

USE OF INORGANIC NATURAL NANOTUBES AND SYNTHETIC
CARBON NANOTUBES IN POLY(LACTIC ACID)

A THESIS SUBMITTED TO
THE GRADUATE SCHOOL OF NATURAL AND APPLIED SCIENCES
OF
MIDDLE EAST TECHNICAL UNIVERSITY

BY

CANAN ESMA YENİOVA ERPEK

IN PARTIAL FULFILLMENT OF THE REQUIREMENTS
FOR
THE DEGREE OF DOCTOR OF PHILOSOPHY
IN
CHEMICAL ENGINEERING

JANUARY 2015

Approval of the thesis

**USE OF INORGANIC NATURAL NANOTUBES AND SYNTHETIC
CARBON NANOTUBES IN POLY(LACTIC ACID)**

submitted by **CANAN ESMA YENİOVA ERPEK** in partial fulfillment of the requirements for the degree of **Doctor of Philosophy in Chemical Engineering Department, Middle East Technical University** by,

Prof. Dr. Gülbin Dural Ünver
Dean, Graduate School of **Natural and Applied Sciences**

Prof. Dr. Halil Kalıpçılar
Head of Department, **Chemical Engineering**

Prof. Dr. Ülkü Yılmaz
Supervisor, **Chemical Engineering Dept., METU**

Assoc. Prof. Dr. Güralp Özkoç
Co-Supervisor, **Chemical Engineering Dept., Kocaeli Uni.**

Examining Committee Members:

Prof. Dr. Erdal Bayramlı
Chemistry Dept., METU

Prof. Dr. Ülkü Yılmaz
Chemical Engineering Dept., METU

Prof. Dr. Halil İbrahim Ünal
Chemistry Dept., Gazi University

Prof. Dr. Göknur Bayram
Chemical Engineering Dept., METU

Assist. Prof. Dr. Erhan Bat
Chemical Engineering Dept., METU

Date

02.01.2015

I hereby declare that all information in this document has been obtained and presented in accordance with academic rules and ethical conduct. I also declare that, as required by these rules and conduct, I have fully cited and referenced all material and results that are not original to this work.

Name, Last Name: CANAN ESMA YENİOVA ERPEK

Signature :

ABSTRACT

USE OF INORGANIC NATURAL NANOTUBES AND SYNTHETIC CARBON NANOTUBES IN POLY(LACTIC ACID)

Erpek Yeniova, Canan Esma

Ph.D., Department of Chemical Engineering

Supervisor: Prof. Dr. Ülkü Yılmaz

Co-supervisor: Assoc. Prof. Dr. Güralp Özkoç

January 2015, 274 Pages

Poly(lactic acid) (PLA) is one of the most important biodegradable aliphatic polyesters, which has attracted great attention in the recent years owing to its excellent material properties. The main objective of this study was to process and characterize Halloysite nanotube (HNT)/PLA nanocomposites. The constituents were observed to be incompatible when processed by classical melt mixing methods, without HNT pre-treatments or addition of plasticizers which act as compatibilizer.

In order to achieve the desired physical properties different mixing methods were tried: Direct melt mixing for 3 minute (DM3), direct melt mixing for 10 minute (DM10), masterbatch melt mixing (MMA), solvent casting followed by melt mixing (SC), suspension addition to melt mixing (SA). In addition, HNT minerals were subjected to different pre-treatments: Purification of HNT (p-HNT), functionalization of HNT by grafting with organo-silane (o-HNT), modification

of HNT with quaternary salt (m-HNT), and evacuation pre-treatment (e-HNT) to improve the compatibility between PLA and HNT. Among the pre-treated HNT minerals, only the samples prepared by e-HNT showed nanocomposite formation due to the removal of water layer that had remained between the layers of silicate which might hinder the desired compatibilization.

For plasticization of PLA, and to provide compatibilization between PLA and HNT two types of blends were processed: PLA plasticized with poly(ethylene glycol) (PEG), P-PLA, and PLA toughened with elastomeric thermoplastic polyurethane (TPU), T-PLA. Addition of HNT was observed to greatly contribute to the improvement of the elongation at break of T-PLA polymers due to the relatively better compatibilization effect of TPU.

The results obtained in this study with the local ESAN HNT were cross checked with a reference imported Nanoclay HNT. Also, the comparison of the properties of HNT based composites with the properties of composites prepared with synthetic carbon nanotube (CNT) was performed. According to results, HNT minerals have no chance to compete with CNT as a filler in PLA matrix unless: The residual water between silica layers are removed or a perfect compatibilizer is used.

Keywords: Poly(lactic acid), Halloysite Nanotube, Carbon Nanotube, Nanocomposite

ÖZ

İNORGANİK DOĞAL NANOTÜPLER VE SENTETİK KARBON NANOTÜPLERİN POLİ(LAKTİK ASİT) İÇİNDE KULLANIMI

Erpek Yeniova, Canan Esma
Doktora, Kimya Mühendisliği Bölümü
Tez Yöneticisi: Prof. Dr. Ülkü Yılmaz
Ortak Tez Yöneticisi: Doç. Dr. Güralp Özkoç

Ocak 2015, 274 Sayfa

Poli(laktik asit) (PLA), gerek endüstriyel olarak elde edilmesi gerekse de petrokimyasal polimerlere yakın özellikleri sebebiyle en sık kullanılan biyobozunur alifatik polyesterlerden bir tanesidir. Bu çalışmada amaçlanan Halloysit nanotüp (HNT)/PLA nanocompozitlerinin işlenmesi ve karakterizasyonudur. Klasik karıştırma metodları, ön işlem uygulanmamış HNT veya plastikleştirici etkisi olan uyumlaştırıcı kullanılmaması durumlarında PLA ve HNT'nin uyumsuz oldukları gözlenmiştir.

Arzu edilen fiziksel özellikleri elde etmek için farklı karıştırma metodları kullanılmıştır: 3 dakika doğrudan eriyik karıştırma (DM3), 10 dakika doğrudan eriyik karıştırma (DM10), masterbatch eriyik karıştırma (MMA), çözeltide karıştırma ardından eriyik karıştırma uygulaması (SC) ve eriyik karıştırmaya suspansiyon eklenmesi (SA). Ayrıca, HNT mineralleri PLA ve HNT arasındaki uyumun artırılması amacıyla farklı ön işlemlere tabi tutulmuşlardır: saflaştırma

(p-HNT), HNT yüzeyinin organo-silan ile fonksiyonlaştırılması (o-HNT), HNT yüzeyinin alkil tuzları ile modifikasyonu (m-HNT) ve vakumlu tahliye ön işlemleri (e-HNT). Ön işlem uygulanmış HNT'ler içerisinde sadece e-HNT mineralleri ile hazırlanmış numunelerde nanokompozit oluşumu gözlenmiştir. Buna neden olarak PLA ve HNT arasında istenen reaksiyonları engellediği düşünülen su tabakasının uzaklaştırılması gösterilebilir.

PLA'nın plastikleştirilmesi ve PLA/HNT arasındaki uyumun sağlanması amacıyla iki çeşit karışım hazırlanmıştır; Poli(etilen glikol) (PEG) ile plastikleştirilmiş PLA, P-PLA, ve termoplastik poliüretan ile tokluğu artırılmış PLA, T-PLA. HNT eklenmesi yapılan T-PLA karışımlarının tokluğunda ciddi derecede bir artış gözlenmiştir. Bu artış TPU'nun PLA ve HNT arasındaki uyumu artırmasından kaynaklanmaktadır.

Bu çalışma sırasında yerel ESAN HNT ile elde edilen sonuçların ithal edilen Nanoclay HNT ile karşılaştırması yapılmıştır. Ayrıca, HNT bazlı kompozitlerin özellikleri, sentetik karbon nanotüpler (CNT) ile hazırlanmış nanokompozitlerin özellikleri ile karşılaştırılmıştır. Elde edilen sonuçlara göre HNT minerallerinin silika tabakaları arasında barındırdıkları su tamamen arındırılmadığı veya iyi bir uyumlaştırıcı kullanılmadığı sürece bu dolgu malzemeleri PLA matrisi içerisinde CNT'lerin gösterdikleri etkiyi gösterememektedirler.

Anahtar Kelimeler: Poli(laktik asit), Halloysit Nanotüp, Karbon Nanotüp, Nanokompozit

To my parents

ACKNOWLEDGEMENTS

This page is the most difficult part of my thesis since there are many special people that I couldn't list and express my feelings in a few pages. During this long period of time they became a part of my life and contributed to the evolution of this thesis.

Among them my special thanks goes to my supervisor Prof. Dr. Ülkü Yılmaz who gave me the opportunity to be his student. Also, I'm indebted to my co-supervisor Assoc. Prof. Dr. Güralp Özkoç who provided me a chance to work in one of the best polymer science laboratories in Turkey. Both of them have always been very kind and supportive in a way that I truly appreciate. Without their constructive tolerance this thesis could not be finished.

I would like to express my gratitude to Prof. Dr. Erdal Bayramlı and Prof. Dr. Göknur Bayram for their presence and fruitful discussions during the progress of my study. For their kind help during my experiments I would like to thank Şebnem Kemaloğlu Doğan, Hümeysra Şirin, Nevin Gamze Karslı Yılmaz and Sibel Yıldız from Kocaeli University Chemical Engineering Department Plastics and Rubber Technology Research Group. Also, I wish to extend my acknowledgements to my dear friends Eda Açıık and Merve Çınar from Middle East Technical University for their valuable friendship and support.

I can count many words to describe the meaning of his presence in my life and how important he is to me. But, I am sure that each of them will be deficient to express my true feelings. Thank you my love Enver Erpek for always being by my side!

I would like to offer my sincerest gratitude to my family for their love and support whole through my life. With their stubborn insistence they made me to carry out this work and they deserve the biggest compliment.

This study was financially supported by The Scientific and Technological Research Council of Turkey (TÜBİTAK) by 111M822 coded project and Domestic Doctorate Fellowship Program.

TABLE OF CONTENTS

ABSTRACT	v
ÖZ	vii
ACKNOWLEDGEMENTS	x
TABLE OF CONTENTS	xii
LIST OF FIGURES	xviii
LIST OF TABLES	xxx
LIST OF EQUATIONS	xxxii
NOMENCLATURE	xxxiii
CHAPTERS	
1 INTRODUCTION	1
2 BACKGROUND INFORMATION	3
2.1 Biopolymers	3
2.1.1 Poly(lactic acid): Main Features and Production	5
2.2 General Structure of Layered Silicates (Phyllosilicates)	7
2.3 Di-octahedral 1:1 Minerals: The Kaolin Group	8
2.3.1 Identification of Halloysite	9
2.3.2 Differentiation of Halloysite from Other Kaolin Minerals	11
2.4 Functionalization of Halloysite Nanotubes with Organo-silanes	12
2.5 Polymer-Layered Silicate (Phyllosilicate) Nanocomposites and Structure Types	13
2.6 Biopolymer Poly(lactic acid) Nanocomposites	15

2.7	Nanocomposite Synthesis Methods.....	16
2.7.1	In-situ Polymerization	16
2.7.2	Solution Intercalation Method.....	17
2.7.3	Melt Intercalation Method	18
2.8	Polymer Blending and Plasticization.....	19
2.9	Polymer Processing	21
2.9.1	Extrusion	22
2.9.2	Injection Molding	25
2.10	Chain Extension Mechanism.....	25
2.11	Carbon Nanotubes (CNT).....	27
2.12	Composite Characterization Techniques	28
2.12.1	Mechanical Analysis.....	28
2.12.2	X-Ray Diffraction Analysis (XRD).....	34
2.12.3	Scanning Electron Microscopy (SEM).....	36
2.12.4	Transmission Electron Microscopy (TEM)	36
2.12.5	Thermal Analysis	37
2.13	Previous Studies	40
3	EXPERIMENTAL.....	51
3.1	Materials	51
3.1.1	Polymer Matrix	51
3.1.2	Plasticizer and Toughening Agent	52
3.1.3	Halloysite Nanotube (HNT).....	52
3.1.4	Carbon Nanotube (CNT)	54
3.1.5	Silane Coupling Agents	55

3.1.6	Quaternary Alkyl Salt	55
3.1.7	Other Chemicals	56
3.2	Characterization of local ESAN HNT	57
3.3	HNT Pre-treatments.....	58
3.3.1	HNT purification (p-HNT)	58
3.3.2	HNT Surface Functionalization with Silane Coupling Agents (o-HNT)	59
3.3.3	HNT Surface Modification with Alkyl Salt (m-HNT)	62
3.3.4	Evacuation Pre-treatment (e-HNT)	62
3.4	Different Composite Preparation Methods	64
3.4.1	Direct Melt Mixing Method (DM)	64
3.4.2	Masterbatch Melt Mixing Method (MMA)	65
3.4.3	Solvent Casting Followed by Melt Mixing Method (SC)	66
3.4.4	Suspension Addition to Melt Mixing (SA)	67
3.5	Characterization of Functionalized HNT Minerals and Composites	68
3.5.1	Fourier Transform Infrared Spectroscopy (FTIR) Analysis	68
3.5.2	X-Ray Diffraction (XRD) Analysis.....	68
3.5.3	Scanning Electron Microscopy (SEM).....	69
3.5.4	Transmission Electron Microscopy (TEM)	69
3.5.5	Tensile Test	69
3.5.6	Impact Test.....	70
3.5.7	Dynamic Mechanical Analysis (DMA)	70
3.5.8	Vertical Force Measurement	71
3.5.9	Differential Scanning Calorimetry (DSC)	72
3.5.10	Thermal Gravimetric Analysis (TGA).....	72

3.5.11	Hydrolytic Degradation Tests	72
3.6	Experimental Design	73
4	RESULTS AND DISCUSSION	75
4.1	Characterization and Purification of Local ESAN Halloysite	75
4.2	Effects of Different Melt Mixing Methods on the Properties of Un- plasticized PLA/HNT Composites	82
4.2.1	X-Ray Diffraction Results	84
4.2.2	Scanning Electron Microscopy	92
4.2.3	Transmission Electron Microscopy	97
4.2.4	Tensile Properties	99
4.2.5	Impact Results	106
4.2.6	Dynamic Mechanical Analysis (DMA)	108
4.2.7	Differential Scanning Calorimetry Analysis (DSC)	118
4.2.8	Hydrolytic Degradation	123
4.3	Effects of Different HNT Pre-treatments on the Properties of Un- plasticized PLA/HNT Composites	129
4.3.1	Functionalization of HNT with Organo-silane	131
4.3.2	X-Ray Diffraction Results	137
4.3.3	Scanning Electron Microscopy	140
4.3.4	Transmission Electron Microscopy	144
4.3.5	Tensile Properties	146
4.3.6	Impact Results	148
4.3.7	Dynamic Mechanical Analysis (DMA)	149
4.3.8	Differential Scanning Calorimetry Analysis (DSC)	152

4.4	Effects of Plasticizer and Toughening Agent on the Properties of PLA/HNT Composites	154
4.4.1	X-Ray Diffraction Results	156
4.4.2	Scanning Electron Microscopy	161
4.4.3	Transmission Electron Microscopy	166
4.4.4	Tensile Properties	167
4.4.5	Impact Results	172
4.4.6	Dynamic Mechanical Analysis (DMA)	174
4.4.7	Differential Scanning Calorimetry Analysis (DSC).....	182
4.4.8	Hydrolytic Degradation	191
4.5	Use of Chain Extender in PLA/HNT P-PLA/HNT Composites and Their Properties	195
4.5.1	X-Ray Diffraction Results	196
4.5.2	Scanning Electron Microscopy	197
4.5.3	Tensile Properties	200
4.5.4	Dynamic Mechanical Analysis (DMA)	205
4.5.5	Differential Scanning Calorimetry Analysis (DSC).....	209
4.5.6	Hydrolytic Degradation	212
4.6	Comparison between the Properties of PLA/CNT and PLA/HNT Unplasticized and Plasticized Composites	214
4.6.1	Scanning Electron Microscopy	215
4.6.2	Transmission Electron Microscopy	219
4.6.3	Tensile Properties	221
4.6.4	Impact Results	225
4.6.5	Dynamic Mechanical Analysis (DMA)	226

4.6.6	Differential Scanning Calorimetry Analysis (DSC).....	232
4.6.7	Hydrolytic Degradation	234
5	CONCLUSIONS	237
	REFERENCES	241
	APPENDICES	
	A: TGA RESULTS OF PLA/HNT COMPOSITES.....	259
	B: MECHANICAL TEST RESULTS	263
	CURRICULUM VITAE	271

LIST OF FIGURES

FIGURES

Figure 2.1. Schematic of PLA production via pre-polymer and lactide (Henton et al. 2005)	6
Figure 2.2. (a) Tetrahedron; (b) O_{oct} (OH, F, Cl) orientation in cis-octahedron and trans-octahedron (O_a and O_b refer to apical and basal oxygen atoms) (Brigatti et al. 2006)	8
Figure 2.3. Schematic diagrams of (a) the crystalline structure of HNT (10 Å); (b) the structure of the nanotube (Yuan et al. 2008)	10
Figure 2.4. Possible interaction mechanism between Halloysite nanotubes and organo-silanes.....	13
Figure 2.5. Effect of shear on clay platelets (Dennis et al. 2001)	19
Figure 2.6. Complex die shapes; (a) Compensate die swell, (b) Sheet coating, (c) Wire coating (Schey 1987).....	22
Figure 2.7. Intermeshing twin screw extruder (Keskkula and Paul 1996).....	24
Figure 2.8. Single and multiwall carbon nanotubes	27
Figure 2.9. Standard dog-bone shape sample and tensile testing machine (Seymour 1996).....	29
Figure 2.10. Stress-strain curve of a typical polymeric material.....	30
Figure 2.11. Performing impact test	31
Figure 2.12. The relationship of the applied sinusoidal strain to stress for a typical polymeric material.....	34
Figure 2.13. Diffraction of X-rays by planes of atoms (Kroschwitz 1990).....	35
Figure 2.14. Differential scanning calorimeter instruments.....	38
Figure 2.15. A typical DSC curve	39

Figure 2.16. SEM micrographs taken on the fracture surfaces of the nanocomposites (a) Nanotube debonding/pull-out, (b) Nanotube bridge (crack bridging).....	46
Figure 3.1. Chemical structure of PLA.....	52
Figure 3.2. TEM micrographs of (a) Nanoclay HNT (b) ESAN HNT.....	53
Figure 3.3. TEM Micrograph of Nanocyl 7000 CNT.....	54
Figure 3.4. Chemical structure of (4-carboxybutyl)triphenyl phosphonium bromide (CBTPB).....	56
Figure 3.5. Ethylene glycol (EG) treatment procedure for local ESAN HNT.....	57
Figure 3.6. Sedimentation Procedure for Halloysite Purification.....	59
Figure 3.7. Silanization Procedure.....	61
Figure 3.8. Evacuation pre-treatment system schematic.....	63
Figure 3.9. Melt mixing equipment; (a) Micro-compounder, (b) Screw design of Micro-compounder, (c) Microinjection-molder.....	65
Figure 3.10. Masterbatch melt mixing procedure (MMA).....	66
Figure 3.11. Solvent casting followed by melt mixing procedure (SC).....	66
Figure 3.12. Suspension addition to melt mixing (SA).....	67
Figure 3.13. Tensile test specimen.....	70
Figure 3.14. The schematic of axial force measurement setup.....	71
Figure 3.15. Experimental Design.....	74
Figure 4.1. XRD pattern of raw ESAN HNT.....	77
Figure 4.2. Comparison of the XRD patterns of raw ESAN HNT and purified ESAN HNT samples.....	78
Figure 4.3 Comparison of the XRD patterns of EG treated and raw ESAN Halloysite samples.....	81
Figure 4.4. XRD pattern of PLA/ESAN HNT composites prepared by DM3 method; (a) ESAN HNT, (b) PLA/10wt% ESAN HNT, (c) PLA/5wt% ESAN HNT, (d) PLA/3wt% ESAN HNT, (e) Neat PLA.....	87

Figure 4.5. XRD pattern of PLA/Nanoclay HNT composites prepared by DM3 method; (a) Nanoclay HNT, (b) PLA/10wt% Nanoclay HNT, (c) PLA/5wt% Nanoclay HNT, (d) PLA/3wt% Nanoclay HNT, (e) Neat PLA.....88

Figure 4.6. XRD pattern of PLA/5wt% ESAN HNT composites prepared by different processing methods; (a) Direct melt mixing for 3 minute (DM3), (b) Direct melt mixing for 10 minute (DM10), (c) Masterbatch melt mixing (MMA), (d) Solvent casting followed by melt mixing method (SC), (e) Suspension addition to melt mixing (SA)91

Figure 4.7. SEM micrographs of pure PLA subjected to 3 minute mixing95

Figure 4.8. SEM micrographs of PLA based composites containing 5wt% HNT and prepared by DM3 method; (a) ESAN 250x, (b) ESAN 2000x, (c) Nanoclay 250x, (d) Nanoclay 2000x.....96

Figure 4.9. TEM micrographs of PLA/5wt% ESAN HNT composites; (a) Scale bar is 0.4 μ m, (b) Scale bar is 100 nm, (c) Scale bar is 0.2 μ m98

Figure 4.10. Stress-strain curve of pure PLA.....99

Figure 4.11. Tensile strength (MPa) of PLA/HNT based composites prepared by DM3 method 101

Figure 4.12. Strain at break of PLA/HNT based composites prepared by DM3 method..... 102

Figure 4.13. Effect of different processing techniques on the tensile strength (MPa) of PLA/ESAN HNT composites (DM3: Direct Melt Mixing-3 minute, DM10: Direct Melt Mixing-10 minute, MMA: PLA Masterbatch Melt Mixing, SC: Solvent Casting Followed by Melt Mixing Method, SA: Suspension Addition to Melt Mixing) 103

Figure 4.14. Effect of different processing techniques on the strain at break values of PLA/ESAN HNT composites (DM3: Direct Melt Mixing-3 minute, DM10: Direct Melt Mixing-10 minute, MMA: PLA Masterbatch Melt Mixing, SC: Solvent Casting Followed by Melt Mixing Method, SA: Suspension Addition to Melt Mixing) 104

Figure 4.15. Effect of different processing techniques on the tensile strength (MPa) of PLA/Nanoclay HNT composites (DM3: Direct Melt Mixing-3 minute, DM10: Direct Melt Mixing-10 minute, MMA: PLA Masterbatch Melt Mixing, SC: Solvent Casting Followed by Melt Mixing Method, SA: Suspension Addition to Melt Mixing)	105
Figure 4.16. Effect of different processing techniques on the strain at break values of PLA/Nanoclay HNT composites (DM3: Direct Melt Mixing-3 minute, DM10: Direct Melt Mixing-10 minute, MMA: PLA Masterbatch Melt Mixing, SC: Solvent Casting Followed by Melt Mixing Method, SA: Suspension Addition to Melt Mixing)	106
Figure 4.17. Impact strength (MPa) of PLA/HNT based composites prepared by DM3 method	108
Figure 4.18. Storage Modulus (E') versus temperature data for PLA/ESAN HNT composites prepared by DM3 method	111
Figure 4.19. Loss Modulus (E'') versus temperature data for PLA/ESAN HNT composites prepared by DM3 method	111
Figure 4.20. $\tan \delta$ versus temperature data for PLA/ESAN HNT composites prepared by DM3 method	112
Figure 4.21. Storage Modulus (E') versus temperature data for PLA/Nanoclay HNT composites prepared by DM3 method	113
Figure 4.22. Loss Modulus (E'') versus temperature data for PLA/ Nanoclay HNT composites prepared by DM3 method	114
Figure 4.23. $\tan \delta$ versus temperature data for PLA/ESAN Nanoclay composites prepared by DM3 method	114
Figure 4.24. Effect of different processing techniques on the Storage Modulus, E' , (Pa) of PLA/5wt%ESAN HNT composites (DM3: Direct Melt Mixing-3 minute, DM10: Direct Melt Mixing-10 minute, MMA: PLA Masterbatch Melt Mixing, SC: Solvent Casting Followed by Melt Mixing Method, SA: Suspension Addition to Melt Mixing)	115

Figure 4.25. Effect of different processing techniques on the Loss Modulus, E'' , (Pa) of PLA/5wt%ESAN HNT composites (DM3: Direct Melt Mixing-3 minute, DM10: Direct Melt Mixing-10 minute, MMA: PLA Masterbatch Melt Mixing, SC: Solvent Casting Followed by Melt Mixing Method, SA: Suspension Addition to Melt Mixing)	116
Figure 4.26. Effect of different processing techniques on the $\tan \delta$ of PLA/5wt%ESAN HNT composites (DM3: Direct Melt Mixing-3 minute, DM10: Direct Melt Mixing-10 minute, MMA: PLA Masterbatch Melt Mixing, SC: Solvent Casting Followed by Melt Mixing Method, SA: Suspension Addition to Melt Mixing)	117
Figure 4.27. DSC thermograms of PLA/ESAN HNT composites prepared by DM3 method	121
Figure 4.28. DSC thermograms of PLA/Nanoclay HNT composites prepared by DM3 method	122
Figure 4.29. Hydrolysis samples of PLA/ESAN HNT composites prepared by DM3 method; (a) 0wt% HNT, (b) 3wt% HNT, (c) 5wt% HNT, (d) 10wt% HNT	126
Figure 4.30. Hydrolytic degradation results of PLA/ESAN HNT composites prepared by DM3 methods.....	127
Figure 4.31. Hydrolytic degradation results of PLA/Nanoclay HNT composites prepared by DM3 methods.....	127
Figure 4.32. FTIR spectrum of Nanoclay HNT mineral modified with functional organo-silanes.....	134
Figure 4.33. TGA spectrums of organo-silane modified and un-modified Nanoclay HNT	136
Figure 4.34. XRD pattern of PLA/5wt% Nanoclay HNT composites prepared by HNT subjected to different pre-treatments; (a) raw HNT, (b) purified HNT (p-HNT), (c) Organo-silane functionalized HNT (o-HNT), (d) Quaternary salt modified HNT (m-HNT), (e) Evacuated HNT (e-HNT)	139

Figure 4.35. SEM micrographs of PLA based composites containing 5wt% Nanoclay; (a) HNT 250x, (b) HNT 2000x, (c) p-HNT 250x, (d) p-HNT 2000x, (e) o-HNT 250x, (f) o-HNT 2000x, (g) m-HNT 250x, (h) m-HNT 2000x, (i) e-HNT 250x, (j) e-HNT 2000x	142
Figure 4.36. Transmission Electron Microscopy of PLA/e-HNT composite; (a) Scale bar is 0.4 μ m, (b) Scale bar is 100nm.....	145
Figure 4.37. Schematic drawing of sample used in TEM analysis	145
Figure 4.38. Effect of different HNT pre-treatments on the tensile strength (MPa) of PLA/5wt%Nanoclay composites (p-HNT: Purified Nanoclay, o-HNT: Functionalized Nanoclay with γ -APS, m-HNT: Modified Nanoclay with Alkyl Sat, e-HNT: Evacuated Nanoclay)	147
Figure 4.39. Effect of different HNT pre-treatments on the strain at break values of PLA/5wt%Nanoclay composites (p-HNT: Purified Nanoclay, o-HNT: Functionalized Nanoclay with γ -APS, m-HNT: Modified Nanoclay with Alkyl Salt, e-HNT: Evacuated Nanoclay)	148
Figure 4.40. Effect of different HNT pre-treatments on the impact strength (kJ/m ²) of PLA/5wt%Nanoclay composites (p-HNT: Purified Nanoclay, o-HNT: Functionalized Nanoclay with γ -APS, m-HNT: Modified Nanoclay with Alkyl Sat, e-HNT: Evacuated Nanoclay)	149
Figure 4.41. Effect of different HNT pre-treatments on the Storage Modulus, E', (Pa) of PLA/5wt% Nanoclay HNT composites (p-HNT: Purified Nanoclay, o-HNT: Functionalized Nanoclay with γ -APS, m-HNT: Modified Nanoclay with Alkyl Sat, e-HNT: Evacuated Nanoclay).....	150
Figure 4.42. Effect of different HNT pre-treatments on the Loss Modulus, E'', (Pa) of PLA/5wt% Nanoclay HNT composites (p-HNT: Purified Nanoclay, o-HNT: Functionalized Nanoclay with γ -APS, m-HNT: Modified Nanoclay with Alkyl Sat, e-HNT: Evacuated Nanoclay).....	151
Figure 4.43. Effect of different HNT pre-treatments on the tan δ of PLA/5wt% Nanoclay HNT composites (p-HNT: Purified Nanoclay, o-HNT: Functionalized	

Nanoclay with γ -APS, m-HNT: Modified Nanoclay with Alkyl Sat, e-HNT: Evacuated Nanoclay)	152
Figure 4.44. XRD pattern of P-PLA/ESAN HNT composites; (a) ESAN HNT, (b) P-PLA/3wt% ESAN HNT, (c) P-PLA/5wt% ESAN HNT, (d) P-PLA/10wt% ESAN HNT	158
Figure 4.45. XRD pattern of P-PLA/Nanoclay HNT composites; (a) Nanoclay HNT, (b) P-PLA/3wt% Nanoclay HNT, (c) P-PLA/5wt% Nanoclay HNT, (d) P-PLA/10wt% Nanoclay HNT	159
Figure 4.46. XRD pattern of T-PLA/5wt% HNT composites; (a) ESAN HNT, (b) Nanoclay HNT, (c) T-PLA/5wt% ESAN HNT, (d) T-PLA/5wt% Nanoclay HNT	160
Figure 4.47. SEM micrographs of P-PLA composites (a) 0wt% HNT 250x, (b) 0wt% HNT 2000x, (c) 5wt% ESAN 250x, (d) 5wt% ESAN 2000x, (e) 5wt% Nanoclay 250x, (f) 5wt% Nanoclay 2000x.....	163
Figure 4.48. SEM micrographs of T-PLA composites (a) 0wt% ESAN 250x, (b) 0wt% ESAN 2000x, (c) 3wt% ESAN 250x, (d) 3wt% ESAN 2000x, (e) 5wt% ESAN 250x, (f) 5wt% ESAN 2000x, (g) 10wt% ESAN 250x, (h) 10wt% ESAN 2000x	164
Figure 4.49. TEM Micrographs of composites containing 5wt% ESAN HNT; (a)P-PLA, (b) T-PLA composite (Scale bar is 0.4 μ m)	166
Figure 4.50. Stress-strain curves of pure PLA, P-PLA and T-PLA	167
Figure 4.51. Effect of different compatibilizers on the tensile strength (MPa) of PLA/ESAN HNT composites (P-PLA: PEG plasticized PLA, T-PLA: TPU toughened PLA).....	169
Figure 4.52. Effect of different compatibilizers on the strain at break values of PLA/ESAN HNT composites (P-PLA: PEG plasticized PLA, T-PLA: TPU toughened PLA).....	170
Figure 4.53. Effect of different plasticizers on the tensile strength (MPa) of PLA/Nanoclay HNT composites (P-PLA: PEG plasticized PLA, T-PLA: TPU toughened PLA).....	171

Figure 4.54. Effect of different plasticizers on the strain at break values of PLA/Nanoclay HNT composites (P-PLA: PEG plasticized PLA, T-PLA: TPU toughened PLA).....	172
Figure 4.55. Effect of elastomeric TPU on the impact strength (kJ/m^2) of PLA/ESAN HNT composites (T-PLA: TPU toughened PLA).....	173
Figure 4.56. Effect of elastomeric TPU on the impact strength (kJ/m^2) of PLA/Nanoclay HNT composites (T-PLA: TPU toughened PLA)	174
Figure 4.57. Storage Modulus (E') versus temperature data for PLA, P-PLA and T-PLA polymers	176
Figure 4.58. Loss Modulus (E'') versus temperature data for PLA, P-PLA and T-PLA polymers.....	176
Figure 4.59. $\tan \delta$ versus temperature data for PLA, P-PLA and T-PLA polymers	177
Figure 4.60. SEM micrograph of PLA plasticized with PEG (P-PLA).....	177
Figure 4.61. Storage Modulus (E') versus temperature data for P-PLA/ESAN HNT composites.....	179
Figure 4.62. Loss Modulus (E'') versus temperature data for P-PLA/ESAN HNT composites.....	179
Figure 4.63. $\tan \delta$ versus temperature data for P-PLA/ESAN HNT composites	180
Figure 4.64. Storage Modulus (E') versus temperature data for T-PLA/ESAN HNT composites.....	180
Figure 4.65. Loss Modulus (E'') versus temperature data for T-PLA/ESAN HNT composites.....	181
Figure 4.66. $\tan \delta$ versus temperature data for.....	181
Figure 4.67. DSC thermograms of P-PLA/ESAN HNT composites.....	186
Figure 4.68. Cooling thermograms for P-PLA/ESAN HNT composites	187
Figure 4.69. DSC thermograms of P-PLA/Nanoclay HNT composites	188
Figure 4.70. DSC thermograms of T-PLA/ESAN HNT composites	189
Figure 4.71. DSC thermograms of T-PLA/Nanoclay HNT composites.....	190

Figure 4.72. Hydrolysis samples of PLA, P-PLA and T-PLA polymers.....	192
Figure 4.73. Hydrolytic degradation results of PLA, P-PLA and T-PLA polymers	192
Figure 4.74. Hydrolytic degradation results of P-PLA/ESAN HNT composites	193
Figure 4.75. Hydrolytic degradation results of T-PLA/ESAN HNT composites	194
Figure 4.76. SEM Micrographs of PLA/PDI composite (a) 0wt% ESAN HNT250x, (b) 0wt% ESAN HNT 2000x, (c) 5wt% ESAN HNT 250x, (d) 5wt% ESAN HNT 2000x.....	198
Figure 4.77. SEM Micrographs of P-PLA/PDI composite (a) 0wt% ESAN HNT 250x, (b) 0wt% ESAN HNT 2000x, (c) 5wt% ESAN HNT 250x, (d) 5wt% ESAN HNT 2000x.....	199
Figure 4.78. Effect of chain extender on tensile strength (MPa) of PLA/HNT composites.....	201
Figure 4.79. Effect of chain extender on strain at break of PLA/HNT composites	201
Figure 4.80. Effect of chain extender on tensile strength (MPa) of P-PLA/HNT composites.....	202
Figure 4.81. Effect of chain extender on strain at break of P-PLA/HNT composites.....	202
Figure 4.82. Vertical force measurements for PLA and P-PLA blends in the presence of PDI	203
Figure 4.83. Effect of chain extender on the PEG migration; (a) Weight loss (%) versus time plot, (b) P-PLA and P-PLA/PDI samples at the end of 2 years.....	204
Figure 4.84. Storage Modulus (E') versus temperature data for PLA/PDI/5wt%HNT composites	206
Figure 4.85. Loss Modulus (E'') versus temperature data for PLA/PDI/5wt%HNT composites.....	206
Figure 4.86. Tan δ versus temperature data for PLA/PDI/5wt%HNT composites	207

Figure 4.87. Storage Modulus (E') versus temperature data for P-PLA/PDI/5wt%HNT composites	207
Figure 4.88. Loss Modulus (E'') versus temperature data for P-PLA/PDI/5wt%HNT composites	208
Figure 4.89. Tan δ versus temperature data for P-PLA/PDI/5wt%HNT composites	208
Figure 4.90. Effect of PDI on the crystallization behavior of P-PLA/HNT composite	211
Figure 4.91. Hydrolytic degradation results on PLA/PDI mixture and PLA/PDI/HNT composites	212
Figure 4.92. Hydrolytic degradation results of P-PLA/PDI mixture and P-PLA/PDI/HNT composites	213
Figure 4.93. SEM Micrograph of PLA composites containing 5wt% (a) ESAN HNT 250x, (b) ESAN HNT 2000x, (c) CNT 250x, (d) CNT 2000x.....	216
Figure 4.94. SEM Micrograph of P-PLA composites containing 5wt% (a) ESAN HNT 250x, (b) ESAN HNT 2000x, (c) CNT 250x, (d) CNT 2000x.....	217
Figure 4.95. SEM Micrograph of T-PLA composites containing 5wt% (a) ESAN HNT 250x, (b) ESAN HNT 2000x, (c) CNT 250x, (d) CNT 2000x.....	218
Figure 4.96. TEM Micrographs of PLA/5wt% CNT composite; (a) Scale bar is 0.2 μ m, (b) Scale bar is 100nm	219
Figure 4.97. TEM Micrographs of composites containing 5wt% CNT; (a) P-PLA Scale bar is 1 μ m, (b) P-PLA Scale bar is 0.2 μ m, (c) T-PLA Scale bar is 1 μ m, (d) T-PLA Scale bar is 0.2 μ m.....	220
Figure 4.98. Tensile strength (MPa) of PLA/CNT nanocomposites and their comparison with PLA/ESAN HNT composites	222
Figure 4.99. Strain at break values of PLA/CNT nanocomposites and their comparison with PLA/ESAN HNT composites	222
Figure 4.100. Tensile strength (MPa) of P-PLA/CNT nanocomposites and their comparison with P-PLA/ESAN HNT composites	223

Figure 4.101. Strain at break values of P-PLA/CNT nanocomposites and their comparison with P-PLA/ESAN HNT composites	223
Figure 4.102. Tensile strength (MPa) of T-PLA/CNT nanocomposites and their comparison with T-PLA/ESAN HNT composites	224
Figure 4.103. Strain at break values of T-PLA/CNT nanocomposites and their comparison with P-PLA/ESAN HNT composites	224
Figure 4.104. Impact strength (kJ/m ²) of PLA/CNT nanocomposites and their comparison with PLA/ESAN HNT composites.....	225
Figure 4.105. Impact strength (kJ/m ²) of T-PLA/CNT nanocomposites and their comparison with T-PLA/ESAN HNT composites	226
Figure 4.106. Storage Modulus (E') versus temperature data for PLA/CNT composites.....	227
Figure 4.107. Loss Modulus (E'') versus temperature data for PLA/CNT composites.....	227
Figure 4.108. Tan δ versus temperature data for PLA/CNT composites.....	228
Figure 4.109. Storage Modulus (E') versus temperature data for P-PLA/CNT composites.....	229
Figure 4.110. Loss Modulus (E'') versus temperature data for P-PLA/CNT composites.....	229
Figure 4.111. Tan δ versus temperature data for P-PLA/CNT composites	230
Figure 4.112. Storage Modulus (E') versus temperature data for T-PLA/CNT composites.....	230
Figure 4.113. Loss Modulus (E'') versus temperature data for T-PLA/CNT composites.....	231
Figure 4.114. Tan δ versus temperature data for T-PLA/CNT composites	231
Figure 4.115. DSC thermograms of P-PLA, P-PLA/ESAN HNT and P-PLA/CNT composites.....	233
Figure 4.116. Hydrolytic degradation results of PLA/CNT composites	234
Figure 4.117. Hydrolysis samples of PLA/CNT composites; (a) 0wt% CNT, (b) 3wt% CNT, (c) 5wt% CNT, (d) 10wt% CNT.....	235

Figure 4.118. Hydrolytic degradation results of P-PLA/CNT composites.....	236
Figure 4.119. Hydrolytic degradation results of T-PLA/CNT composites.....	236
Figure A. 1 TGA spectrums of PLA/ESAN HNT composites prepared by DM3 method.....	259
Figure A. 2 TGA spectrums of PLA/Nanoclay HNT composites prepared by DM3 method.....	260

LIST OF TABLES

TABLES

Table 3.1. Properties of PLA matrix (PLI005).....	51
Table 3.2. Properties of Nanoclay HNT	53
Table 3.3. Characterization of Nanocyl 7000	54
Table 3.4. Silane coupling agents used in this study	55
Table 3.5. Other chemicals used for in this study	56
Table 3.6. Sedimentation procedure experimental parameters	59
Table 4.1 Chemical analysis of raw and purified Halloysite (Performed by ESAN Eczacıbaşı A.Ş.).....	79
Table 4.2 Thermal transition behavior and crystalline fraction (%) of PLA/ HNT composites.....	120
Table 4.3. Effects of different processing techniques on thermal transition behavior and crystalline fraction (%) of PLA/5wt% ESAN HNT composites ...	123
Table 4.4. Effects of different HNT pre-treatments on thermal transition behaviors and crystalline fraction (%) of PLA/5wt% Nanoclay HNT composites.....	153
Table 4.5. Average domain size of PLA/TPU blend and its ESAN based composites.....	165
Table 4.6. Thermal transition behavior and crystalline fraction (%) of P-PLA/HNT composites.....	185
Table 4.7. Basal spacing (Å) results of ESAN based PLA and P-PLA composites containing 3wt% PDI.....	196
Table 4.8. Effects of PDI on thermal transition behavior and crystalline fraction (%) of PLA/5wt% HNT composites.....	210
Table 4.9. Thermal transition behavior and crystalline fraction (%) of PLA/CNT composites.....	232
Table A.1. TGA data of PLA/HNT composites prepared by DM3 method	261

Table B.1. Tensile strength results (MPa).....	263
Table B.2. Elongation at break results	266
Table B.3. Impact strength (kJ/m ²) results.....	269

LIST OF EQUATIONS

EQUATIONS

Equation 2.1	29
Equation 2.2	33
Equation 2.3	33
Equation 2.4	35
Equation 2.5	38
Equation 3.1	62

NOMENCLATURE

- A_0 : Initial cross section, mm^2
 d : Interlayer spacing, Å
 D : Distance between grips of tensile test specimen, mm
 d_{av} : Average dispersed phase domain size, nm
 E^* : complex modulus, MPa
 E' : Storage modulus, MPa
 E'' : Loss modulus, MPa
 F : Applied force, N
 L : Overall length of tensile test specimen, mm
 L_i : Initial gauge length of tensile test specimen, mm
 L_0 : Final gauge length of tensile test specimen, mm
 t : time, s
 T : Thickness of tensile and impact test specimen, mm
 T_g : Glass Transition Temperature, $^{\circ}\text{C}$
 T_m : Melting Temperature, $^{\circ}\text{C}$
 T_c : Crystallization Temperature, $^{\circ}\text{C}$
 W : Width of narrow section of tensile test specimen, mm

Greek Letters

α -crystal: Pseudo-orthorhombic, pseudo-hexagonal or orthorhombic crystal form

β -crystal: Orthorhombic or trigonal crystal form

σ : Engineering stress, MPa
 σ^0 : Stress amplitude, MPa
 σ^* : Complex stress, MPa
 σ_m : Tensile strength, MPa
 ε : Engineering strain, mm/mm
 ε^* : Complex strain, mm/mm
 ε^0 : Strain amplitude, mm/mm
 θ : Scattering angle, °
 λ : Wavelength, nm
 γ -APS: γ -aminopropyltriethoxy silane
 γ -GPS: γ -glycidoxypropyl trimethoxy silane
 γ -MPS: γ -methacryloxypropyltrimethoxy silane
 δ : phase shift, °
 $\tan \delta$: Loss tangent
 ω : angular frequency of oscillation, rad/s
 χ_c : crystalline fraction, %
 ΔH_m : Latent heat of melting, kJ/kg
 ΔH_c : Latent heat of crystallization, kJ/kg
 ΔH^* : Latent heat of fusion of a 100% crystalline polymer, kJ/kg

Abbreviations

AEAPTMS: N- β -(aminoethyl)- γ -aminopropyltrimethoxy silane

ATBC: Acetyl tri-n-butyl citrate

BET: Brunauer, Emmett and Teller method

CBTPB: (4-Carboxybutyl)triphenyl Phosphonium Bromide quaternary salt
CCVD Catalytic Carbon Vapor Deposition
CEC: Cation Exchange Capacity
CNT: Carbon Nanotube
DM: Direct Melt Mixing Method
DM3: Direct Melt Mixing Method (3 Minutes)
DM10: Direct Melt Mixing Method (10 Minutes)
DMA: Dynamic Mechanical Analysis
DSC: Differential Scanning Calorimetry
EG: Ethylene Glycol
e-HNT: Evacuation Pre-treatment
EPDM: Ethylene Propylene Diene Monomer
FTIR: Fourier Transform Infrared Spectroscopy
HDPE: High Density Polyethylene
HDT: Heat Deflection Temperature
HNT: Halloysite Nanotube
m-HNT: HNT Modified With Quaternary Salt
MMA: Masterbatch Melt Mixing Method
MMT: Montmorillonite
MWCNT: Multi Wall Carbon Nanotube
o-HNT: HNT Functionalized by Grafting with Organo-silane
PCL: Polycaprolactone
PEG: Poly(ethylene glycol)
PET: Polyethylene Terephthalate
PDI: 1,4-phenylene diisocyanate
p-HNT: Purification of HNT

PLA: Poly(lactic acid)
PLGA: Poly(lactic-co-glycolic acid)
PMMA: Poly(methyl methacrylate)
PP: Polypropylene
P-PLA: PEG Plasticized PLA
PS: Polystyrene
PVC: Poly(vinyl chloride)
SA: Suspension Addition to Melt Mixing
SC: Solvent Casting Followed by Melt Mixing Method
SEM: Scanning Electron Microscopy
SSP: Solid State Polymerization
SWCNT: Single Wall Carbon Nanotubes
TEM: Transmission Electron Microscopy
TGA: Thermal Gravimetric Analysis
T-PLA: TPU Toughened PLA
TPU: Thermoplastic Polyurethane
XRD: X-Ray Diffraction

CHAPTER 1

INTRODUCTION

Concerns about the resistance of petrochemical based polymers for degradation, declining raw material resources, contamination during their recycling etc. bring questions about their extensive usage. At this point, biopolymers present a solution to these concerns.

PLA is the most commonly preferred biopolymer due to its reasonable price and availability in the market. However, its mechanical and thermal properties may need to be enhanced. For this purpose, PLA/Halloysite nanotube (HNT) composites were prepared in this study by using different techniques. HNT, is a naturally occurring alumina silicate exhibiting unique surface chemical properties. It can adopt a variety of morphologies, but the most common form is an elongated hollow tubular structure with a large aspect ratio.

The study composed of mainly five sections. In the first section, in order to obtain homogeneous dispersion of clay particles in the polymer matrix, different melt mixing methods were tried and they were compared with each other. These methods are;

- Direct Melt Mixing Method (DM)
 - o 3 minute mixing time (DM3)
 - o 10 minute mixing time (DM10)
- Masterbatch Melt Mixing Method (MMA)
- Solvent Casting Followed by Melt Mixing Method (SC)
- Suspension Addition to Melt Mixing (SA)

In the second section of the study, PLA composites were prepared by using HNT minerals subjected to different pre-treatments. These are;

- Purification of HNT (p-HNT)
- Functionalization of HNT by Grafting with Organo-silane (o-HNT)
- Modification of HNT With Quaternary Salt (m-HNT)
- Evacuation pre-treatment (e-HNT)

For improvement of PLA toughness and compatibilization of PLA/HNT interface, two different polymers were used to prepare PLA blends in the third section of the study. These are;

- PEG plasticized PLA (P-PLA)
- TPU toughened PLA (T-PLA)

In the fourth section, PLA/HNT composites were prepared in the presence of a chain extender, PDI, in order to prevent the degradation of PLA molecules due to high processing temperatures and hidden water that exists between the layers of HNT mineral. The technique was also applied to P-PLA blends to see the effect of chain extender on plasticized composites.

Owing to HNT's unique crystal structure resembling that of carbon nanotubes (CNT) and their potential to replace this expensive synthetic materials, CNT and HNT based composite comparison was performed in the last section of the study. In each section, composites were subjected to morphological, mechanical, thermal and hydrolytic degradation analysis.

CHAPTER 2

BACKGROUND INFORMATION

2.1 Biopolymers

Polymers form the backbones of plastic materials, and are continually being employed in an expanding range of areas. In terms of their advantages, i.e. low cost and high-speed production, high mechanical performance, good barrier properties, and good heat sealing, non-renewable petrochemical based polymers encourage the industry to use them. On the other hand, environmental concerns related to their resistance for degradation, declining raw material resources, contamination during their recycling etc. bring in mind questions about their extensive usage (Amass, Amass and Tighe 1998). In addition, rising global population greatly enhances the amount of plastic wastes being sent to landfills. Due to lack of landfill space, demand for using less oil, and/or finding alternative sources, and issue of global warming caused by increasing amounts of carbon dioxide in the atmosphere have provoked scientists and producers to go green.

The above mentioned concerns are negligible for biopolymers concerning the biodegradation process that takes place in nature. The future outlook for advancement in the area of biodegradable plastics is promising. These plastics begin their lifecycle as renewable resources, and then they are formed into the specific end products and used by consumer. Ideally, the biopolymer will be disposed in a bio waste collection, and later composted to go through various

biodegradation steps including direct enzymatic scission, progressive enzymatic dissimilation and conversion of short chains by microorganisms (Aminabhavi, Balundgi and Cassidy 1990). Biodegradation is defined as changes in chemical structure, loss of mechanical and structural properties, and finally, changing into other compounds like water, carbon dioxide, minerals, and intermediate products like biomass and humic materials under the action of naturally occurring microorganisms, such as bacteria, fungi, and algae. The natural environments contain chemical, biological, and physical forces with impinging factors like temperature, humidity, pH, O₂ presence, and so on, which determine the rate and products of the biodegradation process (Jamshidian et al. 2010).

There are mainly four feedstocks that biopolymers are derived from. Animal sources provide collagen and gelatin, while marine sources provide chitin which is processed into chitosan. The remaining two feedstock areas, microbial biopolymer feedstock and agricultural feedstock, are the ones receiving the most attention (Kolybaba et al. 2003).

Sectors where applications for biopolymers have introduced include medicine, packaging, and agriculture. Manufacturers of automotive parts are also responding to societal and governmental demands for environmental responsibility and utilizing biodegradable polymers in vehicle interiors. Vehicle interior part, such as headrest and seat, manufacturers are using non-degradable polyurethane foam that is covered with a layer of polyvinylchloride or polyethylene (Maldanis 2009). Several manufacturers are currently modifying automotive parts to become environmental friendly. Mazda is one of those manufacturers. As an alternative to PVC, films used for seat covers and door trims are produced from a bio-fabric called “Mazda Biotech material” consisting of poly(lactic acid) (PLA). Mercedes, Mitsubishi and Ford are other manufacturers that tend to use biopolymers.

2.1.1 Poly(lactic acid): Main Features and Production

Poly(lactic acid) (PLA) is a common polymer based on agricultural (crop growing), biological (fermentation), and chemical (polymerization) sciences and technologies. It has one of the highest potentials among bio-based polymers due to its reasonable price and availability in the market. Another positive point of PLA production in comparison to other hydrocarbon-based polymers is the control of CO₂ balance after their composting (Jamshidian et al. 2010).

In addition to environmental friendly characteristics, PLA has unique properties such as good appearance, high mechanical strength, low toxicity and good barrier properties. For tensile modulus and flexural modulus, PLA has the highest value in comparison to PS, PP, and HDPE. However, it needs plasticization owing to its low notched izod impact resistance and elongation at break values (Dorgan, Lehermeier and Mang 2000).

Depending on the stereochemistry and thermal history, PLA can be either amorphous or semi-crystalline in the solid state. Higher D-isomer content leads to lower crystallinity, whereas higher L-isomer content displays a reverse effect (Zhang et al. 2008). For semi-crystalline PLA, glass transition temperature (T_g , ~50-80°C) and melting point (T_m , ~175°-185°C) are important for determining the use temperature for various applications. Amorphous PLA has relatively lower T_g and T_m than semi-crystalline PLA, which is better to be used for heat-sealing and thermoforming applications. Below T_g , PLA behaves as a glass with the ability to creep until cooled to its β transition temperature of approximately -45°C. Below this temperature PLA will only behave as a brittle polymer.

Carothers (at DuPont) investigated the production of PLA as early as 1932. He was only able to produce a low molecular weight PLA by heating lactic acid under vacuum while removing the condensed water (Direct condensation polymerization). Today, two other ways are possible for the polymerization of

lactic acid; direct poly-condensation in an azeotropic solution, and polymerization through lactide formation.

In the first method, azeotropic solution helps to decrease the distillation pressure and facilitates PLA separation from the solvent by application of molecular sieves. Cargill Dow LLC, has developed continuous process of polymerization through lactide formation. The process starts with lactic acid produced by fermentation of dextrose and followed by a continuous condensation reaction of aqueous lactic acid to produce low molecular weight PLA pre-polymer. Next, the low molecular weight oligomers are converted into a mixture of lactide stereoisomer using a catalyst. After vacuum distillation, purification, high molecular weight PLA is produced using an organo tin-catalyzed, ring-opening lactide polymerization in the melt (Henton et al. 2005). The illustration of this process is given in Figure 2.1.

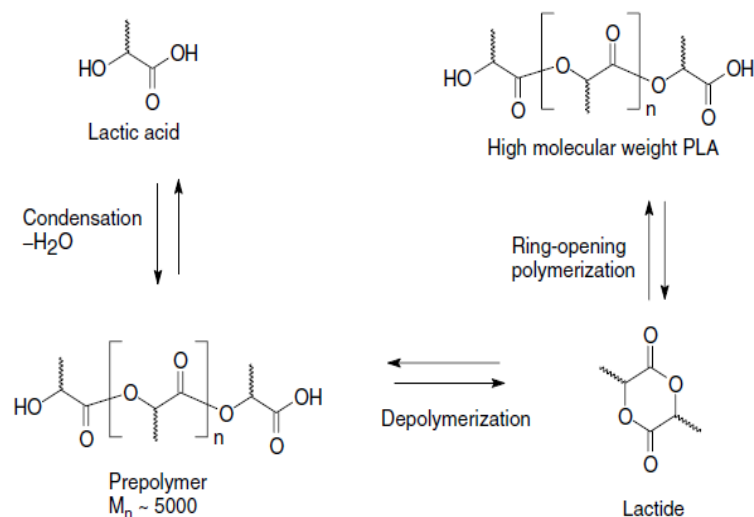


Figure 2.1. Schematic of PLA production via pre-polymer and lactide (Henton et al. 2005)

2.2 General Structure of Layered Silicates (Phyllosilicates)

Clay minerals, for the most part, belong to the group of silicates having layered structures, and classified as phyllosilicates. Their crystal lattices are generated by a combination of tetrahedral and octahedral sheets. Each tetrahedron consists of a cation, Si^{4+} , Al^{3+} , or Fe^{3+} , coordinated to four O atoms, and linked to adjacent tetrahedral by sharing three corners to form an infinite two-dimensional 'hexagonal' mesh pattern (Figure 2.2-a). In the octahedral sheet, connections between each octahedron to neighboring octahedral are made by sharing edges. The edge-shared octahedral form sheets of hexagonal or pseudo-hexagonal symmetry (Figure 2.2-b). Octahedral cations are usually Al^{3+} , Fe^{3+} , Mg^{2+} , or Fe^{2+} .

Phyllosilicates can be classified in two groups according to their layer structure. The 1:1 layer structure consists of the repetition of one tetrahedral and one octahedral sheet, while in the 2:1 layer structure one octahedral sheet is sandwiched between two tetrahedral sheets. In the 1:1 phyllosilicates each layer is about 0.7 nm thick. One surface of the layer consists entirely of basal oxygen atoms belonging to the tetrahedral sheet, while the other surface is composed of mostly OH groups from the octahedral sheet. In the 2:1 structure, the tetrahedral sheets are inverted and two-thirds of the octahedral hydroxyl groups are replaced by tetrahedral apical oxygen atoms (Brigatti, Galan and Theng 2006).

Cation exchange capacity (CEC) is a measure of the ability of a mineral to hold positively charged ions. This capacity is believed to be largely by broken bonds around the edge of silica – alumina units, isomorphic substitution in the clay structure and in some cases replacement of the hydrogen of exposed hydroxyls as in case of Halloysite (HNT) minerals.

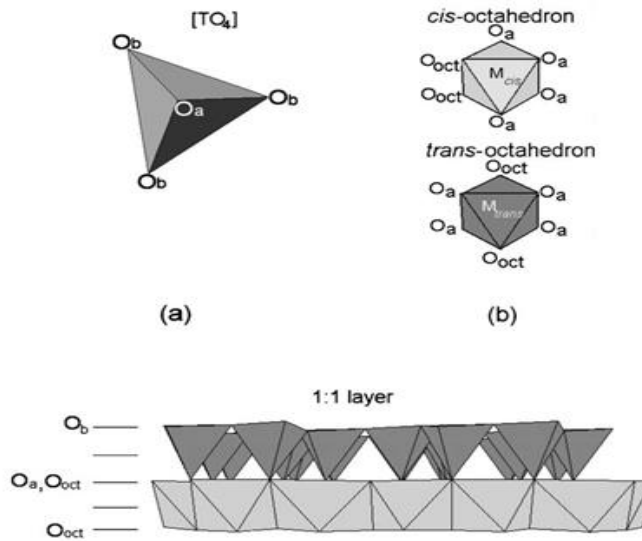


Figure 2.2. (a) Tetrahedron; (b) O_{oct} (OH, F, Cl) orientation in cis-octahedron and trans-octahedron (O_a and O_b refer to apical and basal oxygen atoms) (Brigatti et al. 2006)

2.3 Di-octahedral 1:1 Minerals: The Kaolin Group

The primary structural unit of this group is a layer composed of one octahedral sheet condensed with one tetrahedral sheet. According to the number of octahedral sites occupied in a unit cell, this group can be divided into two: tri-octahedral (six sites) and di-octahedral (four sites). Di-octahedral minerals include kaolinite, Dickite, Nacrite, and Halloysite (HNT), which consist of the octahedral and tetrahedral sites occupied by aluminum and silica respectively. The formation of kaolinite group is mainly by hydrothermal alteration or weathering of feldspars under acid conditions. Halloysite is a member of this group formed in soils.

2.3.1 Identification of Halloysite

As a naturally occurring alumina silicate Halloysite (HNT), $\text{Al}_2\text{Si}_2\text{O}_5(\text{OH})_4 \cdot n\text{H}_2\text{O}$, exhibits unique surface chemical property due to the multi-layered structure with hydroxyl groups on its surface. It is chemically similar to kaolinite, dickite or nacrite, but differing mainly in the morphology of crystals and unit layers that are separated by a monolayer of water molecules (Churchman and Carr 1975).

Owing to absence of isomorphic substitution in either octahedron or tetrahedron sheet; cations or anions cannot occupy the space between the layers and they are held together by hydrogen bonding between hydroxyl groups in the octahedral sheets and oxygen in the tetrahedral sheets of the adjacent layers. The cation exchange capacity (CEC) of HNT depends on the amount of hydration, as $2\text{H}_2\text{O}$ has 5–10 m.e./100 g, while $4\text{H}_2\text{O}$ has 40–50 m.e./100 g (Carroll 1959).

The HNT particle can adopt a variety of morphologies, but the most common form is an elongated hollow tubular structure with a large aspect ratio similar to that of carbon nanotubes (CNT). Tubular structure results from the wrapping of the clay layers around onto themselves to form hollow cylinders under favorable geological conditions. The curling process is driven by reduction of the inherent strain in the structure with the intercalation of water between layers and by the mismatch in the periodicity between oxygen sharing tetrahedral silica sheets and adjacent octahedral aluminum sheets. The HNT external surface is composed of siloxane (Si-O-Si) groups, whereas the inner side and edges of the tubes consists of (Al-OH) groups (Churchman and Carr 1975, Yuan et al. 2008). The schematic representations of the crystalline structure of HNT (10Å) and the structure of a single tubular HNT particle are shown in Figure 2.3 (Yuan et al. 2008).

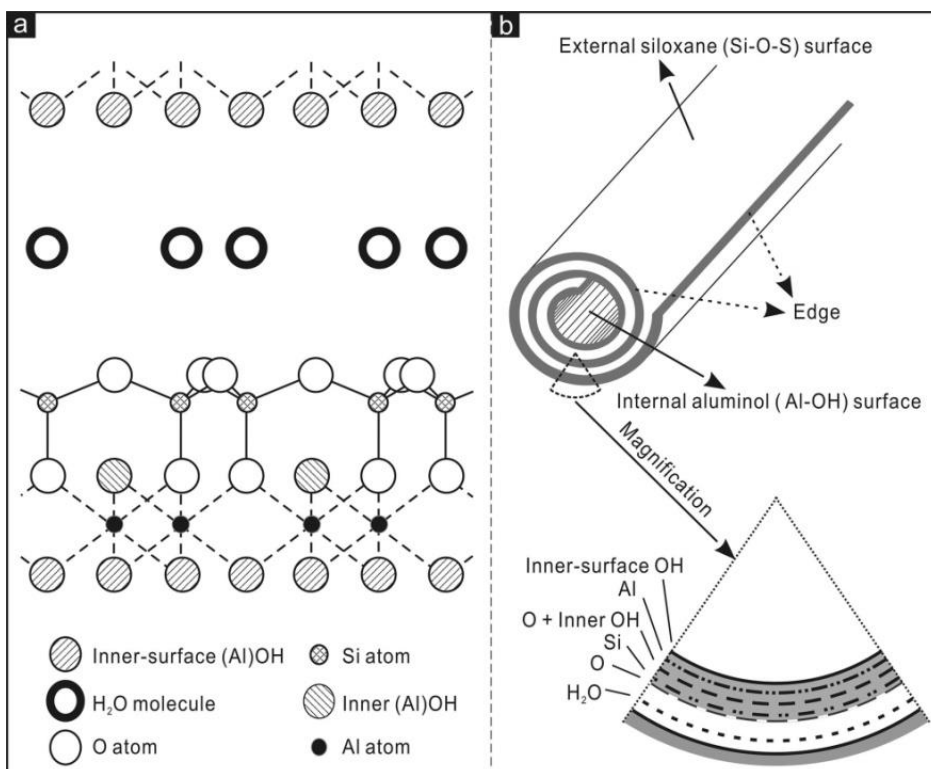


Figure 2.3. Schematic diagrams of (a) the crystalline structure of HNT (10 Å); (b) the structure of the nanotube (Yuan et al. 2008)

The peculiar structure and morphological features of HNTs depend on the fact that they contain water (hydrated HNT/Endellite) or have contained water in their interlayer (dehydrated HNT/Meta-Halloysite). Hydrated Halloysite has a basal spacing of 10 Å, which is ~3 Å (thickness of water monolayer) larger than that of kaolinite or dehydrated HNT. The interlayer water is weakly held, so that 10 Å spacing can readily be decreased to 7 Å by drying. This form of HNT possesses some problems of identification since its XRD pattern resembles that of many kaolinites, with which it is commonly admixed.

According to the study of Brindley (Brindley and Goodyear 1948), at each stage of the dehydration process the basal plane 001 peaks in the XRD patterns of the HNT appear in either or both of two narrow regions of the spectrum (9.5-10.1 Å and 7.5-7.9 Å). These regions describe the hydrated and dehydrated states of the HNT respectively. Thus, it can be said that there are no forms of HNT intermediate between those states. However, the interlayer water cannot be totally removed and dehydration process retains a certain amount of residual water between the silicate layers.

2.3.2 Differentiation of Halloysite from Other Kaolin Minerals

It is hard to differentiate HNT (7Å) from kaolinite minerals based on their XRD patterns. But, patterns that possess broader peaks (>0.3 2θ) and larger basal spacing (>7.15 Å), as well as relatively intense non-basal peaks (peaks ~ 3.57 Å) strongly point the presence of HNT (Hillier and Ryan 2002) and confidently assign the lower crystallinity of HNT than kaolinite (Churchman and Carr 1975).

The widespread use of ethylene glycol solvation in clay mineral studies makes it a particularly useful and simple test to determine the presence of HNT. The presence of interlayer water is central to the definition of HNT and appears to be a prerequisite for the intercalation of ethylene glycol. The response to ethylene glycol solvation involves a decrease in intensity of the 7.2 Å reflection peak but an increase in the intensity of the peak at 3.58 Å and is related to an interstratification effect (Macewan 1946). Hillier (Hillier and Ryan 2002) aims to reaffirm MacEwan's observations regarding HNT. They observed that 7.2 Å / 3.58 Å peak height intensity ratio was reversed with ethylene glycol treatment while kaolinite showed no obvious changes in peak intensities. It seems that ethylene glycol only replaces the partial water layer in HNT (7 Å). However, this does not result in the opening of basal spacing at least not to a noticeable extent;

just a complex is formed by the partial reaction between HNT and ethylene glycol (Brigatti et al. 2006). On the other hand, the fully hydrated 10 Å form of HNT can form a one layer complex with ethylene glycol with a resultant spacing of ~10.9 Å (Hillier and Ryan 2002).

Many investigations have been accomplished to show the different behavior of HNT towards certain other organic compounds compared to other kaolin minerals. One of them claim that clay minerals of the kaolin group can be expanded to approximately 14 Å along the c-axis by grinding or soaking in potassium acetate (KOAc). After KOAc is washed out, kaolinite returns to its characteristic 7 Å spacing, whereas wet HNT contracts to about 10 Å (Ray and Bousmina 2005).

The other method that may distinguish HNT from disordered kaolinite is a test of reaction to formamide. The response within 30 minutes is indicative of HNT, while kaolinite reacts more slowly in a period of hours or days or weeks.

2.4 Functionalization of Halloysite Nanotubes with Organo-silanes

Large diameter of the HNT lumen and hydroxyl groups on outer surface available for functionalization makes it potentially suitable for the accommodation of a range of guests. Functionalization of clays has been explored as a way to improve clay dispersion in a polymer matrix, thus increasing the mechanical properties of resultant polymer-clay nanocomposites. Organo-silane coupling agents have a great affinity to react with the Al – OH groups on the edge and Si – O groups on the surface of HNT. Although, it is hard to achieve an interaction between the interlayer Al – OH groups and silane, insertion of polymer matrix between the

clay layers may be achieved by organo-silane treatment of HNT. A possible interaction mechanism between HNT and organo-silanes is given in Figure 2.4.

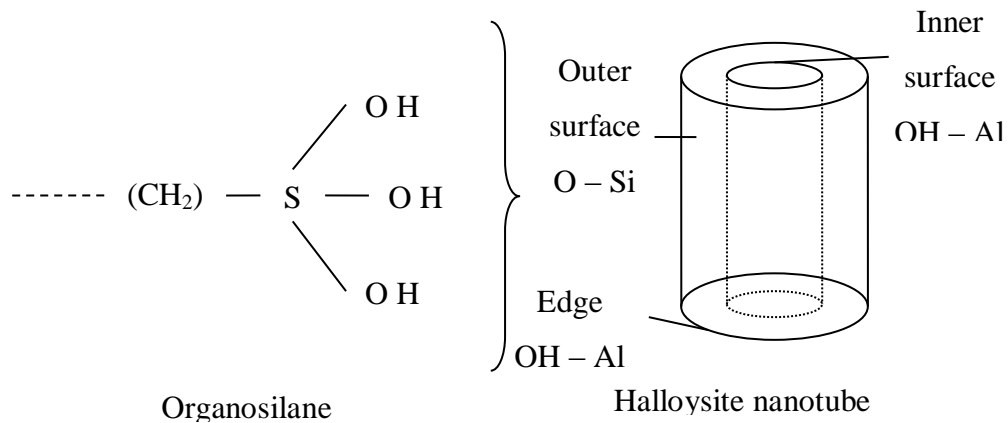


Figure 2.4. Possible interaction mechanism between Halloysite nanotubes and organo-silanes

2.5 Polymer-Layered Silicate (Phyllosilicate) Nanocomposites and Structure Types

In order to improve the stiffness and the toughness of the polymers, they are filled with particles. In this combination, each material retains its identity. According to the definition of International Union of Pure and Applied Chemistry “composite materials in which at least one of the phases has at least one dimension of the order of nanometers” are called nanocomposites (Chen B. 2008). There are various applications for these due to their transparency, low density, reduced

flammability, low permeability, and enhanced thermal and mechanical properties (Zanetti 2000).

Among all the potential nanocomposites, those based on clay and layered silicates attract attention because they are produced easily and their intercalation chemistry has been studied for a long time (Theng 1974, Ogawa 1997).

Polymer-layered silicate nanocomposites have several advantages owing to their nanometer size particle distribution. First of all, they are lighter in weight compared to conventional composites. Also, their mechanical properties are relatively superior to unidirectional fiber reinforced polymers, because reinforcement from the inorganic layers will occur in two, rather than in one dimension. In addition, their fabrication techniques which are much easier and cheaper than the fabrication of conventional composites make polymer-layered silicate nanocomposites preferable.

Nanocomposite formation is achieved only if the desired structure is obtained. The structure mainly depends on components used, synthesizing methods, strength of the interfacial interactions and the clay loading. Hence, it is not always possible to achieve a nanocomposite when a nano-filler is mixed with polymer matrix. In order to obtain a nanocomposite, the dispersion of the clay platelets should be in nanometer range (Mark and Kroschwitz 2003, Ray and Okamoto 2003). For layered silicate nanocomposite formation, the clay layers should be completely pushed apart to create a disordered array and they should be uniformly dispersed to form exfoliated or delaminated structure. Or, at least the polymer chains should be inserted between the silicate layers, while the stacking order remains the same as in micro composites. This type of structure is called intercalated structure. If polymer and clay are incompatible, the clay platelets remain as large stacks and no polymer chain get inserted between the layers. This types of composites are called conventional composites, and they display poor physical properties (Dennis et al. 2001).

2.6 Biopolymer Poly(lactic acid) Nanocomposites

Biodegradable polymers have great commercial potential, but some of the properties, such as brittleness, low heat distortion temperature, high gas permeability, low melt viscosity for further processing etc. restrict their use in a wide-range of applications. Therefore, modification of them through innovative technology has been the subject of research (Ray and Bousmina 2005).

PLA exhibits flexural properties, impact strength and processability that are not suitable for a number of end-use applications. Recently, the utility of inorganic nanoparticles as additives to enhance the performance of PLA has been established. Various nano-reinforcements currently being developed for PLA are nanoclays (Paul et al. 2005, Ozkoc and Kemalolu 2009), cellulose nanowhiskers (Mohanty, Drzal and Misra 2003), and carbon nanotubes (Hapuarachchi and Peijs 2010).

Carbon nanotube (CNT) based polymer composites exhibit exceptional mechanical, thermal and electrical properties. However, extremely high cost and the difficulties in preparation of CNT and its nanocomposites have been a challenge. Particular interest was devoted to composites of polymers and HNT particles owing to the unique crystal structure of HNT resembling CNT. Therefore, HNT particles may have the potential to replace the expensive CNT because of their tubular structure in nano-scale and also due to their similarity to the other layered clay minerals, such as montmorillonite, having the possibility to be further intercalated chemically or physically (Deng et al. 2008).

Unlike CNT, which always have an entangled structure, these nanotubes are straight with no entanglement, which makes HNT dispersion in viscous polymer matrix easier compared with CNT. Also, HNT has the same geometry as multi wall carbon nanotube (MWCNT), but it has an advantage in comparison to CNT, since HNT does not stick to the matrix (Ye et al. 2007). Owing to its crystal

structure, it is nearly impossible to exfoliate the HNT particles in polymer matrix. Also, due to the small basal spacing, the intercalation of HNT by polymers and additives is hard to achieve and needs to be improved.

2.7 Nanocomposite Synthesis Methods

In order to prepare polymer-layered silicate nanocomposites, there are several methods. All of these methods yield a fine dispersion of the nano-filler in the matrix depending on the type of the constituents. Although these methods can be categorized into four groups, they can be modified and combined to increase the effectiveness of the nanocomposite preparation method.

2.7.1 In-situ Polymerization

This method is known to be the first method used in the preparation of polymer-clay nanocomposites. It has been used by the Toyota Researchers for polyamide-6 based nanocomposites (Usuki et al. 1995). In this method, polymer-clay nanocomposite is synthesized by the insertion of a monomer into host compound (layered silicates, either natural or modified) containing inter-planar spaces (channels or other cavities) followed by the polymerization of the monomer. The polymer obtained is called intercalated if confined between layers (Zanetti, Lomakin and Camino 2000).

The second stage of the in-situ method, polymerization, requires an initiator. This initiator can be heat, radiation, diffusion of an organic initiator or a catalyst. The driving force for in-situ polymerization method is the polarity of monomer

molecules. Owing to the high energy surface, the polar molecules are attracted to clay surface that causes them to diffuse between the gallery spaces of clay minerals. After this step, the polymerization reaction starts and overall polarity of intercalated molecules is lowered. Finally, the clay layers are delaminated by the organic molecules.

This nanocomposite preparation method results in remarkable improvements in the physical properties. However, the limited capacity due to complex process restricts its usage. Also, the presence of additives in the system results in complicated reactions, that makes the materials complicated in large scales.

2.7.2 Solution Intercalation Method

In this technique, a polymer dissolved in a solvent is added to the solvated clay and let to intercalate between the disperse layers. It is known that, layered silicates can be easily dispersed in an adequate solvent owing to the weak forces that stack the layers together (Alexandre and Dubois 2000). After waiting for the adsorption of polymer onto the dispersed sheets, the solvent is evaporated in the next step of the process. Fortunately, the layers do not collapse back after this step and resemble sandwiching the polymer to form an ordered multilayer structure.

In this method, entropy is the driving force. Entropy is gained by the desertion of the solvent molecules and balanced by the decrease in conformational entropy due to intercalation of polymer chains. Hence, large number of solvent molecules must be desorbed from the clay to accommodate the incoming polymer chains (Kornmann, Lindberg and Berglund 2001). The suitability of this method to polymers with no or little polarity attracts attention. However, the use of large amounts of inorganic solvents that is environmentally unfriendly and economically prohibitive is one of the major drawbacks

2.7.3 Melt Intercalation Method

This method is the most commonly preferred nanocomposite preparation method due to its simple and environmental friendly process. It is broadly applied to many commodity and engineering polymers, from non-polar polystyrene, polyolefin, weakly polar PET to strongly polar polyamide. In this method, nanocomposites are obtained by direct polymer melt intercalation, where molten polymer chains diffuse into the space between the clay layers (Vaia, Ishii and Giannelis 1993, Vaia et al. 1995). The main difference between this method and other preparation methods is that strong shear forces act on the system and no solvent is required.

The possible clay delamination pathway can be seen from Figure 2.5. By the help of shear stress, clay stacks are decreased in height by sliding platelets apart from each other. After the insertion of polymer chains between the layers, the ends of the platelets are pushed apart to become delaminated. The most important factor in this method is the diffusion of polymer chains between the clay layers, that is driven by physical or chemical interactions. Residence time in extruder facilitates the diffusion, and as more polymer enters between the layers they appear to peel apart, especially, near the edge of clay galleries (Dennis et al. 2001).

The process is accomplished above the melting temperature of the polymer matrix in either static or flow conditions in order to complete the diffusion of macromolecules into the interlayer spaces. If layer surfaces are sufficiently compatible with the polymer, and melt processing conditions are optimized, formation of intercalated and/or exfoliated nanocomposite can be achieved according to the degree of penetration.

In addition to the shear forces, matrix viscosity and the mean residence time also affect the degree of the dispersion. But, the most important parameter in clay delamination is the chemical compatibility between the polymer matrix and the

filler. Hence, it was reported that clay treatment plays the dominating role for final morphology of nanocomposites (Cho and Paul 2001, Dennis et al. 2001).

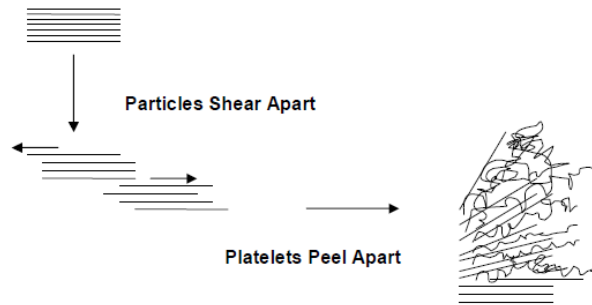


Figure 2.5. Effect of shear on clay platelets (Dennis et al. 2001)

2.8 Polymer Blending and Plasticization

Combinations of two or more polymers at different chemical compositions are called polymer blends, and they combine the performance and economic advantages of each constituent (Keskkula and Paul 1996). In addition to many advantages related to their physical properties, they also offer benefits for manufacturers such as improved processability.

The properties of the blends mainly depend on the equilibrium interphase, interfacial behavior, physical and chemical interactions, phase morphology, etc. However, the most important factor that affects the properties of blends is the miscibility between the components. Miscible blends are almost similar to random co-polymers, and the mechanical properties follow nearly linear relations

with composition. However, for partially miscible blends the components form separate phases and the properties depend on the arrangement of these phases and the nature of the interface (Utracki 2002, Ting, Pearce and Kwei 1980). Properties like stiffness, strength, transition temperatures and softening temperature are dominated by the properties of the component with higher fraction which forms the continuous phase in the blend. The distribution of the dispersed phase, component with low fraction, affects the failure properties, especially those related to ductility. For instance, dimensions of the dispersed phase domains and their shape have a great effect on impact properties.

The most commonly used way of polymer blending is performed for improving the impact strength of resins which are highly brittle at room temperature. The polymers used for the purpose of impact modification are elastomeric materials. Their incorporation into rigid polymer matrix causes the formation of a dispersed elastomeric phase which increases the toughness of the rigid polymer. The dispersed phase arranges in the continuous rigid polymer in nearly spherical drops. As the concentration of dispersed phase increases, the morphology development during the melt mixing comprise processes, such as drops stretching into threads and breakup of these threads into smaller droplets, then finally coalescence of the droplets into larger ones due to cohesive forces between domains and interfacial mobility of the dispersed phase (Akkapeddi et al. 2001).

In this study, TPU elastomeric material was used to increase the toughness of the rigid PLA. Also, it was aimed to use TPU as a compatibilizer between PLA and the filler Halloysite nanotubes (HNT).

Another method used to increase the toughness of the rigid polymers is plasticization by the addition of small molecules or low molecular weight polymers. However, at present there is no way to characterize absolutely the behavior of a plasticizer in terms of some fundamental property, because the behavior of the plasticizer is tied up with the polymer to which it is inserted into and also the previous history of the polymer (Immergut and Mark 1965)

But, in general, plasticizers change both thermal and mechanical properties of the main matrix by;

- lowering the rigidity at room temperature,
- increasing the elongation at break at room temperature,
- increasing the impact strength,
- shifting both α and β relaxation peaks to lower temperatures.

2.9 Polymer Processing

Continuous manufacture of a product from polymeric materials; plastics, elastomers and composites, can be performed by a wide variety of distinct methods. Selection of a process depends on many factors including the capacity of the production, dimensional accuracy and surface finish, form and detail of the product, type of material and size of the final product. In general, all methods are formed by three phases which are heating, shaping and cooling (Strong 2000).

According to their functions polymer processing techniques can be categorized in different groups. The first group involves the continuous manufacture of uniform cross-section products. Extrusion, extrusion covering, film blowing and calendaring belong to this group. The techniques involving the shaping of a deformable polymer are performed against a mold surface. Coating, rotational molding and sintering techniques are in this group. The final group involves the filling of a mold cavity and composed of casting, compression molding, transfer molding, injection molding and reaction injection molding. For the preparation of composite samples, extrusion and injection molding techniques are used in this study.

2.9.1 Extrusion

Extrusion is the act of pushing and squeezing out polymer melt by applying pressure. This type of process is used to produce products in the form of profiles, sheets, films and plastic granules that are used by all the other plastics manufacturing processes. Extrusion is also used for composite preparation in which plastic resins are melted to add fillers, colorants, and other additives into the molten plastics (Rauwendaal 1990).

Extruders permit multiple processes in a single machine; melting, mixing, metering, venting etc. In the first step of the extrusion, plastics granules or pellets and any other materials are fed into a hopper attached to the extruder. Then, the materials are passed through the melting zone and finally the die imparts a shape to the molten plastic stream which is immediately cooled. Extruder dies can have complex shapes as shown in Figure 2.6 to compensate for die swell, distribute material across the width of a sheet or coat a wire (Schey 1987).

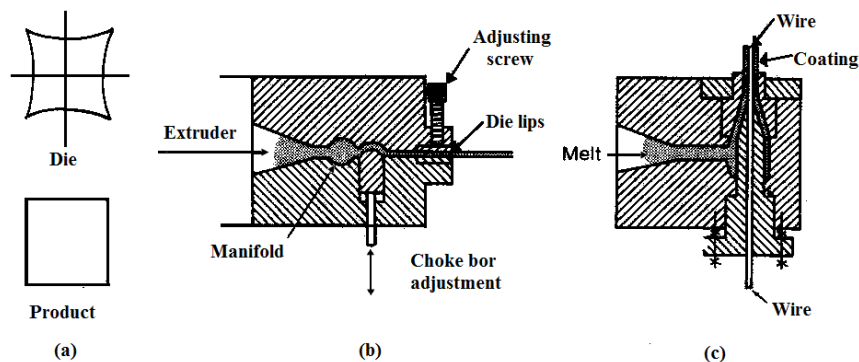


Figure 2.6. Complex die shapes; (a) Compensate die swell, (b) Sheet coating, (c) Wire coating (Schey 1987)

There are three main extruder types: screw extruders, ram extruders and drum or disk extruders. In the extrusion process in screw extruders, the polymer and additives are fed to the cavity between screw and extruder barrel from the hopper. This section is zoned into parts which are individually heated and cooled depending on the material and process parameters. Screws turning inside the extruder barrel convey the plastic forward into a heated region of the barrel where the combination of external heating and heating from viscous dissipation melts the plastic. Then, the molten polymer is transmitted to the die section to form the basic shape of the desired product (Fisher 1976).

The most important components of an extruder are their screws. Screws of an extruder directly affect the performance of the machine. The main functions of screws are conveying the plastic granules, melting the material, conveying the molten material, and mixing the plastic melt to obtain homogeneity. Continuous screw extruders can be classified in two main groups: single screw and multiple screw extruders. Twin screw extruders belong to multiple screw extruders and are mostly preferred in composite preparations.

Twin screw extruders offer many advantages to the modern processor. They are widely employed for difficult compounding applications, de-volatilization, chemical reaction, and profile extrusion of thermally sensitive materials. Some of their advantages are good mixing, good heat transfer rate, good control over stock temperatures and large melting capacity. Their more positive pumping action compared to single screw extruders is also an attractive way of twin screw extruders. Material transport in single screw extruder occurs by frictional drag in solid conveying zone and by viscous drag in the melt conveying zone. On the other hand, the transport in an intermeshing twin screw extruder is a positive displacement type of transport (Rauwendaal 1990). There are several design variables for twin screw extruders such as the meshing type of the screws, screw rotation directions. Figure 2.7 shows a drawing of intermeshing twin-screw extruder. Intermeshing screws can be employed in a co-rotating or counter-

rotating pattern. Co-rotating pattern extruders support high contact with the barrel and improve the efficiency of heating and mixing. In the counter-rotating patterns, pumping is more efficient when compared to co-rotating screw systems. However, total shear applied to the material is low in these systems and makes co-rotating screw pattern more preferential for composite preparations.

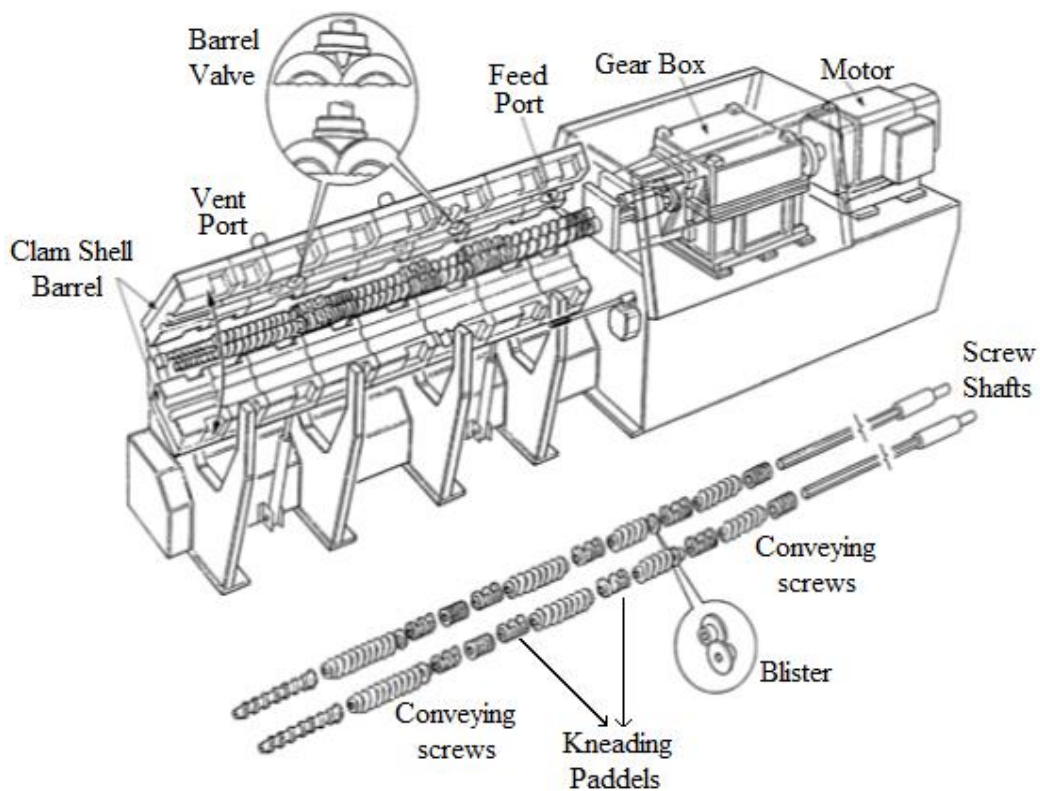


Figure 2.7. Intermeshing twin screw extruder (Keskkula and Paul 1996)

2.9.2 Injection Molding

Injection molding is the most commonly used manufacturing process for the production of discrete parts that can have complex and variable cross sections as well as a range of surface textures and characteristics (Strong 2000). The cycling injection molding process is composed of three steps: filling, packing and cooling. In the first stage, molten polymer is pushed through a nozzle to a cooled cavity of a closed mold. This stage gives the shape of the plastic and consists of the first two steps, filling and packing. During the filling step, the pressure exerted on the polymer melt by screw section is kept constant, whereas in the packing step the pressure builds up. In the final stage, sufficient time is allowed for the plastic to solidify. This step is called as cooling, and the pressure is maintained high to minimize shrinkage and shape changes (Middleman 1977). The temperature control system of the injection unit is used to control the temperature of the melt. It should be maintained above the T_m of the polymer to provide effective filling and packing steps. The temperature is kept below T_g and T_m in the cooling step, then the opening of the mold is followed by part ejection.

2.10 Chain Extension Mechanism

To gain their optimum mechanical and processing properties, thermoplastic polymers must have a good balance of backbone structure. The backbone structure depends on the monomers and or pre-polymers, but can be modified with chemical species named as chain extenders.

Chain extension is a mechanism where di- or poly-functional low molecular weight material is reacted with the carboxyl and/or hydroxyl end groups of the

polymeric material to rejoin the broken chains that result from the chain scission during melt processing. To recover the drop of intrinsic viscosity and reduced molecular weight, chain extension by reactive extrusion process is an attractive choice compared to other methods used for the enhancement of these properties, such as solid state polymerization (SSP). Owing to the low polymerization temperature, low diffusion rate of the condensation water out of the pellets and low mobility of end groups in the solid state, the required residence time in the SSP process is long.

Degradation upon thermal processing owing to several undesirable reactions is a problem that comes up during the processing of PLA. Some of these reactions are hydrolysis, inter-chain trans-esterification, and intra-molecular trans-esterification. The water based hydrolysis degradation mechanism of PLA results in a chain split into two sub-chains. The molecular weight reduction of polyesters is primarily caused by the hydrolysis of the ester linkage, randomly taking place in the polymer. The inter-molecular trans-esterification affects the sequence of different polymeric segments, whereas intra-molecular trans-esterification leads to polymer degradation and the formation of cyclic polylactide oligomers. At a certain level, the de-polymerization of PLA can cause a change in physical, mechanical and thermal properties. Thus, in order to increase the usability of PLA, its molecular weight must be maintained or increased during compounding, injection molding or extrusion with the aid of chain extension reactions.

Poly(lactic acid) synthesized by direct melt poly-condensation has reactive functional groups, such as hydroxyl and carboxyl, and its reduced molecular weight, intrinsic viscosity and other physical properties can be improved through chain extension in the melt using existing melt reactors, or single or twin screw extruders (Pilla et al. 2009). Modification of PLA through chain extension directly amplifies the shear intensity. However, as the chain extender content is raised the shear intensity decreases owing to reduced polar interactions from neat to highly chain extended PLA (Corre et al. 2011).

2.11 Carbon Nanotubes (CNT)

Carbon Nanotubes can be said to be at the intersection of carbon fibers and fullerene (Ebbesen 1997). Their unique structure and electronic properties makes them attractive for nanocomposites preparation. They can be classified in two types: single wall carbon nanotubes (SWCNT) and multiwall carbon nanotubes (MWCNT) as can be seen from Figure 2.8. MWCNTs were discovered earlier than SWCNTs and they are composed of 2 to 30 concentric graphitic layers in diameters from 10 to 50 nm with an aspect ratio more than 1000. On the other side, SWCNTs have much thinner diameters that range from 1 to 1.4 nm. The length of nanotubes can be up to centimeters, giving them an astonishing aspect ratio (length/diameter ratio) of 10^7 (Xanthos 2005).

CNTs are made up of rolling graphene sheet into a cylinder. However, rolling up graphene is not the actually only way in which a nanotube forms. Their synthesis techniques have evolved considerably in the last years giving them potential to be used in electronic circuits (Yao, Kane and Dekker 2000), composites, thin films (Huang et al. 2004), hydrogen storage etc.

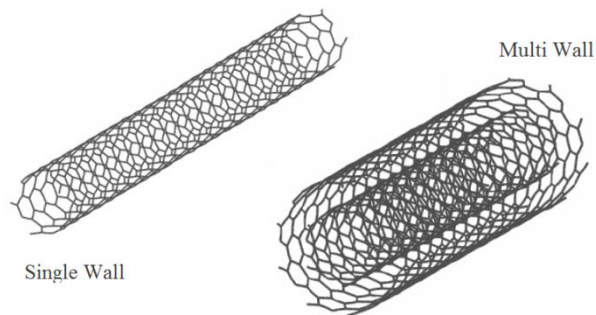


Figure 2.8. Single and multiwall carbon nanotubes

2.12 Composite Characterization Techniques

To understand the properties of the newly developed materials and the applications that the materials can be used for, some characterization techniques are required. These techniques may be mechanical, morphological or thermal.

2.12.1 Mechanical Analysis

Among the physical and chemical properties of composite materials, the most important ones are mechanical properties. Strength, hardness, ductility and stiffness are some of the important mechanical properties and can be analyzed by using standardized testing techniques. Establishment and publication of these standards are often coordinated by professional societies. In the United States, the most active organization is the American Society for Testing and Materials. In this study, mechanical analyses of the samples were performed by tensile and impact tests.

2.12.1.1 Tensile Test

In tensile tests, the force required to fracture a specimen and the extent to which it elongates are measured. The load is applied with a gradual increase and uniaxially along the axis of the specimen. A standard dog-bone shape sample and testing machine can be seen in Figure 2.9. As can be seen from the figure the ends of the specimen are clamped into the jaws of the testing machine. As the jaws are separated by the application of the force, the specimen elongates and finally breaks when the load is higher than the force that the specimen can resist.

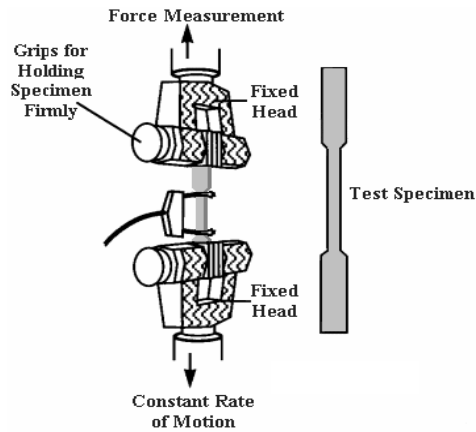


Figure 2.9. Standard dog-bone shape sample and tensile testing machine (Seymour 1996)

As a result of tensile test, an instantaneous load F (N) versus elongation (mm) chart is obtained. Load and elongation values are converted into stress σ (MPa) and strain ε (mm/mm) by using the initial gauge length of the specimen. The calculations can be seen from Equation 2.1, where, F : Applied force, A_0 : Initial cross section, L_0 : Initial length, L_i : Final length.

$$\sigma = \frac{F}{A_0}$$

$$\varepsilon = \frac{L_i - L_0}{L_0}$$

Equation 2.1

Figure 2.10 shows the stress – strain curve of a typical polymeric material. Tensile strength, σ_m , is the maximum tensile stress sustained by the specimen during the tension test. Young’s modulus (modulus of elasticity) is the ratio of stress (nominal) to corresponding strain below the proportional limit of the material.

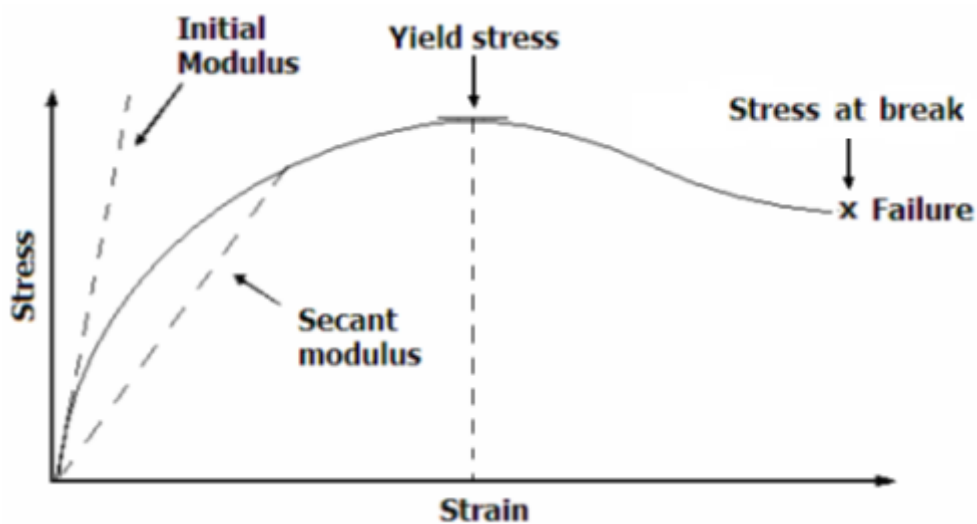


Figure 2.10. Stress-strain curve of a typical polymeric material

2.12.1.2 Impact Test

The ability of a component to withstand a sudden impact is an important issue. To measure this ability impact tests are used. They exactly measure the energy required (absorbed) for failure upon a rapid stress loading onto the standard specimen (Seymour 1996). This absorbed energy is a measure of the toughness of the material and used to study the temperature dependent ductile/brittle transition.

In this high strain rate test, a number of techniques can be employed to measure the impact strength of a polymer. In the izod and charpy impact tests a pendulum with hammer like weight strikes a specimen, and the energy required to break the specimen is determined from the loss in kinetic energy of the weight. Figure 2.11 shows a schematic of how to perform izod and charpy impact tests. In charpy test, the specimen is held parallel to the surface by fixing the specimen at each end. The hammer used in the charpy test has one or two knife edges, which gives a three or four-point impulsive bending. In the izod test, the specimen is fastened vertical to the surface and held at one end while holding the striker at the other end (Bower 2002).

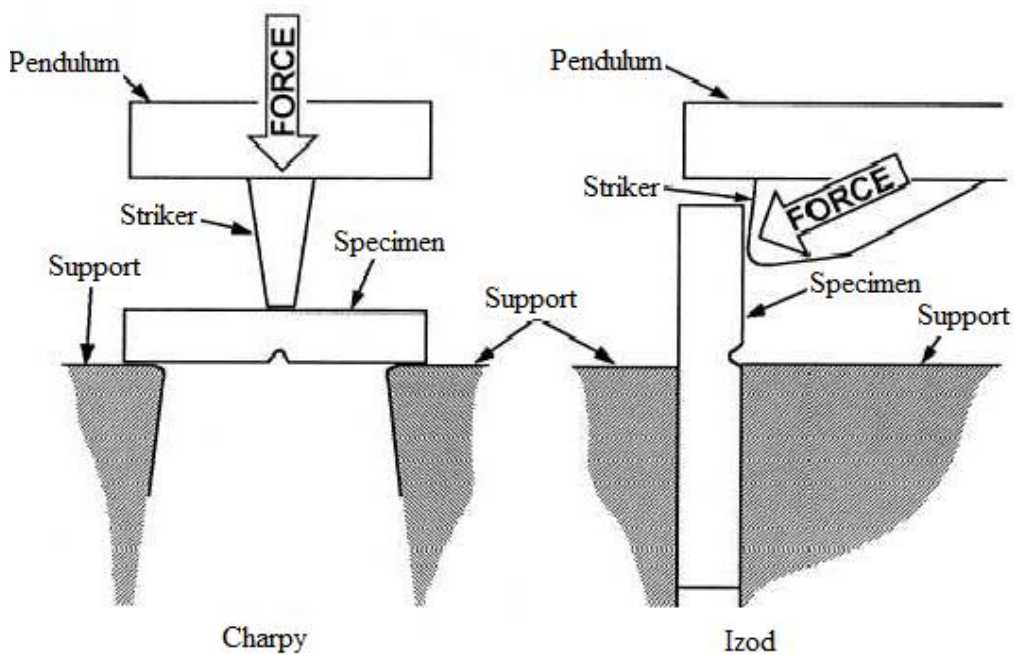


Figure 2.11. Performing impact test

2.12.1.3 Dynamic Mechanical Analysis (DMA)

In dynamic mechanical analysis, material properties are characterized as a function of temperature, time, frequency, stress, atmosphere or a combination of these parameters. The deformation is applied to the sample in a cyclic manner to obtain information about the relaxation behavior of the test piece and stress-strain relation is monitored while changing the temperature. There are various loading options for this mechanical testing method, such as, reversed bending, axial tension, torsion and shear. In this study, a tension mode was used to analyze the PLA composites.

Dynamic mechanical analysis is one of the best options to understand the viscoelastic nature of polymeric materials. The viscoelastic nature has two components; dynamic and elastic. The first one is controlled by the viscous component. In this sense, strain continues to increase until the stress is removed and is not recoverable. The elastic component reacts instantaneously to the applied stress and is completely recovered if the stress is removed.

During the tests, vibration applied to the sample is generally sinusoidal, and this sinusoidal load gives rise to a sinusoidal deformation as can be seen from Figure 2.12. For ideal elastic materials, a sinusoidal stress proportional to the strain amplitude is produced, and it is in-phase with sinusoidal stress. But, for ideal viscous materials, the stress and strain are out of phase by 90° . For viscoelastic materials like polymers, there is a phase shift (δ) between 0 and 90° depending on the elastic/viscous characteristic of the material.

Complex variable, σ^* (complex stress), ε^* (complex strain) and E^* (complex modulus) can be used to analyze this phenomena. These variables can be described by Equation 2.2, where, σ^0 and ε^0 are stress and strain amplitude respectively, ω is the angular frequency of oscillation (rad/s) and t is time (s);

$$\begin{aligned}\varepsilon^* &= \varepsilon^0 \times e^{i\omega t} \\ \sigma^* &= \sigma^0 \times e^{i(\omega t + \delta)} \\ E^* &= \frac{\sigma^*}{\varepsilon^*} = \left(\frac{\sigma^0}{\varepsilon^0}\right) \times e^{i\delta} = \left(\frac{\sigma^0}{\varepsilon^0}\right) \times \cos \delta + \left(\frac{\sigma^0}{\varepsilon^0}\right) \times \sin \delta\end{aligned}$$

Equation 2.2

As can be seen from Equation 2.2, the complex modulus can be expressed in two components: in-phase component storage modulus (E') and out of phase component loss modulus (E''). Also, the ratio of energy dissipated to energy stored is calculated by dividing the E'' to E' values, which gives loss tangent (tan δ). These calculations can be followed from Equation 2.3.

$$\begin{aligned}E' &= \left(\frac{\sigma^0}{\varepsilon^0}\right) \times \cos \delta \\ E'' &= \left(\frac{\sigma^0}{\varepsilon^0}\right) \times \sin \delta \\ \tan \delta &= \frac{E''}{E'} = \frac{\sin \delta}{\cos \delta}\end{aligned}$$

Equation 2.3

Modulus values change with temperature and transitions in materials can be seen as changes in the E' or tan δ curves. This includes not only the glass transition and the melt, but also other transitions that occur in the glassy or rubbery plateau.

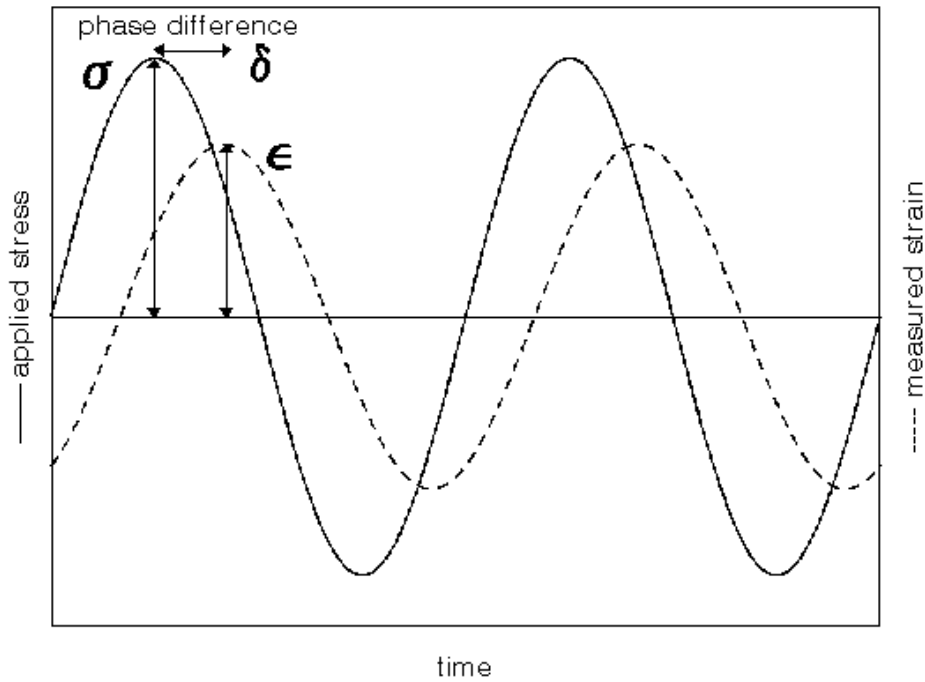


Figure 2.12. The relationship of the applied sinusoidal strain to stress for a typical polymeric material

2.12.2 X-Ray Diffraction Analysis (XRD)

This method is one of the oldest and most widely used techniques available to define the crystallographic structure, such as crystal lattice spacing, crystal size and perfection, the crystallinity and the degree of preferred orientation in polycrystalline samples. During the analysis a beam of x-rays impinges on a solid material and is partially absorbed while a portion of this beam is scattered in all directions by the electrons associated with each atom or ion that lies within path of the beam. These scattered beams interfere with each other and produce a diffraction pattern that varies with scattering angle (Kroschwitz 1990).

Figure 2.13 shows the diffraction from two scattering planes, due to two consecutive clay layers or other crystallographic planes of the layers that are separated by a distance d and intercept x-rays of wavelength λ at the incident angle θ . For a given set of lattice plane with an inter-plane distance of d (Å), the condition for a diffraction (peak) to occur can be simply written as Equation 2.4, which is the Bragg's law. In this thesis, XRD method was used to identify the nanocomposite structure by observing the position, shape, and intensity of basal reflections from the distributed silicate layers. In an exfoliated nanocomposite, the extensive layer separation associated with the delamination of the original silicate layers in the polymer matrix results in the disappearance X-ray peaks. On the other hand, for intercalated nanocomposites, the finite layer expansion associated with polymer intercalation results in the appearance of a new basal reflection corresponding to larger gallery height.

$$\lambda = 2 \times d \times \sin \theta$$

Equation 2.4

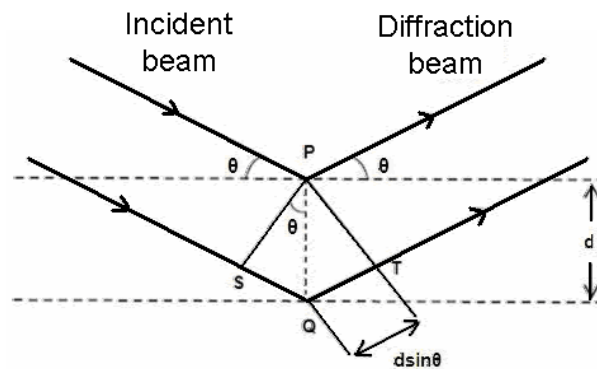


Figure 2.13. Diffraction of X-rays by planes of atoms (Kroschwitz 1990)

2.12.3 Scanning Electron Microscopy (SEM)

Scanning electron microscopy (SEM) is a method for high-resolution imaging of surfaces. It is preferred due to the great depth of focus, relatively simple image interpretation and ease of sample preparation. SEM uses electrons to form images contrary to light microscopes which use visible light. The large depth of field of SEM analysis allows a large amount of the sample to be in focus at one time and produces images of high resolution. Before the analysis, the surface of the specimen is coated with gold-platinum under vacuum to make the sample conductive (Callister 1997, Kroschwitz 1990).

During the analysis, the surface of a specimen to be examined is scanned with an electron beam and the resulting electrons emitted (back-scattered) from the sample are collected to form an image of the surface. The image on the screen, which may be photographed, represents the surface features of the specimen.

2.12.4 Transmission Electron Microscopy (TEM)

In this microscopy technique, a beam of electrons is focused onto a specimen causing an enlarged version to appear on a fluorescent screen or layer of photographic film. It is often used with thin materials (less than 100 nm thick) in which different regions within the sample absorb electrons differently. By the help of this method, objects on the order of a few angstroms (10^{-10} m) can be seen and details in the cell or different materials down to near atomic levels can be studied (Bower 2002).

The wavelength of electrons is dependent on their energy, and can be tuned by adjustment of accelerating fields. The electrons that travel through vacuum in the column of microscope are emitted by a light source at the top of the microscope.

In the TEM analysis, electromagnetic lenses are used to focus the elements into very thin beam, instead of glass lenses that focus the light in the microscope. The electron beam then travels through the specimen to be studied. Depending on the density of the material present, some of the electrons are scattered and disappear from the beam. At the bottom of the microscope, the un-scattered electrons hit a fluorescent screen, which gives rise to a shadow image of the specimen with its different parts displayed in varied darkness according to their density. The image can be studied directly by the operator or photographed with a camera.

2.12.5 Thermal Analysis

2.12.5.1 *Differential Scanning Calorimetry (DSC)*

Differential scanning calorimetry (DSC), is a technique of non-equilibrium calorimeter. It measures the difference in the amount of heat required to increase the temperature of a sample and reference as a function of temperature. Throughout the test, both sample and reference are maintained at nearly the same temperature. When the sample undergoes a phase transition or other physical transformations, depending on whether the process is endothermic or exothermic, heat flows to the sample compared to reference to balance the temperature. The difference of the heat flow between the sample and reference is sent to an output device which results in a plot of the differential heat flow as a function of temperature, which is called DSC curve.

Figure 2.14 shows different instruments for DSC analysis. According to the figure there are two types of instruments; 'heat flux' in which heat is transferred to the sample and reference through a disk made of the alloy and 'power compensation' instrument using separate heaters for the sample and reference (Billmeyer 1984).

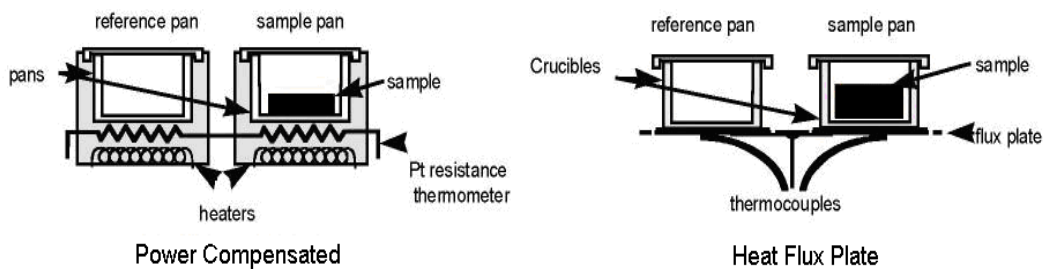


Figure 2.14. Differential scanning calorimeter instruments

As can be seen from Figure 2.15, a DSC curve clarifies three important points for polymeric materials; Glass transition temperature (T_g), crystallization temperature (T_c) and melting temperature (T_m). Glass transition is called a second order transition, whereas transitions like melting and crystallization, which do have latent heats, are called first order transitions.

Another important point that can be deduced from DSC curve is the crystalline fraction (%) of the polymeric material. It is calculated by using Equation 2.5, where, ΔH_m : Latent heat of melting (kJ/kg), ΔH_c : Latent heat of crystallization (kJ/kg), and ΔH^* : Latent heat of fusion of a 100% crystalline polymer (93 kJ/kg) (Latent heat of melting, ΔH_m , and latent heat of crystallization, ΔH_c , are determined from the area under the melting and crystallization peaks in the curve.);

$$\text{Crystalline Fraction (\%)} = \chi_c = \frac{|\Delta H_M - \Delta H_C|}{\Delta H^*} \times 100$$

Equation 2.5

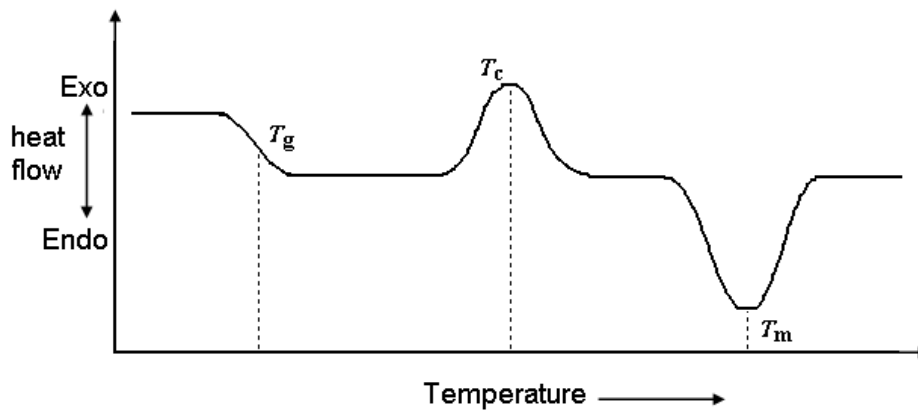


Figure 2.15. A typical DSC curve

2.12.5.2 Thermal Gravimetric Analysis (TGA)

In this analysis, the weight loss of a sample is measured as a function of temperature. There may be various reasons for weight loss, such as, drying or chemical reactions that release gases. This data gives the material weight as a function of increasing temperature, and this information can be used to characterize the materials exhibiting a weight change due to decomposition, oxidation, or dehydration (Billmeyer 1984). In this study, TGA was used to investigate the surface modification of HNT minerals.

In this method, the sample is located into an alumina pan and suspended from an analytical balance used to measure the weight loss. The balance is set to zero, and the sample cup is heated according to a predetermined thermal cycle. The balance transmits the weight signal to the computer for storage, along with the sample temperature and the elapsed time.

2.13 Previous Studies

Layered silicates are generally used with low or intermediate polarity polymers as reinforcing filler. There are a number of investigations based on layered silicate/PLA nanocomposites which mainly aim to form exfoliated distribution of clay layers. Improvement in material properties, such as storage modulus, flexural strength, flexural modulus, gas barrier property, and heat distortion temperature is a common observation both in the presence of modified or unmodified Montmorillonite (MMT) clays (Ray et al. 2002a, Ray et al. 2003b, Ray et al. 2003a, Pluta et al. 2002, Zhou and Xanthos 2008). Especially, organic modification of the clay surface results in better dispersion and hence better mechanical properties. XRD analysis of many investigations showed that the high affinity between organically modified clay and the PLA is sufficient to form an intercalated structure (Pluta et al. 2002, Ray et al. 2002b).

Various investigations also have been performed on PLA based nanocomposites reinforced with carbon nanotubes in terms of their tensile strength, thermo-mechanical properties (Krul et al. 2007, Chiu et al. 2008), electrical properties (Chiu et al. 2008, Wu et al. 2008), viscoelastic properties (Wu et al. 2008), crystallization behavior (Kim et al. 2010) etc. Results showed that adding CNT induces positive changes in the properties mentioned above. The concerns related to the cost and processability of the CNT, encourage researchers to find new alternatives. Halloysite is one of those alternatives with its promising properties.

Unlike the vast literature on MMT or CNT-based nanocomposites, HNT mineral inclusion to biodegradable PLA, which is the scope of this study, is relatively less investigated. Halloysite nanotubes cannot be exfoliated due to their tubular structure formed by wrapping of the clay layers. Also, enhancement of the basal spacing can hardly be achieved by insertion of polymer chains between the spacing of clay layers. Hence, modification of the HNT surface is essential (Liu et al. 2011, Zhang et al. 2010, Wan et al. 2009). Recently, three researches were

published on PLA/HNT nanocomposites prepared by melt blending. Two of the studies deal with the HNT minerals modified with quaternary ammonium salt. Also, one of them modifies the pre-modified mineral with organo-silane. Both studies reveal an enhancement in the tensile properties, thermal stability and impact properties of the composites (Prashantha et al. 2013, Murariu et al. 2012). The literature on the modification process of clay surface will be mentioned later. The other study is concerned with the improvement of the surface interaction between un-modified HNT and PLA by introducing maleic anhydride grafted PLA (Chow, Tham and Seow 2013).

Like various researches performed in the literature, the referred PLA/HNT nanocomposite studies mentioned hereby were carried out by “Melt Mixing” method. The other processing technique observed in literature for PLA/HNT nanocomposites is electrospinning (Touny et al. 2010, Qi et al. 2010). This method is used especially for fabricating continuous nano-fibers, from the viewpoint of drug delivery and tissue engineering applications. In the study performed by Touny (Touny et al. 2010), the PLA/HNT nanocomposite fibers produced by electrospinning technique were characterized by XRD and SEM analysis. The work investigating the optimum values for the electrospun process parameters revealed that 10% wt/v solution concentration and 10% wt/wt HNT content produces uniform fibers. Antibiotic drug loaded HNTs were mixed with poly(lactic-co-glycolic acid) (PLGA) solution to form drug delivery systems in the study of Qi (Qi et al. 2010). The system was successfully fabricated in the form of nano-fibers to improve therapeutic efficacy and safety of drug by delivering it at a rate dictated by the need of the physiological environment. According to the results obtained from this study, drug loaded HNT not only significantly improved the mechanical properties of the fibrous material, but also prolonged the release rate of the drug.

In the literature, contrary to the shortage on PLA/HNT nanocomposite investigations, it is possible to find researches on PLA/kaolinite nanocomposites

(Cabedo et al. 2006, Matusik, Stodolak and Bahranowski 2011). Kaolinite mineral is almost similar to dehydrated HNT, except water molecules between layers and tubular morphology are observed in HNT. Its chemically modified form, which was specifically designed to be melt blended with poly(lactic acid), was used in PLA/PCL blends by Cabedo (Cabedo et al. 2006). The semi-crystalline PCL acts as a plasticizing agent when melt blended with PLA and slightly increases its thermal stability. The evenly distributed silicate layers within the biodegradable polymer blend show an improvement in the mechanical properties: but the main advantage of kaolinite clay is the increase in gas barrier properties of the polymer matrix. In another PLA/kaolinite nanocomposite study (Matusik et al. 2011), kaolinite nanotubes were transformed from planar morphology into nano-tubular morphology by applying an intercalation/de-intercalation method that was used to prepare PLA based nanocomposites by Matusik et al. The results were compared with the ones on nanocomposites obtained by the inclusion of poorly ordered kaolinite and HNT – kaolinite mixture to see the effect of tubular morphology. Better mechanical properties were obtained for PLA/nano-tubular kaolinite nanocomposites compared to that are prepared with other clay minerals. The presence of highly dispersed nano-tubular kaolinite particles in the polymer matrix which contributed to the improvement of PLA mechanical properties was observed using AFM. Moreover, the interaction between the functional groups of PLA and the hydroxyl groups of the inner surface of nano-tubular kaolinite was confirmed by the intensity decrease of the O-H stretching absorption band. While enhancing the mechanical properties of PLA with organo-fillers, it is important not to sacrifice from the biodegradation rate. Matusik did not observe any evident changes in the degradation rate between pure PLA and PLA nanocomposites.

The surface chemistry of HNT minerals is readily modified enabling applications in nanocomposites, enzyme immobilization and controlled releases. Relying on the attribute that HNT minerals display an increased dispersion in viscous thermoplastic polymers, in literature HNTs have been incorporated into various

polymer matrices. Recently, an increasing number of research groups have studied the fabrication and characterization of polyamide/HNT nanocomposites (Ray et al. 2003b, Ray et al. 2003a, Pluta et al. 2002, Zhou and Xanthos 2008, Ray et al. 2002b). Höchstötter (Hedicke-Hochstotter, Lim and Altstadt 2009b, Hedicke-Hochstotter, Lim and Altstadt 2009a) and Marney (Marney et al. 2008) introduced unmodified HNT minerals into polyamide 6 matrix by melt extrusion in a twin screw extruder. At low HNT levels, an increased strength and stiffness as well as an enhanced elongation at break values were obtained. However, relatively high additive concentrations (>15 wt%) are required to achieve fire retardant property of nanocomposites associated with montmorillonite additives. Dispersion of HNT in Polyamide 12 matrix with different processing methods was investigated by Lecouvet (Lecouvet et al. 2011). A better dispersion was observed in nanocomposites prepared by using twin screw mini-compounder compared to nanocomposites formed in a batch internal mixer. The study revealed increase in linear viscoelastic properties and the dynamic storage modulus values with increasing HNT loading.

Thermoplastic polymer/HNT nanocomposite researches revealed that there lies a great potential for further improvement of the properties of HNT nanocomposites with a suitable chemical surface treatment. Especially, polypropylene based nanocomposites require modification of HNT particles by alkyl ammonium ions or organo-silanes. Grafting of γ -methacryloxypropyltrimethoxysilane (γ -MPS) onto HNT surface was studied by Du to investigate the effect of modification on thermal stability and flame retardant properties of polypropylene (PP) (Du, Guo and Jia 2006a). The modification of HNT results in a uniform dispersion although some aggregates are found in the HNT filled PP nanocomposite. In their following work, they grafted polypropylene on to HNT and investigated its compatibility effect on polypropylene/HNT nanocomposites (Du et al. 2006b). The mechanical properties and crystallization behavior of PP/HNT composites have been investigated by Ning (Ning et al. 2007). They also detected a well dispersion of HNT nanocomposites in PP matrix and a good interfacial interaction

with PP. However, not much enhancement on mechanical properties of PP/HNT composites had been achieved owing to constant crystallinity and spherulite size of PP. Halloysite can also be grafted by poly(methyl methacrylate) (PMMA) for the purpose of toughening. Liu (Liu et al. 2011) performed PMMA grafted Halloysite nanocomposites and introduced into poly(vinyl chloride) (PVC) matrix by melt compounding to achieve a ductile fracture behavior.

Another widely studied topic for HNT nanocomposites is their effect on Ethylene Propylene Diene Monomer (EPDM). Since EPDM does not contain any polar groups in its backbone it is incompatible with Halloysite nanotubes. Due to this fact, a Malaysian group, Ismail and his coworkers, (Ismail et al. 2008) observed a limited intercalation of HNT layers. However, from microscopic analysis fine dispersion of HNT particles in the matrix was observed. Especially, inclusion of EPDM chains into lumen of the HNTs and edge-to-edge and/or edge-to-face zigzag structures at high HNT loadings were clearly detected. This avoidance from agglomeration can be attributed to charge distribution (outer and inner surface carry net negative charge, whereas the edge is amphoteric with positive charge at low pH), unusual crystal shape and non-polar characteristics of EPDM. The well dispersion in EPDM matrix and zigzag structure are expressed as the main reasons for the increases in tensile strength, stiffness and ductility of EPDM/HNT nanocomposites. The same Malaysian group reported a similar work (Pasbakhsh et al. 2010) by adding maleic-anhydride grafted EPDM (MAH-g-EPDM) to EPDM/HNT nanocomposites to increase the compatibility between matrix and HNT surface. From FTIR analysis, formation of hydrogen bonding between outer and inner surfaces of the HNTs with MAH-g-EPDM was observed. Compared to previous work, greater intercalation was achieved with compatibilized nanocomposites owing to insertion of maleic anhydride into the HNT interlayer space. The improved interfacial interactions between EPDM and HNT by MAH-g-EPDM lead to enhancement of the tensile modulus. However, at high HNT loadings two different phases, EPDM-rich and HNT rich phases, were

found which were regarded as the main reason for reduction of the tensile strength and elongation at break values at high HNT loadings.

Like PLA, main matrix of this study, the main drawback of cured epoxies is their low fracture toughness, poor resistance to crack initiation and propagation, and inferior impact strength. In recent years, many efforts have been made to modify epoxies with layered MMTs. But, it is hard to achieve remarkable improvements in fracture toughness of epoxies. Deng (Deng et al. 2008) tried the cheap alternative of expensive CNT to improve the properties of epoxies. Improvement of fracture toughness with an optimum amount of HNT was clearly observed. The enhancement was not as great as the ones reported for epoxy/CNT nanocomposites, but, comparable with the nanocomposites that consist of modified-MMT, although much more evenly distributed silica particles were present for this type of composite. Hence, it can be concluded that supporting a better dispersion of HNT particles may result in better mechanical properties. Another study that uses HNT as impact modifier for epoxy was performed by Ye (Ye et al. 2007). In this study, HNTs were well dispersed in the epoxy but in two different dispersion forms: HNT and epoxy rich. When a more detailed investigation was performed in HNT rich regions by TEM analysis, it was seen that the spaces between the HNTs were actually filled by epoxy. This morphology was regarded as the starting point of 400% improvement of the impact strength. The toughening mechanism underlying this morphology is explained by nanotube debonding/pull-out seen in the crack initiation region of fracture surface and by the formation of several micro-cracks in which several nanotubes bridge the two surfaces of these cracks (Figure 2.16). This kind of morphology was observed in the tough and strong HNT rich parts of the nanocomposites, leading to dissipation of energy. This crack-bridging morphology was also reported by Hochstotter in HNT reinforced polyamide 6 matrix (Hedicke-Hochstotter et al. 2009b). When compared with the elongation properties of polyamide nanocomposites filled with organically modified montmorillonite, HNT containing nanocomposites showed enhancement as a result of this morphology.

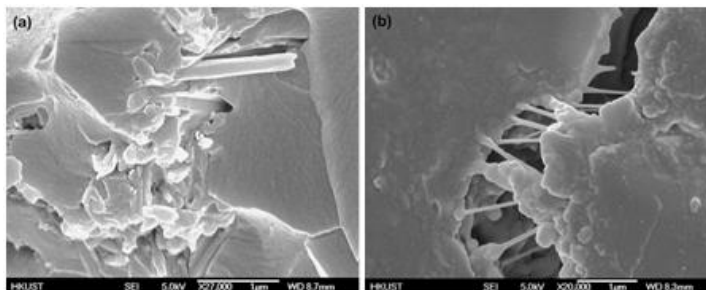


Figure 2.16. SEM micrographs taken on the fracture surfaces of the nanocomposites (a) Nanotube debonding/pull-out, (b) Nanotube bridge (crack bridging) (Ye et al. 2007)

Either modification of polymer backbone with unsaturated polar groups or functionalization of clay surface with coupling agents can be used to improve the compatibility between polymer matrix and clay surface. As mentioned above, functionalization of clay surface with organo-silanes has been explored in recent years as a way to improve clay dispersion in polymer matrix, thus increasing the mechanical properties of resultant nanocomposites (Yuan et al. 2008, Du et al. 2006a, Pasbakhsh et al. 2010, Hashemifard, Ismail and Matsuura 2011, Wang et al. 2008). In this study, modification of HNT is performed with organo-silanes having amino, epoxy and acrylic functional groups. In literature, grafting of γ -aminopropyltriethoxy silane (γ -APS) onto HNT with various pretreatment conditions was investigated by Yuan (Yuan et al. 2008). Owing to strong hydrogen bonds between layers, most of the interlayer inner surface Al – OH groups are unavailable for grafting, and interlayer distances of γ -APS-modified clay samples remain unchanged. However, it is clear that the modification is accompanied by the consumption of inner-surface Al – OH groups suggesting that the vast majority of grafting occurred on the Al – OH groups at the internal surface of the lumen or the Al – OH groups at the edges or external surface

defects. Moreover, grafting on Si – O groups on the external surface is also achievable. The most interesting observation driven from FTIR results is that in addition to grafting at the internal wall, edges, and external surface, hydrolyzed γ -APS might also oligomerize or even polymerize with surface water, and the oligomerized γ -APS further reacts with grafted γ -APS to form a cross-linked network. Among the pretreatments applied before silanization, evacuation showed the best performance. Thus, it can be said that removal of air from the lumen is useful for enhancing the loading of γ -APS, and hence on increasing the extent of grafting or oligomerization. Studies performed by Ismail and his group on the effect of the HNT loading on the properties of EPDM and EPDM/MAH-g-EPDM nanocomposites were mentioned previously. In the study of EPDM/modified HNT nanocomposites (Pasbakhsh et al. 2010), they modified HNT particles by γ -methacryloxypropyltrimethoxy silane (γ -MPS) to improve their dispersion in ethylene propylene diene monomer (EPDM). They also observed a partial grafting of γ -MPS on the surface Si-O groups and edge Al-OH groups and penetration of γ -MPS into the lumen of the nanotubes. As a result of good dispersion, tensile properties and elasticity were enhanced reasonably.

Another work on organo-silane grafting on to HNT for the application of mixed matrix membrane in gas separation was conducted by Hashemifard (Hashemifard et al. 2011). The silane agent was N- β -(aminoethyl)- γ -aminopropyltrimethoxy silane (AEAPTMS) and silanation of HNT occurred via reaction of 3 methoxy groups in AEAPTMS with the OH groups in HNT. The modification of the outer surface of the HNT particles was proven by in-plane Si-O stretching peak observed at 1080.8 cm^{-1} . Results showed that, the silanated HNT particles tended to be separated from each other but started to be re-agglomerated at higher silane concentration.

Wang (Wang et al. 2008) explored a different method and a wider way to the surface modification of Halloysite with 3-chloropropyltrimethoxysilane (CPTMS) followed by the introduction of peroxide groups on the surface (for the present

work only the first step of the Wang's study would be considered). The method is a so-called reverse atom transfer radical polymerization (RATRP) and modified HNT was used as an inorganic substrate. By the help of XPS, SPM and thermogravimetric analyses, successful grafting of silane on the HNT surface was determined. In the light of these researches, the modification of purified Halloysite nanotubes will be performed in this study. Then they will be inserted in plasticized and un-plasticized PLA matrix to form nanocomposites.

The low fracture toughness is the undesired property of PLA. Although it is possible to increase the strength of PLA by the well dispersion of layered silicate, it may be possible to enhance the toughness in a limited manner. A feasible strategy to decrease the brittleness of PLA is blending it with materials like polyethylene glycol (PEG), polycaprolactone (PCL), Acetyl tri-n-butyl citrate (ATBC) or lactide monomer, which are expected to act as plasticizing agent. The efficiency of the plasticizer can be evaluated in terms of glass transition temperature (T_g) shift to lower values and elongation at break property improvement (Zhang et al. 2010, Wan et al. 2009, Hu et al. 2003b, Hu et al. 2003c, Hu et al. 2003a, Martin and Averous 2001, Baiardo et al. 2003). In the study performed by the research group of Kocaeli University Chemical Engineering Department Plastics and Rubber Technology Research Group, 20% PEG was introduced to improve the fracture toughness of the PLA (Ozkoc and Kemalolu 2009). The modulus value, reduced to half of that of pure PLA with plasticizer addition, was tried to be recovered by organoclay addition. However, desired improvement could not be achieved owing to poor distribution of organoclay in PLA matrix. Although they do not form an exfoliated structure, HNT displays a fine distribution by the insertion of polymer chains into the lumen of the nanotube and attraction between the nanotube outer surface and edge (Baiardo et al. 2003). Hence, inclusion of HNT to plasticized PLA was expected to be efficient in terms of the improvement of the strength of plasticized PLA.

Biodegradation rate is the most outstanding property of the PLA. Upon disposal in the environment, PLA is hydrolyzed into low molecular weight oligomers and then mineralized into CO₂ and H₂O by the microorganisms present in the environment. The rate determining step in the degradation of PLA is hydrolysis, which is a self-catalyzed reaction owing to increased carboxylic acid end group concentration in the medium. Hydrolytic degradation under phosphate buffer and composting behavior of PLA/MMT nanocomposites take attention in literature (Paul et al. 2005, Ozkoc and Kemalolu 2009, Ray et al. 2002a, Ray et al. 2003b, Zhou and Xanthos 2008, Ray et al. 2002b). Most of the studies revealed that the biodegradation of the PLA nanocomposites takes place more rapidly than the unfilled PLA (Paul et al. 2005, Ray et al. 2002a, Ray et al. 2002b). Hydrolytic degradation preferentially takes place in amorphous regions, leading therefore to an increase in the polymer global crystallinity. Paul (Paul et al. 2005) and his co-workers observed an increase in the opacity of the samples during degradation period owing to an evolution in the crystallinity of the polymer matrix due to the nucleating ability of the fillers. Increase in crystallinity was also proven by crystallization enthalpy measurements with calorimetry. In contrast to studies mentioned above, Ozkoc and Kemalolu (Ozkoc and Kemalolu 2009) claimed that with increasing crystallinity by the inclusion of clay results in a lower biodegradation rate, 30% weight loss happens in the first 30 days for PLA, while only 10% is lost at the end of 100 days for PLA and plasticized nanocomposites. According to the mechanical results of this study, organo-filler does not improve the tensile strength of PLA, whereas it gives a higher Young's modulus. These contradictory results bring the question: Does increasing crystallinity with organoclay addition impede the hydrolytic degradation that takes place in amorphous regions or accelerate the degradation by the nucleating ability of the fillers. Roy and his co-workers attempted to investigate the hydrolytic degradation of PLA/Halloysite nanocomposites and compare it with the degradation of PLA/MMT nanocomposites (Roy, Hakkarainen and Albertsson 2012). It has been shown that, the mass loss (after 8 weeks) was of the same order for all the

compositions studied. However, the water-soluble product distribution of the oligomeric lactic acids showed that shorter oligomers were formed in the case of montmorillonite composites. Our study is the first; examining the response of the degradation rate of plasticized and un-plasticized PLA when it is reinforced with modified and unmodified HNT.

In order to improve the mechanical properties further, it is a good idea to impede the thermal degradation of PLA during melt-mixing. Recently, a large volume of research has been devoted to enhance the molecular weight and strength of virgin, reprocessed or recycled thermoplastics. The most promising of these chemical methods has been the use of di- or multi-functional chemical compounds called chain extenders. Chain extenders can also function to prevent the reduced thermal degradation of poly(lactic acid) nanocomposites after clay loading due to the presence of organo-modifier. The studies conducted by Najafi (Najafi et al. 2012b, Najafi, Heuzey and Carreau 2012a) and Meng (Meng, Heuzey and Carreau 2012) investigated the thermal degradation, mechanical and rheological properties of poly(lactic acid) based nanocomposites prepared in the presence of organically modified Cloisite® 30B nanoclay. As a result of these studies, it was seen that the nanoclay particles were well dispersed and affected the rheological properties strongly. Moreover, with better distribution and larger exfoliation extent desired mechanical properties can be achieved. In this study, thermal degradation of PLA was tried to be prevented and mechanical properties were tried to be improved by using 1,4-phenylene diisocyanate (PDI) as chain extender.

CHAPTER 3

EXPERIMENTAL

3.1 Materials

3.1.1 Polymer Matrix

As polymer matrix, Poly(lactic acid) manufactured by Natureplast (PLI005) was used. PLI005 is a thermoplastic resin developed for injection molding. The material was dried before processing at 60°C for 12 hours. Some properties and chemical structure of PLI005 are given in Table 3.1 and Figure 3.1 respectively.

Table 3.1. Properties of PLA matrix (PLI005)

Physical Property	Unit	Value	Standard
Specific Gravity		1.25	ISO 1183
Melt Index (190°C / 2.16 kg)	g/10 min	10 – 30	ISO 1183
Melting Range	°C	150 – 200	
Degradation Temperature	°C	240 – 250	
HDT (1.8 MPa)	°C	50	ISO 75-2

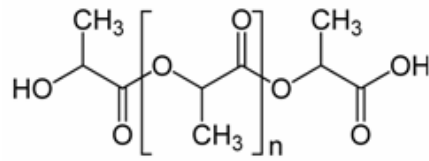


Figure 3.1. Chemical structure of PLA

3.1.2 Plasticizer and Toughening Agent

In order to obtain high toughness two different polymers were blended with PLA matrix; Poly(ethylene glycol) (PEG) and thermoplastic polyurethane (TPU). PEG, approved by FDA (Food and Drug Administration) in terms of its biodegradable properties, was obtained from Sigma Aldrich with an average molecular weight of 8000g/mole in dust form. The elastomeric material TPU, with a trade name of Estane® 2102-90A, was obtained from Lubrizol Advanced Materials.

3.1.3 Halloysite Nanotube (HNT)

The HNT minerals used for this study were provided by ESAN Eczacıbaşı A.Ş. The source of this local HNT is Bandırma/Turkey. In this study, this mineral is called as ESAN HNT. Chemical analysis of the sample is given in the results part of this dissertation (see Table 4.1). To compare the results of local ESAN HNT, an imported HNT, which has the same chemical and morphological structure as the local HNT, was used. It was obtained from Sigma-Aldrich in the form of powder and is called as Nanoclay HNT. Properties of the Nanoclay HNT can be seen from Table 3.2. Before each extrusion and modification procedure, HNT minerals were subjected to vacuum drying at a temperature of 105°C for 24 hours.

Table 3.2. Properties of Nanoclay HNT

Property	Value
Diameter × Length	30-70 nm × 1-3 μm
Color	75-96, Hunter Brightness
Surface Area	64 m ² /g
Capacity	8.0 meq/g CEC
Density	2.53 (true specific gravity)

The TEM micrographs of the clay minerals ESAN and Nanoclay HNT are shown in Figure 3.2. ESAN mineral with 20 – 30 nm diameter and 200 – 600 nm length displays layered structure morphology with a 7 - 8 nm wall consisting approximately 10 layers. Nanoclay sample exhibits the same structure as ESAN does, except for its higher length.

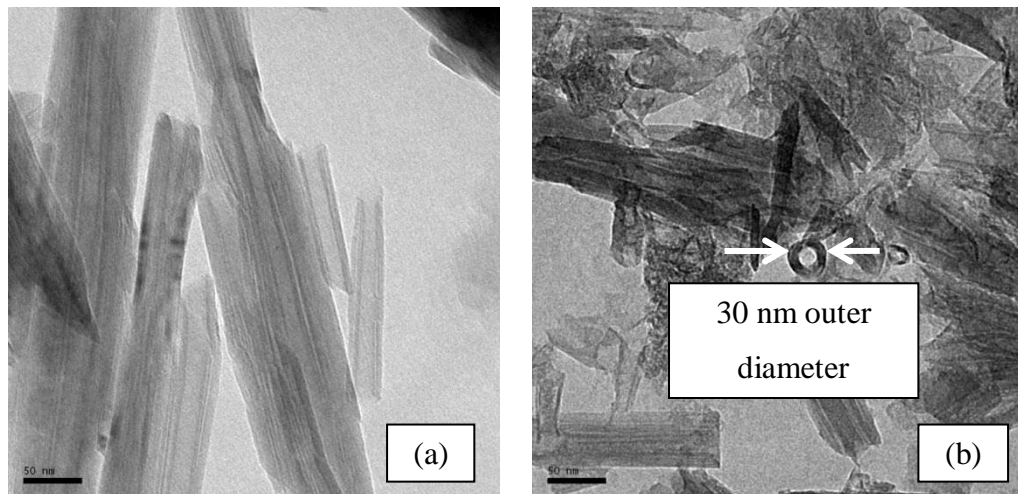


Figure 3.2. TEM micrographs of (a) Nanoclay HNT (b) ESAN HNT

3.1.4 Carbon Nanotube (CNT)

As synthetic nano-filler, thin multi-wall carbon nanotube was utilized. The carbon nanotube used in this study was obtained from Nanocyl with a trade name of Nanocyl 7000, which was produced via the catalytic carbon vapor deposition (CCVD) process. Characteristics of Nanocyl 700 is tabulated in Table 3.3. and the TEM micrograph supplied by the manufacturer is given in Figure 3.3.

Table 3.3. Characterization of Nanocyl 7000

Property	Value	Method of Measurement
Average Diameter (nm)	9.5	TEM
Average Length (μm)	1.5	TEM
Carbon Purity (%)	90	TGA
Metal Oxide (%)	10	TGA
Surface Area (m^2/g)	250 – 300	BET

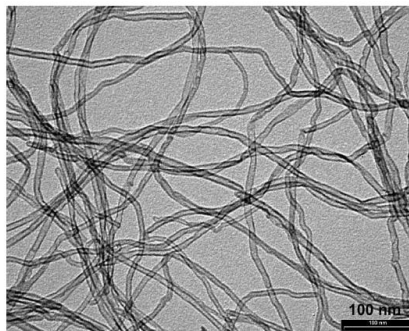
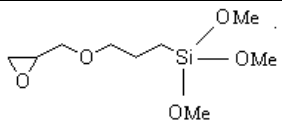
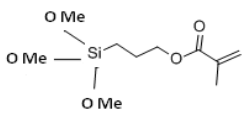
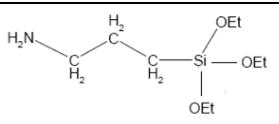


Figure 3.3. TEM Micrograph of Nanocyl 7000 CNT

3.1.5 Silane Coupling Agents

For the functionalization of HNT surface, three different silane coupling agents were used. The chemical structure, feature and trade name of the organo-silane can be seen from Table 3.4.

Table 3.4. Silane coupling agents used in this study

Material	Chemical Structure	Feature	Trade name
γ -glycidoxypropyl trimethoxysilane (γ -GPS)		Epoxy functional	KH-560
γ -methacryloxypropyl trimethoxysilane (γ -MPS)		Acrylic functional	KH-570
γ -aminopropyl triethoxysilane (γ -APS)		Amino functional	KH-550

3.1.6 Quaternary Alkyl Salt

For the modification of HNT surface, (4-carboxybutyl)triphenyl phosphonium bromide (CBTPB) quaternary salt obtained from Sigma Aldrich was used. The chemical structure of the quaternary salt is given in Figure 3.4.

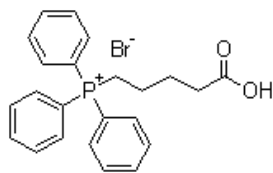


Figure 3.4. Chemical structure of (4-carboxybutyl)triphenyl phosphonium bromide (CBTPB)

3.1.7 Other Chemicals

The other chemicals used in this study are given in Table 3.5 with their chemical structures and purpose of use. All of them are obtained from Sigma-Aldrich

Table 3.5. Other chemicals used for in this study

Chemical	Structure	Purpose of Use
1,4-phenylene diisocyanate (PDI)		Chain extender to prevent degradation reactions
Sodium Pyrophosphate ($\text{Na}_4(\text{P}_2\text{O}_7)$)		Dispersant agent in HNT purification process
Ethylene Glycol		For HNT characterization
Ethanol		To form hydrolysis medium for silane coupling agents
Chloroform		As solvent in SC method
Citrus Solvent (ELECTRON [®])	Proprietary Blend	As solvent in SA method

3.2 Characterization of local ESAN HNT

Before the characterization of ESAN HNT, which was supplied in the form of massy bulk, it was ground with a lab scale grinder to obtain a dust like form and then subsequently sieved through 45 μ m. Drying conditions of the HNT mineral was designated as 105 °C for 12 hours under vacuum.

It is hard to differentiate HNT (7Å) from kaolinite minerals. In order to verify the presence of HNT mineral, ethylene glycol (EG) treatment is the most commonly used test method (Hong and Mi 2006). During the treatment, ethylene glycol saturated clay sample was obtained by suspending the powder sample in a solution at ambient temperature for 24 hours. At the end of 24 hours, the clear ethylene glycol was decanted and the excess glycol was removed by working the mixture on a 0.45 mm polycarbonate filter paper under vacuum. Then, the ethylene glycol was evaporated in an oven until the suspension has the proper consistency. The ethylene glycol treatment procedure can be seen from Figure 3.5.

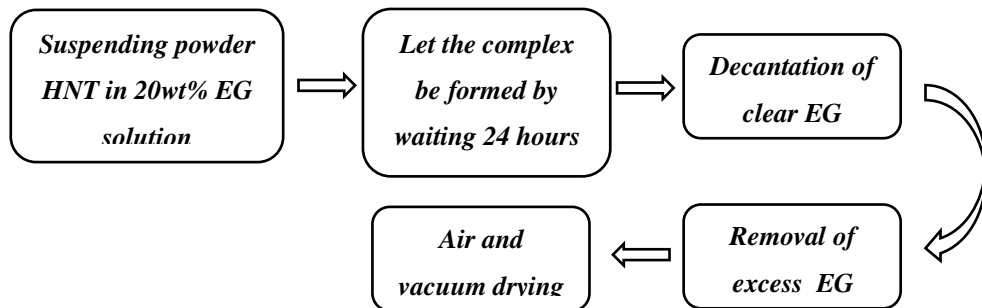


Figure 3.5. Ethylene glycol (EG) treatment procedure for local ESAN HNT

3.3 HNT Pre-treatments

3.3.1 HNT purification (p-HNT)

HNT can occur intermixed with other clay minerals and it may also contain non-clay impurities as well. Non-clay minerals and other impurities in HNT vary considerably in different deposits. Some deposits are exceptionally pure and contain only minor quantities, consisting chiefly of pyrite, silica, dolomite, iron-bearing minerals and non-crystalline materials, and manganese oxides. However, in most deposits, silica is the principal impurity; it occurs in the form of feldspar, illite, cristobalite, quartz, chert and is in poorly crystalline form. Gibbsite and manganese minerals can also occur in some HNT depending on the geological deposit (Kennedy 1990).

In order to remove the impurities found in the ESAN HNT, sedimentation procedure was applied. During the procedure Halloysite and dispersant agent were dispersed in distilled water. After fully dispersed slurry was obtained, the suspension was left for sedimentation. At the end of sedimentation, supernatant liquid was siphoned and centrifuged at 6000 rpm for 15 minutes. Sediment obtained in centrifuge tubes was smeared from the bottom of each bottle and subsequently air dried, and then vacuum dried at 105 °C approximately for 48 hours. Particle size of HNT, amount of dispersant agent, amount of distilled water and sedimentation period were varied to obtain the maximum amount of pure HNT as shown in Table 3.6 . The parameters used in the 5th procedure were found to be the optimum ones which resulted in approximately 20 gr of pure HNT at the end of the sedimentation. The sedimentation procedure is shown in Figure 3.6. After HNT purification their characterizations were performed by XRD analysis, whether the purification was successful or not. XRD analysis will be explained in the composite characterization part.

Table 3.6. Sedimentation procedure experimental parameters

# of Trial	1	2	3	4	5
HNT amount (gr)	60	60	60	60	60
HNT particle size (μm)	<125	<125	<125	<125	<45
Amount of $\text{Na}_4(\text{P}_2\text{O}_7)$ (gr)	---	3	3	6	6
Amount of water (ml)	1600	1600	3600	1600	1600
Sedimentation period (hour)	5	5	5	1	1

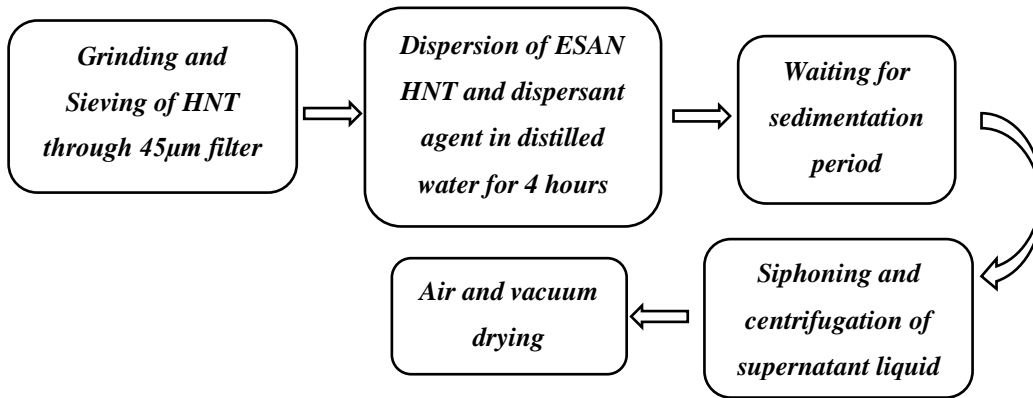


Figure 3.6. Sedimentation Procedure for Halloysite Purification

3.3.2 HNT Surface Functionalization with Silane Coupling Agents (o-HNT)

A general procedure applied for grafting of silica-based materials was used in this study (Yuan et al. 2008, Vansant, Van Der Voort and Vrancken 1995). During the functionalization procedure, three different types of organo-silanes having

different functional groups (amino, epoxy and acrylic) and alkoxy groups (methoxy and ethoxy) were used. The main aim to use organo-silanes having different alkoxy groups is to investigate the effect of the alkoxy chain length on the conversion of alkoxy silanes to hydrophilic silanols by hydrolysis and the affinity of organo-silane to react with the Al – OH groups on the edge and Si – O groups on the surface of HNT. Also, the effect of different functional groups on the interaction between functionalized HNT and polymer matrix is the reason of using organo-silanes with different functional groups.

As shown in Figure 3.7, the first step of the silanization procedure is ethanol-water solution preparation in a polyethylene beaker to use for hydrolysis prior to surface treatment. Stability of aqueous silane solutions varies from hours for the simple alkyl silanes to weeks for the amino functional silanes. Both hydrolysis and condensation are reversible, and alcohol reverses the silane hydrolysis stabilizing the solution of silanols for a period of time. The slowest hydrolysis and condensation rate for alkoxy silanes is at approximately pH 7 and 4 respectively. Thus, acid catalyzed silanization procedures result in “fast hydrolysis + slow condensation” which maximize the solution life for silanol species to prevent the limited water solubility of most commercial alkoxy silanes, until the groups are converted to hydrophilic silanol groups by hydrolysis. However, this limited water solubility case is not valid for amino functional silanes. Thus, the pH of the ethanol – water solution was adjusted to 4.5 – 5.5 by adding acetic acid for the treatments performed with γ -glycidoxypropyl trimethoxysilane (γ -GPS) and γ -methacryloxypropyltrimethoxysilane (γ -MPS). But the solution pH was kept neutral for silanization conducted in the presence of γ -aminopropyltriethoxysilane (γ -APS). After adjusting the pH of the solution, silane was added with stirring to yield the desired final concentration, and 30 minutes was allowed for hydrolysis / silanol formation. HNT nanotubes were dispersed in the solution and the suspension was refluxed at 80°C for 24 hours under constant stirring. At the end of 24 hours the dispersion was centrifuged at 6000 rpm for 5 minutes. Until neutralization, the modified mineral was washed with ethanol and left for drying.

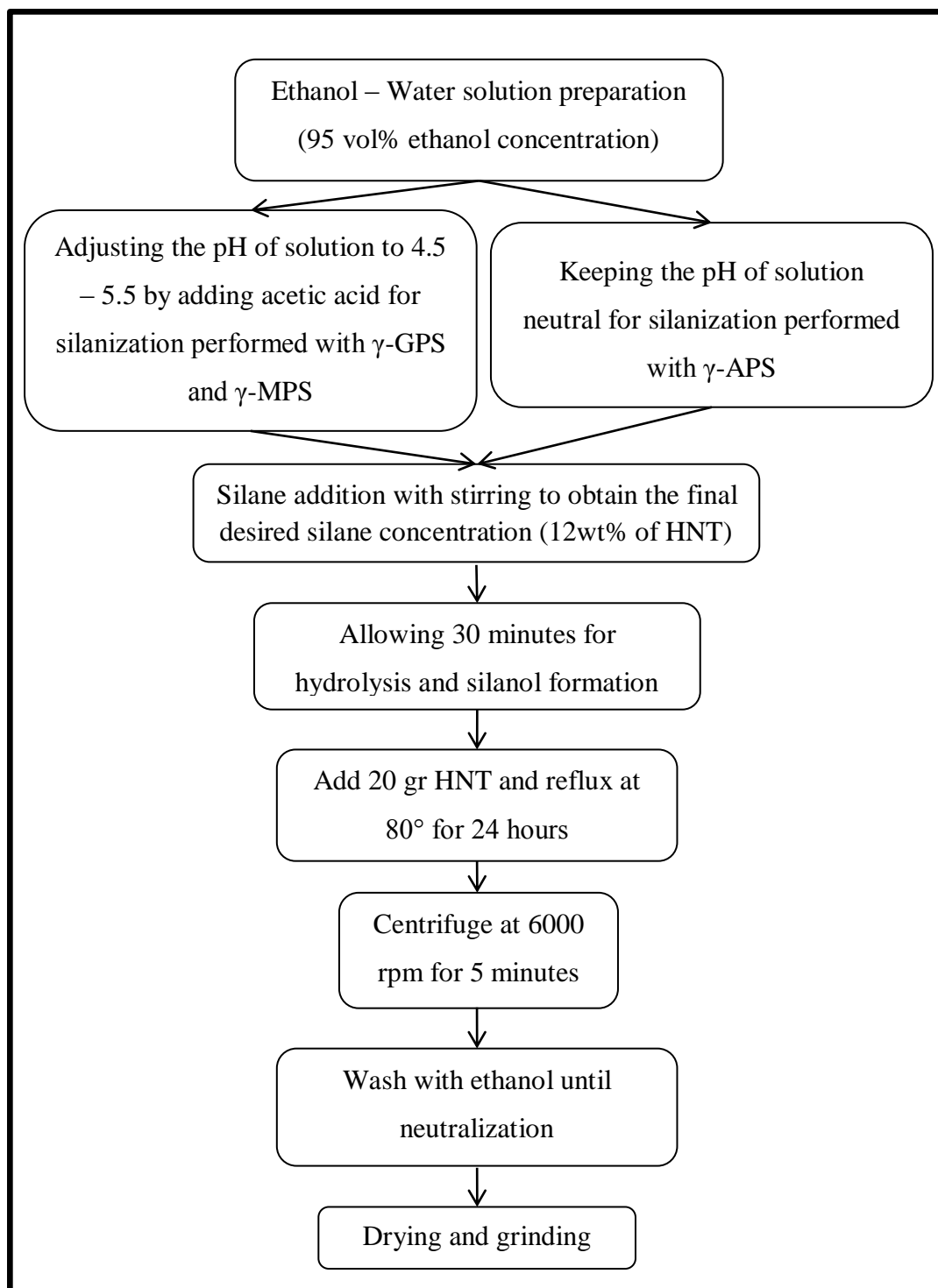


Figure 3.7. Silanization Procedure

3.3.3 HNT Surface Modification with Alkyl Salt (m-HNT)

For the modification purpose phosphonium based quaternary salt was used. In the first step of the procedure 50% ethanol-water mixture was prepared. Then, clay and calculated amount of modifier were added to this mixture and let to reaction to occur by stirring at 80°C for 4 hours. After 4 hours, the dispersion was centrifuged at 5000 rpm for 5 minutes and washed with 50% ethanol-water mixture. The clay minerals were washed until all of the ions were removed. After each centrifugation, the supernatant liquid was titrated with AgNO₃ to check the remaining ions. Then, the modified mineral was left for drying under vacuum.

The amount of surfactant (mg) is determined with the following equation:

$$A \text{ (mg of surfactant)} = \frac{\text{CEC (mmol)}}{100\text{gr Halloysite}} \times 1.1 \times \frac{1\text{mol}}{1000\text{mmol}} \times \frac{\text{MW (gr) of surfactant}}{1\text{mol}} \times \frac{1000\text{mg}}{1\text{gr}} \times \text{Amount of Halloysite (gr)}$$

Equation 3.1

3.3.4 Evacuation Pre-treatment (e-HNT)

In addition to HNT surface purification and functionalization, a different pre-treatment was applied to clay minerals. Instead of classic vacuum incubator, drying was performed by the help of a turbo-molecular vacuum pump with a maximum capability of 1×10^{-2} - 1×10^{-3} mbar vacuum. The drying temperature was

not changed and kept at 105°C. This pre-treatment was called as “evacuation pre-treatment” and performed to remove interlayer water that could not be wiped out by classical drying method. The schematic of the system where the drying was performed can be seen from Figure 3.8.

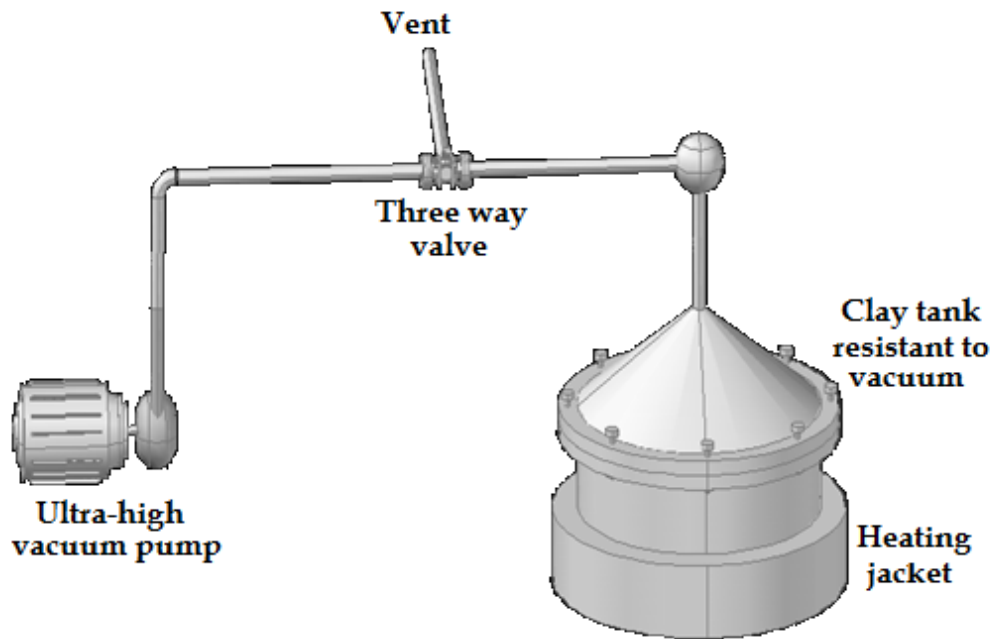


Figure 3.8. Evacuation pre-treatment system schematic

3.4 Composite Preparation Methods

3.4.1 Direct Melt Mixing Method (DM)

In this method PLA based composites were prepared by using a co-rotating twin screw laboratory scale compounder (15 mL Micro-compounder, DSM Xplore) that was operated in batch mode. The processing parameters were kept constant at 100 rpm screw speed, 180 °C barrel temperature. In order to eliminate oxidative degradation, the barrel was swept with argon, and at the end of the specified mixing period the extrudate was taken by changing the position of the valve to guide the polymer to the die and subsequently injection molded by 12 ml DSM Xplore Microinjection molder to obtain ISO 527-2/5A tensile bars and ISO 180 impact bars. Photographs of the Micro-compounder and Microinjection molder can be seen in Figure 3.9.

Different mixing times were used to investigate the effect of increasing residence time on the dispersion of clay minerals in PLA matrix:

- Direct Melt Mixing for 3 minutes (DM3)
- Direct Melt Mixing for 10 minutes (DM10)

In addition to PLA/HNT composites, P-PLA/HNT, T-PLA/HNT, PLA/PDI/HNT and PLA/CNT/HNT composites were also prepared by using this technique due to its simple processing and effectiveness.

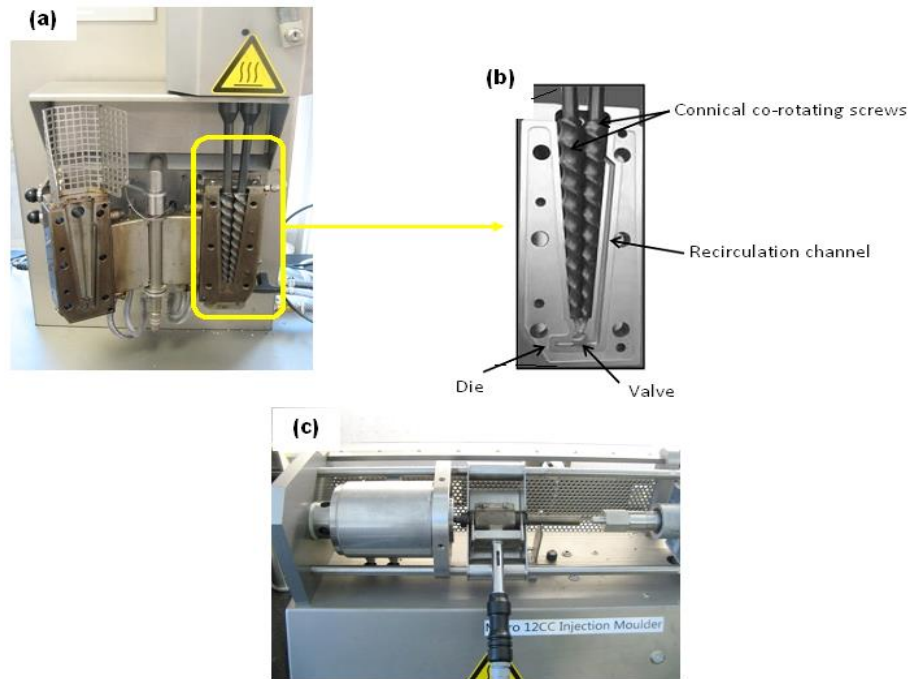


Figure 3.9. Melt mixing equipment; (a) Micro-compounder, (b) Screw design of Micro-compounder, (c) Microinjection-molder

3.4.2 Masterbatch Melt Mixing Method (MMA)

In this composite preparation technique, a modified melt mixing procedure consisting two simultaneous extrusion steps, was applied. The procedure of this method can be seen from Figure 3.10. During both of the extrusion steps, all the parameters that were kept constant in direct melt mixing method were used and the residence time was adjusted to 3 minutes.

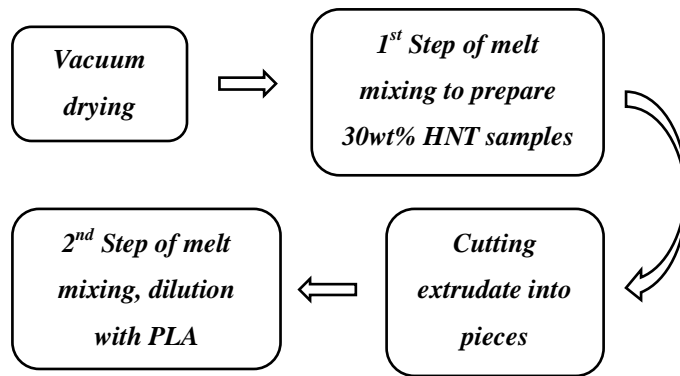


Figure 3.10. Masterbatch melt mixing procedure (MMA)

3.4.3 Solvent Casting Followed by Melt Mixing Method (SC)

This method is a modified version of masterbatch melt mixing method (MMA). Instead of the 1st extrusion step, solvent casting was applied to prepare 30wt% HNT masterbatch. The procedure is shown in Figure 3.11.

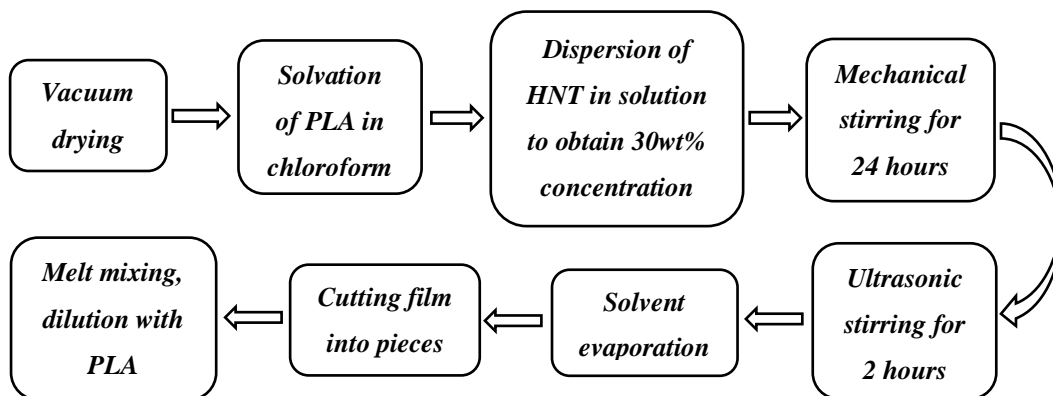


Figure 3.11. Solvent casting followed by melt mixing procedure (SC)

3.4.4 Suspension Addition to Melt Mixing (SA)

This method benefits from the dispersive effect of a liquid solvent. It also includes the melt mixing step as in the other processing techniques mentioned earlier. In this method, residence time was adjusted to 6 minutes owing to the slurry addition. The procedure of this method is given in Figure 3.12.

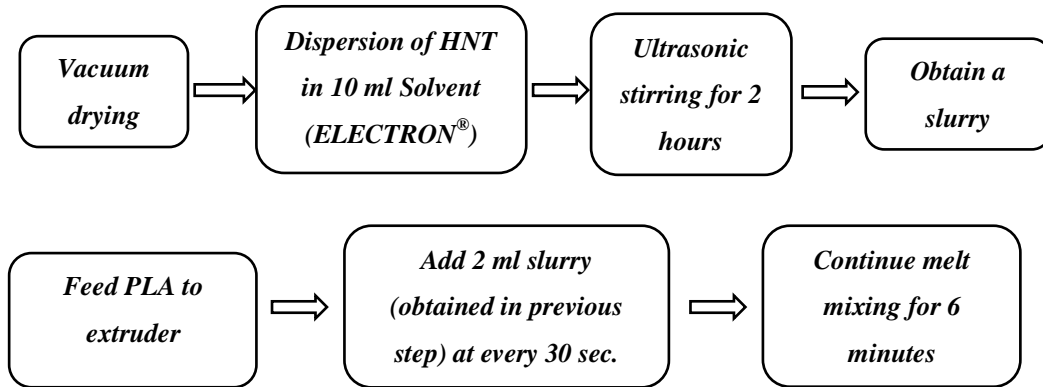


Figure 3.12. Suspension addition to melt mixing (SA)

3.5 Characterization of Functionalized HNT Minerals and Composites

Several characterization techniques were used in this study to understand the physical behavior of the composite materials and functionalized HNT minerals. The techniques used in this study include morphological, mechanical, thermal and hydrolytic degradation tests.

3.5.1 Fourier Transform Infrared Spectroscopy (FTIR) Analysis

FTIR analysis was used to obtain qualitative information about functionalization of HNT minerals. Hence, the chemical reactions occurring between the HNT surface and silane coupling agents were investigated with this analysis.

HNT minerals were ground thoroughly with KBr at approximately 1–3% by weight and pressed into a pellet with a thickness of about 1 mm. FTIR spectra were collected at ambient temperature after 4 scans at 4 cm^{-1} resolution in the region of $4000\text{--}650\text{ cm}^{-1}$ on a Spectrum 100 FTIR spectrometer.

3.5.2 X-Ray Diffraction (XRD) Analysis

The XRD patterns were recorded from $2 - 45^\circ 2\theta$ using Cu-K α radiation successively on the same samples and collected at a scan rate of $2^\circ 2\theta/\text{min}$ with a 10 mm divergence slit, variable anti-scatter slit, 0.3 mm receiving slit and tube settings of 40 kV – 40 mA. Change in basal spacing of the HNT layers were calculated by XRD analysis by the help of Bragg's law.

3.5.3 Scanning Electron Microscopy (SEM)

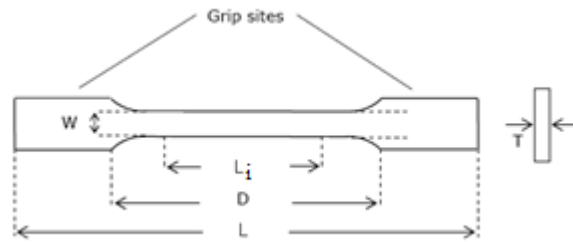
Morphological properties of the composites were investigated using a SEM JEOL JSM-6510LV Scanning Electron Microscope (SEM). Samples for SEM were prepared by coating the impact fracture surface of the composites with gold to eliminate arcing of the beam.

3.5.4 Transmission Electron Microscopy (TEM)

For TEM analysis, ultra-sections were cryogenically cut with a diamond polymer knife at a temperature of -100°C by using LEICA UC EM6 Ultramicrotome. These samples were examined by a TECNAI F30 Transmission Electron Microscope at an acceleration rate of 120 kV in UNAM National Nanotechnology Research Center.

3.5.5 Tensile Test

Tensile properties of the samples were analyzed using an Instron Universal Testing Machine. During the test, the specimen was placed in the grips of the testing machine, taking care that it was properly aligned and the grips were tightened evenly and firmly enough to prevent the slippage of the specimen. Crosshead speed was applied as 10 mm/min, based on the gauge length of 25mm and strain rate of 0.4min^{-1} . Five samples were tested from each batch and the average values of tensile strength (MPa) and strain break were reported with the standard deviation. The schematic representation of the tensile bar sample is illustrated in Figure 3.13.



$L = 75 \text{ mm}$, $D = 40 \text{ mm}$, $L_i = 25 \text{ mm}$ (gauge length), $W = 4 \text{ mm}$, $T = 2.1 \text{ mm}$

Figure 3.13. Tensile test specimen

3.5.6 Impact Test

Notched Izod impact tests were performed based on ISO 180 standard with a Ceast machine model 9050. Five samples were tested from each batch and the average values were reported with the standard deviation.

3.5.7 Dynamic Mechanical Analysis (DMA)

For the determination of thermo-mechanical properties dynamic mechanical analysis (DMA) was performed by the help of Metravib 01dB 50N Dynamic Mechanic Analyzer. Spectra were recorded in the tensile mode at a scanning rate of $1^\circ\text{C}/\text{min}$ from room temperature to 150°C at a frequency of 1 Hz . DMA specimens were cut from the injection molded tensile test specimens in the form of rectangular bars; height: 30 mm , thickness: 4 mm and depth: 2.1 mm .

3.5.8 Vertical Force Measurement

In order to obtain an idea about the melt viscosity of the composites during extrusion, vertical force measurements were recorded. A representative schematic of the system setup, connected to micro-compounder for vertical force measurement, can be seen from Figure 3.14 (Ozkoc, Bayram and Quaedflieg 2008). The main idea underlying behind this setup is the measurement of vertical force exerted by the barrel of the micro-compounder opposing the pushing forces imposed by the screws toward the bottom. During this process, polymer melt is pumped through the recirculation channel. The load cell used for the measurements is in 10 kN range and balanced by the barrel rotating around a stationary vertical axis. The vertical force data were recorded at every 30 seconds.

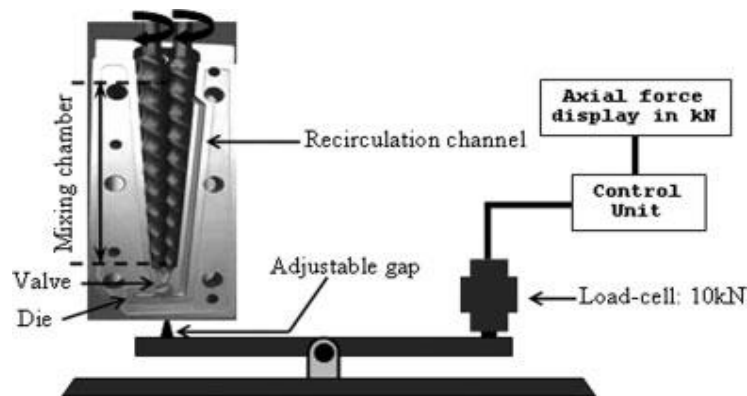


Figure 3.14. The schematic of axial force measurement setup (Ozkoc et al. 2008)

3.5.9 Differential Scanning Calorimetry (DSC)

Thermal transition behavior and crystalline fraction (%) of composites and blends were investigated by DSC. The measurements were conducted on Mettler Toledo DSC 1 Star System. Each sample was run at a scanning rate of 10 °C/min in a nitrogen atmosphere. Samples were heated from 30 to 200 °C at 10 °C/min, annealed for 3 min at 200 °C, and cooled to 0 °C at a rate of 10 °C/min. The scan cycle was then repeated.

3.5.10 Thermal Gravimetric Analysis (TGA)

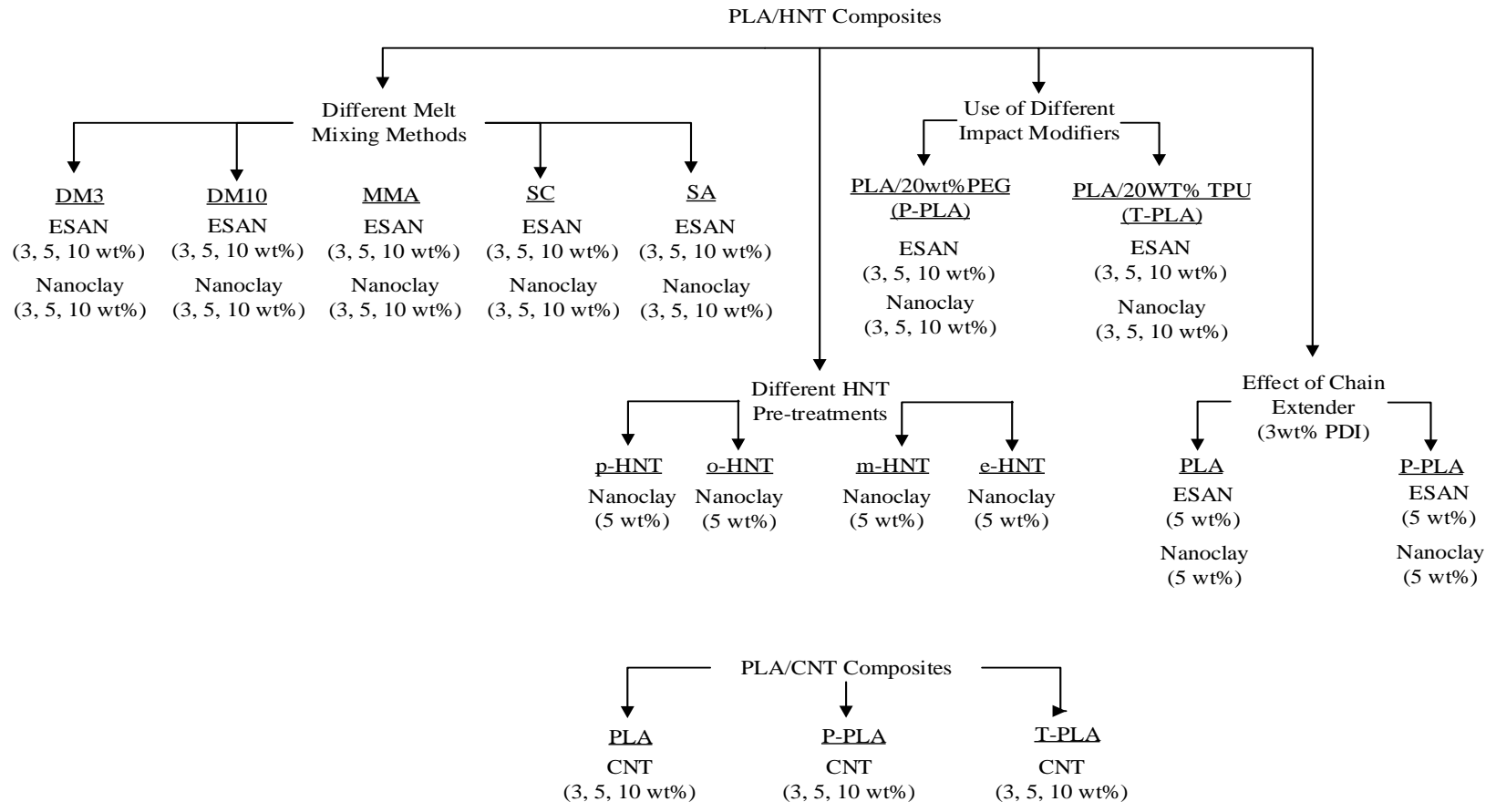
To investigate the functionalization of HNT minerals, silane coupling agent treated HNT samples were subjected to TGA analysis. It was performed by Perkin Elmer Pyris 1 Thermogravimetric Analyzer (TGA) with a heating rate of 20°C/min from room temperature to 900°C under air flow.

3.5.11 Hydrolytic Degradation Tests

The hydrolytic degradation, which is the first and rate determining step of biodegradation, was investigated in phosphate buffer solution (pH= 7.4) under a constant temperature of 60 °C. The degradation rate was determined from the weight loss. Samples with approximately 0.45 mm thickness were placed in a bottle containing 25 ml solution. These bottles were then placed in a water bath that remained at constant temperature during the whole degradation period. Then, the weights of samples were recorded at specified periods after drying.

3.6 Experimental Design

The experimental design of this study is shown in Figure 3.15. It consists of five sections: different melt mixing methods, different HNT pre-treatments, use of different impact modifiers, use of chain extender and preparation of PLA/CNT composites.



74

Figure 3.15. Experimental Design

CHAPTER 4

RESULTS AND DISCUSSION

4.1 Characterization and Purification of Local ESAN Halloysite

In the first part of this dissertation it is attempted to characterize the mineralogical characteristics of the local Halloysite (HNT) mineral from Bandırma/TURKEY supported by ESAN Eczacıbaşı. These minerals are ubiquitous in soils and rocks, and there are numerous types of particle shapes, hydration and purity states for these minerals. Before preparing polymer composite, it is important to determine the specifications of the mineral that will be used as filler.

The simplest way to understand the type of the mineral, its hydration state and impurities in it is to analyze its crystal structure. In the XRD pattern of the raw ESAN HNT shown in Figure 4.1 the peaks mentioned with bordered labels refer to the Halloysite mineral. Especially the peaks at ~ 7.2 Å and ~ 3.6 Å represent the basal and non-basal peaks of dehydrated HNT (Meta Halloysite) sample respectively. Since the sample has been dried before XRD analysis, no trace of Hydrated Halloysite (Endellite with 10 Å basal spacing) appears. Basal peaks of air dried sample can be seen from the small figure shown on the left top of the Figure 4.1. It reveals the pattern of an Endellite with a basal spacing of ~ 10 Å, indicating that there is a significant amount of hydrated HNT in the sample which contains water layers between its silicate layers (Churchman and Carr 1975, Keller and Johns 1976).

As mentioned before, HNT minerals usually contain non-clay particles and some impurities depending on the geological conditions that occurred during the formation of the minerals. When the XRD result of raw ESAN HNT is analyzed, it is seen that the non-clay particles are most likely Gibbsite, Quartz and Feldspar (Joussein et al. 2005). These particles cannot delaminate in a polymer matrix because of the absence of silicate layers and they have lower CEC (mmol/100g) values. Also, ions other than Na^+ (or Li^+), such as Ca^+ , are not exchangeable during the cation exchange reaction, since they act as multivalent cation reservoirs (Lagaly 2006). Hence, these non-clay particles, impurities and ions in layered silicates should be removed to increase CEC of the minerals and provide better dispersion in polymer matrices.

Although there are several works on Bentonite purification (Seyidoglu and Yilmazer 2012, Song et al. 2005), for Halloysite nanotubes the number of these studies are a few. In the study of Liu (Liu et al. 2008), Halloysite nanotubes were purified before they were modified with silane coupling agents and results showed better dispersion of clay minerals in the polymer matrix. In this study, non-clay impurities and un-desired ions are removed by sedimentation method. As can be seen from Figure 4.2, peaks resembling non-clay particles disappear except for the one that belongs to Gibbsite. It is also important to note that, XRD pattern of reference Nanoclay Halloysite; obtained from Sigma-Aldrich, perfectly matches with that of raw ESAN Halloysite (will be discussed in the next section). This raises the question whether purification is necessary for the preparation of composites. To provide a solution to this question, properties of composites containing raw and purified ESAN Halloysite were compared and the results are given in “Effect of Halloysite Pre-treatment” chapter.

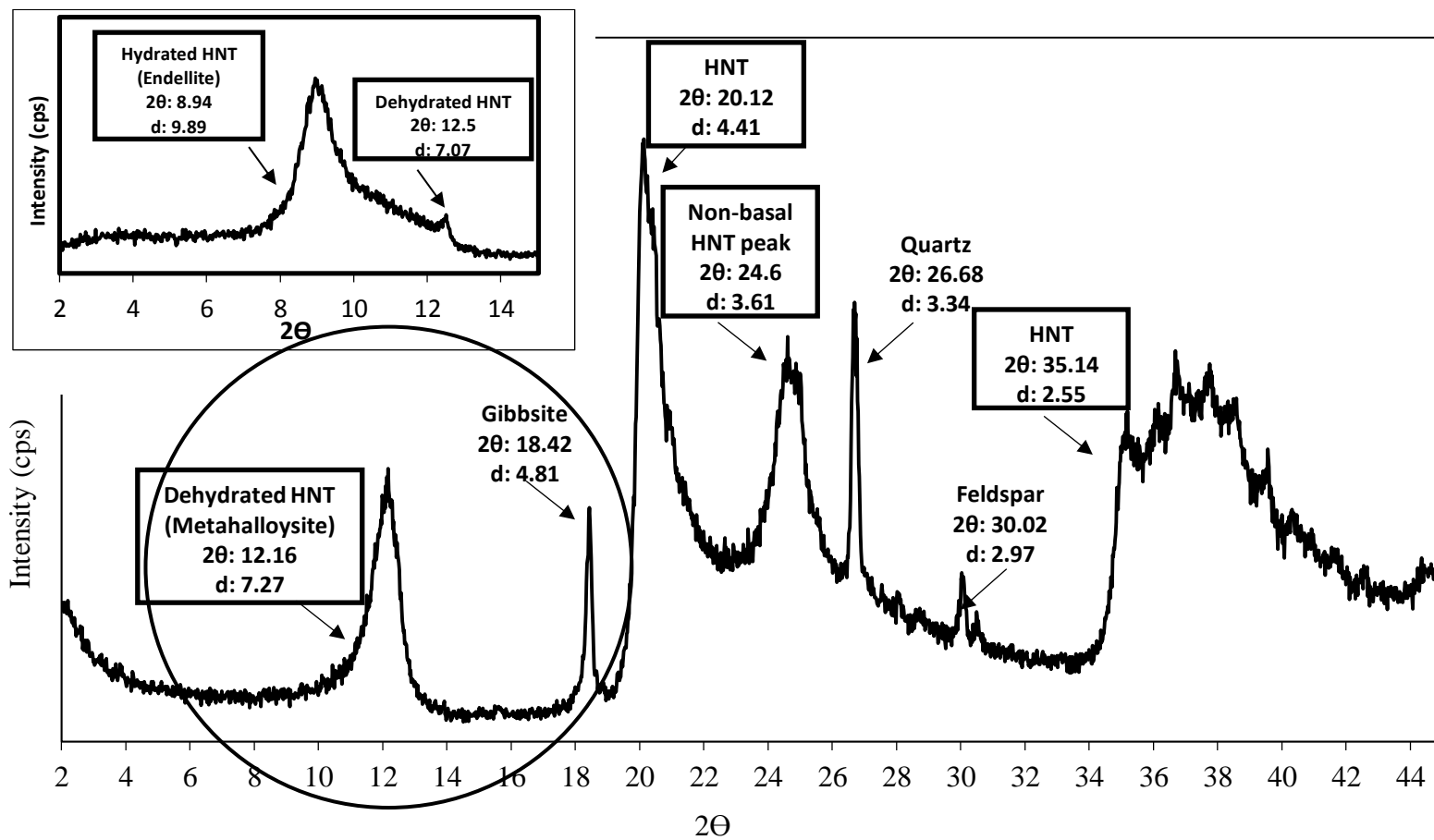


Figure 4.1. XRD pattern of raw ESAN HNT

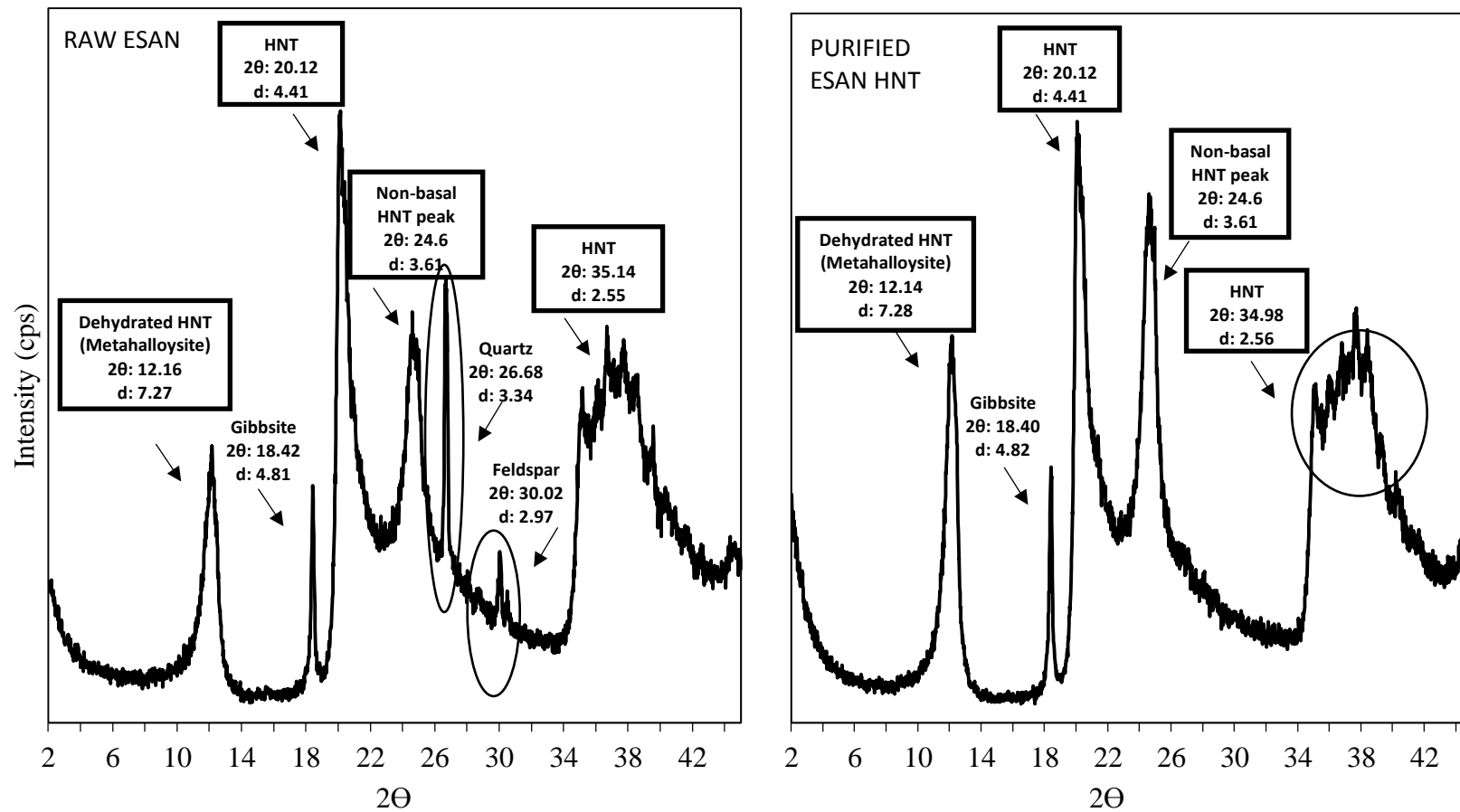


Figure 4.2. Comparison of the XRD patterns of raw ESAN HNT and purified ESAN HNT samples

Chemical analysis is also performed to analyze the component distribution and purification state of the mineral (Table 4.1). Oxides, such as CaO, MgO, Na₂O and K₂O, and colorants, such as Fe₂O₃ and TiO₂, separated from the clay mineral by precipitating and their weight percent decrease as a result of purification.

Table 4.1 Chemical analysis of raw and purified Halloysite (Performed by ESAN Eczacıbaşı A.Ş.)

Components	Raw Halloysite (wt %)	Purified Halloysite (wt %)
SiO ₂	43.55	47.03
Al ₂ O ₃	38.49	41.20
Fe ₂ O ₃	0.68	0.34
TiO ₂	0.13	0.06
CaO	0.27	0.10
MgO	0.02	0.01
Na ₂ O	0.43	0.40
K ₂ O	0.33	0.27
Others	16.10	10.59

For the characterization of local ESAN Halloysite mineral, XRD analysis was performed and the results are given in Figure 4.1. When its XRD pattern is compared with that of reference Nanoclay Halloysite, it confirms that the mineral is a Halloysite with some purity in it. However, identification of Halloysite is ambiguous because its X-Ray diffraction pattern resembles that of many Kaolinites, which is commonly admixed with Halloysite (Brigatti et al. 2006). Use of the XRD patterns of the minerals to differentiate them is not enough. Hence, several methods had come out to reveal the actual identity of the sample. Most commonly, morphology or intercalation reactions take attention for this

purpose. The tubular morphology of ESAN sample (see Figure 3.2) can be used to identify the mineral as Halloysite which has a characteristic shape in the form of hollow tubes. However, there are several studies that identify Kaolinite mineral in tubular shape (Churchman and Carr 1975, Churchman 1990). Eventually, differentiation of the Halloysite and Kaolinite minerals based on particle shapes can be misleading.

On the other hand, intercalation methods are much more precise for HNT recognition. To understand this situation better, it can be asserted that due to the water monolayer between the silicate layers of HNT, the intercalation of the mineral with polar compounds is easier than the intercalation of Kaolinite, which does not previously contain water layer. The most widely used intercalation procedure for this purpose is to saturate the clay sample with ethylene glycol (EG) (Hillier and Ryan 2002). This treatment let the water layer between the basal spacing be replaced with EG leading to a complex formed by the partial reaction between HNT and EG. Hence, the XRD pattern of Halloysite characteristically changed following solvation with EG. This change is called as MacEwan effect and involves a decrease in the height intensity of the basal peak around 7.2 Å and an increase in the height intensity of non-basal peak around 3.6 Å (Hillier and Ryan 2002, Macewan 1946, Macewan 1948). This effect can be seen from Figure 4.3 for ESAN Halloysite. After the treatment of clay sample with EG, the intensity of the basal peak decreases and the intensity of non-basal peak increases which strongly points that the sample is mainly comprised of Halloysite mineral and does not contain kaolinite mineral. According to study performed by Hillier and his co-workers (Hillier and Ryan 2002), the XRD patterns of Halloysite samples obtained from “Macaulay Institute Mineral Collection” indicate that the basal spacing around 7.2 Å is the most intense peak for their samples and glycolation results in a reverse in basal/non-basal peak intensity ratio. However, for ESAN HNT sample, non-basal peak is the most intense peak both before and after glycolation. This may arise from the origin of the Halloysite sample, but it is not an indication of the Kaolinite mineral.

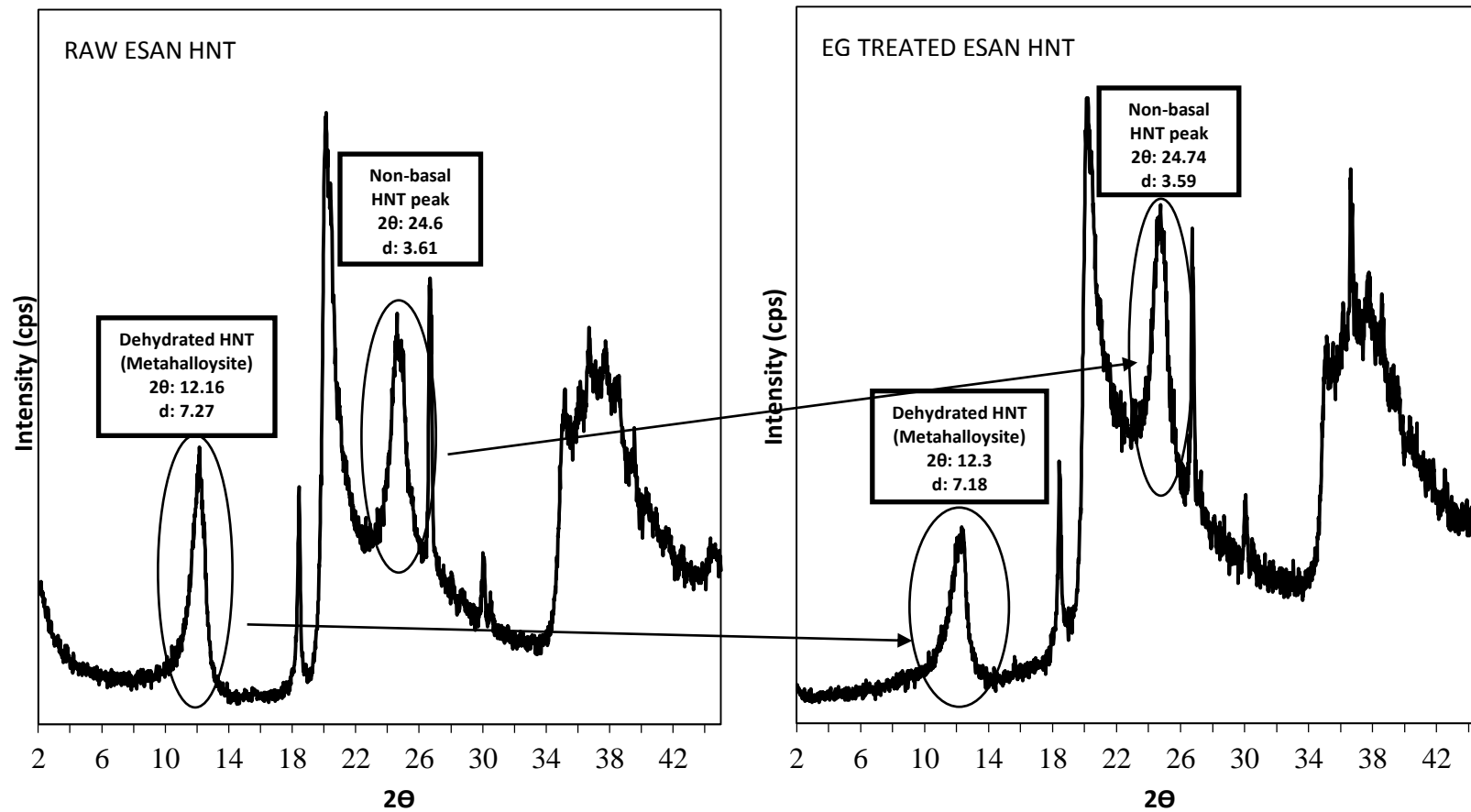


Figure 4.3 Comparison of the XRD patterns of EG treated and raw ESAN Halloysite samples

4.2 Effects of Different Melt Mixing Methods on the Properties of Unplasticized PLA/HNT Composites

Polymer nanocomposites or composites can be prepared using different methods, such as melt mixing, solution processing or in-situ polymerization as described in the background information part of the dissertation. Among these methods, the easiest and the most commonly used one is melt mixing. Being environmentally friendly and adaptable to industrial processes makes melt mixing the preferred method. For this technology, there are several laboratory or industrial scale equipment used to disperse the nano-filler homogeneously in the polymer matrix. In this study, a mini compounder with a twin screw design was employed for melt mixing. However, the control factors considered to affect the dispersion state of the nano-fillers were changed and direct melt mixing method was modified to achieve better mechanical and thermal results.

Mixing methods employed for this study are explained in detail in the experimental part. The following list is a short summary of the melt mixing methods and control factors altered during experiments:

- Direct Melt Mixing Method (DM)
 - o 3 minute mixing time (DM3)
 - o 10 minute mixing time (DM10)
- Masterbatch Melt Mixing Method (MMA)
- Solvent Casting Followed by Melt Mixing Method (SC)
- Suspension Addition to Melt Mixing (SA)

Each mixing method has its own advantages and disadvantages respectively. Direct melt mixing method (DM) can be said to be the easiest way to process. However, its ability to meet the dispersion requirement for the nanocomposites of incompatible polymer and filler couples might not be enough. At this point, masterbatch dilution technique (MMA) offers an alternative to direct melt mixing

method. The most commonly encountered masterbatch method is to prepare a concentrated sample by melt mixing in the first extrusion step and then diluting it with the matrix in the second extrusion. In this method, the particles to be dispersed find a chance to encounter with the compatibilizer or the polymer matrix first. In addition, particles are subjected to extrusion more than once which may contribute to their dispersion state. Not only mixing twice, but also high viscosity of the masterbatch (because of high loading) during the first extrusion step may help to enhance the dispersion process (Prashantha et al. 2009). Other advantages of masterbatch mixing method are: easy processing which is similar to direct melt mixing method and more controllable composite production. The main problem that may be encountered in masterbatch processing is the primary aggregates that are formed during the first extrusion step. In such a case, it becomes hard to delaminate them in the second extrusion step, and the process results in a reduction of desired composite properties. Hence, it is important to choose the optimum masterbatch composition that would give sufficient shear stress during extrusion but not result in primary aggregates.

The initial step of masterbatch method can be modified in several ways. In this work, solvent casting method (SC) was used instead of the first extrusion step. Then, the solvent free masterbatch was melt mixed with polymeric material in the second step.

In solvent casting method, the polymer is first dissolved in a solvent, and the filler is added. This method is also called as solvent intercalation method due to the adsorption of polymer onto delaminated layers of clay filler with the help of solvent and ultrasonic stirring. It can be said that this technique employs the capability of the liquid phase to disperse the filler particles better than the solid phase can. During the evaporation of solvent, the clay layers do not collapse back, and they retain their basal spacing. While the solvent molecules are evaporating, the system gains entropy and conformational entropy diminishes which acts as the driving force of the method (Byun et al. 2012). The drawbacks of this method are

use of environmentally unfriendly solvents which complicate the processing and removal of the solvent from the system. In order to stimulate the driving force of the system, all solvent molecules should be removed by applying high vacuum to supply a low conformational entropy.

In the last method, a clay/solvent suspension is simultaneously added to polymer processing extruder via a peristaltic pump (SA). This method utilizes the advantage of liquid phase homogeneity as in solvent casting method and increase the chance of the diffusion of polymer chains between silicate layers. Also, it shares the same environmental disadvantage with solvent casting method. However, high processing temperature abolishes the necessity to use high vacuum drying for solvent removal.

As discussed above each processing technique has its own advantages and disadvantages. Still all of them may provide a homogeneous dispersion of clay particles in the polymer matrix and intercalation of the silicate layers. Effects of different processing methods on morphological, mechanical and thermal properties of PLA/Halloysite based composites are given in detail in the following parts.

4.2.1 X-Ray Diffraction Results

Investigating the position, shape and intensity of the basal reflection from the clay layer makes XRD analysis the best way to identify the structure of nanocomposite (Alexandre and Dubois 2000). All clay mineral containing composites are monitored with this analysis to see if there is an increase in the basal spacing between silicate layers.

Clay minerals are hydrous aluminum silicates which are classified as phyllosilicates or layered silicates. These mineral groups are generally subjected to natural isomorphic substitution within the silicate layers. During this

substitution negative charges are generated owing to the replacement of Al^{+3} by Mg^{+2} or by Fe^{+2} , or Mg^{+2} replaced by Li^{+} . Some cations, such as Na^{+} , Li^{+} or Ca^{+2} , are positioned between the layer galleries to balance these negative charges (Tjong 2006, Pethrick 2000). This characteristic of layered silicate is not observed for Halloysite mineral. Owing to absence of isomorphic substitution, cations or anions cannot occupy the space between the layers. Instead, hydrogen bonding between the hydroxyl groups in the octahedral sheets and oxygen in the tetrahedral sheets of the adjacent layers hold the layers together. Hydroxyl and oxygen linkages may be assumed to favor the compatibility between silicate and polar PLA polymer couple. But, for composites prepared by DM method this assumption becomes invalid as can be understood from un-changed basal spacing of the clay minerals shown in Figure 4.4. Instead, there is a small right shift in the 7.2 Å basal peak, which indicates a reduction of the gap. Although the XRD pattern broadens and its intensity decreases as the clay content increases, shift of peak to the higher 2theta values represents a micro filled composite formation with lower surface area compared to nanocomposites and nominal level of interaction between filler and polymer (Ray and Okamoto 2003, Mark and Kroschwitz 2003). In this type of composites, layered silicates do not function as nano-structured fillers and do not exfoliate and/or intercalate with polymer chains. Instead, they act as if they are micro fillers which have no dimension in the order of nanometer.

In the study performed by Touny and his co-workers (Touny et al. 2010), PLA/HNT composites prepared by electro-spinning method resulted in entire disappearance of HNT peaks at 5wt% HNT content. This finding was interpreted as HNT loading may not be enough to diffract XRD beam, or PLA chains had diffused between the layers and caused the HNT particles to lose their parallel stacking and become disordered. Among these interpretations, the first one seems more meaningful since the peaks become visible at 10wt% HNT loading and show an ordered structure for the composites with basal peak around 12°. Unchanged basal spacing for PLA/HNT composites was also observed in the

study performed by Liu (Liu, Zhang and Zhou 2013). According to XRD analysis of this study, the interlayer spacing remained the same and PLA chains did not enter the clay gallery. It was suggested that the polymer chains might have been blocked by hydrogen bonds positioned between the layers instead of cations. However, the disappearance of the reflection of HNT around 20° was emphasized. The presence of the interaction of polymer chains with filler particles was suggested, and the disappearance of the reflection was attributed to the preferential orientation of nanotubes in the composites like oriented tile patterns that was caused by shear force created during melt mixing. In this study, HNT peaks above 34° and each impurity peak completely disappeared, whereas there were still traces of the presence of peaks around 20° and 25° . Hence, to understand the interaction between PLA and HNT and the “tile oriented” structure, it is important to check the TEM results of the composites.

In this thesis, Nanoclay is the reference HNT used to check the results obtained by using local ESAN HNT. Both minerals have the similar chemical composition as can be understood from the XRD pattern of Nanoclay which perfectly resembles to that of ESAN HNT, except more intense peaks that were observed for Nanoclay. Although there is no chemical difference between these two minerals, their particle sizes are different from each other. Both minerals have the similar inner and outer diameter, in the range of 20 – 70 nm, whereas Nanoclay HNT has a greater aspect ratio (L/D ratio) compared to ESAN due to its greater length. This size difference may explain the better reflection and hence more intense peaks observed for Nanoclay sample as can be seen from Figure 4.5 with much more visible peaks around 12° and 25° . As in the case of PLA/ESAN HNT composites, there is no basal peak left-shift that would have indicated intercalation in PLA/Nanoclay composites. Also, change in clay loading from 3 to 10wt% does not affect the dispersion state of particles in the polymer matrix. But, increase in clay amount resulted in a broader pattern as in the case of PLA/ESAN HNT composites. Effects of these two HNT minerals on thermal and mechanical properties of PLA composites are further discussed in the following sections.

However, it can be assumed that their similar morphological structures may give rise to similar composite properties. Impurity peaks are also become invisible for Nanoclay HNT, whereas peaks beyond 34° are slightly explicit especially for composite containing 3wt% Nanoclay.

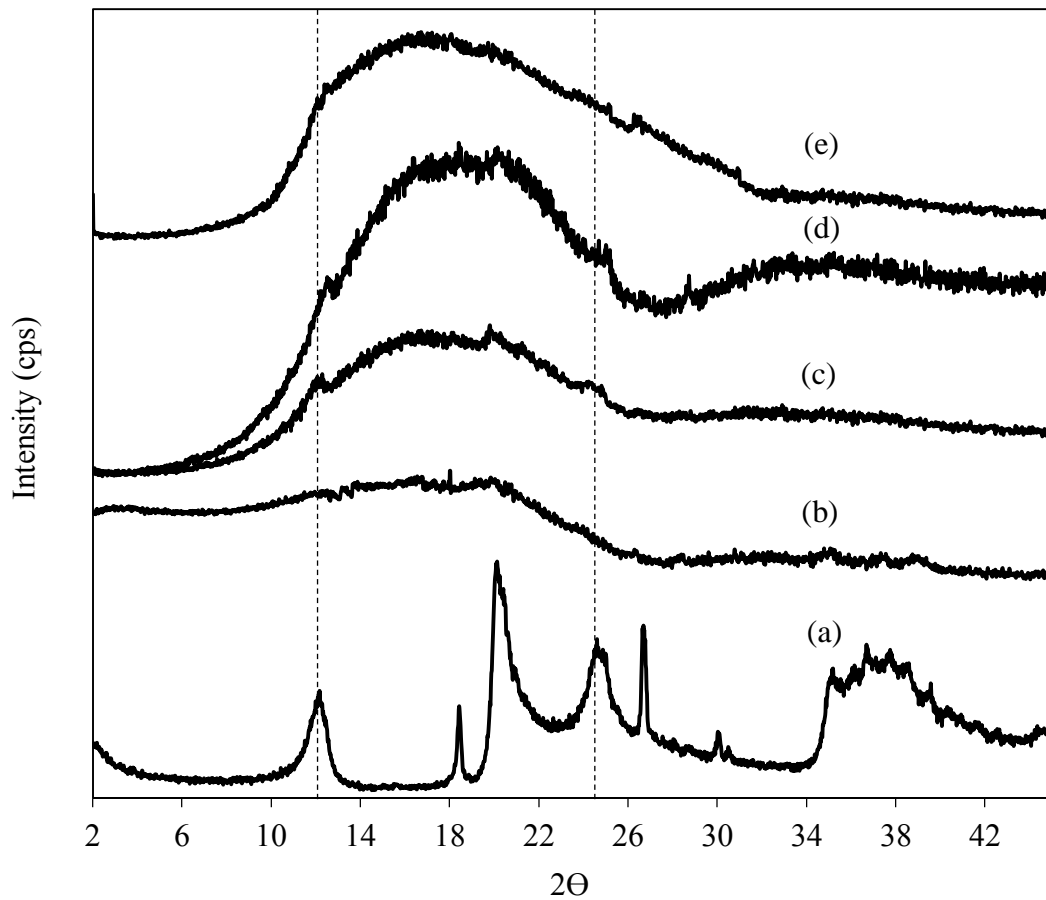


Figure 4.4. XRD pattern of PLA/ESAN HNT composites prepared by DM3 method; (a) ESAN HNT, (b) PLA/10wt% ESAN HNT, (c) PLA/5wt% ESAN HNT, (d) PLA/3wt% ESAN HNT, (e) Neat PLA

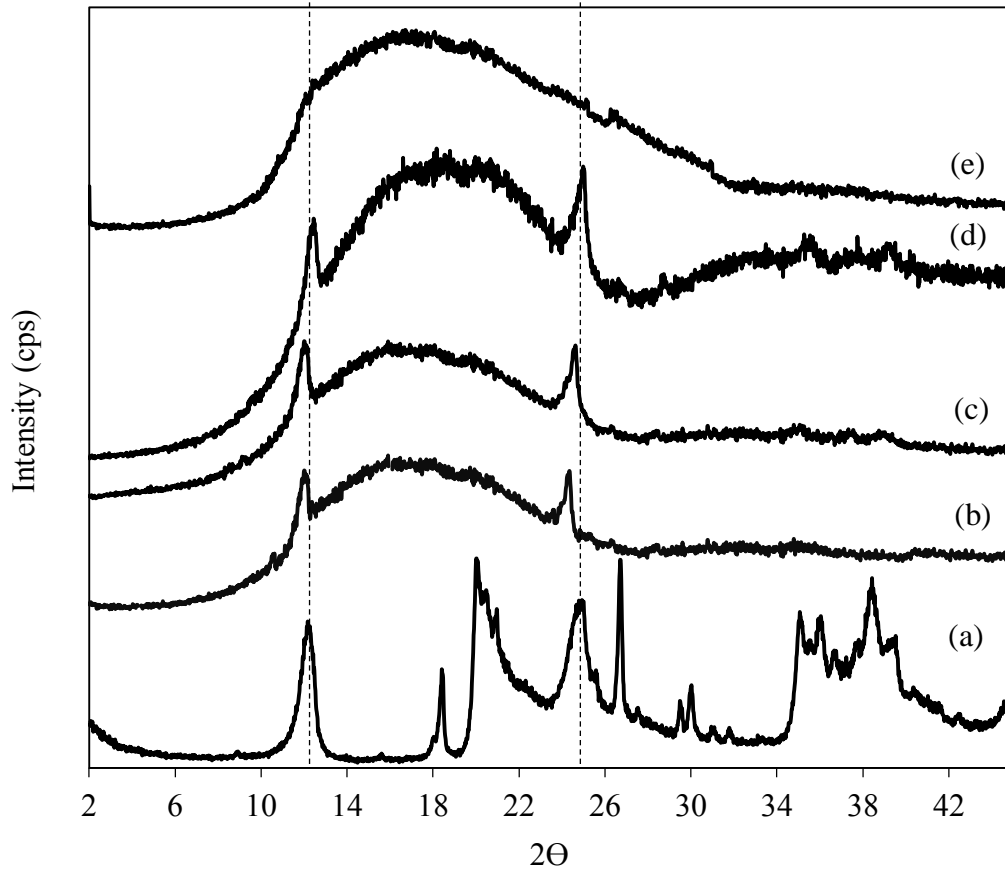


Figure 4.5. XRD pattern of PLA/Nanoclay HNT composites prepared by DM3 method; (a) Nanoclay HNT, (b) PLA/10wt% Nanoclay HNT, (c) PLA/5wt% Nanoclay HNT, (d) PLA/3wt% Nanoclay HNT, (e) Neat PLA

In addition to unchanged basal spacing of HNT minerals, the crystalline structure of the PLA remains unchanged with mineral addition. Neat PLA displays only a broad scattering reflection around 16° indicating a low crystalline fraction which may be formed during the cooling step of the molding process (see Figure 4.4 and Figure 4.5). HNT minerals do not cause a significant shift in the reflection peak, and this semi-crystalline structure is preserved with inclusion of the minerals

regardless of the nature of the clay. However, with increasing clay loading the patterns get broader around PLA reflection angle for both types of HNT. This may be attributed to the formation of less perfect crystals and hence lowered crystalline fraction (Carli, Crespo and Mauler 2011). These findings will be investigated and further discussed in thermal and morphological properties parts of the dissertation.

Even if intercalated and/or exfoliated structures could not be obtained, dispersed particle homogeneity should be improved in conventional composites to achieve better physical composite properties. One of the ways to provide a better dispersion is to optimize the processing method and conditions. In this study, four different processing methods were tried. The first one is the previously mentioned DM3 method. As mentioned, this method does not give rise to fine dispersion of clay particles in PLA matrix which may be due to insufficient shear stress during mixing. There are several control parameters, such as temperature, screw speed, screw orientation, mixing time etc. for direct melt mixing (DM) method that can be altered to achieve desired properties. For this study, all parameters were kept constant, except for the mixing time. To provide high shear, time elapsed for composite mixing was increased from 3 to 10 minutes and called as DM10 method. XRD pattern of PLA/5wt% ESAN HNT composites prepared by DM10 method can be seen from Figure 4.6 showing no improvement in intercalation or particle dispersion in polymer matrix. Also, in this method PLA matrix faces with thermal degradation risk during the process. However, its crystalline structure does not change as in DM3 method.

A previous work shows the contribution of HNT mineral on the mechanical properties of Poly(lactic acid) composite prepared by masterbatch dilution method (Prashantha et al. 2013). According to study; although there is a sharp interface between HNT and PLA, and there are many debonded nanotubes that are pulled out from the polymer matrix, the composites display good dispersion, especially at 2 and 4wt% clay loadings. To see the effect of masterbatch mixing on

PLA/ESAN HNT composites, 30wt% HNT containing masterbatch samples were prepared and then they were diluted with PLA to 5wt% (MMA Method). Since the samples were subjected to extrusion more than once, it can be assumed that the higher shear force exerted to break-up the clay agglomerates may facilitate the intercalation process (Homminga et al. 2005). According to this assumption, formation of nanocomposite may depend on favorable chemical compatibility between its constituents, but, there should be significant shear force influence to set apart the clay layers from each other. However, for this study the compatibility between PLA and HNT, or shear force applied during masterbatch mixing may not be adequate to insert the PLA chains between rolled silicate layers as can be seen from Figure 4.6.

Instead of increasing mixing shear force by applying several extrusion steps, processes that benefits from the better particle dispersion capability of a liquid phase could be a solution to dispersion problem. The third and fourth methods used in this study employ a solvent to disperse HNT particles. In the third method, solvent was used to prepare a PLA masterbatch which was diluted with PLA in the following extrusion step (Solvent Casting Followed by Melt Mixing Method - SC). Although melt mixing offers a better intercalation of silicate layers, solvent casting may prevent the formation of clay agglomerates. In addition, solvent casting may decrease the degradation risk addressed in two step extrusion process (Finnigan et al. 2004). However, no improvement was observed both in intercalation state and the dispersion state of the clay particles (see Figure 4.6). Solvent casting method is known to be generally suitable for polymers with little or no polarity (Ray and Okamoto 2003). Polar characteristic of PLA and HNT may be detrimental to achieve the desired success in particle dispersion with SC method.

In contrast to third method, HNT suspension was directly injected to extruder in process in the fourth method (Suspension Addition to Melt Mixing - SA). This method also did not also give rise to intercalated structure formation as well.

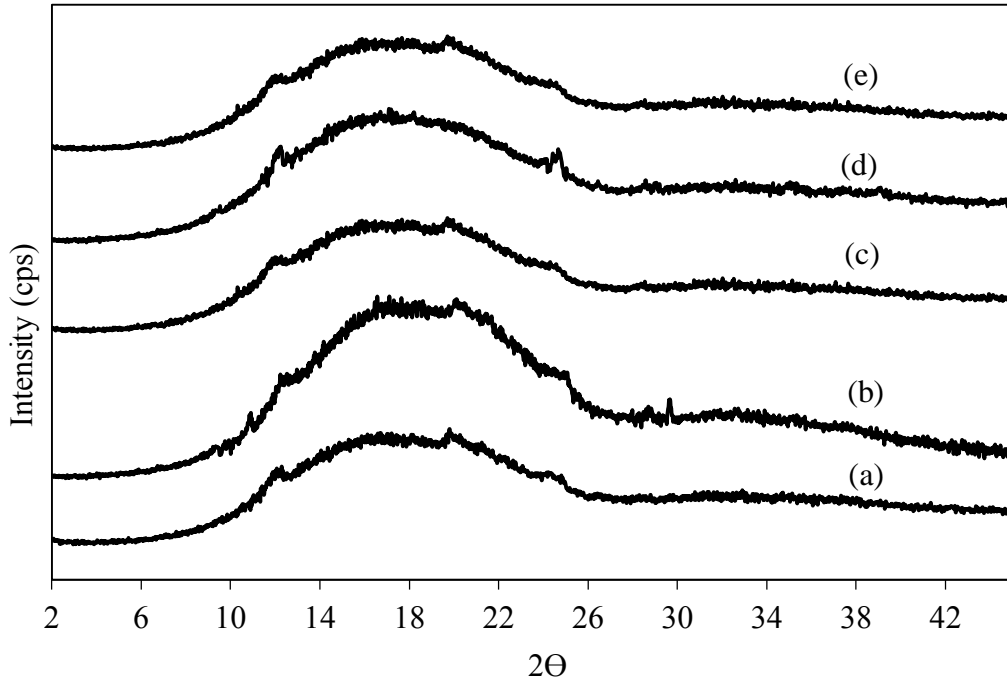


Figure 4.6. XRD pattern of PLA/5wt% ESAN HNT composites prepared by different processing methods; (a) Direct melt mixing for 3 minute (DM3), (b) Direct melt mixing for 10 minute (DM10), (c) Masterbatch melt mixing (MMA), (d) Solvent casting followed by melt mixing method (SC), (e) Suspension addition to melt mixing (SA)

For nanocomposite formation, an exfoliated or at least an intercalated structure should be achieved. However, this formation could not be observed for PLA/HNT composites processed by different methods. Hence, it can be said that the compatibility between the constituents is not enough and should be enhanced by using a third matrix as compatibilizer or by the modification of HNT minerals to provide a better interaction between polymer and filler. These trials are mentioned in the following sections. In the continuation of this section morphological, mechanical and thermal properties of the PLA/HNT composites are also given.

4.2.2 Scanning Electron Microscopy

The impact fracture surfaces of the PLA/HNT composites were analyzed by SEM to observe their morphological characteristics. Brittle characteristic of PLA resulted in straight crack propagation lines rather than tortuous ones and a smooth fractured surface as can be seen from Figure 4.7. This property enhances further growth of propagation lines after initial crack formation and makes it easier to fracture PLA with only a small amount of energy (Nielsen 1962, Chow et al. 2013). With addition of HNT, the smooth surface of PLA was roughened in some parts indicating an interphase formation between PLA and HNT. However, the improvement in surface roughness was not enough to have a prominent effect on stress concentration.

In addition to XRD analysis, SEM is a good method to observe the dispersion state of clay minerals in polymer matrix, and also it is a chance to understand the changes experienced by PLA in mechanical and thermal performance by the addition of HNT mineral. On the contrary to XRD results, Figure 4.8 shows a fine dispersion of HNT minerals with a distribution below 1 μ m particles. Well dispersion could be attributed to weak tube-tube interactions yielding an edge-to-edge or edge-to-face zigzag structure that made them easy to be dispersed in matrix by shear forces. Interaction between PLA and HNT via hydrogen bonding might have also caused a fine dispersion of particles (Liu et al. 2013, Ismail et al. 2008). Instead of a homogeneous distribution, gigantic agglomerates which attain a particle size of 20 μ m dominated the microstructure.

There may be several causes leading to agglomeration. Surface incompatibility and insufficient shear during processing are the most common ones among them. Well distributed HNT particles in addition to agglomerated particles, may lower the doubt about the incompatibility between PLA and HNT, and may lead one to consider insufficient shear stress. Hence, in the first part of the study different processing techniques were performed to increase shear stress or benefit from the

distributive effect of liquid phase. However, no significant improvement could be obtained on the morphology and also on the mechanical properties of the composites. This result might show that there is still insufficient shear and it should be made better by different techniques, or PLA and HNT are not compatible enough to yield better physical properties.

In the study performed by Liu and his co-workers an interesting dispersion is observed by SEM which shows that only end faces (visible circular dots) of the nanotubes in the fracture surface (Liu et al. 2013). This was attributed to the preferential orientation of nanotubes in the composites like oriented tile patterns formed by shear force created during melt mixing. However, 3-dimensional dispersion can be clearly seen in this study with both end faces (dot structures) and side faces (ribbon structures) in the fracture surface. To achieve the mentioned tile pattern does not seem to be possible with the materials and processing techniques used in this part of the study.

The elongated structure of the HNT can be clearly seen as ribbon shapes from the SEM micrographs shown in Figure 4.8. They are observed to be covered by the matrix and pulled out from the matrix indicating an interaction between HNT surface and PLA was formed (Hedicke-Hochstotter et al. 2009b). Although there is an interaction between the constituents, compatibility and better physical properties could not be obtained. A sharp interface between PLA and HNT, and some debonded nanotubes were also formed, instead of embedded ones into matrix due to this inadequate compatibility, which indicates a weak interface between PLA and HNT. Debonded HNT particles might be the second reason of unimproved mechanical properties, in addition to the agglomerated structure.

During fracture many cracks are formed inevitably and these nonlinear micro-cracks tend to grow until they interfere with each other. In some parts of the PLA/HNT composites the elongated hollow tubular structures connect the two surfaces of these cracks due to large aspect ratio of HNT mineral. Their function as bridge between the micro-cracks generally contribute to the toughening

mechanism by stabilizing the micro-cracks and stopping their development into large and harmful cracks, and results in better mechanical properties (Ye et al. 2007, Deng et al. 2008). These kinds of observations suggest a strong adhesion between the polymer matrix and filler particles.

However, PLA/HNT composites prepared in this study contain many agglomerates as mentioned above. These clusters resemble micro sized rigid inclusions. When they confront with a crack they cause plastic deformation and relatively easier fracture of the material. Hence, the bridges formed between the cracks were suppressed by the agglomerates and did not facilitate an improvement in mechanical properties.

In addition, broken bridging nanotubes formed during crack opening are not observed with x2000 magnification in SEM analysis, however there should be some due to the PLA/HNT interaction. According to the study performed by Ye et al. a sword and sheath structure is formed after the breakdown of the tubes (Ye et al. 2007). Also, after the fracture of outer layers, the inner layers of the tubes are pulled out due to weaker Van Der Waals action among nanotubes, compared to their bonding strength with the matrix. Unnoticeable fractured nanotube structures might be the result of low resolution of SEM analysis or insufficient bonding strength between HNT and PLA.

As mentioned in the XRD results part, intercalated and/or exfoliated structures could not be achieved for the PLA/HNT composites. However, it is expected to obtain at least inclusion of PLA chains into the lumen of the nanotubes and hydrogen bonding formation. In homogeneously distributed parts of the sample, integrity of this assumption could be observed. However, HNT rich phase formation and strong tendency for the agglomeration in many parts exhibit the non-inclusion of PLA chains.

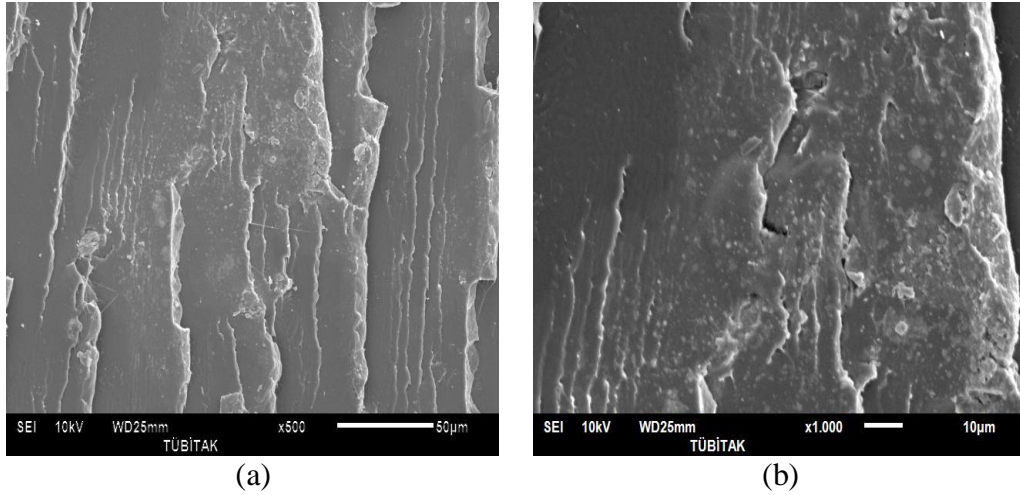


Figure 4.7. SEM micrographs of pure PLA subjected to 3 minute mixing

SEM micrographs of PLA/HNT composites containing Nanoclay are also given in Figure 4.8. A much more fine distribution is observed for the imported HNT containing composites compared to the ones prepared with local ESAN HNT. Since both minerals have the same chemical structure, the better distribution might be caused by the higher aspect ratio of Nanoclay. As can be seen from the SEM micrographs, the amount of agglomerated structures is less in PLA/Nanoclay composites. In addition, visible end faces of the nanotubes in the fracture surface are more prominent for imported clay mineral. However, the better distribution did not give rise to a significant enhancement of mechanical properties which will be discussed in the following section.

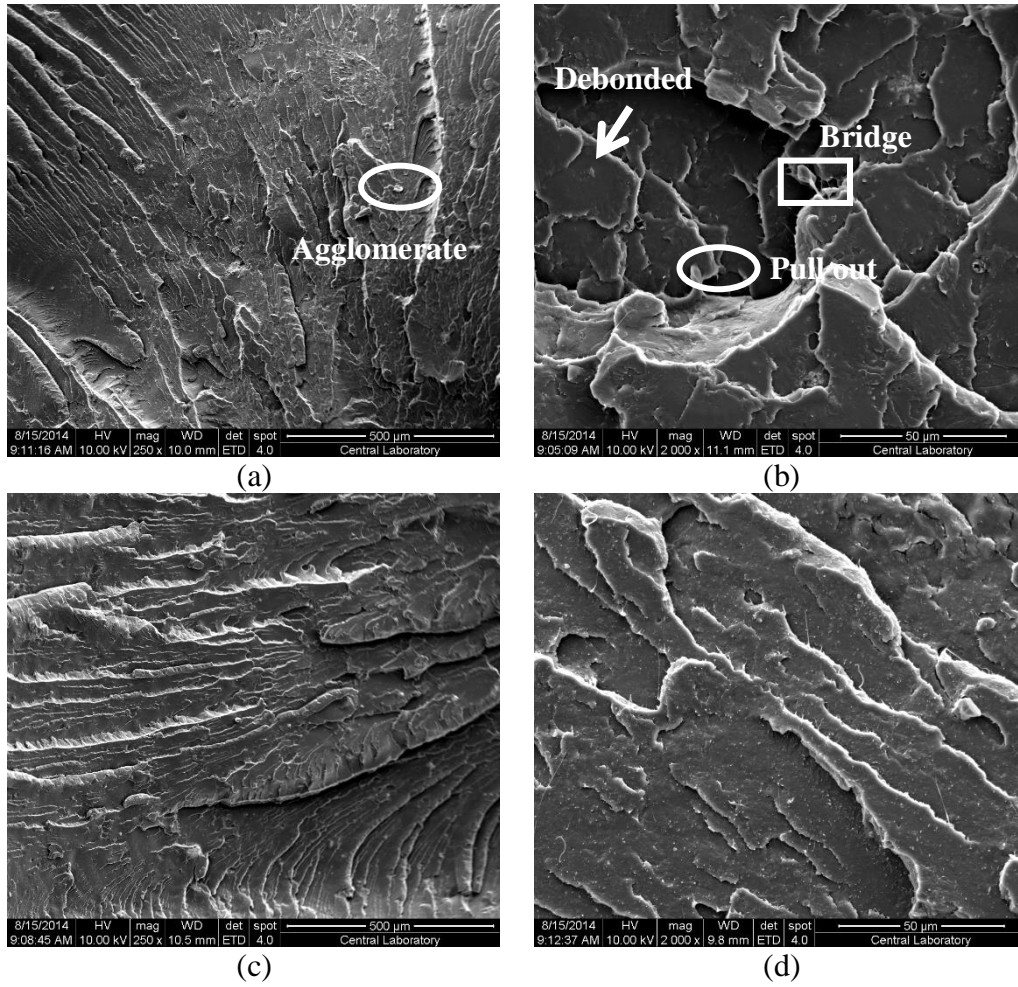


Figure 4.8. SEM micrographs of PLA based composites containing 5wt% HNT and prepared by DM3 method; (a) ESAN 250x, (b) ESAN 2000x, (c) Nanoclay 250x, (d) Nanoclay 2000x

4.2.3 Transmission Electron Microscopy

In order to validate the results obtained in XRD analysis and to observe the internal nanometer scale morphological characteristics transmission electron microscopy (TEM) was used. The visible black spots in Figure 4.9 represent the HNT particles. For well dispersed structures as shown in Figure 4.9-a, these spots appear separately, and the tubular structure of HNT becomes more visible. However, it is hard to observe intercalation and/or exfoliation for these tubular particles.

For PLA/HNT composites prepared with direct melt mixing method well dispersion can be seen in many parts of the sample (Figure 4.9-a). The tubular particles do not form an exfoliated structure, while their basal spacing can be enlarged to host polymer chains. This formation is generally attributed to the well interaction between polymer and clay particles. Although no intercalation can be observed for PLA/HNT composites, well distributed sections are clear. Especially, edge-to-edge or edge-to-face zigzag structures are noticed as can be seen from Figure 4.9-b. Hence, it can be said that the interaction between PLA and HNT is not enough to create a well distribution. However, the weak interaction between the nanotubes enforces the distribution.

In addition to well distributed clay particles, many agglomerates are seen from Figure 4.9-c. These agglomerated structures mainly dominate the morphological characteristics of the composite and result in recessed physical properties as will be discussed in the following part.

One more observation can be mentioned based on the TEM micrographs. According to this observation, instead of a tile pattern, a 3-dimensional distribution of the clay particles in the matrix can be seen.

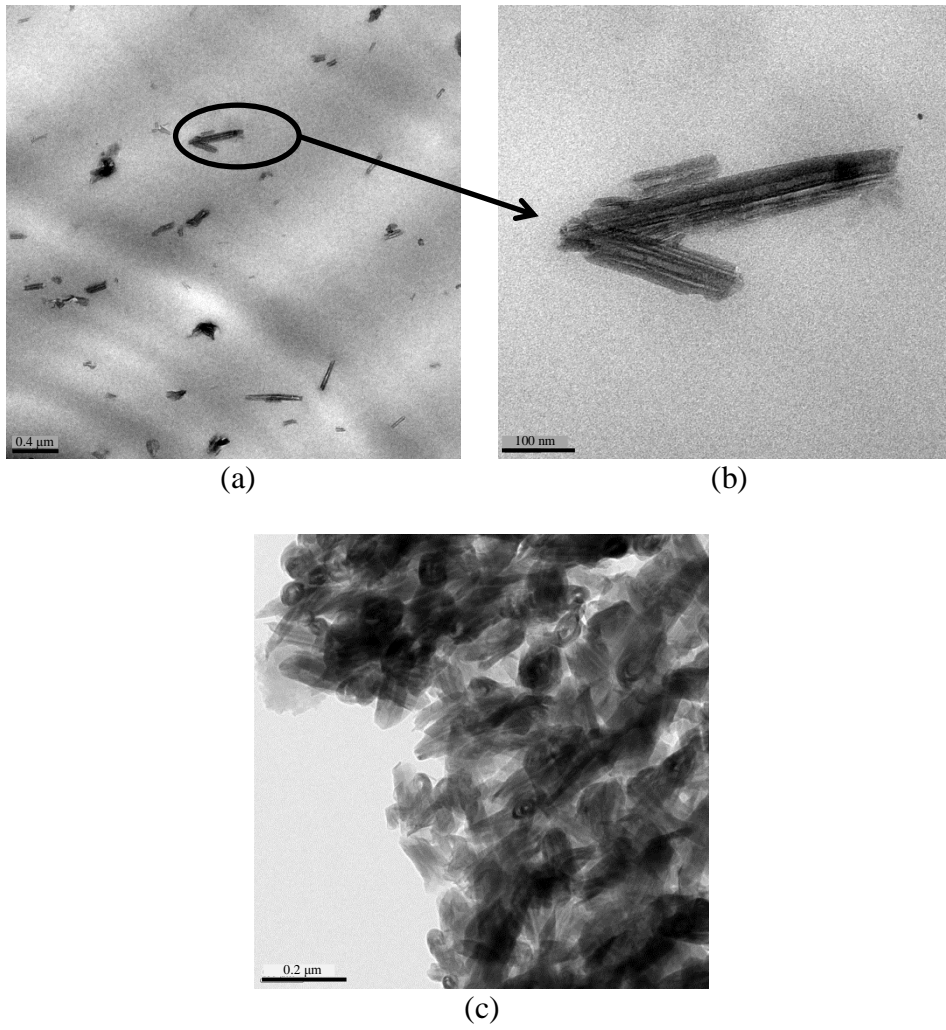


Figure 4.9. TEM micrographs of PLA/5wt% ESAN HNT composites; (a) Scale bar is 0.4μm, (b) Scale bar is 100 nm, (c) Scale bar is 0.2μm

4.2.4 Tensile Properties

Mechanical analysis is the most commonly referenced method to understand the physical properties of the polymeric materials. Especially, typical tensile tests are performed to obtain the response of the composites to the applied force and the extent of elongation they experience before failure. A typical stress-strain curve for PLA used in this study can be seen from Figure 4.10. The smooth surface of PLA enables rapid crack formation at small deformations and results in brittle characteristics. With a tensile strength of 63.5 MPa at yield point and an elongation of 16% at fracture, PLA found commercial applications in packaging market. In addition, biodegradable PLA represents a stronger and durable feature compared to many brittle polymers by displaying a yield in its stress-strain curve. However, PLA should be improved in terms of toughness to widen its usage area.

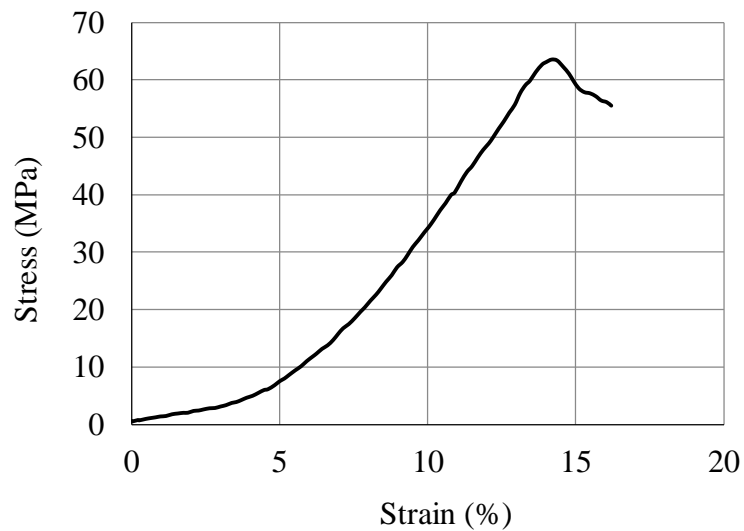


Figure 4.10. Stress-strain curve of pure PLA

Tensile tests were performed to PLA/HNT composites to obtain the tensile strength and strain at break values. To achieve the desired mechanical properties, it is necessary to obtain a good dispersion of filler material in the polymer matrix. Especially for nanocomposites, a full dispersion with intercalated and/or exfoliated structures is required to obtain an enhancement in mechanical properties. As mentioned in the XRD results part, inclusion of raw HNT particles into PLA matrix does not give rise to the formation of nanocomposites, although there is an interaction between them.

The effect of clay loading and clay type on the tensile properties (tensile strength and strain at break values) of PLA based nanocomposites are shown in Figure 4.11 and Figure 4.12. Some of the previous PLA/HNT studies mentioned an evolution in the strength of the nanocomposites up to a clay loading, and beyond that loading no further increase in tensile strength (Liu et al. 2013, Murariu et al. 2012). In contrast to these studies, in this study no enhancement was achieved in tensile strength independent of clay loading and clay type. This may be attributed to both the absence of an intercalated structure and 3-dimensional distribution of clay particles instead of a tile pattern distribution.

Moreover, a slight reduction was observed for each and every composite. Even if a nanocomposite is not formed, a slight enhancement is expected in the strength and stiffness of the conventional composites containing high aspect ratio and high strength fillers. However, the opposite of this case was observed and strength of the composites declined (Stiffness of the materials are investigated in dynamic mechanical analysis part of the dissertation). The reduction in strength can be a result of agglomerates attaining particle size of 20 μ m that act as stress builder and trigger catastrophic failure of the material. On the other side, debonded nanotubes might also cause the reduction in tensile strength by creating an air void during the fracture.

Compared to ESAN HNT, Nanoclay displays a relatively higher tensile strength. Larger aspect ratio and more homogeneous dispersion of the Nanoclay is the

reason for the higher strength. Especially, 5wt% clay loading can be said to be the optimum filler amount. However, no improvement is observed in the strength of the PLA for both types of clays.

On the contrary to the reduction in strength of the PLA/HNT composites, the elongation at break values show a slight improvement. The bridging effect of nanotubes between the micro-cracks can be deemed to be the factor that is contributing to the toughening mechanism. Indeed, the fracture of these bridges during tensile tests contributes to the enhancement in elongation at break by absorbing extra energy. Specially, 5wt% Nanoclay containing composite yields a 13% improvement in its strain at break value. However, this effect of nanotubes disappears at high clay loading (at 10wt%) probably due to growing agglomerate size distributed in the polymer matrix.

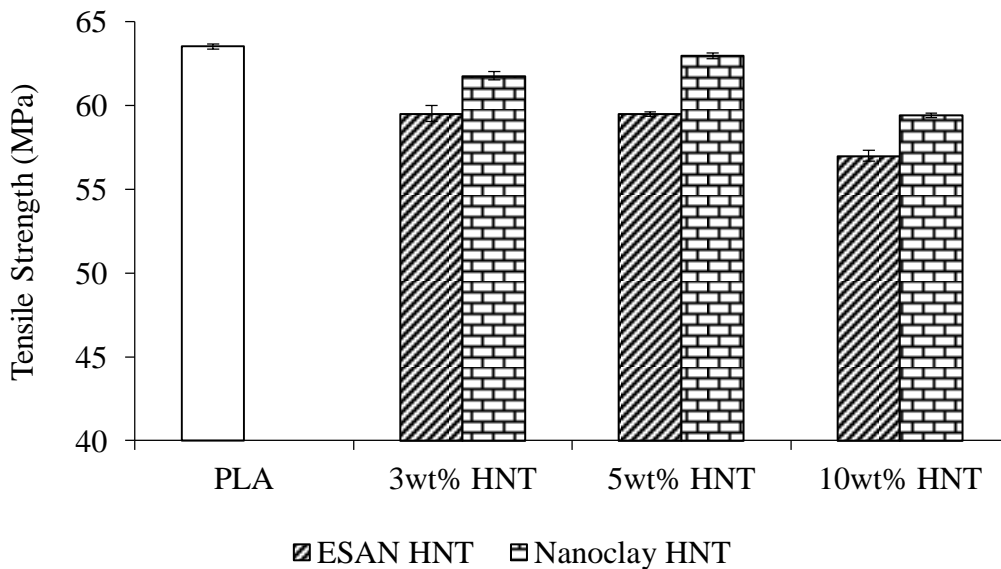


Figure 4.11. Tensile strength (MPa) of PLA/HNT based composites prepared by DM3 method

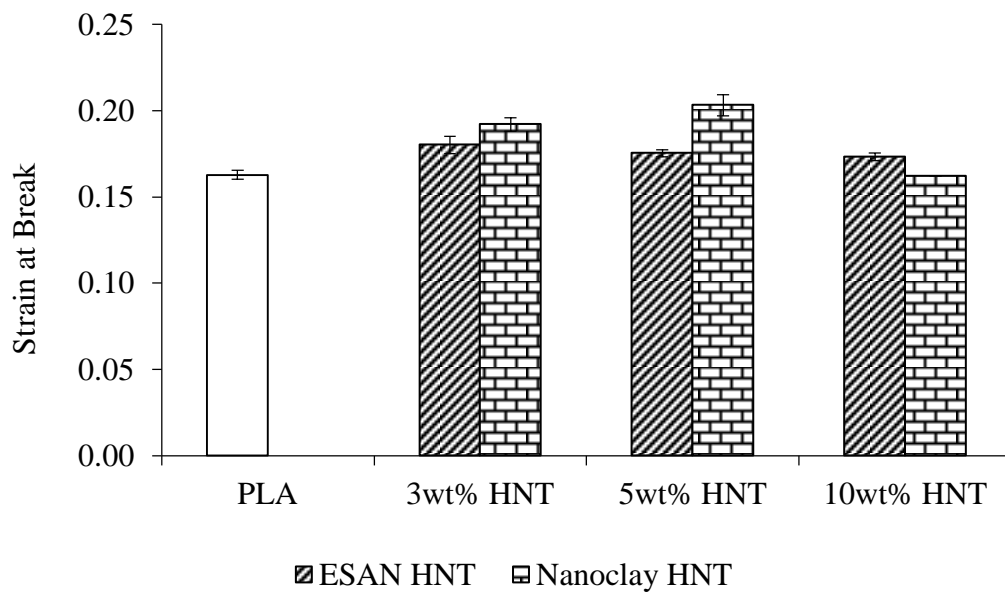


Figure 4.12. Strain at break of PLA/HNT based composites prepared by DM3 method

The results obtained for composites prepared by DM3 method were discussed previously. The comparison between the tensile properties of these composites and the composites prepared by other processing techniques are given in Figure 4.13 and Figure 4.14. Although there is still a reduction in the strength of the composites, the processing techniques with the increased shear stress show a slightly higher strength. Especially, melt mixing method for 10 minute shows a good dispersion as can be understood from the strength value that is close to that of PLA. However, this higher strength results in sacrifice from the elongation at break, and a material similar to PLA in terms of mechanical properties is obtained.

For the composites prepared by SC and SA methods, the desired effect of dispersive liquid phase on the strength of the composites could not be achieved. Instead, plasticization yielding an increase in strain values, 43% for SC method and %68 for SA method, was observed for PLA/5wt% ESAN composites. In addition, this plasticization caused approximately 8% reduction in tensile strength for the SA method. Solvent molecules are responsible for this result. In general, the lower the molecular weight, the higher is the plasticizing effect. Hence, it can be said that this response of PLA is due to the plasticizing effect of the solvent molecules on the polymeric materials which increases the flexibility of the macromolecule chains (Halász and Csóka 2013, Leng, Du and Lu 2010).

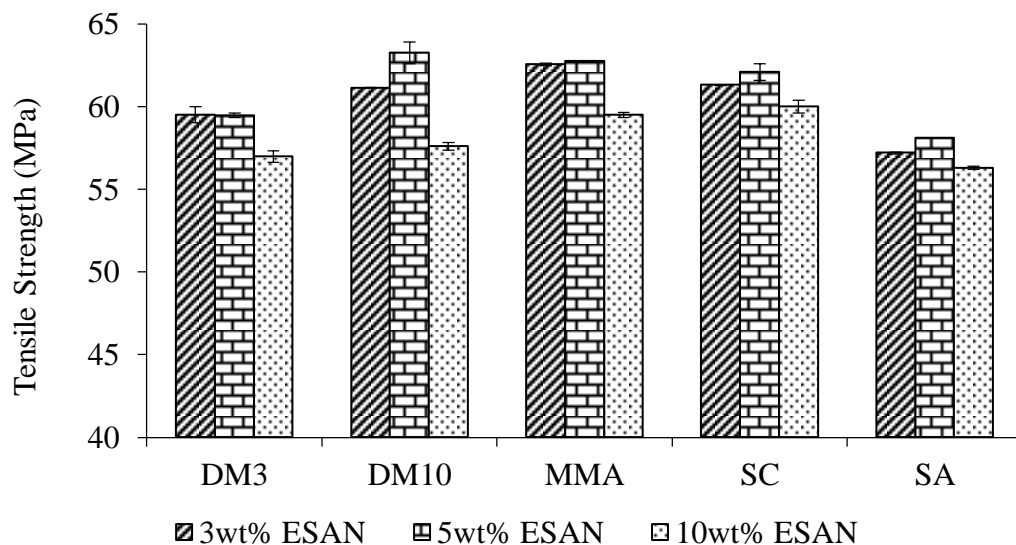


Figure 4.13. Effect of different processing techniques on the tensile strength (MPa) of PLA/ESAN HNT composites (DM3: Direct Melt Mixing-3 minute, DM10: Direct Melt Mixing-10 minute, MMA: PLA Masterbatch Melt Mixing, SC: Solvent Casting Followed by Melt Mixing Method, SA: Suspension Addition to Melt Mixing)

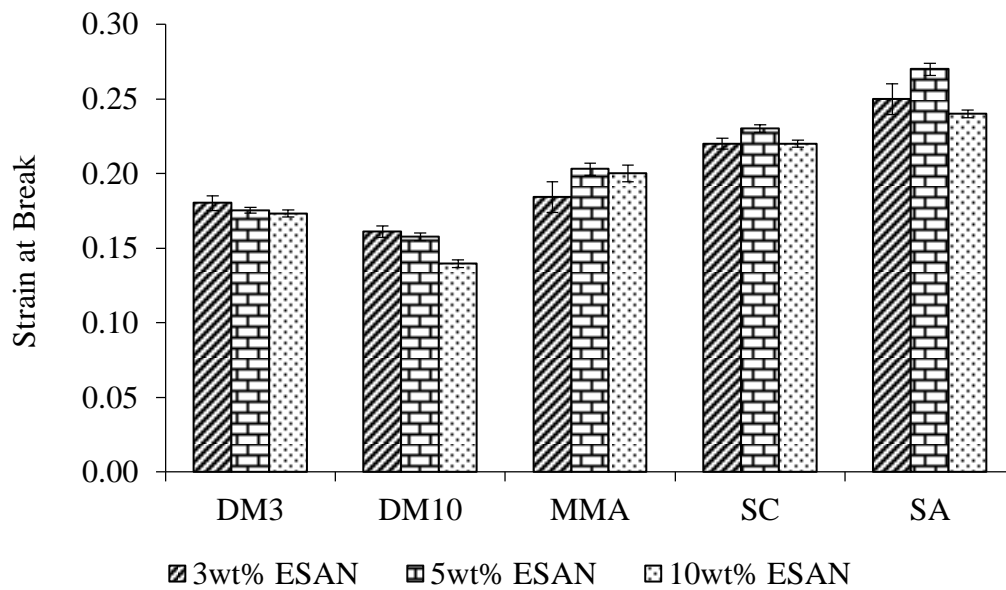


Figure 4.14. Effect of different processing techniques on the strain at break values of PLA/ESAN HNT composites (DM3: Direct Melt Mixing-3 minute, DM10: Direct Melt Mixing-10 minute, MMA: PLA Masterbatch Melt Mixing, SC: Solvent Casting Followed by Melt Mixing Method, SA: Suspension Addition to Melt Mixing)

Effect of different processing techniques on the composites containing reference HNT, Nanoclay, are shown in Figure 4.15 and Figure 4.16. As mentioned previously in DM3 method results, Nanoclay containing composites display slightly higher strength and elongation at break values than local ESAN HNT containing composites do. The same difference between shear stress increasing methods (direct melt mixing for 10 minute-DM10 and PLA masterbatch melt mixing-MMA) and solvent employing methods (solvent casting-SC and suspension addition-SA) observed for ESAN HNT based composites are also observed for Nanoclay containing ones. SC and SA methods for 5wt% clay

containing composites give 56% and 75% improvements in strain at break values respectively.

Among the processing techniques MMA takes attention in terms of stabilizing the strength of the material while improving the flexibility and hence elongation at break. For applications which require a lower strength and a slightly better strain, SA method take attention. However, complexity of the SA method compared to simple melt mixing method restricts the use of this method. In addition, the main aim of nano-fillers is to enhance the strength of composites, while plasticizing can be achieved much more easily by using a third material which is called compatibilizer, impact modifier or plasticizer depending on the intended use.

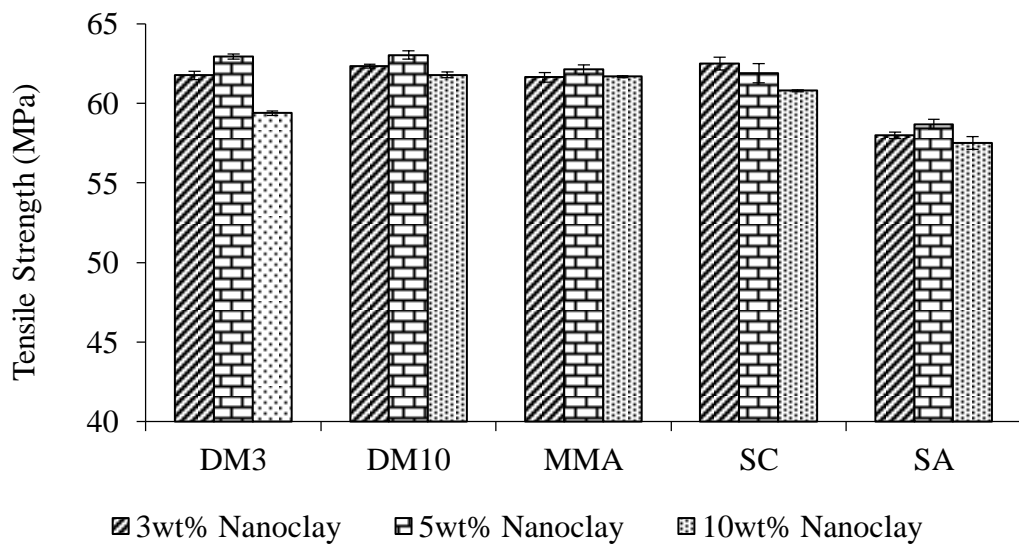


Figure 4.15. Effect of different processing techniques on the tensile strength (MPa) of PLA/Nanoclay HNT composites (DM3: Direct Melt Mixing-3 minute, DM10: Direct Melt Mixing-10 minute, MMA: PLA Masterbatch Melt Mixing, SC: Solvent Casting Followed by Melt Mixing Method, SA: Suspension Addition to Melt Mixing)

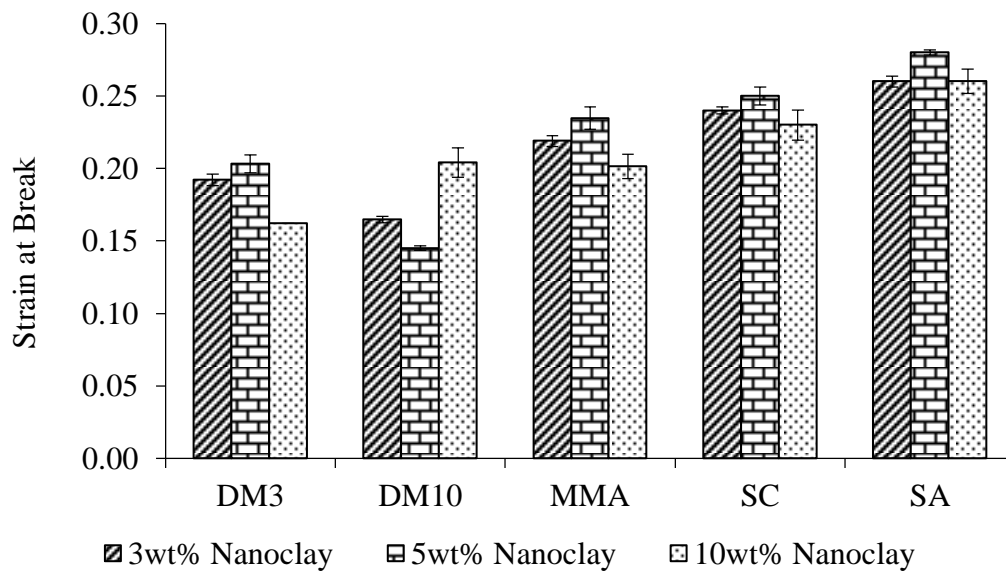


Figure 4.16. Effect of different processing techniques on the strain at break values of PLA/Nanoclay HNT composites (DM3: Direct Melt Mixing-3 minute, DM10: Direct Melt Mixing-10 minute, MMA: PLA Masterbatch Melt Mixing, SC: Solvent Casting Followed by Melt Mixing Method, SA: Suspension Addition to Melt Mixing)

4.2.5 Impact Results

One of the best methods to understand the change in the toughness of a material is to measure the energy it can absorb during a sudden impact. This method is called as impact testing which is a standard method of determining the impact resistance of materials. In that sense, izod impact tests were performed for PLA and its composites based on HNT mineral. Impact strength results obtained from izod tests can be seen from Figure 4.17. PLA is a brittle material with an impact strength value of 12.3 kJ/m².

As mentioned in tensile tests results in the previous section, HNT mineral exhibits similar effects of a plasticizer owing to the bridging effect of nanotubes between the micro-cracks. These bridges cause extra energy absorption during tensile test, and by the help of this effect elongation at break values increase up to 5wt% clay loading. Then, elongation at break values start to decrease due to large agglomerates. However, plasticizing effect of HNT is not enough to improve the toughness of the PLA and impact strength remains around a value of 12 kJ/m². In addition, the results obtained for both clay types; ESAN HNT and Nanoclay HNT, are similar to each other. At higher clay loading which is greater than 5wt% impact strength of the composites decreases approximately by 15%.

According to study performed by Liu and his co-workers, addition of HNT improves the impact strength in contrast with the results obtained in this study. This improvement is around 70% at 10wt% clay loading. Beyond that loading, impact results start to decrease and reach to values lower than that of neat PLA (Liu et al. 2013). This difference between the two studies can be attributed to better distribution of clay minerals obtained in Liu's study. However, for this study large agglomerates which attain particle size of 20µm dominate the microstructure, although there is a homogeneous distribution. For both studies strength values decrease at higher loadings. This reduction in toughness of the PLA/HNT composites with relatively high HNT loading should be attributed to the weakened interfacial interactions at high loadings of nano particles.

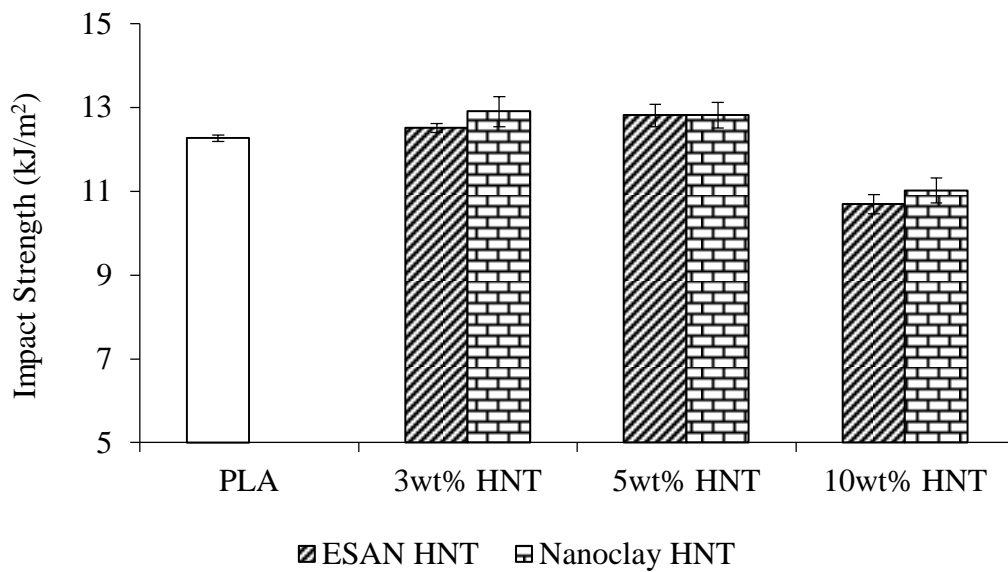


Figure 4.17. Impact strength (MPa) of PLA/HNT based composites prepared by DM3 method

4.2.6 Dynamic Mechanical Analysis (DMA)

Like other polymeric materials PLA displays a viscoelastic characteristic for which the relationship between stress and strain depends on time, or on frequency in the frequency domain. This viscoelastic nature of the PLA/HNT composites was investigated by the help of dynamic mechanical analysis (DMA) in which the dynamic response to periodic forces was measured. For loading, axial tension option was used in this study and stress-strain relationship information was monitored while changing the temperature. Temperature range was kept between room temperature and 150°C during the experiments to observe cold crystallization behavior of the samples in addition to glass transition.

As can be seen from Figure 4.18, for the semi-crystalline PLA storage modulus (E') undergoes a gradual decrease up to 50°C, then rapidly drops and attains a minimum value at 65°C. Further increasing the temperature above 90°C results in a slight rise in the value of E' owing to the enhancement of the rigidity of the sample with cold crystallization process. Above 120°C, E' drops again because of the melting of the polymeric material. Since the storage modulus is conceptually similar to Young's modulus that is calculated from the slope of the initial part of a stress-strain curve, only storage modulus values are given in this study (Vable 2009). Although the two results are not the same they give similar idea about the analysis.

Effect of increasing ESAN HNT loading on E' values can also be seen from Figure 4.18. Increase of E' with increasing filler content can be related to higher energy that is stored per cycle of oscillation. Storage modulus enhancement is a general behavior of reinforced semi-crystalline polymers and it is generally expected to be more distinct at higher temperatures. Remaining rigidity of the fillers throughout the entire temperature range in which the transition of polymeric material from glassy region to rubbery region occurs might be the result for this difference (Wilkinson et al. 2006). For PLA/HNT composites this larger difference at higher temperatures is not the case. Although increasing HNT content results in higher modulus values at room temperature, its effect is not prominent at temperatures above glass transition. The reason of lower reinforcement at higher temperatures might be the lowered contact surface between debonded nanotubes and polymer matrix at higher temperatures which accelerates the chain mobility. Hence, it can be said that the stiffening effect of HNT is mainly observed at lower temperatures.

Loss modulus (E''), which associated with the dissipation of energy as heat, versus temperature graphs of PLA and PLA/HNT composites are given in Figure 4.19. Pure PLA reveals it maximum loss at 56.5°C. Addition of HNT to PLA does not give rise to a distinct shift of the maximum peak to higher or lower temperature

indicating lower or higher chain mobility respectively. Also, E'' value at maximum peak temperature does not increase with increasing filler content.

To observe the glass transition (T_g) temperature clearly, DMA analysis is a good method. The loss tangent ($\tan \delta$) versus temperature results of pure PLA and PLA/HNT composites are given in Figure 4.20. The maximum peak indicating T_g for pure PLA occurs around 66.1°C which is approximately 8°C greater than the result obtained from DSC analysis. This difference is due to the frequency effect of DMA which causes polymer chains to relax at higher temperatures. The detail will be mentioned in the DSC results part. This value is also assigned as α relaxation peak which is believed to be related to the actuation of long range segmental chain movement in the amorphous area. Supporting the tensile results expressing the plasticization effect of nanotubes, no increase can be observed for the T_g values of composites. Instead, an insignificant shift to lower temperatures is displayed.

Another important point takes attention is that the intensity value of the $\tan \delta$ peak at T_g decreases with filler addition. Loss tangent is obtained by the division of loss modulus to storage modulus (E''/E'). As mentioned previously, in the temperature range around T_g , E' values increase, whereas E'' values remain almost the same with filler addition. Hence, decrease in $\tan \delta$ is an expected result. The intensity value of $\tan \delta$ peak is also related to the volume of constrained polymer in the composite due to crystal formation or polymer clay interaction. Constrained polymer means that the volume fraction of chain segments whose mobility is constrained. For this study, the decrease in $\tan \delta$ indicates the higher fraction of mobile chains. This might be attributed to both decreased crystallinity which is also proven with DSC analysis and poor polymer clay interaction.

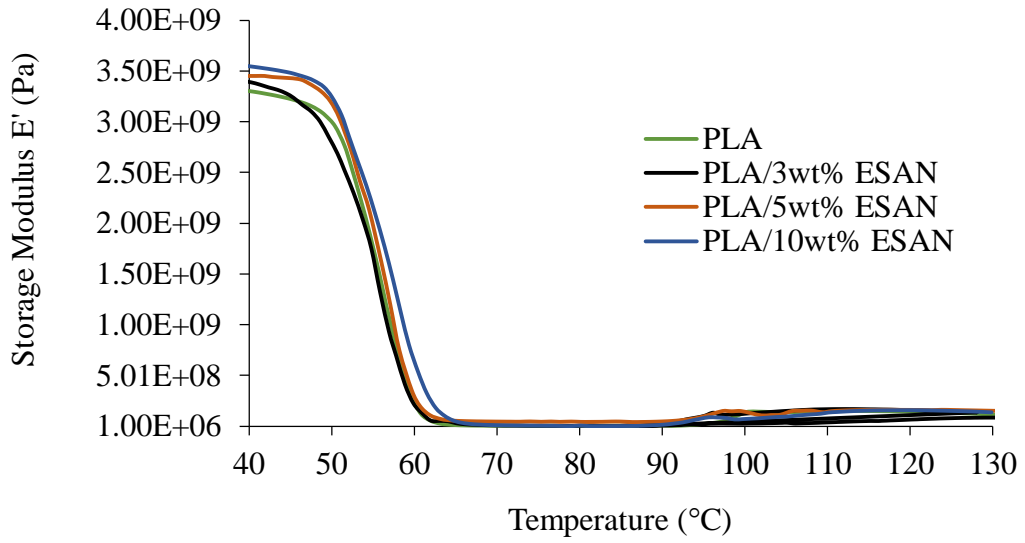


Figure 4.18. Storage Modulus (E') versus temperature data for PLA/ESAN HNT composites prepared by DM3 method

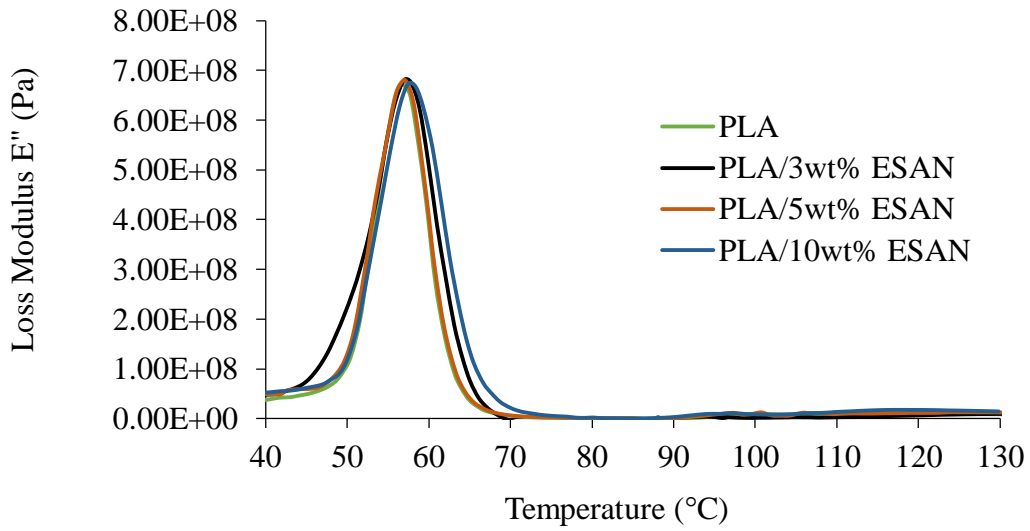


Figure 4.19. Loss Modulus (E'') versus temperature data for PLA/ESAN HNT composites prepared by DM3 method

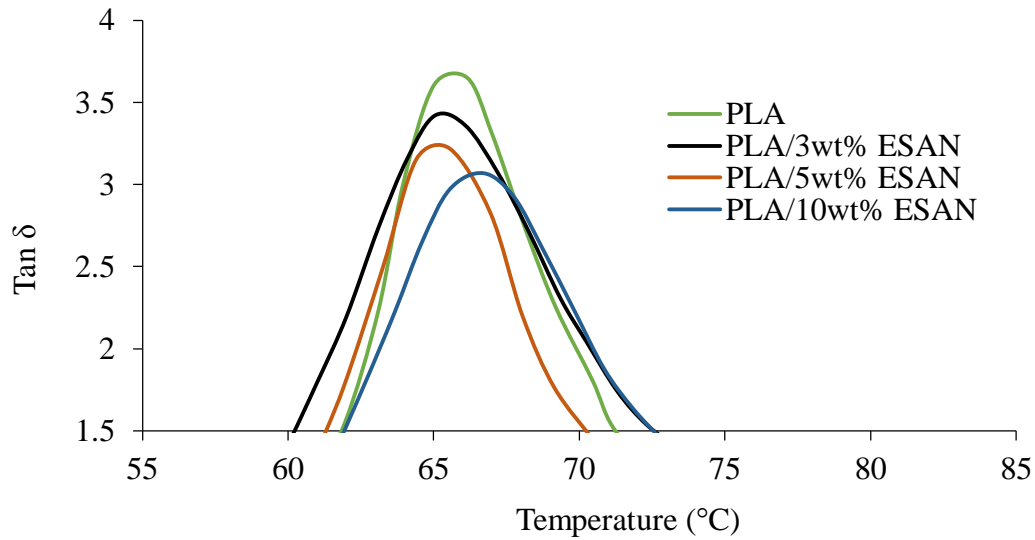


Figure 4.20. Tan δ versus temperature data for PLA/ESAN HNT composites prepared by DM3 method

Nanoclay based composites are also investigated by DMA to compare the viscoelastic properties obtained on ESAN based composites. DMA results are given through Figure 4.21 to Figure 4.23. Although a better dispersion of Nanoclay particles was observed by XRD and SEM analysis, storage modulus of the samples at lower temperatures show a reduction with Nanoclay addition. This result is in contrast to enhancement obtained with ESAN addition to PLA matrix. Since, the HNT particles could not function as nano-filler in the polymer matrix, their dispersion seems to have no effect for the improvement of the stiffness. Instead, the plasticizing effect of particles dominates the mechanical property. However, with increasing clay amount, E' value of the samples increases due to the stiffening effect of fillers which suppresses the plasticizing effect.

The decrease of loss modulus values which cannot be observed from the E' versus temperature plot of PLA/ESAN HNT composites is clear in Figure 4.22. The

trend observed in the storage modulus can be seen in the maximum peak value of E'' . With filler addition, this factor displays a reduction indicating a lowered dissipated energy as heat, whereas it increases with increasing clay content due to the same reason referred to as in storage modulus results.

As can be seen from Figure 4.23 there is small decline in the T_g from 66.1°C for pure PLA to 64.8°C for 10wt% Nanoclay containing composite. However, this reduction can be said to be negligible. In addition, as in the case of PLA/ESAN HNT composites, the intensity of $\tan \delta$ decreases with increasing clay loading due to terminated crystal growth by clay particles and poor compatibility between HNT and PLA.

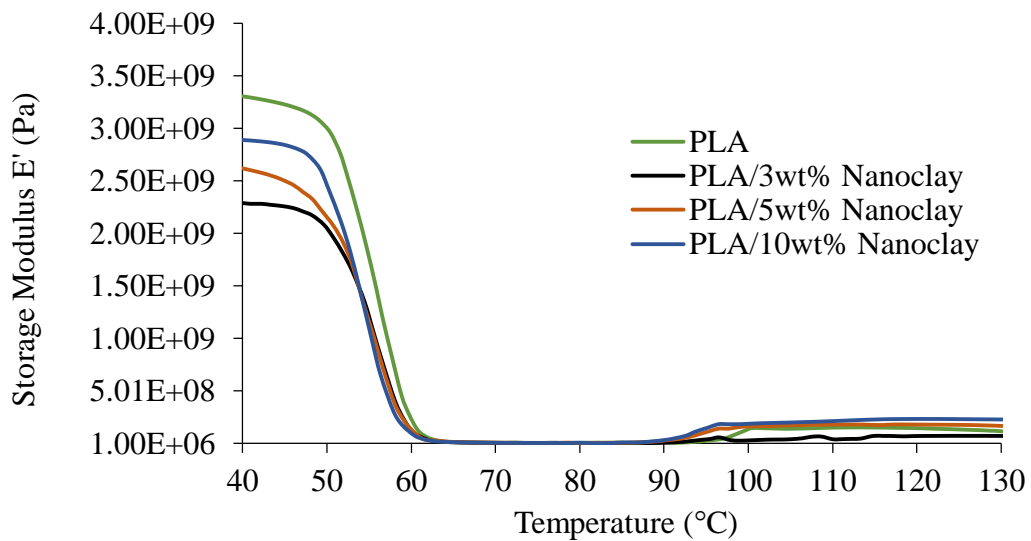


Figure 4.21. Storage Modulus (E') versus temperature data for PLA/Nanoclay HNT composites prepared by DM3 method

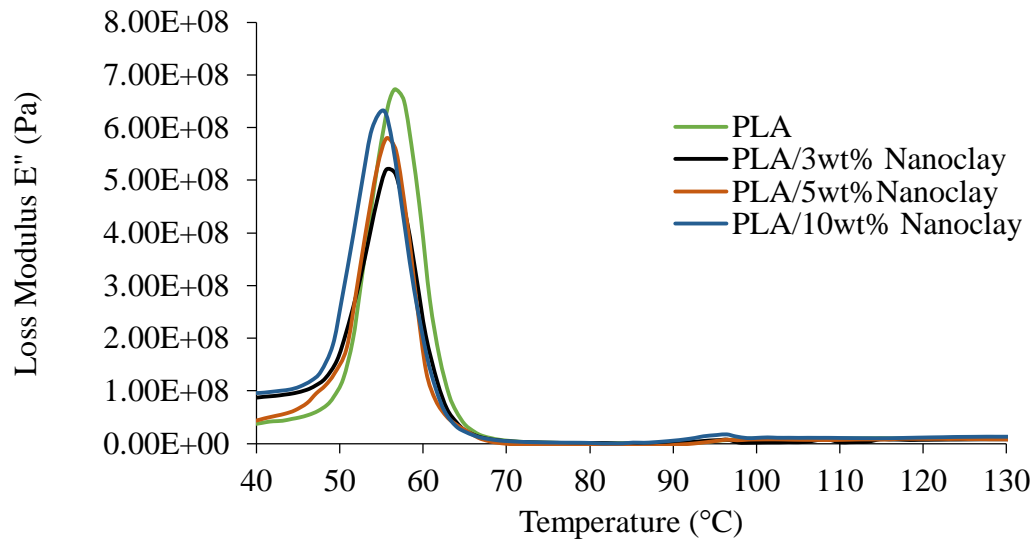


Figure 4.22. Loss Modulus (E'') versus temperature data for PLA/ Nanoclay HNT composites prepared by DM3 method

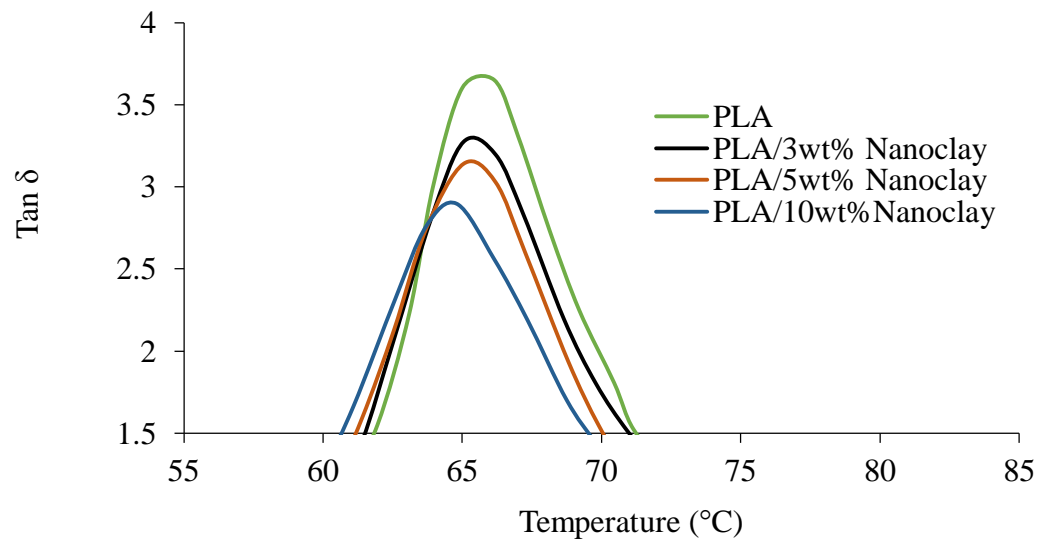


Figure 4.23. Tan δ versus temperature data for PLA/ESAN Nanoclay composites prepared by DM3 method

The in-effectiveness of HNT in terms of stiffness improvement for PLA/HNT composites, prepared by DM3 method, might also be attributed to the agglomerates and hence inhomogeneous distribution of the particles. One of the reasons for agglomeration is insufficient shear, in other words, mechanical force applied during processing. Hence, to find a solution for this problem, different processing techniques were tried as mentioned in detail in previous chapters. Like other properties, dynamic mechanical properties of the composites cannot be improved by the help of increased shear stress or dispersive effect of liquid phase. Effects of different processing techniques on dynamic mechanical properties of PLA/5wt% ESAN HNT composites are given through Figure 4.24 to Figure 4.26.

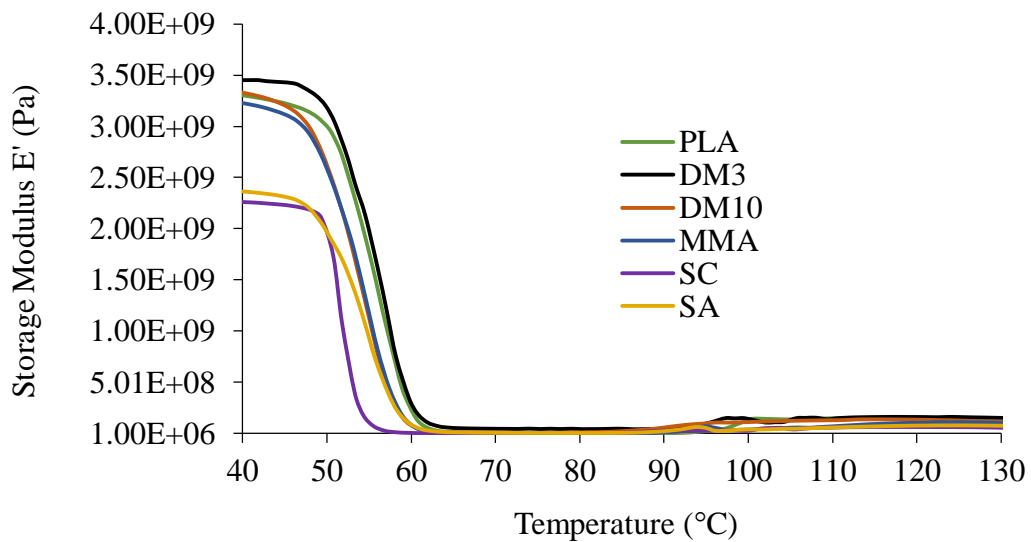


Figure 4.24. Effect of different processing techniques on the Storage Modulus, E' , (Pa) of PLA/5wt%ESAN HNT composites (DM3: Direct Melt Mixing-3 minute, DM10: Direct Melt Mixing-10 minute, MMA: PLA Masterbatch Melt Mixing, SC: Solvent Casting Followed by Melt Mixing Method, SA: Suspension Addition to Melt Mixing)

Although the storage modulus of the composite prepared by DM3 method shows a small enhancement, DM10 and MMA methods result in stable and lower E' respectively at temperatures below T_g (Figure 4.24). For SC and SA methods E' shows a sharp decrease at low temperatures due to the plasticizing effect of the solvent molecules. For the loss modulus, the same trend with storage modulus can be observed from Figure 4.25. With increasing shear stress in MMA and DM10 methods, E'' values decrease and the peak temperature shifts to left indicating more mobile polymer chains. A sharp decrease is also observed in E'' results of composites prepared by SC and SA methods because of small solvent molecules.

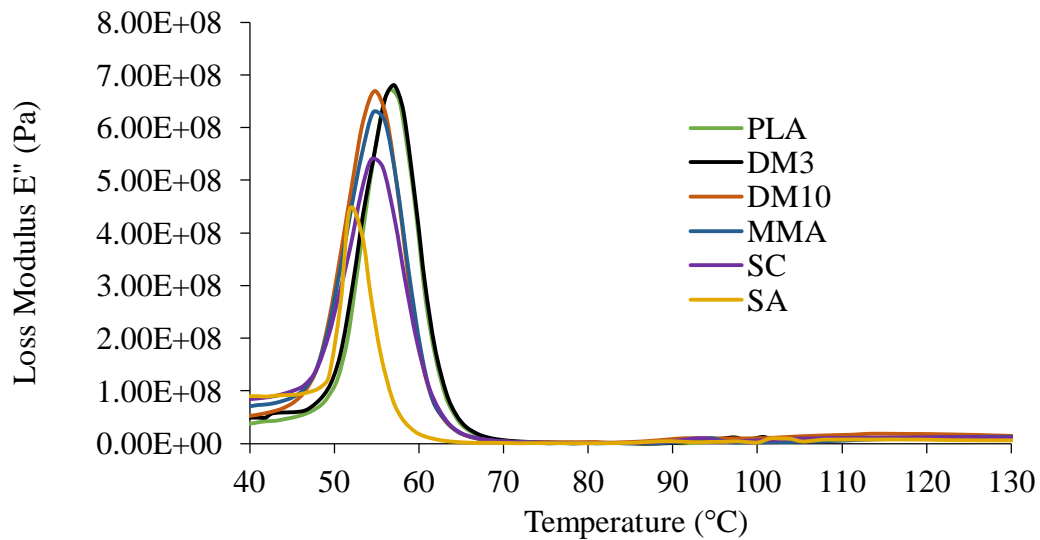


Figure 4.25. Effect of different processing techniques on the Loss Modulus, E'' , (Pa) of PLA/5wt%ESAN HNT composites (DM3: Direct Melt Mixing-3 minute, DM10: Direct Melt Mixing-10 minute, MMA: PLA Masterbatch Melt Mixing, SC: Solvent Casting Followed by Melt Mixing Method, SA: Suspension Addition to Melt Mixing)

Change in $\tan \delta$ versus temperature plot with different processing techniques support the results observed in E' and E'' versus temperature plots. According to these plots, solvent based methods yields an undesired decrease in the stiffness and T_g values of the composites due to solvent molecules functioning as plasticizer. In addition, the methods in which higher shear rates are applied by increasing residence time and number of extrusion steps show a decrease in T_g values. This might be due to the degradation of PLA subjected to extra heat during processing.

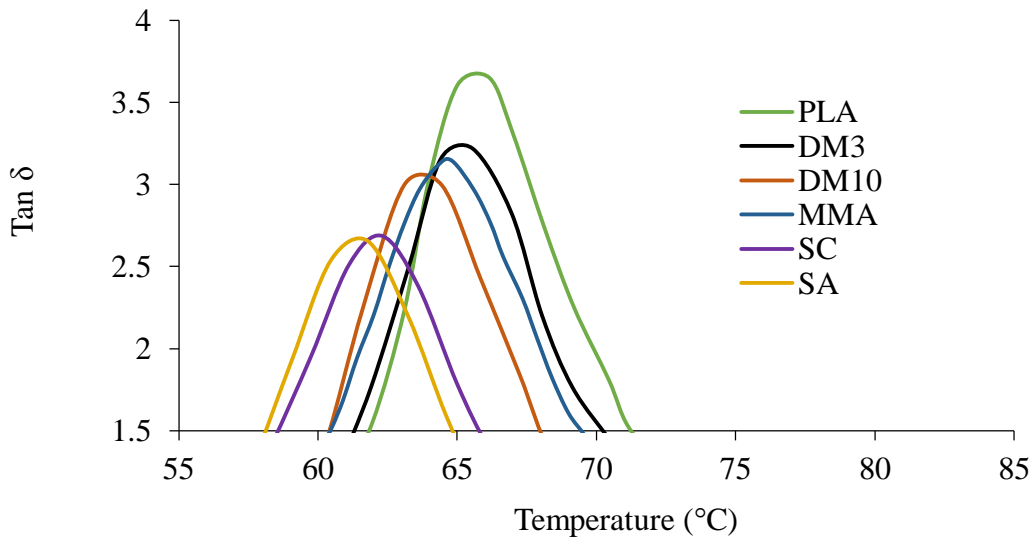


Figure 4.26. Effect of different processing techniques on the $\tan \delta$ of PLA/5wt%ESAN HNT composites (DM3: Direct Melt Mixing-3 minute, DM10: Direct Melt Mixing-10 minute, MMA: PLA Masterbatch Melt Mixing, SC: Solvent Casting Followed by Melt Mixing Method, SA: Suspension Addition to Melt Mixing)

4.2.7 Differential Scanning Calorimetry Analysis (DSC)

With the thermo-analytical technique of differential scanning calorimetry (DSC) thermal properties of the PLA/HNT composites were detected. Transition temperatures and % crystallinity are the monitored results to interpret the thermal behavior of the composites. To eliminate the thermal history of the polymeric materials two heating runs were performed and the second run was taken into account.

PLA is a semi-crystalline polymer whose mechanical and physical properties are governed by its crystal structure (Henton et al. 2005). The PLA grade used for this study exhibits a glass transition temperature at 57.8°C, crystallization temperature at 120.3°C and melting point at 148.1°C as can be seen from Figure 4.27 and Table 4.2. The difference between the T_g results of DMA and DSC analysis are due to the different principles in determining T_g . In DMA, the hysteresis between the applied force and the response of the polymer chains is measured under repeated strains in a cyclic manner. This frequency effect yields a delayed T_g , at which polymer chains relax, and this method is considered to be much more accurate than the one obtained by DSC method. However, in DSC method, the enthalpy change in heating and cooling process is measured (Sperling 2006). A broad and weak endotherm overlaps with T_g of PLA owing to “enthalpy relaxation” of polymer chains (Kodal, Sirin and Ozkoc 2014). Enthalpy relaxation is explained as the relaxation process of oriented amorphous chains which become motionless in an un-equilibrium state. This orientation forms during the injection molding process in which polymeric materials are cooled below their T_g so rapidly. When they are re-heated above T_g , they show a relaxation indicated by a weak endotherm around transition temperature.

Although crystallization of PLA is negligible on cooling, it crystallizes on heating which produces a crystalline phase through a cold crystallization process. In addition, it displays a very low crystalline fraction (χ_c) which is just 2%. For some

PLA grades, two melting peaks occur indicating formation of different crystal structures, melting of crystalline regions of various size, perfections formed during cooling or presence of fractions of low molecular weight (Murariu et al. 2012, Fukushima et al. 2011).

Effects of addition of ESAN HNT on the thermal and crystallization behavior of the PLA composites are shown in Figure 4.27. The T_g , T_m and T_c hardly change with addition of HNT as can be seen from Table 4.2. In the literature, shift of crystallization temperature to lower temperatures was observed for PLA/HNT composites, and this shift was attributed to the ability of HNT to serve as a nucleating agent for PLA (Liu et al. 2013, Prashantha et al. 2013). In addition, the difference between the area under crystallization and melting peaks increases with increasing HNT content indicating an increase in the crystalline fraction. However, in this study, the surface area which will improve the nucleation of crystal structure could not be formed between polymer and HNT.

The crystalline fraction (χ_c) of PLA decreases with increasing HNT content due to lowered heat of melting as can be seen from Table 4.2. This reduction also proves that the surface area that would have triggered the nucleation is not formed. In polymer composites, another reason that may cause lowered χ_c is agglomerates at higher loadings leading to reduction of the number of available nucleation sites. This reduction is independent of the amount of clay. Hence, it can be said that the main reason is mainly weak interface, instead of agglomerates formed during the processing. According to literature, materials that have plasticizing effect may crystallize the PLA more easily at lower temperatures due to increased chain mobility (Jang et al. 2007, Chow et al. 2013). On the contrary to semi-plasticizing effect of HNT, no improvement can be observed for the crystallization of PLA.

For the Nanoclay based composites, thermal and crystallization behavior are shown in Figure 4.28. Transition temperatures and crystallinity are also given in Table 4.2. The same observations obtained for ESAN HNT indicating a poor compatibility between the constituents of the composite was also obtained for the

reference Nanoclay. While there is no remarkable change in transition temperatures, heat of melting (ΔH_m) shows a decrease with addition of HNT yielding a lower (χ_c).

Table 4.2 Thermal transition behavior and crystalline fraction (%) of PLA/ HNT composites

Sample	T _g (°C)	T _c (°C)	ΔH _c (J/kg)	T _m (°C)	ΔH _m (J/kg)	X _c (%)
PLA	57.8	120.3	22.04	148.1	24.21	2.3
PLA/3wt% ESAN HNT	58.5	120.7	22.83	148.9	22.15	0.7
PLA/5wt% ESAN HNT	58.0	120.0	22.31	148.0	22.58	0.3
PLA/10wt% ESAN HNT	58.1	118.5	22.12	148.0	22.32	0.2
PLA/3wt% Nanoclay HNT	58.7	121.6	22.24	149.6	22.23	0.0
PLA/5wt% Nanoclay HNT	58.3	121.2	21.68	148.4	21.79	0.1
PLA/10wt% Nanoclay HNT	58.3	119.0	21.75	148.0	21.75	0.1

Effects of different processing techniques on DSC results are given in Table 4.3. The higher residence time or shear stress applied during processing and the dispersive effect of liquid phase do not give rise to higher T_g or crystallinity indicating a better interaction between PLA and HNT. Instead, there is sharp decrease in T_g, T_m and χ_c results, especially for solvent containing methods. This may be due to the plasticizing effect of solvent molecules. For DM10 and MMA methods, decrease in T_g might be due to the degradation of PLA. Melting point of the composites prepared by the methods other than DM3 also shift to lower temperatures. This may be attributed to the lowered crystallinity or less perfect crystalline formation due to incomplete nucleation (Liu et al. 2013).

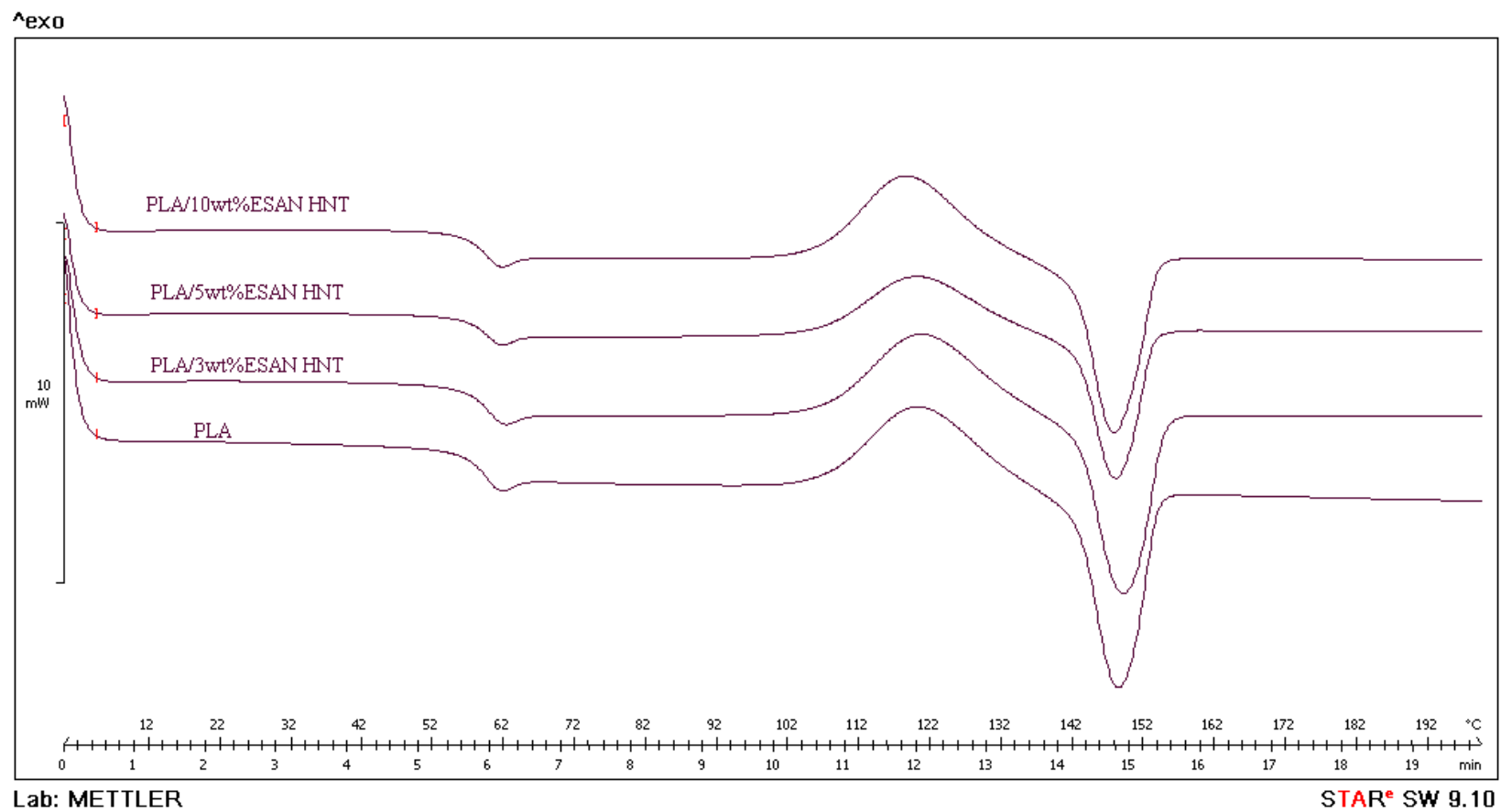


Figure 4.27. DSC thermograms of PLA/ESAN HNT composites prepared by DM3 method

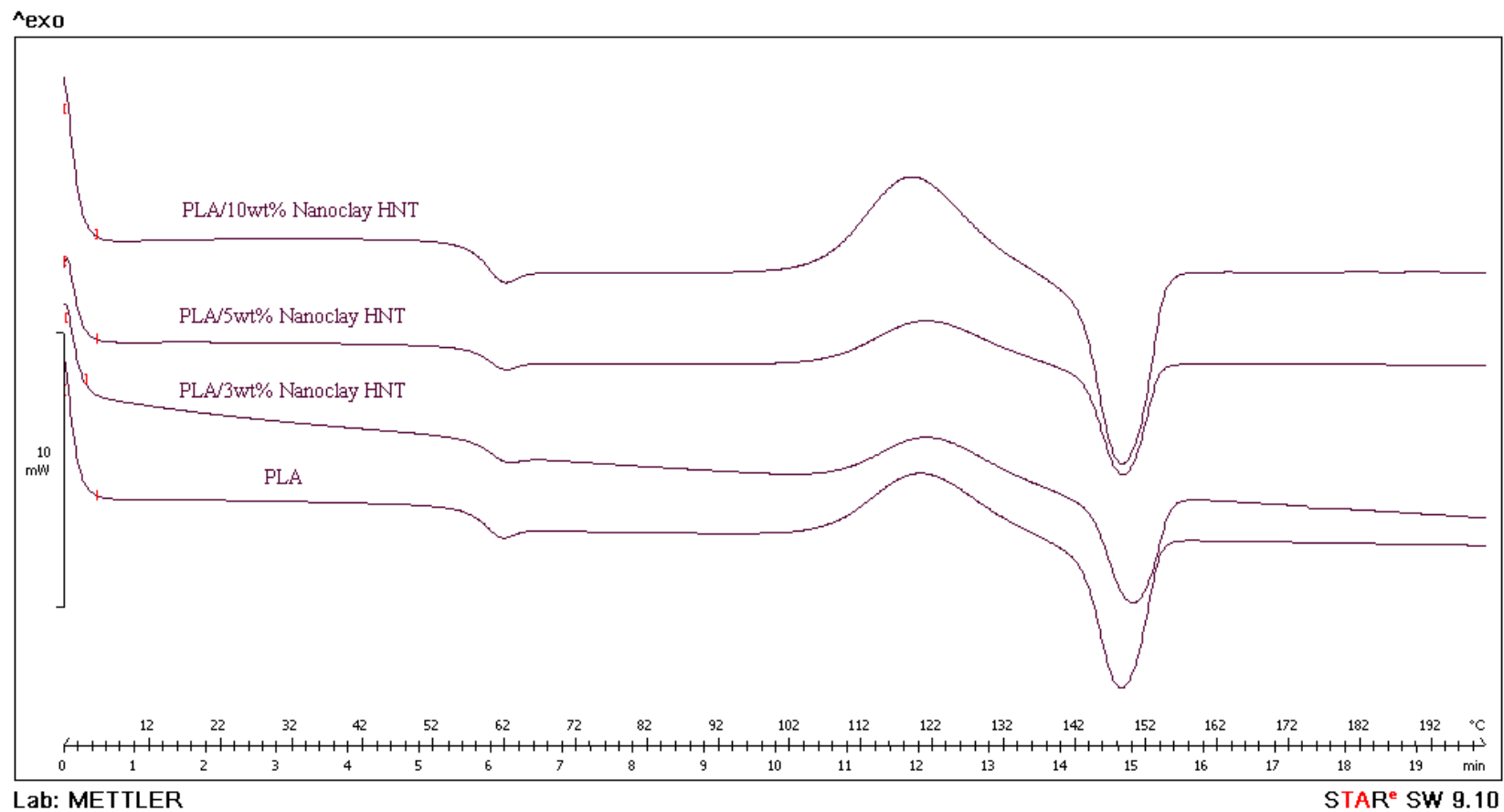


Figure 4.28. DSC thermograms of PLA/Nanoclay HNT composites prepared by DM3 method

Table 4.3. Effects of different processing techniques on thermal transition behavior and crystalline fraction (%) of PLA/5wt% ESAN HNT composites

Method	T_g	T_c	ΔH_c	T_m	ΔH_m	X_c (%)
DM3	58.5	120.7	22.83	148.9	22.15	0.7
DM10	56.3	120.1	22.75	147.3	22.47	0.3
MMA	55.5	121.0	21.95	146.7	21.76	0.2
SC	54.1	119.3	18.75	144.5	18.71	0.0
SA	53.5	120.4	16.41	144.2	16.37	0.0

4.2.8 Hydrolytic Degradation

Biodegradation can be described as changes in chemical structure, loss of mechanical and structural properties and finally changing into other compounds like water, carbon dioxide, minerals and intermediate products like biomass and humic acid (Jamshidian et al. 2010). Chemical degradation of biopolymers via hydrolysis or enzyme-catalyzed hydrolysis is much easier, compared to other polymers, due to hydrolysable bonds in their backbone. The degree of degradation can be estimated from the measurements of mass loss. Hence, mass loss profiles for PLA/HNT composites as a function of hydrolysis time are recorded in this study.

Although composting appears to be a cost effective solution for the degradation of biopolymers, its duration and variability led this study to use the hydrolysis method. Also, composting is a restrictive method in terms of demand on resources and space in composting plants (Jordan and Mullen 2007). Hydrolysis at a temperature around the T_g of PLA is used in this study, since PLA is largely resistant to the molecular weight reduction at ambient conditions in absence of

enzymes. In this manner, the cost arising from the use of enzymes in enzymatic hydrolysis was eliminated.

The polar oxygen linkages make PLA naturally hydrophilic, and its methyl side group confers its hydrophobic properties (Vroman and Tighzert 2009). Decomposition of PLA is affiliated by its hydrophilic characteristics and depends on the surrounding moisture and temperature. During the degradation of PLA, the first stage is the reduction of its molecular weight by hydrolysis before it becomes biodegradable. Elevated temperature is important for hydrolysis to reduce its molecular weight as mentioned above. Also, by the help of elevated temperature a reasonable range of time is provided to monitor the hydrolysis results. This step occurs by the random cleavage of $-C-O-$ ester bond producing fragments of lactic acid, oligomers and other aqueous medium soluble products (Ndazi and Karlsson 2011). In this study, buffer solution was used as the aqueous medium which diffuses into the polymeric material, while oligomer products diffuse outwards.

Visual hydrolysis results of PLA can be seen from Figure 4.29 which shows no weight loss until the 20th day. After that period, a fast degradation starts and it becomes difficult to measure the weight loss of the samples due to extensive fragmentation.

Reinforcement of biodegradable polymers is an important progress in terms of eco-friendly green materials for several applications. However, it is important not to modify the biodegradable properties of PLA while enhancing its mechanical properties. Visual results for ESAN HNT containing composites can also be seen from Figure 4.29 and the % of weight loss versus hydrolysis time plot is given in Figure 4.30. For the composites no change in mass loss can also be observed in the first 20 days. According to Zhang et. al. in this first stage of the degradation the molecular weight of PLA decreases as time passes following a bulk erosion mechanism. However, in the meantime, the crystallinity increases and no observable weight loss occurs in this stage (Zhang et al. 2008). HNT particles

added to PLA do not affect this stage evidently, although hydrolysis of silicate layer based nanocomposites are shown to proceed at slower rates in literature (Roy et al. 2012, Paul et al. 2005).

After 20 days, PLA/HNT composites also display quick erosion but in a slower manner compared to that of pure PLA. This 2nd stage of the degradation starts when the molecular weight and the crystallinity reach a stable level. With the beginning of this stage, the crystalline structure of PLA is further modified as hydrolysis time increases. During this stage, pH and the temperature play a significant role, whereas crystallinity remains constant and the molecular weight in the residue decreases very slowly (Zhang et al. 2008). Hence, this prolonged 2nd stage gives the main idea about the degradation behavior of the composites. At the end of the 2nd stage, lactic acid is formed as the major product of the weight loss. Decelerating degradation rate with increasing clay content, in addition to unchanged rate during the first stage might be the indication of deterioration in barrier properties (Roy et al. 2012).

Hydrolytic degradation of polyester chains is known to take place in the amorphous phase of the polymer matrix and expected to increase its crystalline fraction resulting in an increase in the opacity of the samples (Hakkarainen 2002). Lowered crystalline fraction by the introduction of HNT particles is presumed to cause lower degradation rate due to extra amorphous space formed. Also, HNT particles that prevent crystal formation during processing might cause a slower crystal formation in hydrolysis due to their poor nucleating affect.

The reference nanotube, Nanoclay, based composites display the same degradation behavior as ESAN based composites do. In the first 20 days, which is called the first stage, they do not display a change in the degradation rate, whereas it slows down in the second stage.

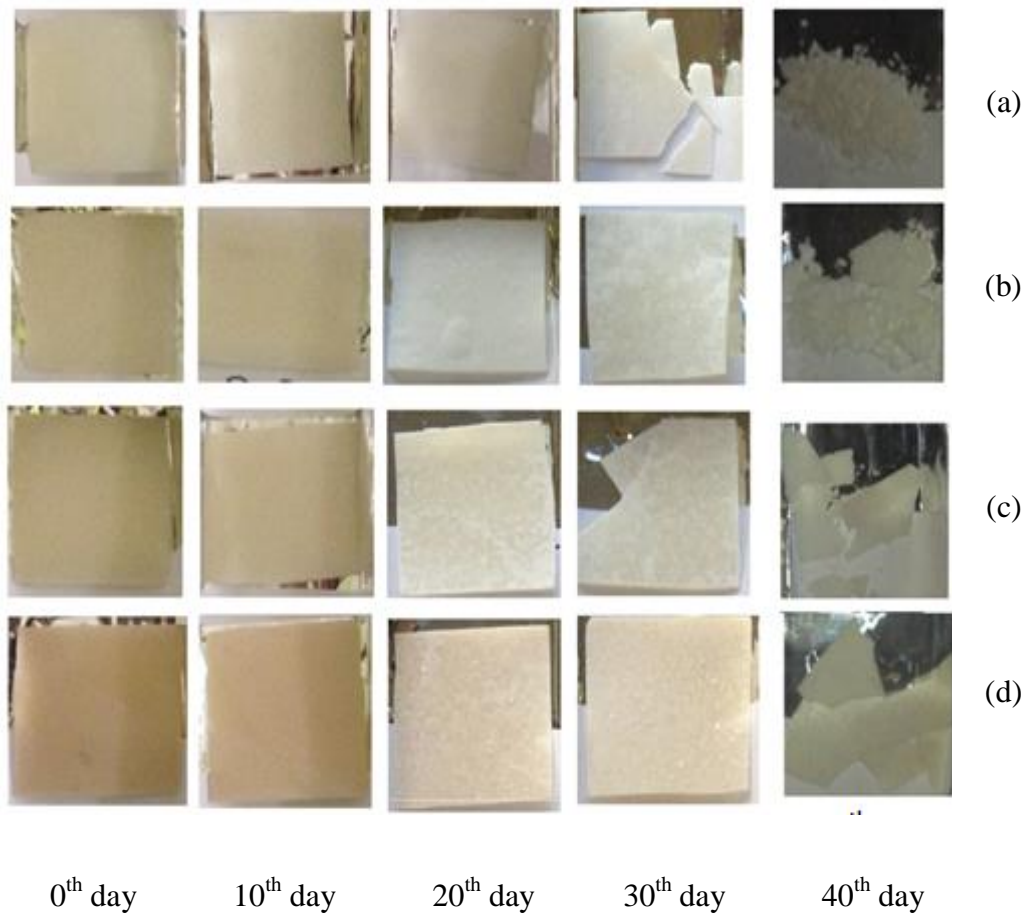


Figure 4.29. Hydrolysis samples of PLA/ESAN HNT composites prepared by DM3 method; (a) 0wt% HNT, (b) 3wt% HNT, (c) 5wt% HNT, (d) 10wt% HNT

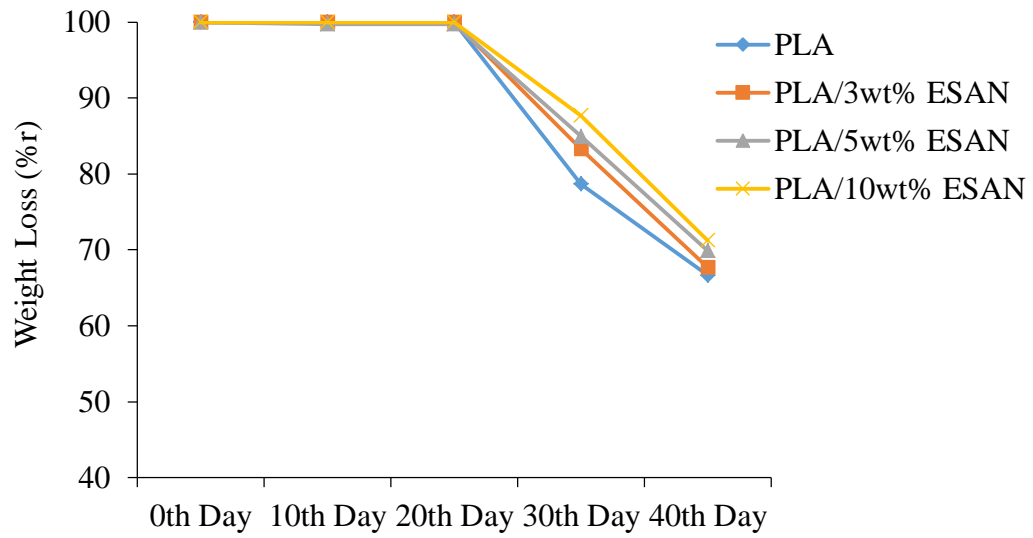


Figure 4.30. Hydrolytic degradation results of PLA/ESAN HNT composites prepared by DM3 methods

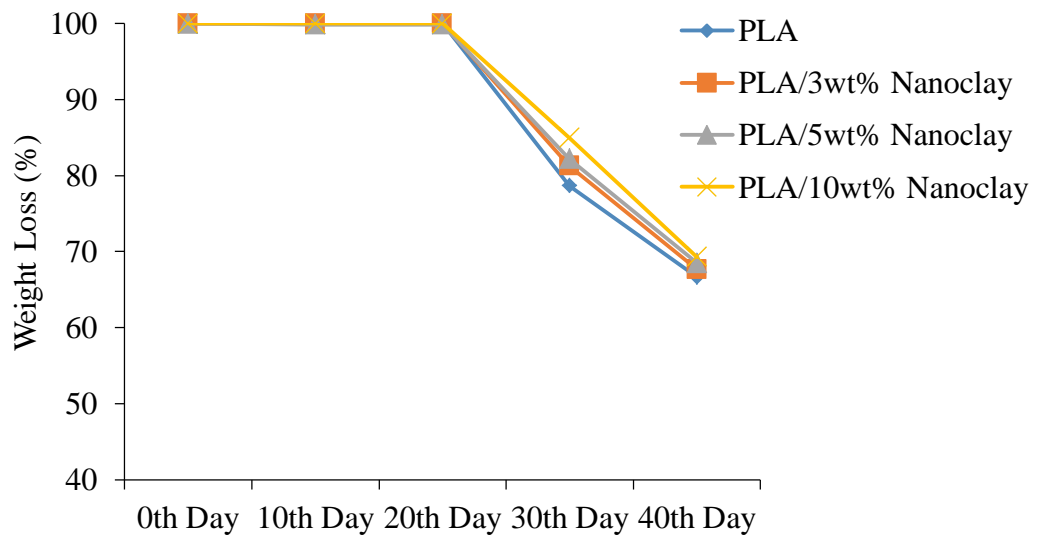


Figure 4.31. Hydrolytic degradation results of PLA/Nanoclay HNT composites prepared by DM3 methods

The morphological, mechanical, thermal and degradation properties of the PLA based composites prepared by using different processing techniques are given in this section. According to these results, there is an incompatibility between the polymer matrix and HNT filler, and no improvement can be obtained for the composite properties. The morphological results also indicate that agglomerated structures are formed during melt processing.

Owing to its simple, environmental friendly and relatively cheap characteristics, DM3 method was preferred for the composite preparation. There are two more options to provide an enhancement in the physical properties. One of these ways is applying a pre-treatment to HNT minerals to form a compatible surface. The second way is to use a third material which serves as a compatibilizer. In the following parts of this dissertation the results obtained by using nanotubes subjected to different pre-treatments and different compatibilizers are given.

4.3 Effects of Different HNT Pre-treatments on the Properties of Unplasticized PLA/HNT Composites

As mentioned in the previous section, the incorporation of layered silicate nanotubes, with a high aspect ratio and relatively high surface area, into PLA matrix does not improve the physical properties of the composites. In other words, a nanocomposite formation could not be achieved with addition of HNT. It is a well-known fact that the properties of composites mainly depend on the chemistry of the polymer matrix, nano-filler type, processing technique and conditions (Pavlidou and Papaspyrides 2008). The third option, different processing techniques, was tried to obtain better properties and no significant improvement could be observed. In this section of the dissertation, trials that were made to modify the nanotube and properties of PLA composites prepared with the modified nanotubes are given.

It is important to create a surface interaction between filler and the polymer matrix. Although there is an interaction between the constituents for PLA and raw HNT composites, the compatibility between them is poor. Hence, different HNT pre-treatments were applied to HNT minerals:

- Purification of HNT (p-HNT)
- Functionalization of HNT by Grafting with Organo-silane (o-HNT)
- Modification of HNT With Quaternary Salt (m-HNT)
- Evacuation pre-treatment (e-HNT)

Different non-clay particles and impurities dependent on the geological conditions are found in HNT minerals. These impurities might cause deterioration of the physical properties of polymer composites due to increased tendency for agglomeration and reduced PLA-HNT surface area. A successful purification with the removal of impurities except Gibbsite was performed and the results are given in the characterization and purification of HNT section. In this section, the

physical properties of the PLA composites prepared with purified HNT (p-HNT) are given and the results are compared with the results on composites prepared by raw HNT.

One of the most commonly used techniques to provide a good interaction between polymer and filler is to functionalize the surface of the filler by organo-silane. During the functionalization of HNT, coupling agents on the organo-silane react with the Al – OH groups on the edge and Si – O groups on the surface of nanotubes (Zhao and Liu 2008). Functionalized HNT (o-HNT) is expected to interact with the polymer matrix more effectively and form covalent bonds between the polymer matrix and the coupling agent of the organo-silanes. In this study, three different types of organo-silanes were used to functionalize the surface of HNT;

- γ -aminopropyl triethoxysilane (γ -APS) modified HNT (APS-o-HNT)
- γ -methacryloxypropyl trimethoxysilane (γ -MPS) modified HNT (MPS-o-HNT)
- γ -glycidoxypropyl trimethoxysilane (γ -GPS) modified HNT (GPS-o-HNT)

Another method to change the chemical structure of fillers and make them more compatible with the polymer is modification by cationic surfactants, such as quaternary alkyl salts. This modification option is generally applied to layered silicates which undergo isomorphic substitution to make these hydrophilic phyllosilicates more hydrophobic (Pinnavaia and Beall 2000). Since no cations and anions exist between the layers of HNT, no isomorphic substitution occurs. But, hydroxyl and oxygen linkages make HNT polar. It may be expected to have a better compatibility between polar PLA and HNT compared to other layered silicates. However, as discussed in the previous section no improvement can be observed for raw HNT based composites. To create an intercalation of quaternary salts between the HNT layers, modification with triphenyl phosphonium bromide (CBTPB) quaternary salt was performed (m-HNT).

After many trials, un-improved physical properties led the study to concentrate on the characteristics of HNT which may hinder the compatibility and even result in degradation of bio based PLA. HNT minerals contain a water layer between their basal spacing which is hard to remove completely by classical drying methods. So, an ultra-high vacuum was applied to HNT particles and it is called as the evacuation method. The emergent HNT particles are then directly fed to extruder to avoid air contact and de-humidification.

4.3.1 Functionalization of HNT with Organo-silane

To use in the preparation of PLA/o-HNT composites, nanotubes are subjected to grafting method of silica based materials (Yuan et al. 2008, Vansant et al. 1995). During the modification of HNT with different types of organo-silanes, ethanol concentration and amount of HNT dispersed in the solvent were varied and only the results obtained by optimum conditions for the modification are given in this dissertation. Also, the composites containing 5wt% Nanoclay were prepared by DM3 owing to relatively better properties obtained in the previous section.

To see the effects of both different functional groups and alkoxy groups, three different organo-silanes were used in this study as mentioned in the experimental part. The main aim to use organo-silanes having different alkoxy groups (methoxy and ethoxy) is to investigate the effects of the alkoxy chain length on the conversion of alkoxy-silane to hydrophilic silanol by hydrolysis and the affinity of organo-silane to react with the Al – OH groups on the edge and Si – O groups on the surface of HNT. The effect of different functional groups on the interaction between functionalized HNT and polymer matrix is the reason of using organo-silanes with different functional groups.

To investigate the formation of organically functionalized HNT, infrared spectrum of the raw Nanoclay and Nanoclay samples, modified with γ -

aminopropyl triethoxysilane (γ -APS), γ -methacryloxypropyl trimethoxysilane (γ -MPS), and γ -glycidoxypropyl trimethoxysilane (γ -GPS) were recorded and the results are displayed in Figure 4.32. HNT can be characterized by a meso/macroscale porous texture because of the wrapping of the layers around themselves. Thus under favorable conditions they exhibit hollow cylindrical structure with mismatch in the periodicity which is composed of Si – O – Si groups on the external surface and Al – OH groups on the internal surface and edge of the layered silicate (Barrientos-Ramirez et al. 2011). These groups are known to be easily attracted by the silanol groups of organosilanes formed by the help of ethanol-water solution (Joussein et al. 2005, Liu et al. 2008). This attraction can be seen from the FTIR results.

In the hydroxyl stretching region, the spectrum of raw Nanoclay HNT exhibits bands around 3693 and 3620 cm^{-1} , that can be attributed to inner-surface free hydroxyl groups and inner hydroxyl groups respectively. The O – H stretching of water gives rise to bands around 3458 cm^{-1} and 3524 cm^{-1} , while O – H deformation of water results in a band around 1634 cm^{-1} representing water adsorbed on clay surface without strong bonding to the clay. The region below 1200 cm^{-1} is characterized by bands associated with Al – O and Si – O. The absorption peaks around 911 cm^{-1} are related to the Al – OH vibration referring to O – H deformation of inner hydroxyl groups. Perpendicular Si – O stretching peaks occur around 1113 and 753 cm^{-1} , while in plane and symmetric stretching of Si – O peaks are centered around 1030 and 794 cm^{-1} (Yuan et al. 2008, Pasbakhsh et al. 2010, Pasbakhsh et al. 2009).

As can be seen from Figure 4.32, γ -APS modified samples exhibit some new FTIR peaks, such as the deformation C – H₂ vibration peak at 1490 – 1468 cm^{-1} and the deformation N – H₂ vibration peak at 1548 cm^{-1} . Also the peak around 2930 cm^{-1} indicates the stretching C – H₂ vibration band that is intensified with surface modification. Water O – H stretching peak centered around 3458 widens with the functionalization of the nanotube. In addition to O – H stretching peak, N

– H₂ stretching peak at 3484 cm⁻¹ becomes observable. In literature, it is possible to find different arguments about this observation. According to Yuan and his co-workers, amino-silanes might oligomerize or even polymerize with surface water in addition to grafting on nanotubes, and the oligomerized amino-silane might further react with grafted amino-silane to form a cross-linked network (Yuan et al. 2008). If prior drying is performed before functionalization or water is not used together with alcohol in the silanization procedure, O – H stretching band due to adsorbed water is not found in the FTIR spectra, and hence it is not possible for silane condensation on the HNT surface to follow this mechanism which forms cross-linked network (Barrientos-Ramirez et al. 2011). In addition to this argument, further widened peak can be attributed to the overlap with the N – H₂ stretching vibration around 3360 cm⁻¹.

The other type of organo-silane used to functionalize the surface of the HNT is acrylate functional γ -MPS. According to FTIR spectrum of γ -MPS modified HNT, absorbance bands at 1723 cm⁻¹ indicating ester groups, 1470 cm⁻¹ of propyl group and 2923 cm⁻¹ bands of methyl are formed indicating the formation of MPS modified nanotubes. Moreover, increasing intensity of the band at 1637 cm⁻¹ may be indicative of the overlap of the peaks of C = C group and O – H deformation of water.

FTIR spectrum of γ -GPS modified HNT represents symmetric stretching of epoxy ring at 1250cm⁻¹. However, the absorption peak of epoxy group at 914 cm⁻¹ could not be observed owing to the overlap with the band related to the O – H deformation of inner hydroxyl groups. In addition, the peak around 1470cm⁻¹ illustrates the propyl group.

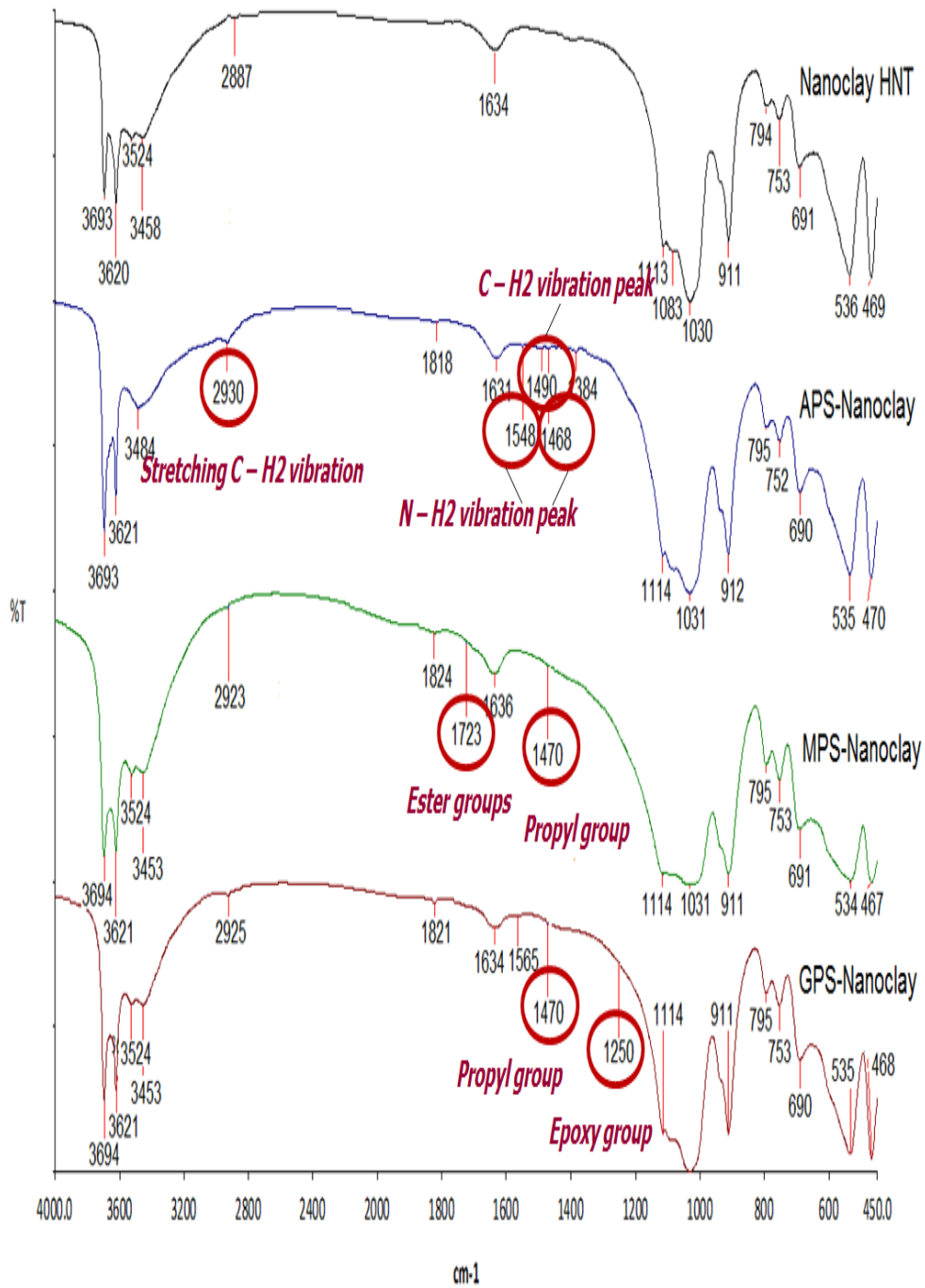


Figure 4.32. FTIR spectrum of Nanoclay HNT mineral modified with functional organo-silanes.

The modification of HNT surface can also be analyzed by investigating the disparities formed in the thermal behavior of the nanotubes whose surfaces are modified by organo-silanes. For this purpose, thermal gravimetric analysis (TGA) was performed and the results for functionalized and un-functionalized Nanoclay HNT minerals are given in Figure 4.33. HNT displays three distinguishable regions in its TGA spectrum owing to weight loss during thermal heating. The first region below 100°C indicates the presence of absorbed free water, whereas the region between 200 and 400°C can be ascribed to the loss of hydration water molecules that can be present between the layers of HNT. The last region is the dehydroxylation at higher temperatures than 400°C and lower temperatures than 600°C. At temperatures above 800°C, degradation of clay particles take place and a new phase is formed (Barrientos-Ramirez et al. 2011, Joussein et al. 2005).

Mass loss between 150 and 200°C is also attributed the hydrogen bonded organo-silanes to the HNT surface in addition to the loss of hydration water molecules between the layers of HNT. This region corresponds to the initial decomposition temperature which is considered to be the temperature at 5wt% loss in the literature (Barrientos-Ramirez et al. 2011). Functionalization results in a lower weight loss up to the end of dehydroxylation region compared to raw Nanoclay due to restricted release of water molecules. Hence, successfully functionalized HNT particles show an enhancement in their thermal stability. Respectively, APS-o-HNT, GPS-o-HNT, and MPS-o-HNT show better thermal stability. At higher temperatures, this sequence is reversed. APS-o-HNT shows the largest weight loss compared to other HNT samples as shown in the circle in Figure 4.33. This can be attributed to lowered residual weight (%) that remained at the end of the degradation of both HNT mineral and organo-silane attached to the surface of HNT. So, it can be said that the best functionalization was achieved by using γ -APS.

If a polarity comparison is made between the organo-silanes used for this study, γ -MPS takes the first line due to the carbonyl groups in its backbone and the

double bonds it contains. The second highest polarity belongs to γ -GPS which contains epoxy group. Hence, the greater ability of γ -APS to attach on the surface of HNT particles can be attributed to its highest non-polarity among the three organo-silanes. Effects of the APS-o-HNT mineral on the physical properties of the PLA composites are given in the following part with the results on composites prepared by HNTs subjected to other pre-treatments mentioned above. Hence, in the following sections, the term o-HNT will be mentioned as APS-o-HNT mineral.

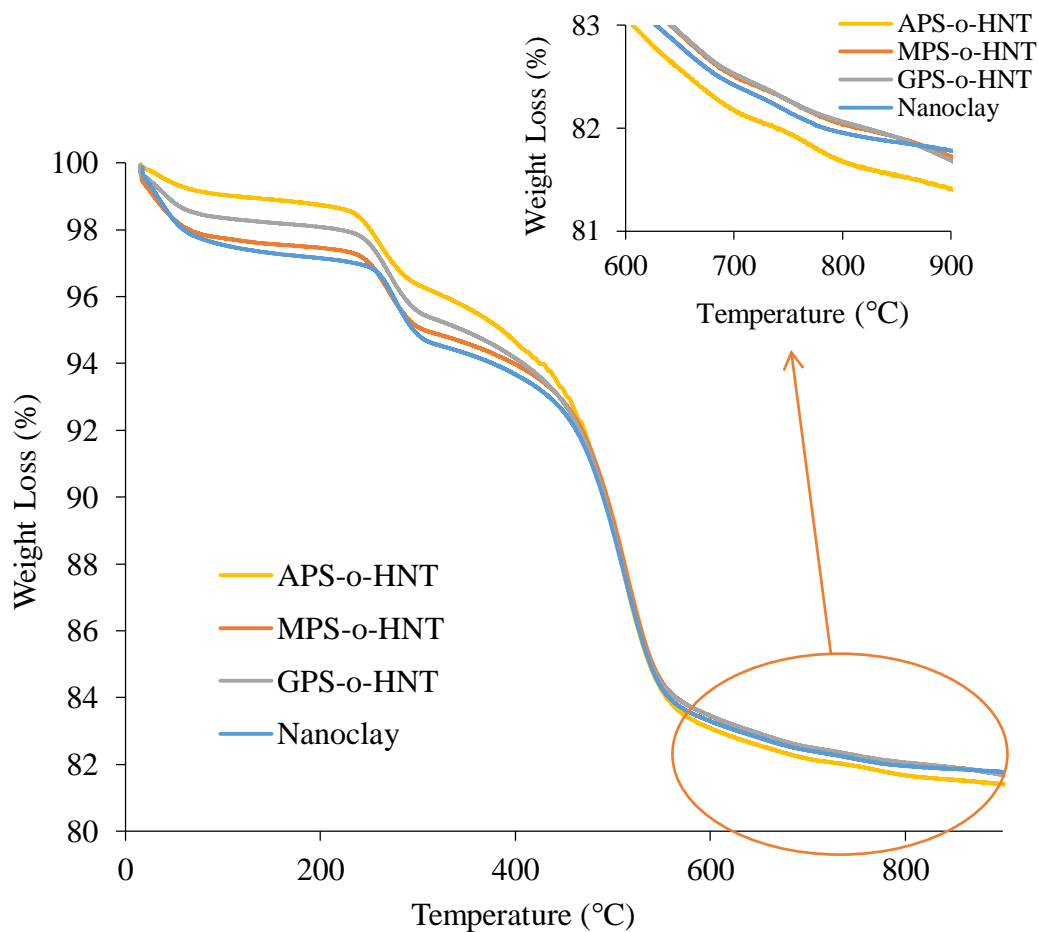


Figure 4.33. TGA spectrums of organo-silane modified and un-modified Nanoclay HNT

4.3.2 X-Ray Diffraction Results

In this part of the study, in-dispersible agglomerates formed by different processing techniques are tried to be wiped out by subjecting the clay particles to different pre-treatments. Also, pre-treatments, especially surface modifications, are generally believed to increase the interaction between the polymer and filler. To see the effects of the pre-treatments on the dispersion of clay particles, XRD analysis was performed and the results are shown in Figure 4.34.

Before surface modification and nanocomposite preparation, purification of clay minerals is a necessary step to remove impurities which may cause agglomeration of particles and hinder the intercalation of polymeric materials between the clay layers (Seyidoglu and Yilmazer 2013). As can be seen from Figure 4.34-b, purification does not contribute to the intercalation process. Although the peak around 20° disappears, basal and non-basal peaks of Nanoclay are still visible. In this study, purification of HNT was performed by sedimentation method and $\text{Na}_4(\text{P}_2\text{O}_7)$ was used as the dispersant agent in distilled water medium. High Na^+ concentration may cause Na^+ ions to act as trapped points which lead to failure in the intercalation of polymer chains into silicate layers. Hence, it can be said that purification has no effect on the distribution of the particles and their intercalation process. In addition, the intensity of the XRD pattern increases with purification. This can be attributed to better reflection and hence to more intense peaks as a result of purified samples.

Greater ability of ethoxy group of γ -APS on the silanol formation compared to methoxy groups of γ -MPS and γ -GPS contributed to better modification of HNT surface. But, the main reason underlying the successful modification is the non-polar characteristics of γ -APS due to the absence of carbonyl and double bond found in γ -MPS and epoxy group found in γ -GPS. On the contrary to increased surface action and compatibility of HNT, no significant change can be observed in the 2θ value of the basal and non-basal peaks of composites prepared with

o-HNT (APS-o-HNT). Failure in intercalated structure formation may depend on various parameters. One of them might be the reactions that are expected to create a connection between amino functional group and PLA did not occur during compounding.

Almost the same observation mentioned above is made for the composite prepared by Nanoclay subjected to modification with (4-carboxybutyl)triphenyl phosphonium bromide (CBTPB) quaternary alkyl salt. It is a well-known fact that modified layered silicates are more compatible with organic polymers due to lower surface energy. Also, as in the case of organic functionalization with silane coupling agents, the functional groups of alkyl salts are expected to react with the polymer chain to increase the adhesion between the filler and the matrix (Giannelis 1999, Krishnamoorti 1996). This trial also ended up in failure in the intercalation of silicate layers and distribution of the clay particles due to lack of reaction.

In both cases, functionalization with silane and modification with alkyl salt, the inhibition of the reactions are considered to be a result of water that had remained between the layers of HNT with classical drying methods. For HNT minerals, it is easy to remove the 3Å thick water layer from the gap at temperatures between 200°C and 400°C as mentioned in the TGA results shown in Figure 4.33. However, there still remains a water portion (Brigatti et al. 2006). Also, for raw and pure HNT, water layers might be the reason of poor distribution of clay particles and un-improved physical properties. In addition to poor distribution, residual water causes a recession in the thermal stability of PLA. This was proven with TGA results which are shown in Appendix A.

In order to overcome this problem on residual water, HNT particles are subjected to a high vacuum and fed to processing by avoiding extreme contact with air to prevent de-humidification. The XRD result of composite prepared by evacuated HNT (e-HNT) can be seen from Figure 4.34-e. In terms of visible basal and non-basal peaks, it is totally different from the other patterns. In normal situations, this

kind of a pattern can be defined as an exfoliated structure in which all the platelets are delaminated. However, exfoliated structures are seemed to be suitable only in layered silicates with platelet morphology. Hence, such an XRD pattern for PLA/e-HNT cannot be interpreted as a sign of an exfoliated structure. However, it can be said that although the layers are not completely delaminated, there is distinctive improvement in the distribution of the particles and even there might be limited intercalation which cannot be determined from this result. So, the formation of nanocomposite was achieved by the help of perfect drying.

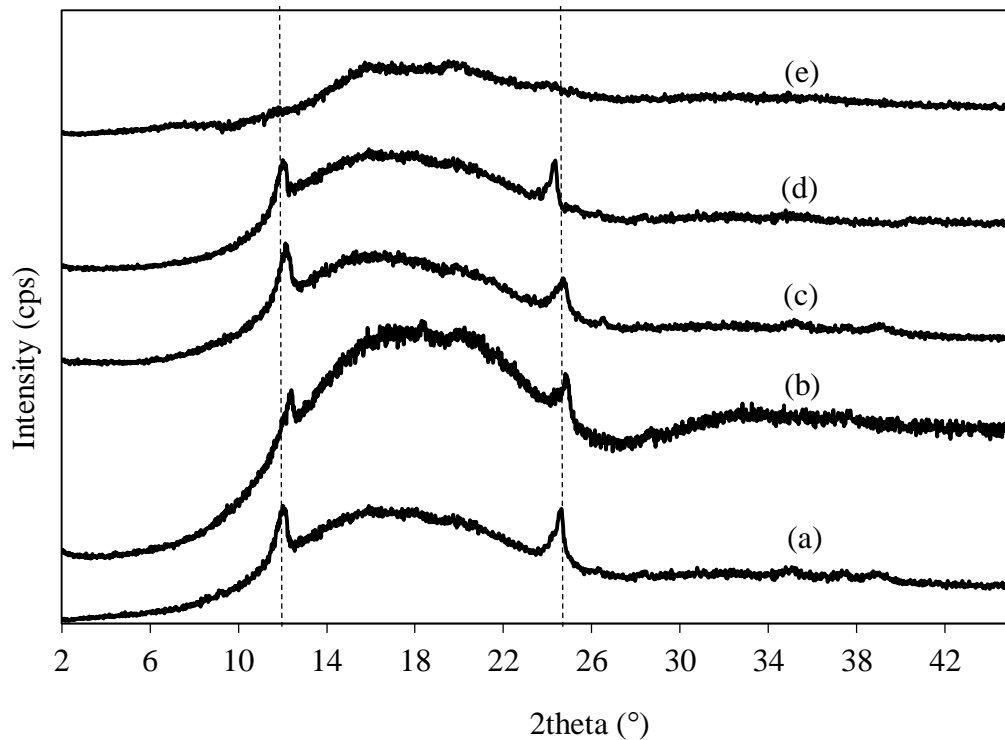


Figure 4.34. XRD pattern of PLA/5wt% Nanoclay HNT composites prepared by HNT subjected to different pre-treatments; (a) raw HNT, (b) purified HNT (p-HNT), (c) Organo-silane functionalized HNT (o-HNT), (d) Quaternary salt modified HNT (m-HNT), (e) Evacuated HNT (e-HNT)

4.3.3 Scanning Electron Microscopy

Effect of different HNT pre-treatments on the morphological structure of PLA based composites are analyzed by SEM. The observations on the composite containing 5wt% un-treated HNT mineral was given in the previous section. Its SEM micrograph can be also seen in Figure 4.35-a, b. According to the analysis, HNT minerals show a fine dispersion with a distribution of particles that are below $1\mu\text{m}$ in the PLA matrix owing to weak tube-tube interactions and/or hydrogen bonding between the filler and the matrix. However, agglomerates attaining particle size of $20\mu\text{m}$ dominate the microstructure and the composite components should be compatibilized better to prevent these formations.

In order to improve the compatibility between PLA and HNT, a purification procedure was applied. The main aim in this treatment is to remove the impurities which may cause agglomeration of particles and hinder the intercalation of polymeric materials between the clay. However, XRD results show that purification does not contribute to the intercalation process which might be due to high Na^+ concentration acting as trapped points and leading to failure in the intercalation of polymer chains into silicate layers. In addition, it causes much more dominant agglomerates as can be seen from Figure 4.35-c, d. They almost attain particle sizes of $30\text{-}40\mu\text{m}$ which are approximately twice that of the biggest agglomerates observed in composites prepared by un-treated HNT. However, composites prepared with p-HNT minerals display more roughened crack propagation lines compared to composites prepared with un-treated and other pre-treated HNT minerals.

To create a surface interaction between the filler and the polymer matrix, HNT minerals were silanated with γ -APS (o-HNT) and modified with phosphonium based quaternary alkyl salt, CBTPB, (m-HNT). The distribution of these two types of pre-treated minerals in the PLA was investigated with XRD analysis in the previous section, and it was seen that both trials resulted in poorly intercalated

structures. The SEM micrographs of the composite prepared with o-HNT and m-HNT can be seen from Figure 4.35-e, f and Figure 4.35-g, h respectively. Both mineral types show a similar distribution in PLA to that observed for un-treated HNT as expected. As explained in the previous part, this result might be attributed to lack of reactions which are expected to occur between the functional groups of organo-silane or alkyl salt and PLA matrix.

The last pre-treatment applied to HNT mineral is the evacuation method applied to remove the water layer that remained between the layers after classical drying methods. Well distribution of e-HNT minerals in the PLA matrix was mentioned in the previous part. SEM analysis of these samples can be seen from Figure 4.35-i, j. According to the micrographs, clay particles are distributed more finely when they are subjected to evacuation compared to HNT minerals subjected to other pre-treatments. However, there are still some aggregates which might deteriorate the mechanical properties of the composites. Answer to this question will be given in the mechanical properties part of this section. In addition, after addition of e-HNT to PLA the smooth surface is unchanged which resulting in high tensile strength.

There are some differences observed in the SEM micrographs of composites prepared by HNT minerals subjected to different pre-treatments. However, all of them show the bridging effect of the HNT mineral observed between the micro-cracks formed during fracture.

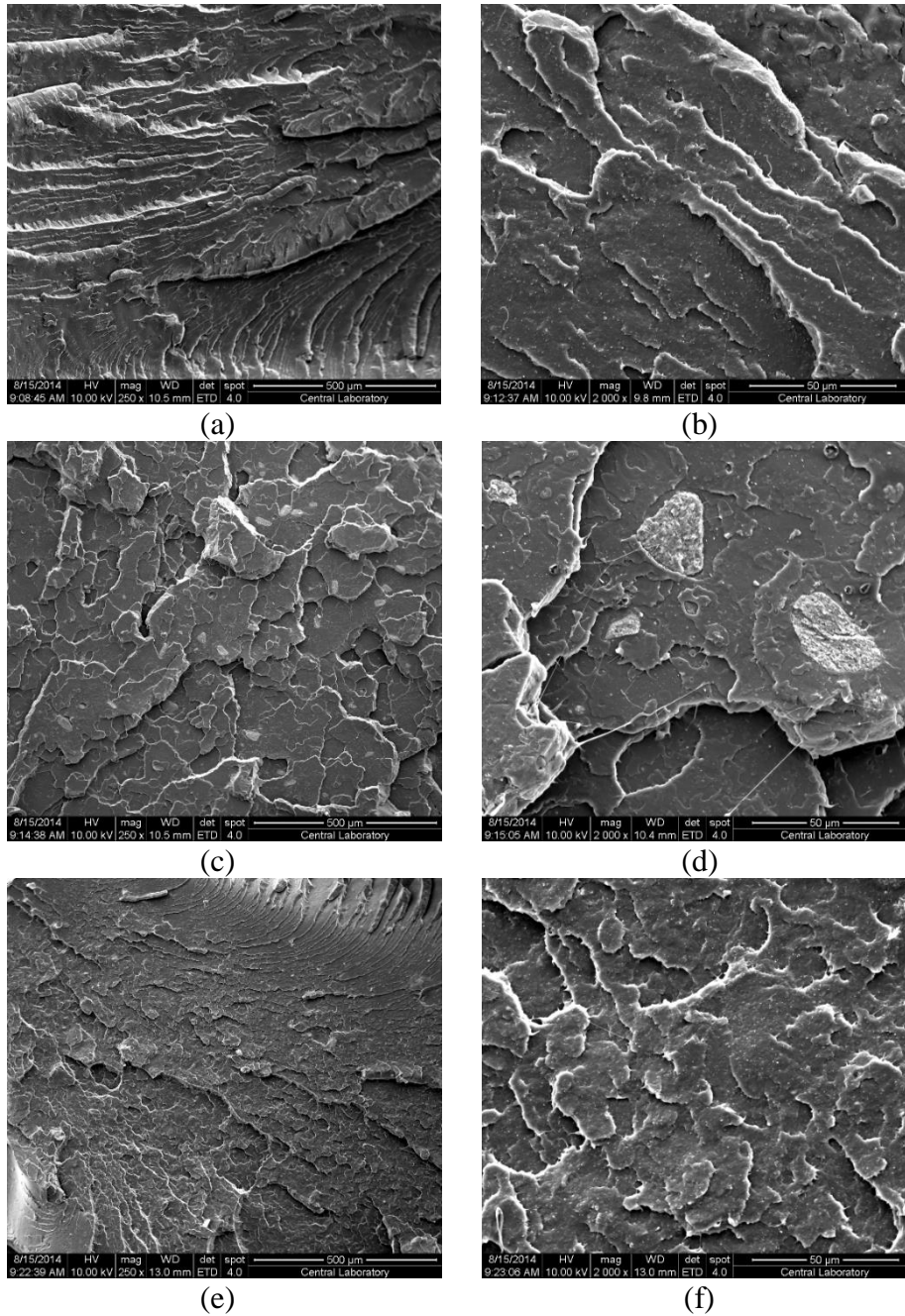
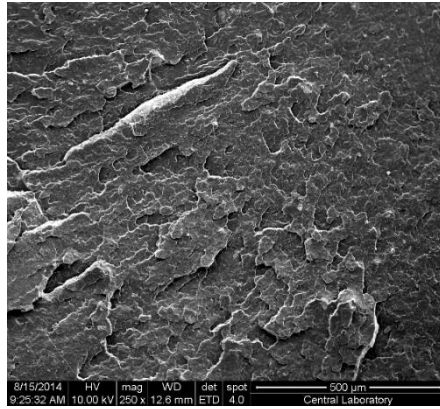
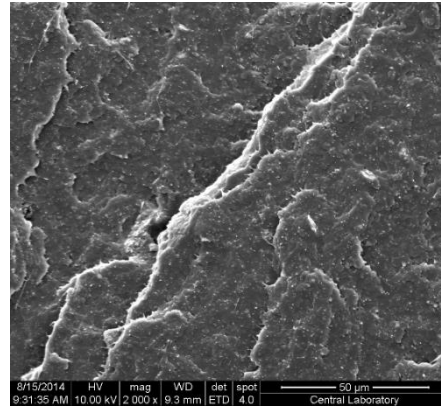


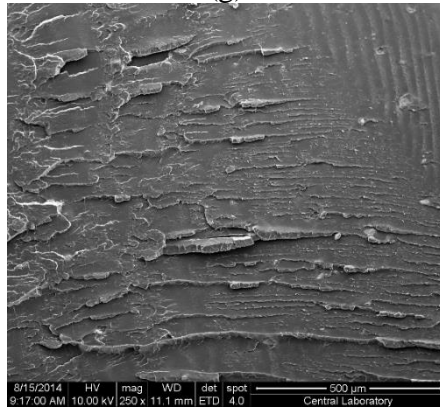
Figure 4.35. SEM micrographs of PLA based composites containing 5wt% Nanoclay; (a) HNT 250x, (b) HNT 2000x, (c) p-HNT 250x, (d) p-HNT 2000x, (e) o-HNT 250x, (f) o-HNT 2000x, (g) m-HNT 250x, (h) m-HNT 2000x, (i) e-HNT 250x, (j) e-HNT 2000x



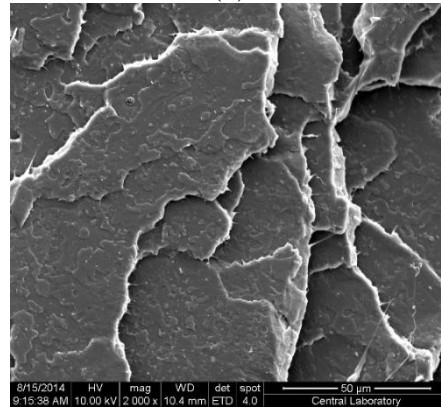
(g)



(h)



(i)



(j)

Figure 4.35 (continued). SEM micrographs of PLA based composites containing 5wt% Nanoclay; (a) HNT 250x, (b) HNT 2000x, (c) p-HNT 250x, (d) p-HNT 2000x, (e) o-HNT 250x, (f) o-HNT 2000x, (g) m-HNT 250x, (h) m-HNT 2000x, (i) e-HNT 250x, (j) e-HNT 2000x

4.3.4 Transmission Electron Microscopy

Different pre-treatments that the HNT particles were subjected to are mentioned previously. Among these treatments the best dispersion results were obtained from the composite samples prepared with evacuated HNT (e-HNT). This treatment was performed to overcome the problem about the water layer that remained after classical drying methods.

According to XRD and SEM results, although the layers of e-HNT mineral are not completely delaminated, there is distinct improvement in the distribution of the particles. In addition, it was suggested that there is limited intercalation. By the help of TEM micrographs shown in Figure 4.36, the well distribution and intercalation of clay particles is proven.

TEM micrographs given in Figure 4.36 show the ultra-section surface that is vertical to molding direction (See Figure 4.37). TEM micrographs were obtained by cutting ultra-thin sections from these surfaces and subjecting them to electron beam. As can be seen from Figure 4.36-a, HNT particles are located parallel to each other and form a “tile order” structure oriented with an angle of 45° to ultra-section surface axis. As mentioned previously these patterns are caused by shear forces created during melt mixing. In addition, 3-dimensional dispersion of HNT particles is not observed when they are subjected to drying under ultra-high vacuum before they are introduced into PLA matrix.

When the water between the basal spacing is totally removed, the interaction between HNT particles decreases while PLA-HNT compatibility increases. As a result, the zigzag structure explained in PLA/HNT composites turns into a ribbon structure with only an edge-to-edge interaction. This ribbon structure can be seen from Figure 4.36-b.

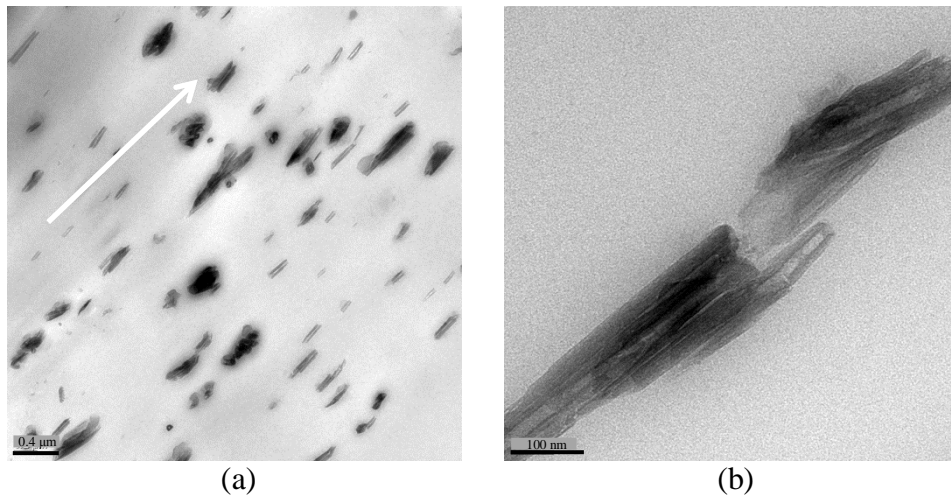


Figure 4.36. Transmission Electron Microscopy of PLA/e-HNT composite; (a) Scale bar is 0.4 μ m, (b) Scale bar is 100nm

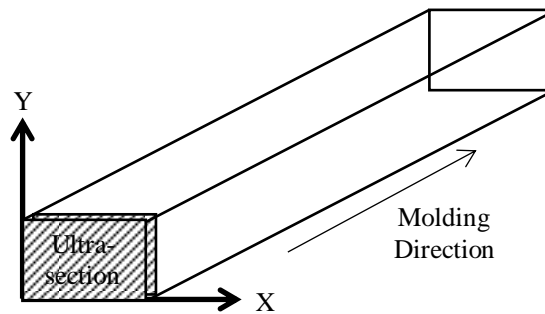


Figure 4.37. Schematic drawing of sample used in TEM analysis

4.3.5 Tensile Properties

Effects of different pre-treatments on the tensile properties of PLA/5wt% Nanoclay composites are given in Figure 4.38 and Figure 4.39. The slight reduction observed in the strength of the composites prepared by raw Nanoclay HNT was discussed in the previous section, and this was attributed to the absence of an intercalated structure and formation of agglomerates attaining particle size of 20 μ m.

Surface modification of HNT particles both with γ -APS and CBTPB were performed to solve the distribution problem by creating a more attractive HNT surface for PLA matrix. Some studies demonstrate the possibility to obtain high performance nanocomposites by the help of surface modification with organo-silane and alkyl salt (Murariu et al. 2012, Prashantha et al. 2013). They display better strength for composites compared to pure PLA. However, no enhancement in tensile strength can be obtained for this study. As mentioned in the XRD results part of this section, the water layer that remained between the layers of silicate might hinder the expected reactions between the functional groups and polymer matrix.

The nanocomposite which was prepared with evacuated HNT (e-HNT) displays a 5% increase in its tensile strength compared to pure PLA as can be seen from Figure 4.38-e. This improvement may lead the study to modify the surface of the e-HNT minerals to obtain much better physical properties of composites prepared by these fillers. However, troublesome production of e-HNT due to high vacuum application may restrict its industrial application. Hence, other solutions should be found to improve the physical properties of PLA/HNT composites.

Among the pre-treatments the worst results are obtained for the composite which is prepared with p-HNT. There is a reduction in its tensile strength of approximately 7% compared to that of PLA.

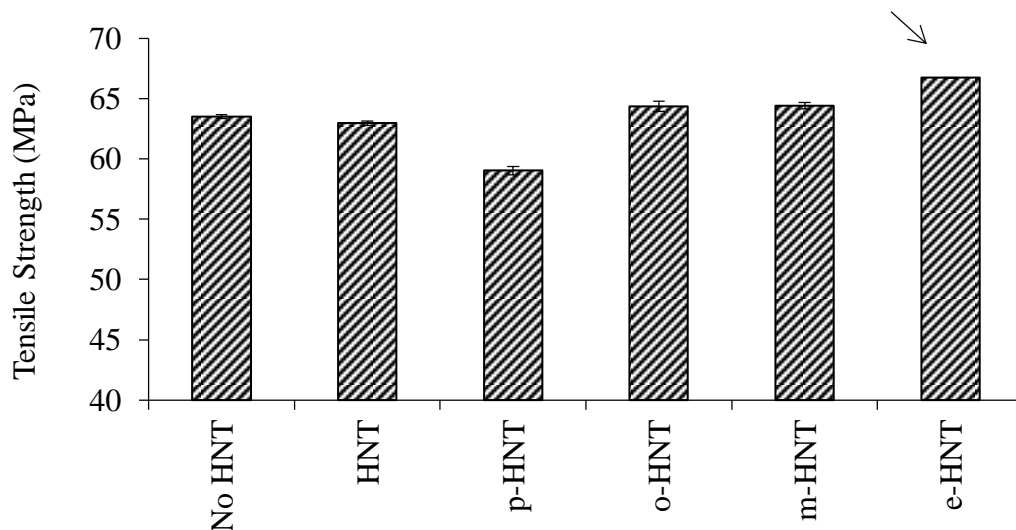


Figure 4.38. Effect of different HNT pre-treatments on the tensile strength (MPa) of PLA/5wt% Nanoclay composites (p-HNT: Purified Nanoclay, o-HNT: Functionalized Nanoclay with γ -APS, m-HNT: Modified Nanoclay with Alkyl Sat, e-HNT: Evacuated Nanoclay)

Bridging effect of the nanotubes on the elongation at break results of PLA/HNT composites was mentioned before. Especially, 5wt% Nanoclay loading results in 13% improvement as mentioned in the discussion of Figure 4.12 and Figure 4.39. However, the other pre-treatments except for purification, which roughens straight crack propagation lines, have no significant effect on strain at break values. For the e-HNT containing nanocomposite, the small reduction in elongation at break is an expected result, because for thermoplastics, a reduction in elongation at break value with clay addition is a common observation due to restricted strain of silicate particles by external stresses (Nielsen and Landel 1993).

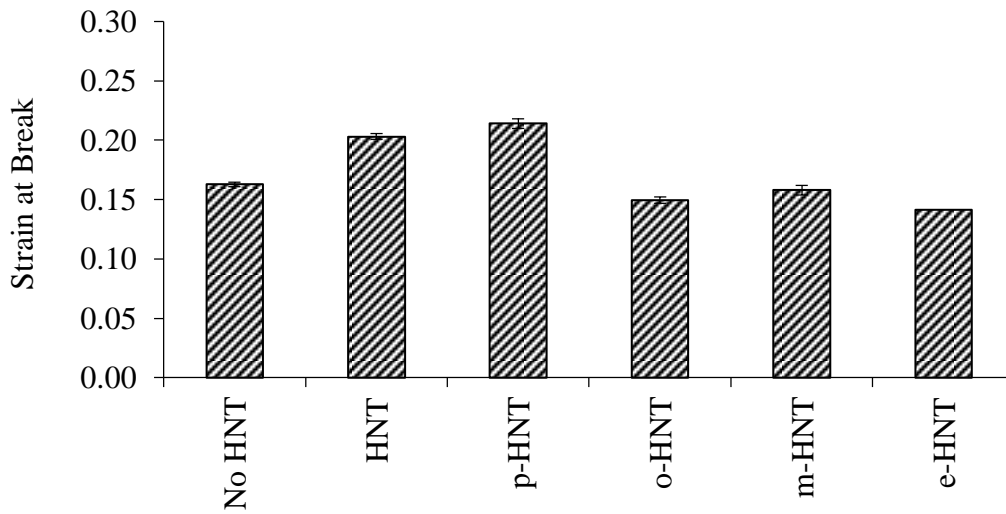


Figure 4.39. Effect of different HNT pre-treatments on the strain at break values of PLA/5wt% Nanoclay composites (p-HNT: Purified Nanoclay, o-HNT: Functionalized Nanoclay with γ -APS, m-HNT: Modified Nanoclay with Alkyl Salt, e-HNT: Evacuated Nanoclay)

4.3.6 Impact Results

Effect of HNT pre-treatments on the impact strength of PLA/HNT composites can be seen from Figure 4.40. According to the results, pre-treatments do not give rise to an improvement in the toughness of the pure PLA. Especially, the composites prepared with purified HNT (p-HNT) might be expected to display better impact properties due to roughened surface. However, the large agglomerates prevent this enhancement. In addition, e-HNT containing composite shows no deterioration in its impact strength although it shows good tensile properties compared to other composites.

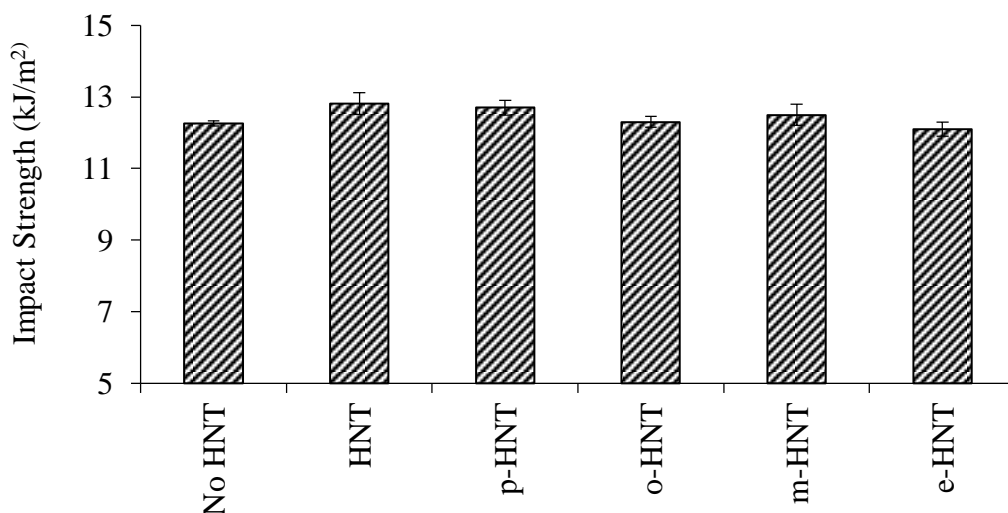


Figure 4.40. Effect of different HNT pre-treatments on the impact strength (kJ/m²) of PLA/5wt% Nanoclay composites (p-HNT: Purified Nanoclay, o-HNT: Functionalized Nanoclay with γ -APS, m-HNT: Modified Nanoclay with Alkyl Sat, e-HNT: Evacuated Nanoclay)

4.3.7 Dynamic Mechanical Analysis (DMA)

The responses of the PLA/Nanoclay HNT composites prepared by clay minerals subjected to different pre-treatments to periodic forces are given through Figure 4.41 to Figure 4.43. In the previous section, the better dispersion of Nanoclay particles in the polymer matrix compared to ESAN HNT and its low storage modulus (E') was mentioned. This was attributed to ineffectiveness of the distribution of clay particles on the stiffness of the composites.

Purification has no effect on the E' values of the PLA/HNT composites which display approximately the same response as the composites prepared by raw

Nanoclay. Although a better stiffness is expected with surface modification of HNT minerals. There is a sharp decrease in the E' values of the composites containing o-HNT and m-HNT at temperatures below the T_g of PLA. Negative effect of the modified clay particles on the storage modulus of the composites might be a result of their high plasticizing effect. However, e-HNT inclusion into PLA matrix results in a higher storage modulus in both the glassy and rubbery regions.

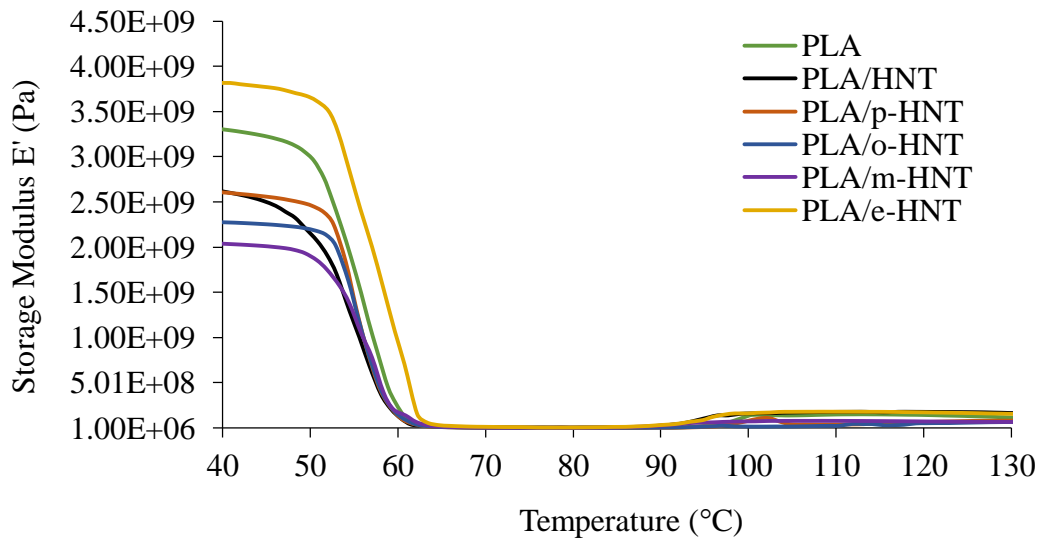


Figure 4.41. Effect of different HNT pre-treatments on the Storage Modulus, E' , (Pa) of PLA/5wt% Nanoclay HNT composites (p-HNT: Purified Nanoclay, o-HNT: Functionalized Nanoclay with γ -APS, m-HNT: Modified Nanoclay with Alkyl Sat, e-HNT: Evacuated Nanoclay)

The viscous portion of the composites also displays an enhancement in modulus values (E') in the presence of e-HNT compared to those which are prepared with raw Nanoclay or Nanoclay samples subjected to other type of pre-treatments. The maximum point peak shifts to higher temperatures due to lowered chain mobility with increasing crystalline fraction. However, this result cannot be proven by loss tangent ($\tan \delta$) versus temperature plots. The maximum point peak neither shifts to higher or lower temperatures. Instead, it remains approximately the same as that of neat PLA. On the other hand, the intensity value of the $\tan \delta$ peak at T_g shifts to higher values indicating a higher volume fraction of constrained polymer.

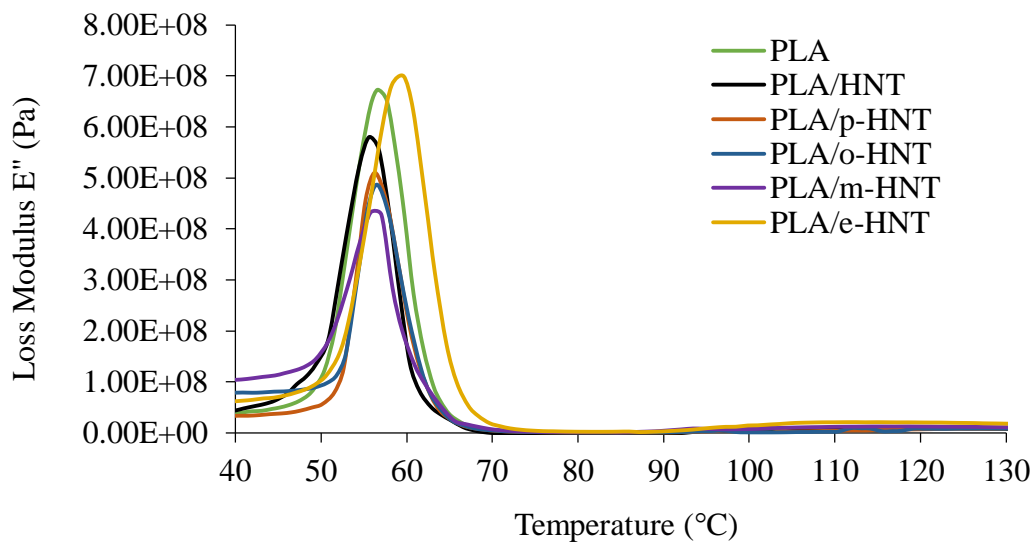


Figure 4.42. Effect of different HNT pre-treatments on the Loss Modulus, E'' , (Pa) of PLA/5wt% Nanoclay HNT composites (p-HNT: Purified Nanoclay, o-HNT: Functionalized Nanoclay with γ -APS, m-HNT: Modified Nanoclay with Alkyl Sat, e-HNT: Evacuated Nanoclay)

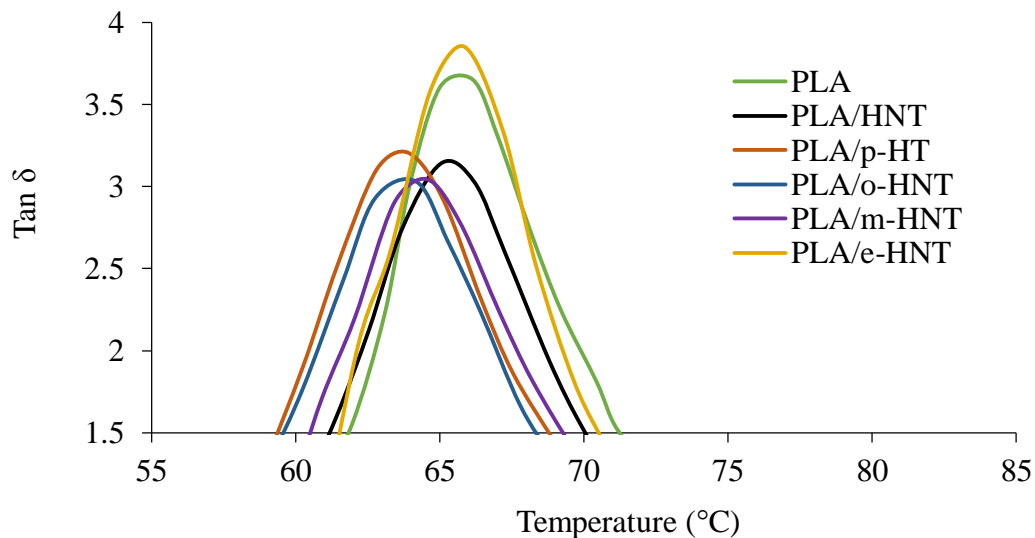


Figure 4.43. Effect of different HNT pre-treatments on the $\tan \delta$ of PLA/5wt% Nanoclay HNT composites (p-HNT: Purified Nanoclay, o-HNT: Functionalized Nanoclay with γ -APS, m-HNT: Modified Nanoclay with Alkyl Sat, e-HNT: Evacuated Nanoclay)

4.3.8 Differential Scanning Calorimetry Analysis (DSC)

To investigate the change in the thermal behavior with HNT pre-treatment, DSC analysis was performed and transition temperatures are given in Table 4.4 with % crystallinity results. The results obtained for composites prepared with Nanoclay subjected to pre-treatments other than evacuation do not display a significant change in their T_g , T_m and T_c , whereas they show a decrease in crystalline fraction (%) as in the case of the composite containing raw Nanoclay HNT.

However, T_g of e-HNT containing nanocomposite shows an increase due to lowered chain mobility. Although the crystalline fraction (%) remains lower than

that of pure PLA, the decrease in chain mobility and higher glass transition temperature is clear. This might be due to restricted movement of polymer chains because of homogeneously distributed clay particles. However, it is obvious that there is no nucleating effect of e-HNT on the PLA matrix.

Another point that takes attention is the reduction in heat of crystallization (ΔH_c) and heat of melting (ΔH_m) for the nanocomposite prepared with e-HNT.

Table 4.4. Effects of different HNT pre-treatments on thermal transition behaviors and crystalline fraction (%) of PLA/5wt% Nanoclay HNT composites

Sample	T_g (°C)	T_c (°C)	ΔH_c (J/kg)	T_m (°C)	ΔH_m (J/kg)	X_c (%)
PLA	57.8	120.3	22.04	148.1	24.21	2.3
PLA/HNT	58.3	121.2	21.68	148.4	21.79	0.1
PLA/p-HNT	58.0	121.2	22.15	148.0	22.17	0.0
PLA/o-HNT	57.8	121.3	22.21	147.8	22.23	0.0
PLA/m-HNT	58.1	121.1	22.36	147.9	22.07	0.3
PLA/e-HNT	59.5	121.6	18.76	149.1	19.78	1.0

Among the pretreatments performed in this study, only evacuation led to formation of nanocomposite and gave reasonable values in terms of the composite physical properties. However, in industrial applications evacuation is hard to achieve due to vacuum application. Hence, other solutions for the formation of nanocomposites are investigated in the following sections.

4.4 Effects of Plasticizer and Toughening Agent on the Properties of PLA/HNT Composites

PLA is a preferable polymer due to its biodegradable characteristics, but suffers from its brittleness. One of the methods to overcome this problem is to use a third material which is biocompatible with the polymer matrix. These types of materials are called compatibilizers, impact modifiers or plasticizers depending on the intended use. In this study these terms will be used interchangeably.

The aim of these types of materials is to toughen the matrix by preventing crazes from developing into cracks. The mechanism underlying behind the toughness improvement with plasticizers is to create large dispersed particles which stop the growth of cracks. These dispersed particles dissipate impact energy by transforming it into deformation of themselves (Bucknall 1977, Kramer and Krauch 1983). In order to provide this improvement, perfect compatibility between polymer matrix and plasticizer is required.

Use of biodegradable polymers in automotive sector, which requires high toughness, is the starting point of this study. Hence, plasticization is required for PLA, for applications requiring high toughness. For nanocomposites, improvement in the strength is possible by the well dispersion of silicate layers and exfoliated structure. However, the toughness is improved in a limited manner (Pavlidou and Papaspyrides 2008). Function of the plasticizer starts at this point as impact modifier whose inclusion to polymer matrix results in better impact properties, toughness and elongation at break values.

In addition, another property of the materials used for toughness improvement is to enhance the compatibility between the matrix and filler to aid the penetration of polymer chains in between the silicate layers. Delaminated clay layers by polymer insertion act as both effective stress concentrator and nucleating agent which improve mechanical and thermal properties. In this study, two types of materials

with different characteristics were used as impact modifier for PLA; Poly(ethylene glycol) (PEG) and Thermoplastic polyurethane (TPU). These materials are called as PEG plasticized PLA (P-PLA) and TPU toughened PLA (T-PLA).

A low molecular weight (8000 g/mol) PEG in the form of powder was chosen as the plasticizer for this study. The reason underlying behind the selection of low molecular weight PEG is its perfect solubility in the amorphous phase of PLA, and previous studies revealing the action of PEG as an effective polymeric plasticizer to improve the crystallization rates of PLA (Kulinski and Piorowska 2005, Hu et al. 2003b, Pluta and Galeski 2002). In the literature, especially organoclay based nanocomposites of PLA/PEG blends attract attention due to their improved physical properties compared to those of pure PLA (Paul et al. 2003, Tanoue et al. 2006). For the determination of optimum PEG concentration, the study performed by the research group of Kocaeli University Chemical Engineering Department Plastics and Rubber Technology Research Group on the plasticized PLA films was used as the reference, and PEG was loaded to composites at 20wt% (Ozkoc and Kemalolu 2009).

The other material used to improve the toughness of the PLA is TPU which is stiffer material than PEG. To compare the effect of TPU with PEG, all parameters during composite preparation were kept constant, such as processing temperature, screw speed, TPU content (20wt%) and etc. TPU is a linear co-polymer composed of hard and soft rubbery segments which provide high elongation at break, moderate tensile strength and Young's modulus, excellent abrasion and tear resistance (Ping et al. 2007). This elastomeric material disperses itself uniformly in the polymer matrix. It reduces the interfacial tension and improves the adhesion. In addition, it is expected for TPU to function as a good compatibilizer between PLA and nano-filler HNT due to its biocompatibility with PLA.

In this section of the study DM3 method was used and HNT minerals were not subjected to pre-treatment due to the reasons explained in the previous sections.

4.4.1 X-Ray Diffraction Results

PEG is a biocompatible polymer known to have a crystalline structure which leads to increased crystallization rate for the PLA matrix. PLA samples display an amorphous dominant initial structure with a broad maximum around 17° which is the peak of homo-crystal form as shown before in Figure 4.4 and Figure 4.5. The trace of this broad structure is also visible in the XRD patterns of PLA/HNT composites. The composites prepared in the presence of the crystalline PEG show a new peak around 16.4° as can be seen from both Figure 4.44 and Figure 4.45. This new formed broad hump is the indication of increased crystallinity by introduction of PEG into PLA matrix. Since PEG has characteristic diffraction peaks between 1 and 3° , they do not attract attention in the following figures.

The plasticizing effect of PEG on the PLA matrix is investigated in the mechanical and thermal properties part of this section. The small molecules like PEG can establish physical interactions such as hydrogen bonding or dipole-dipole interaction with macromolecules like PLA during melt mixing. Hence, the polymer – polymer interaction is mostly replaced with polymer – plasticizer interaction. This phenomenon might provide better molecular movement and hence better intercalation of polymer chains between the silicate layers (Mohapatra, Mohanty and Nayak 2014). Also, PEG molecules are expected to interact with the Si – O outer surface and Al – OH edge and inner surface groups of HNT minerals. Hence, these small molecules might behave as a bridge between the incompatible polymer PLA and filler HNT. However, the unchanged position of basal and non-basal peak with the introduction of PEG indicates that, PEG could not act as a successful compatibilizer between PLA and HNT to provide intercalation.

In the literature, there are many studies indicating well dispersion and intercalated structures that are formed with the introduction of layered silicates into PLA matrix in the presence of PEG. Especially, Montmorillonite (MMT) based

nanocomposites attract attention in which PEG provides high compatibility between PLA and MMT (Mohapatra et al. 2014, Pluta et al. 2006a, Pluta et al. 2006b). For instance, Pluta and his co-workers mention the improvement in the gallery space of layered silicates in the presence of PEG with 1000 g/mole molecular weight (Pluta et al. 2006a). According to study performed with different types of organically modified MMTs, PEG and PLA intercalation into galleries interchanges depending on the modification. In some cases PLA and PEG tend to co-intercalate, whereas for some organoclay types only PEG is stabilized within the clay galleries. The PEG molecule used in this study has an eight times higher molecular weight compared to the PEG used in the mentioned study. High molecular weight of the PEG compared to reference might be the reason of its low compatibilizer effect. In other words, hydrogen bonds positioned between the layers instead of cations might block the insertion of high molecular weight chain insertion between the layers.

Another reason that may cause un-distributed and un-delaminated clay layers is the water layer that remained between the clay galleries as mentioned previously in the effect of pre-treatments part. The water content might inhibit the desired reactions which would have resulted in hydrogen bonding and dipolar interaction between both PEG – HNT and PLA – HNT. Also, possibility of degradation of both PLA and PEG molecules can be said to be the reason of un-improved clay distribution and physical properties as will be mentioned in the following sections.

On the contrary to PLA/HNT composites investigated previously, the disappeared HNT reflection peak around 20° becomes slightly visible for composites containing plasticizer. Hence, the suggestion of the presence of the interaction of polymer chains with filler particles due to preferential orientation of nanotubes in tile patterns is not valid for the plasticized composites.

For the plasticized composites containing reference HNT Nanoclay, the basal and non-basal peak become more visible due to better reflection as mentioned

previously. The positions of these peaks do not show a left or right shift indicating intercalation or gallery collapse respectively as in the case of P-PLA/ESAN HNT composites.

Thus, for both types of clay minerals it can be said that nanocomposite formation did not take place for plasticized composites. Also, change in clay loading from 3 to 10wt% does not affect the dispersion state of particles in the polymer matrix.

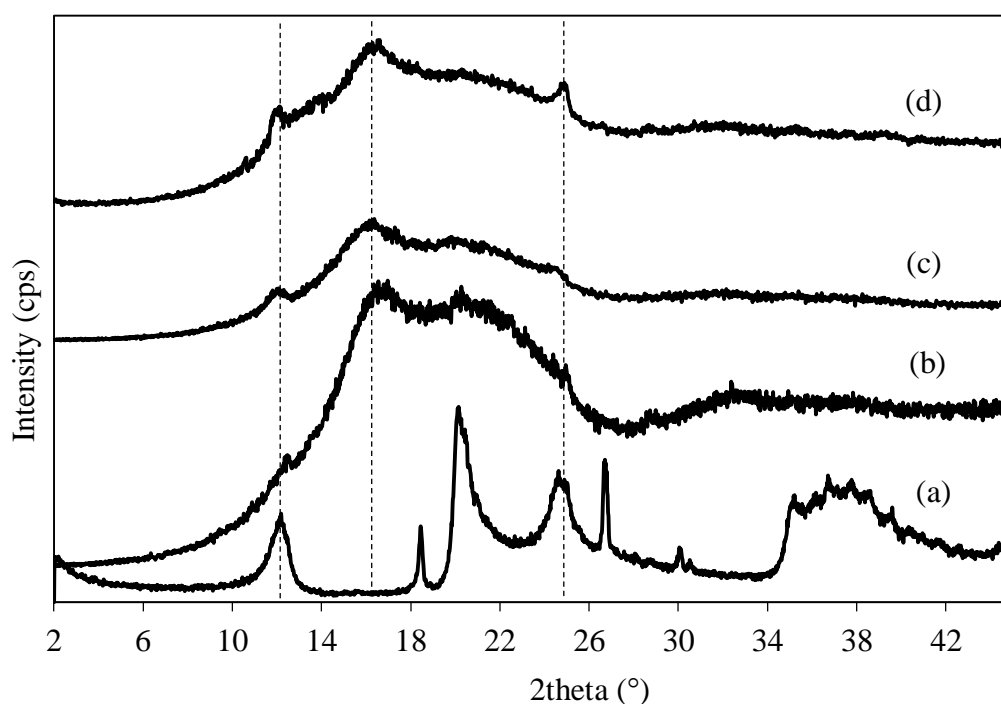


Figure 4.44. XRD pattern of P-PLA/ESAN HNT composites; (a) ESAN HNT, (b) P-PLA/3wt% ESAN HNT, (c) P-PLA/5wt% ESAN HNT, (d) P-PLA/10wt% ESAN HNT

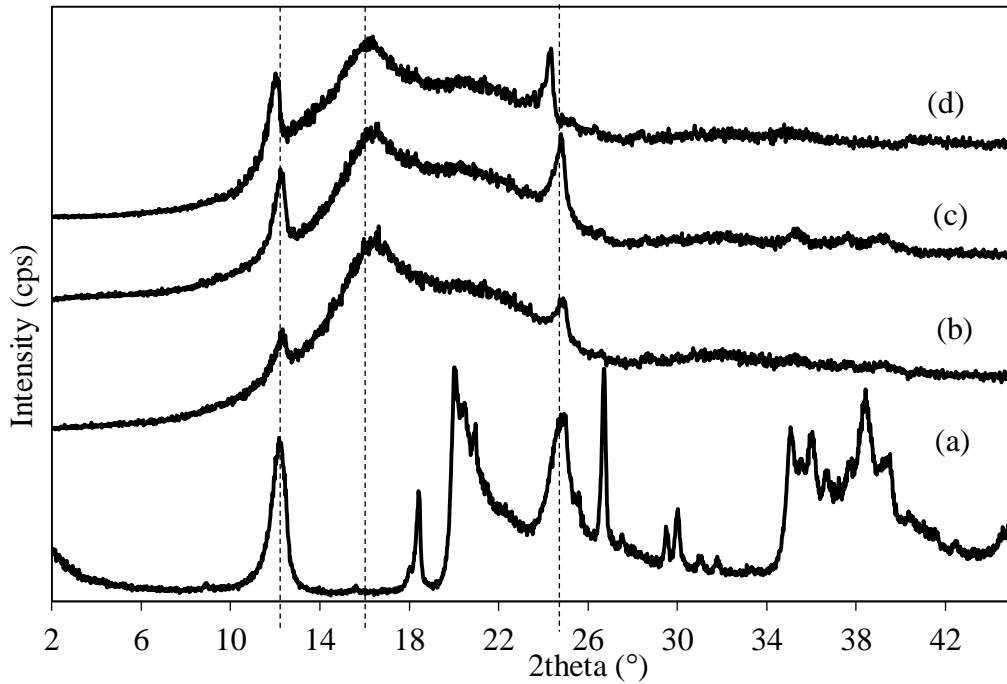


Figure 4.45. XRD pattern of P-PLA/Nanoclay HNT composites; (a) Nanoclay HNT, (b) P-PLA/3wt% Nanoclay HNT, (c) P-PLA/5wt% Nanoclay HNT, (d) P-PLA/10wt% Nanoclay HNT

The second material used to toughen the PLA matrix and form compatibility is TPU, which has flexible mechanical properties. Like PEG, TPU is also a biodegradable polymer which is expected to solve the problem faced in the distribution of clay in polymer matrix and hence un-improved physical properties. XRD results of 5wt% ESAN and Nanoclay HNT containing composites prepared in the presence of this elastomeric material are shown in Figure 4.46. In addition to basal and non-basal peaks of HNT, with TPU introduction to PLA/HNT composites, a new peak is formed exactly at the same position of Gibbsite peak as shown in Figure 4.1 and Figure 4.2. This new peak located around 18° might be an indication of increased crystalline fraction of PLA.

The strong attraction of the ester group of the TPU with PLA and possible grafting of TPU chains on the surface and edge of HNT mineral render a homogeneous distribution. However, the preservation of the basal and non-basal peaks indicates that a significant amount of HNT had retained its original diameter after melt extrusion, for both ESAN and Nanoclay HNT. In the literature, both P-PLA and T-PLA composites yield an improved MMT clay distribution and physical composite properties (Jia et al. in Press). However, this study reveals that this is not possible with HNT minerals which are in the shape of hollow tubular and carry water molecules that cannot be removed by classical drying methods.

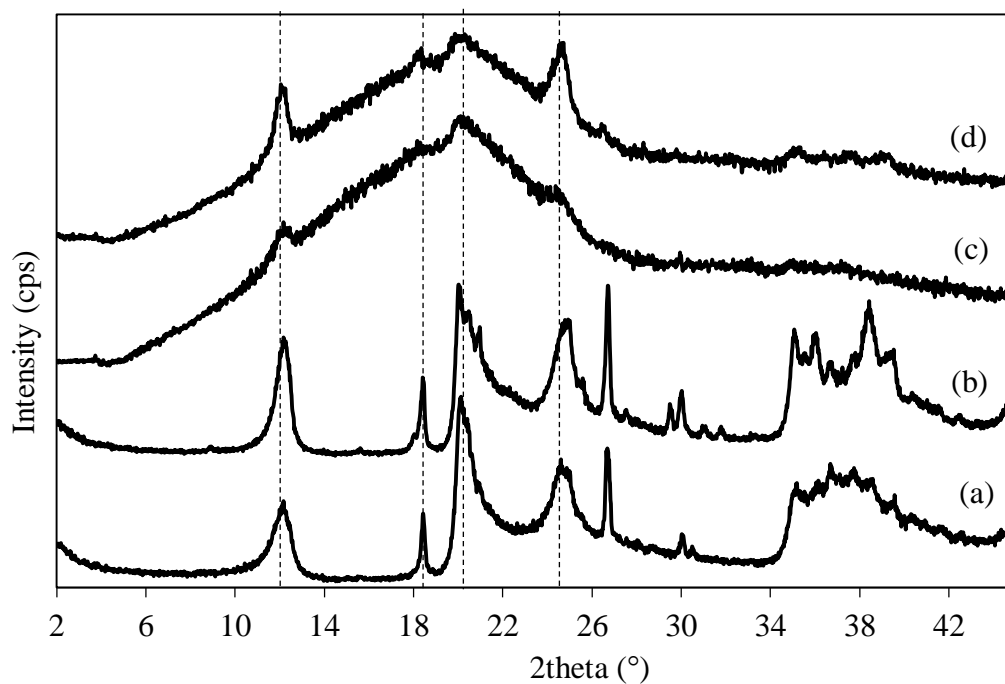


Figure 4.46. XRD pattern of T-PLA/5wt% HNT composites; (a) ESAN HNT, (b) Nanoclay HNT, (c) T-PLA/5wt% ESAN HNT, (d) T-PLA/5wt% Nanoclay HNT

4.4.2 Scanning Electron Microscopy

As mentioned at the beginning of this section two types of materials were used for the modification of brittle polymers, and prevent the problems related with fracture. The SEM micrographs of PLA/PEG (P-PLA) blend and its composites prepared with 5wt% ESAN and Nanoclay HNT can be seen from Figure 4.47.

When PEG is introduced into PLA, surface becomes smoother and a layered structure is formed. It is known that increased roughness of a surface directly affects the toughness of a material. Also, straight crack propagation lines should become shorter and closer to each other to enhance the amount of energy dissipation during fracture. Although a different morphology is observed for this study, mechanical results verify that addition of PEG improves the toughness of PLA. This might be attributed to extensively very long fibrillar structures covering the entire surface. In addition, no phase separation of PEG is observed indicating miscibility of the two components.

HNT minerals added to P-PLA blend lead to re-formation of roughened surface and disappearance of fibrillar structures. This formation does not result in a change in the mechanical properties of the composites as will be mentioned in the following part.

The second type of material is TPU which is used as an elastomeric compatibilizer. The elastomeric materials generally form distributed domains in the main matrix and the failure mechanism of a blend or composite depends on this distribution. The morphology development during melt mixing of these blends comprise processes such as: fluid drops stretching into threads, break-up of the threads into smaller droplets and finally coalescence of the droplets into larger ones (Akkapeddi et al. 2001). SEM micrographs of PLA/TPU (T-PLA) blend and its composites showing the dispersed droplet structure are depicted in Figure 4.48. The average domain sizes which are calculated by using ImageJ 1.32 (Wayne

Rasband National Institutes of Health) software program can also be seen both from Figure 4.48, on the respective micrographs, and Table 4.5. Approximately 50-100 domains were analyzed to get an accurate dimension.

It is a known fact that droplet matrix morphologies improve the impact properties, and small domains make the system more stable due to larger surface area created (Wu 1985, Verhoogt et al. 1994). Addition of HNT to T-PLA blend results in a smaller average domain size. As HNT content increases, the domain size decreases due to clay particles distributed both in the PLA matrix and at the interfaces between PLA and TPU phases. This might be attributed to inhibited cohesive forces between domains and interfacial mobility of the dispersed phase.

In addition to the average domain size, inter-domain distance is an important factor affecting the toughening of the materials. Small inter-particle distance suppresses craze or crack growth and facilitates the overlap of the stress fields around the adjacent domains. By this way, local shear yielding is promoted and high impact energies are absorbed. By decreasing domain size, this parameter also decreases yielding better impact strength as will be mentioned in the mechanical results part.

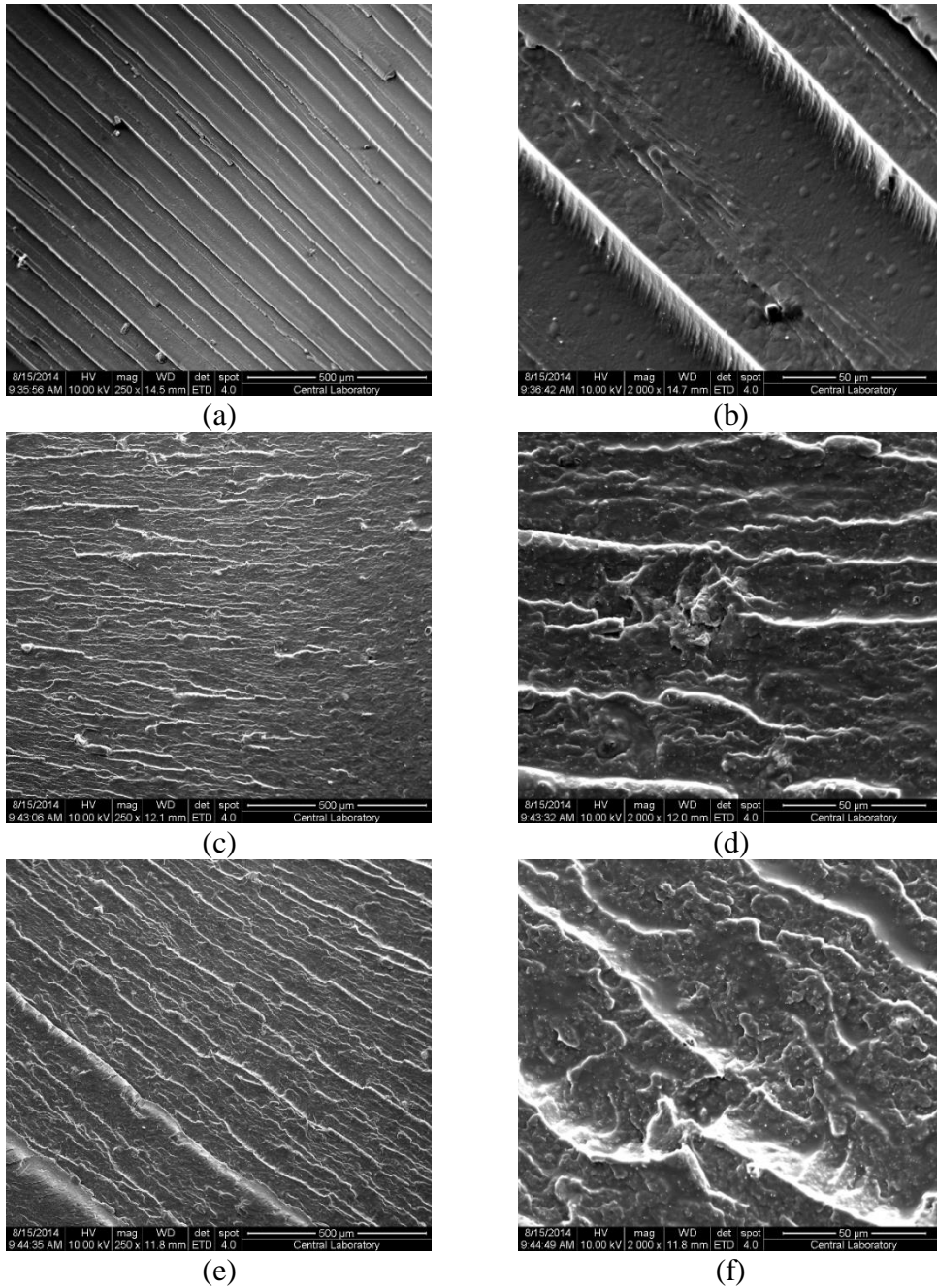


Figure 4.47. SEM micrographs of P-PLA composites (a) 0wt% HNT 250x, (b) 0wt% HNT 2000x, (c) 5wt% ESAN 250x, (d) 5wt% ESAN 2000x, (e) 5wt% Nanoclay 250x, (f) 5wt% Nanoclay 2000x

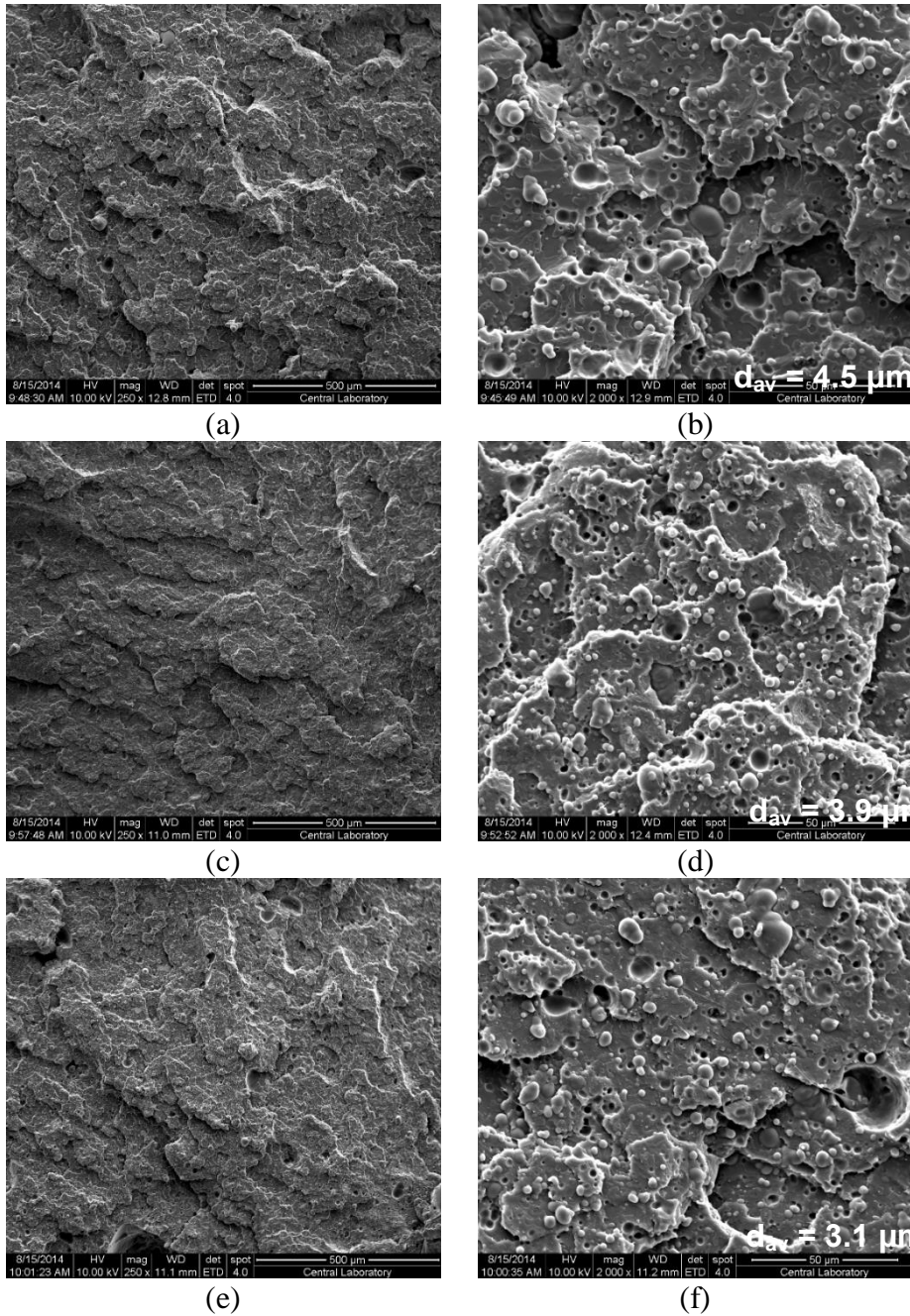


Figure 4.48. SEM micrographs of T-PLA composites (a) 0wt% ESAN 250x, (b) 0wt% ESAN 2000x, (c) 3wt% ESAN 250x, (d) 3wt% ESAN 2000x, (e) 5wt% ESAN 250x, (f) 5wt% ESAN 2000x, (g) 10wt% ESAN 250x, (h) 10wt% ESAN 2000x

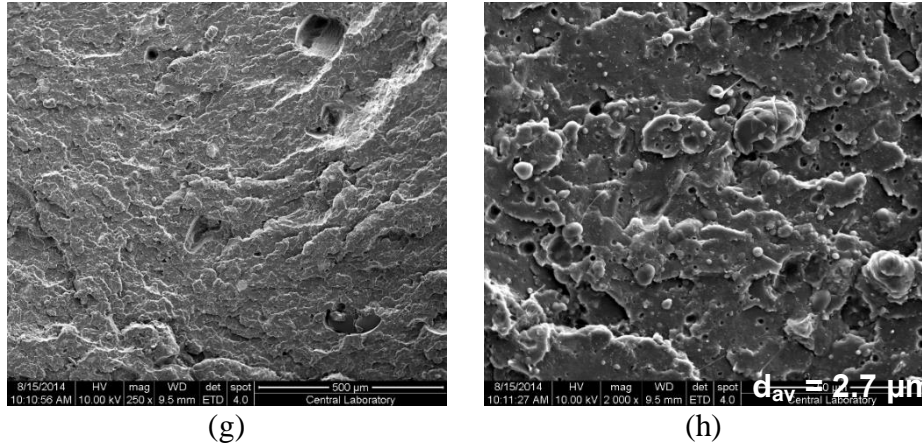


Figure 4.48 (continued). SEM micrographs of T-PLA composites (a) 0wt% ESAN 250x, (b) 0wt% ESAN 2000x, (c) 3wt% ESAN 250x, (d) 3wt% ESAN 2000x, (e) 5wt% ESAN 250x, (f) 5wt% ESAN 2000x, (g) 10wt% ESAN 250x, (h) 10wt% ESAN 2000x

Table 4.5. Average domain size of PLA/TPU blend and its ESAN based composites

Sample	$d_{avg}(\mu\text{m})$
T-PLA	4.5
T-PLA/3wt% ESAN	3.9
T-PLA/5wt% ESAN	3.1
T-PLA/10wt% ESAN	2.7

4.4.3 Transmission Electron Microscopy

P-PLA and T-PLA composites containing 5wt% ESAN HNT are observed by TEM analysis to see the effect of PEG and TPU on the distribution of clay. As mentioned before, PEG is miscible in PLA and does not form a separate phase. In addition, PEG molecules do not contribute to the dispersion of HNT minerals in a desired manner to form a nanocomposite as can be seen from Figure 4.49-a.

When TPU containing composite is analyzed from Figure 4.49-b it is observed that elastomeric phase is observed as the dispersed white region. In accordance with the SEM results, HNT particles are distributed mainly in the PLA matrix and close to the interface between the PLA and TPU matrix. This morphological structure was assumed to be the main cause of decreased domain size and improved impact properties with the addition of HNT.

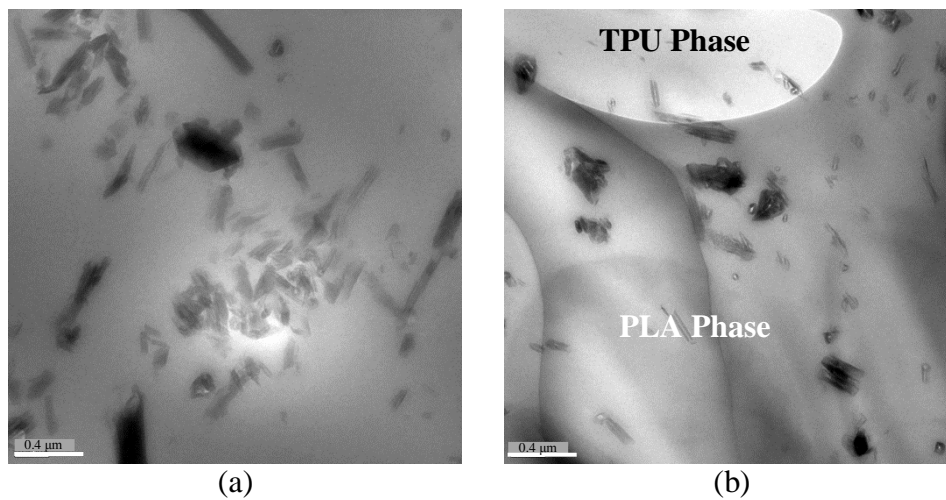


Figure 4.49. TEM Micrographs of composites containing 5wt% ESAN HNT; (a)P-PLA, (b) T-PLA composite (Scale bar is 0.4 μm)

4.4.4 Tensile Properties

The representative stress-strain curves of the plasticizer PEG and elastomer TPU are shown in Figure 4.50. The figure illustrates the soft and tough characteristics of PEG-plasticized PLA (P-PLA) in contrast to hard and strong characteristics of PLA blended with TPU (T-PLA) and compares both of them with neat PLA. These comparisons can also be clearly seen through Figure 4.51 to Figure 4.54.

PLA displays a quite sharp reduction in its tensile strength after plasticization with PEG molecules. However, PEG functions in the desired way and highly improves the strain at break and toughness of PLA. On the contrary, T-PLA blend represents a tensile strength that is in between that of PLA and P-PLA. However, the improvement in the strain at break value of PLA can be said to be poor.

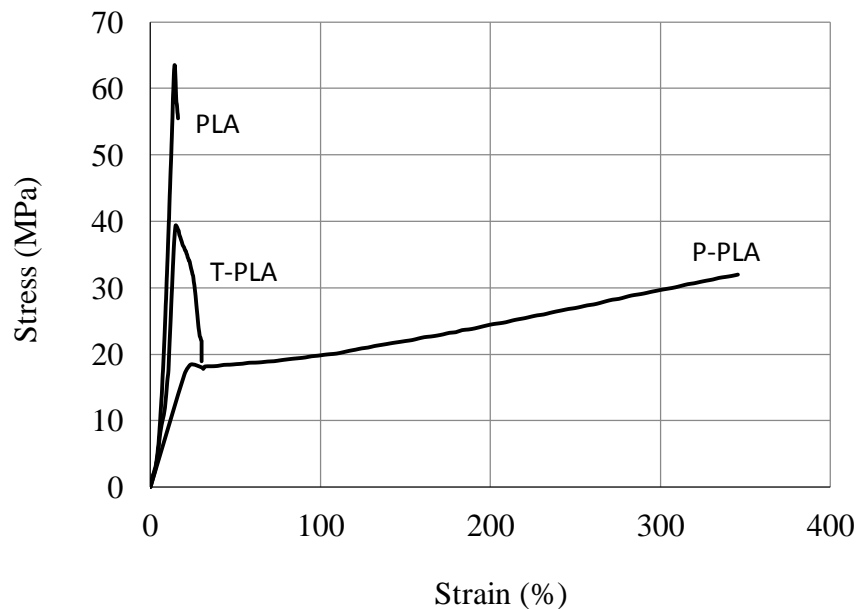


Figure 4.50. Stress-strain curves of pure PLA, P-PLA and T-PLA

As mentioned previously, PEG is loaded to composites at 20wt%. According to both of the studies performed by Özkoç and Pillin with their co-workers, beyond 20wt% loading of PEG, the toughness of the PLA starts to decrease, and this can be attributed to the lack of cohesion between the polymer matrix and PEG due to phase separation formation (Ozkoc and Kemalolu 2009, Pillin, Montrelay and Grohens 2006). At this loading, the strength of PLA decreases approximately by half while contribution of PEG to the strain at break is enormous.

Strength and strain at break results obtained for toughened ESAN based composites are given in Figure 4.51 and Figure 4.52. The unsuccessful distribution of clay particles in the presence of PEG was previously mentioned in the XRD results. This result might be the cause of the reduction in the tensile strength and un-improved strain at break values with HNT addition. However, with increasing clay content from 3 to 10wt%, there is a slight enhancement in the strength of the composites. Micro-filled composites are defined as composites with particle size around 0.01 – 0.04 μ m, whereas in conventional composites the particle size attains a value of around 8 μ m. It can be assumed that HNT containing P-PLA matrix behaves as a conventional composite at low clay loading due to the absence of intercalated structure and poor distribution of clay particles. However, as the clay content increases the force applied to distribute the particles may become more effective due to increased viscosity with addition of clay particle into polymer matrix (Yeniova and Yilmazer 2013). Hence, it can be said that the effect of clay particles to act as filler which increase the melt viscosity of the matrix might be the cause of conversion from conventional composite at low loadings to micro-filled composite at higher loading.

This slight improvement in the tensile strength with increasing clay content results in an insignificant decrease in the strain at break values of P-PLA composites. For reinforced composites, the reduction in elongation at break is an expected result because of the increased stress concentration. According to these results, in-effectiveness of PEG as a compatibilizer is obvious.

TPU behaves in a different manner compared to PEG. To compare the impact of these plasticizers on the physical properties of PLA and PLA/HNT composites, TPU was also added at 20wt%. The tensile strength of the PLA matrix blended with TPU shows a better result compared to that of P-PLA matrix, whereas its elongation at break only doubles compared to that of PLA. The un-improved elongation at break can be attributed to the hard segment of TPU elastomer.

Tensile properties of the T-PLA/ESAN composites are also given in Figure 4.51 and Figure 4.52. Insertion of ESAN HNT to T-PLA matrix does not give rise to a negative or positive effect on the strength values due to absence of intercalated and/or exfoliated structure. However, improvement in the strain at break values with increasing HNT content is noticed. Especially, for 10wt% ESAN HNT loading the strain at break value reaches 1.78.

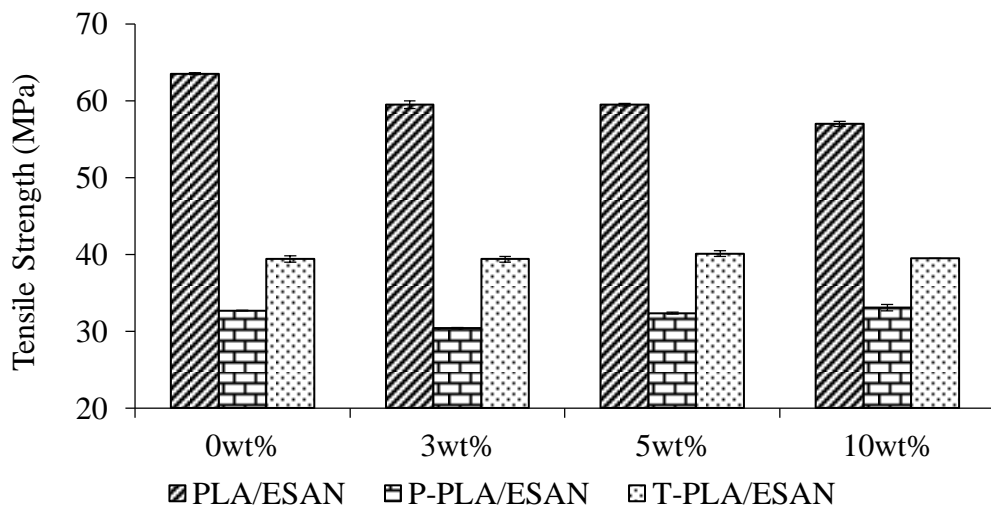


Figure 4.51. Effect of different compatibilizers on the tensile strength (MPa) of PLA/ESAN HNT composites (P-PLA: PEG plasticized PLA, T-PLA: TPU toughened PLA)

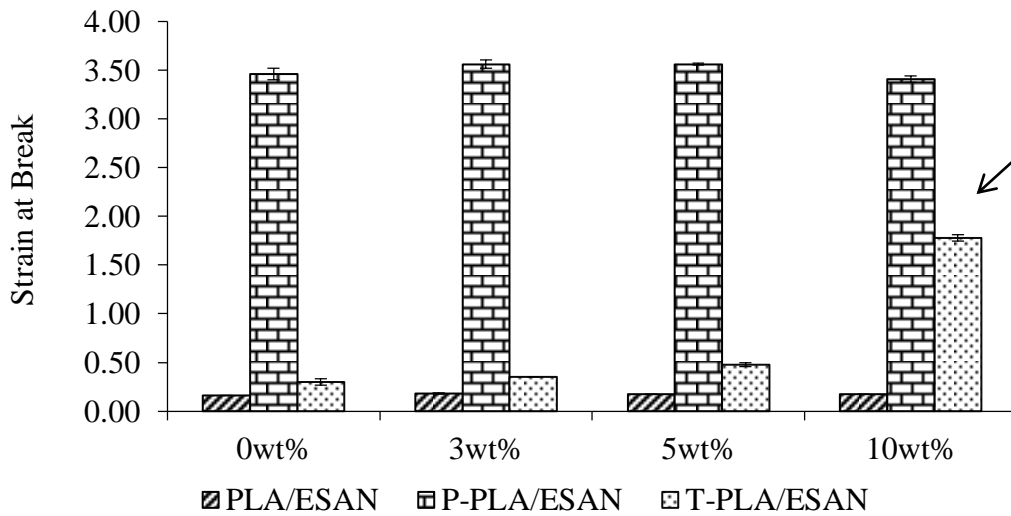


Figure 4.52. Effect of different compatibilizers on the strain at break values of PLA/ESAN HNT composites (P-PLA: PEG plasticized PLA, T-PLA: TPU toughened PLA)

As mentioned in TEM results, HNT particles are distributed mainly in the PLA matrix and close to the interface between the PLA and TPU matrix. The nanotube bridges formed at the interface of PLA and TPU phase might be the reason of the contribution of HNT mineral on the plasticizing effect of TPU. Hence, as the clay content increases, the increased number of reinforced cracks with nanotube bridges provides a well enhancement in elongation at break. The homogeneous distribution of clay particles in the T-PLA matrix compared to that of P-PLA matrix might also contributes to this improvement. As mentioned in the previous part, well distribution of clay particles results in a lowered average TPU domain size and inter-domain size which can also enhance the toughness of the material due to larger surface area created.

The enhancement in strain at break values of T-PLA composites with increasing clay content without deteriorating the tensile strength indicates the ability of TPU to act as a compatibilizer between PLA and HNT. The impact of other positive effects of TPU on the mechanical and thermal properties will be given later.

Tensile properties of Nanoclay based P-PLA and T-PLA composites are given in Figure 4.53 and Figure 4.54. For these composites exactly the same trends are obtained. In P-PLA composite containing 3wt% Nanoclay HNT the strength decreases, and this reduction is recovered with increasing clay content. For T-PLA composites, increasing Nanoclay content also enhances the strain at break values without changing the strength of the composites. However, for Nanoclay based composites slightly better tensile properties can be clearly seen.

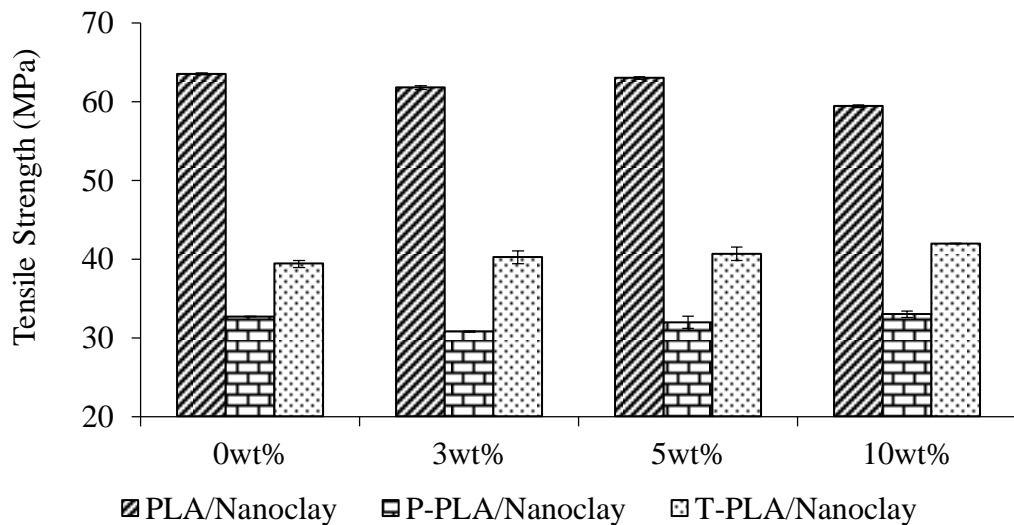


Figure 4.53. Effect of different plasticizers on the tensile strength (MPa) of PLA/Nanoclay HNT composites (P-PLA: PEG plasticized PLA, T-PLA: TPU toughened PLA)

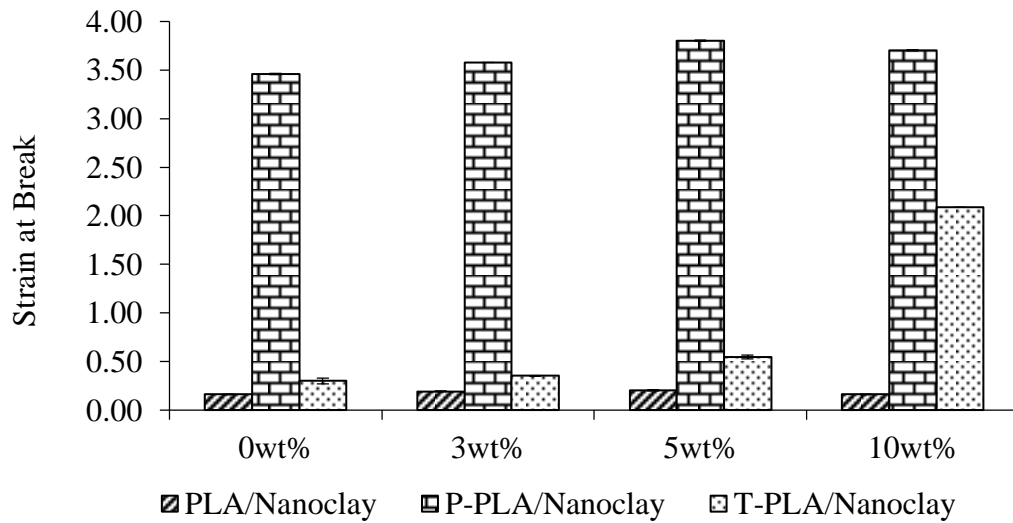


Figure 4.54. Effect of different plasticizers on the strain at break values of PLA/Nanoclay HNT composites (P-PLA: PEG plasticized PLA, T-PLA: TPU toughened PLA)

4.4.5 Impact Results

Impact tests were performed to understand the effect of TPU on the toughness of PLA and its HNT based composites. The results of tests performed for ESAN and Nanoclay HNT based composites are given in Figure 4.55 and Figure 4.56 respectively.

The results are consistent with the strain at break results given in the previous part of this section. TPU almost doubles the impact strength of the PLA owing to the droplet domains that the elastomeric TPU had formed when it was distributed in the polymer matrix. For blends the failure mechanism mainly depends on the average domain size of the dispersed phase. As can be seen from SEM

micrograph of T-PLA blend it forms a dispersed phase with an average domain size of 4.5 μm .

When HNT is introduced into the system, impact strength increases in an abrupt manner. This contribution of HNT to the toughness of the T-PLA was attributed to the better bridging effect of nanotubes between the cracks and reduced average domain size in the presence of distributed clay particles. Also, low inter-domain size enhances the toughness of the material since a larger surface area is created.

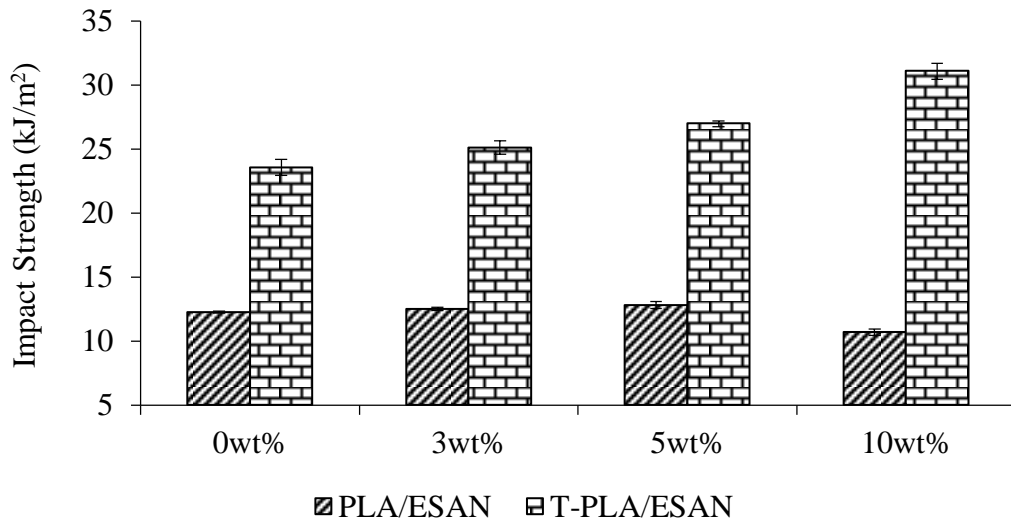


Figure 4.55. Effect of elastomeric TPU on the impact strength (kJ/m²) of PLA/ESAN HNT composites (T-PLA: TPU toughened PLA)

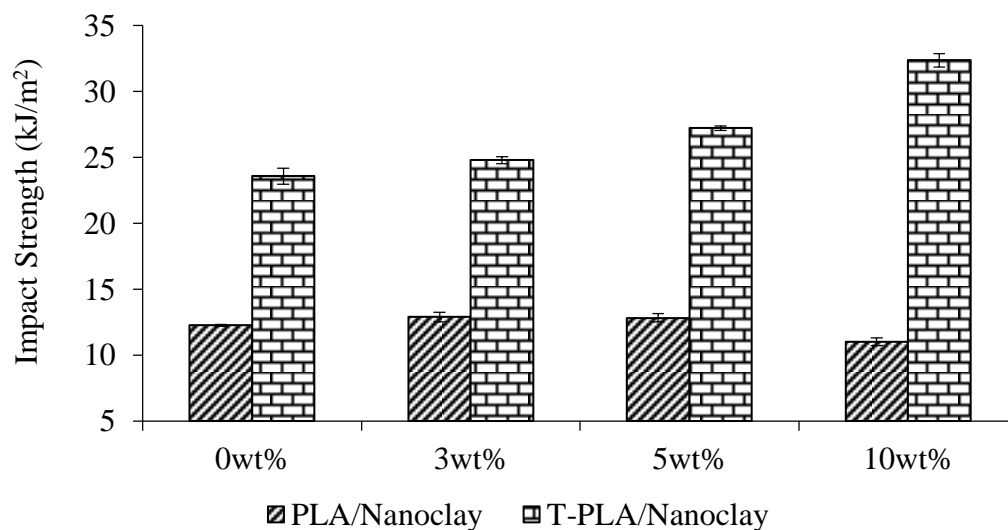


Figure 4.56. Effect of elastomeric TPU on the impact strength (kJ/m^2) of PLA/Nanoclay HNT composites (T-PLA: TPU toughened PLA)

4.4.6 Dynamic Mechanical Analysis (DMA)

Comparison of the dynamic responses of PLA, P-PLA and T-PLA polymers are given through Figure 4.57 to Figure 4.59. The plasticization effect of both PEG and TPU can be clearly seen from these figures. PEG plasticized PLA displays an enormous reduction in its storage modulus at low temperatures and reaches its minimum value at a temperature range of $50 - 60^\circ\text{C}$ compared to pure PLA. The same trend is also observed for T-PLA polymer, but at a higher modulus range due to the contribution of the hard segment of TPU to PLA. For each type of polymer, E' value starts to increase after a certain temperature. For P-PLA this temperature is relatively low compared to PLA and T-PLA. Also, the increase in E' value is greater for P-PLA due to its higher crystalline fraction as will be given in DSC results part.

The reduction in loss modulus also attracts attention with PEG and TPU plasticization. The reduction for P-PLA polymer is much more distinct as can be seen from Figure 4.58. In addition, the maximum peak shifts to extremely low temperatures. However, the maximum peak of T-PLA does not shift to lower temperatures.

In contrast to maximum peak result in E'' versus temperature plot, the maximum loss tangent peak shifts to lower temperatures for T-PLA indicating more mobile polymer chains. For P-PLA polymer, the reduction in T_g is approximately 15°C indicating a perfect plasticizing effect of PEG.

Miscibility is one of the most important factors in blends that affect the physical properties. According to literature in order to understand the miscibility of PEG and TPU in PLA, the loss tangent plots should be investigated in the temperature range between 0 – 50°C (Mohapatra et al. 2014, Pluta et al. 2006a, Mi et al. 2013, Jia et al. in press). If they are partially miscible and there is a phase separation, there exists an extra maximum peak indicating the T_g of PEG rich phase. Since there is no available loss tangent data in this temperature range, morphology of P-PLA should be investigated. Figure 4.60 depicts the SEM micrograph of P-PLA which shows no phase separation for 20wt% of PEG loading to PLA, and it indicates the miscibility between PLA and PEG. Also, for T-PLA polymer, the lack of tangent loss data in the specified temperature range makes it impossible to understand the miscibility between TPU and PLA from dynamic analysis. However, according to the studies performed by Yang-Mi and Jia with their co-workers, the tangent loss versus temperature plot of TPU-PLA blend does give rise to a second maximum peak indicating that these two polymers are immiscible in each other (Mi et al. 2013, Jia et al. in press). This result was also proven by DSC analysis in these studies.

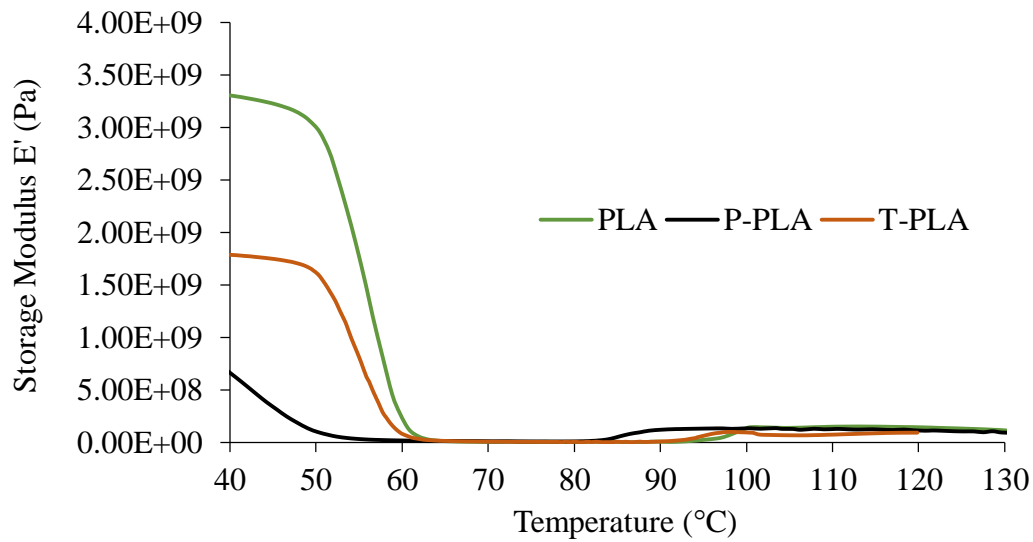


Figure 4.57. Storage Modulus (E') versus temperature data for PLA, P-PLA and T-PLA polymers

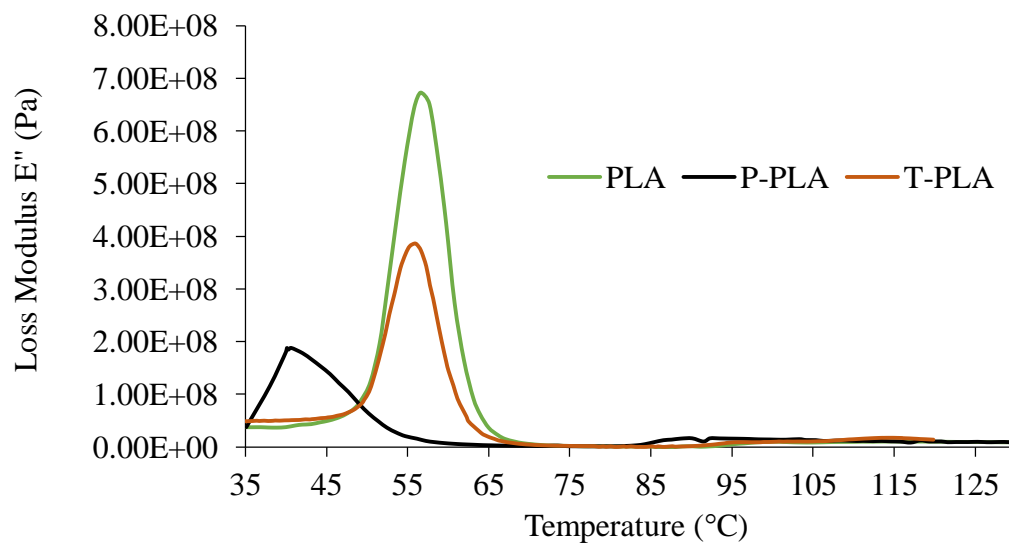


Figure 4.58. Loss Modulus (E'') versus temperature data for PLA, P-PLA and T-PLA polymers

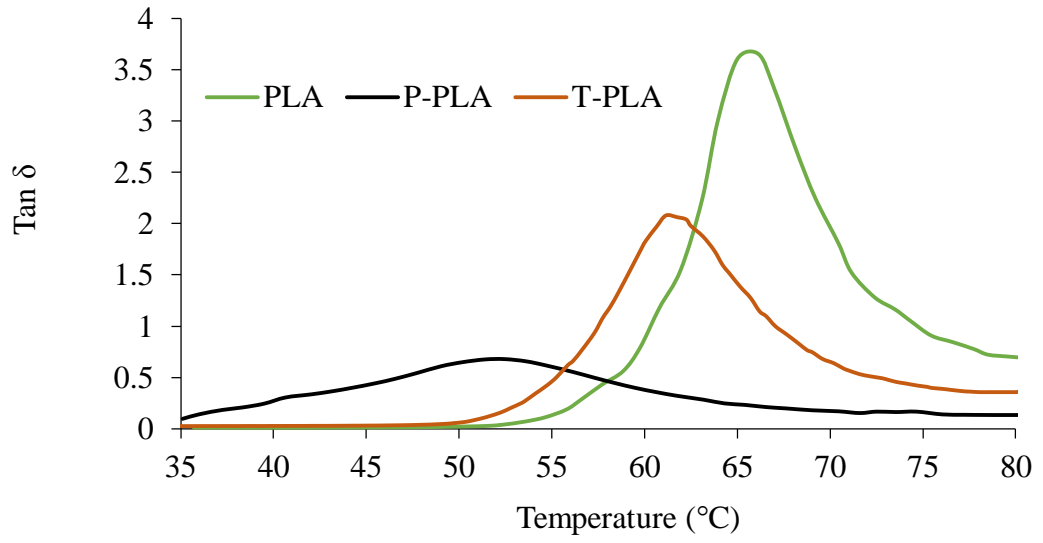


Figure 4.59. Tan δ versus temperature data for PLA, P-PLA and T-PLA polymers

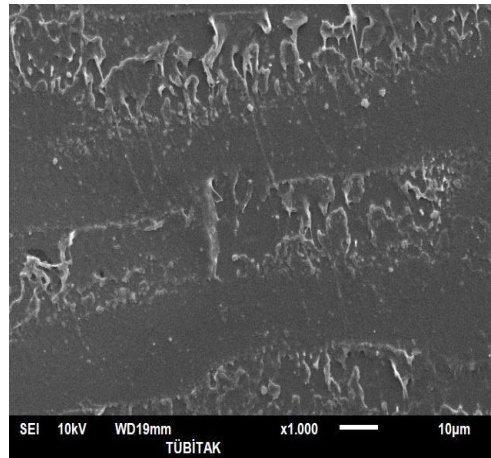


Figure 4.60. SEM micrograph of PLA plasticized with PEG (P-PLA)

DMA results of P-PLA composites containing ESAN HNT are given through Figure 4.61 to Figure 4.63. According to the results, the storage modulus of the composites reduces with addition of HNT, while it is recovered by increasing clay content from 3 to 10 wt%. Especially at 10wt% clay loading, the storage modulus of P-PLA polymer increases highly at low temperatures. In addition, the second E' value rising region of 10wt% ESAN containing P-PLA occurs at a lower temperature region compared to P-PLA indicating a higher crystallinity.

The same trend is also observed in the E'' and $\tan \delta$ versus temperature plots indicating a reduction in DMA properties with ESAN HNT addition, whereas the properties are well recovered with increasing HNT loading up to 10wt% filler. According to these results, it can be said that; although addition of ESAN HNT does not give rise to formation of nanocomposites, its high loading (greater than 5wt%) to P-PLA blend gives rise to the formation of micro-filled composites.

For T-PLA blends, dynamic mechanical analysis was also performed and the results are shown through Figure 4.64 to Figure 4.66. Nanotube incorporation into T-PLA blend results in an increase in the magnitude of both E' and E'' values. Moreover, these results show an increase with increasing clay content. This behavior might be predominantly attributed to improved stress transfer from the nanotubes to the matrix.

In the tensile properties part of this section, the improved plasticizing effect of TPU in the presence of HNT minerals for PLA matrix was mentioned. In general, reduction in T_g is expected with increasing plasticization of composites. However, as can be seen from Figure 4.66, maximum $\tan \delta$ peak does not shift to lower temperatures with increasing clay content. Hence, it can be said that increased flexibility of PLA with addition of TPU could be achieved without deteriorating strength, modulus and transition temperatures. The other thermal properties will be discussed in detail in the following part.

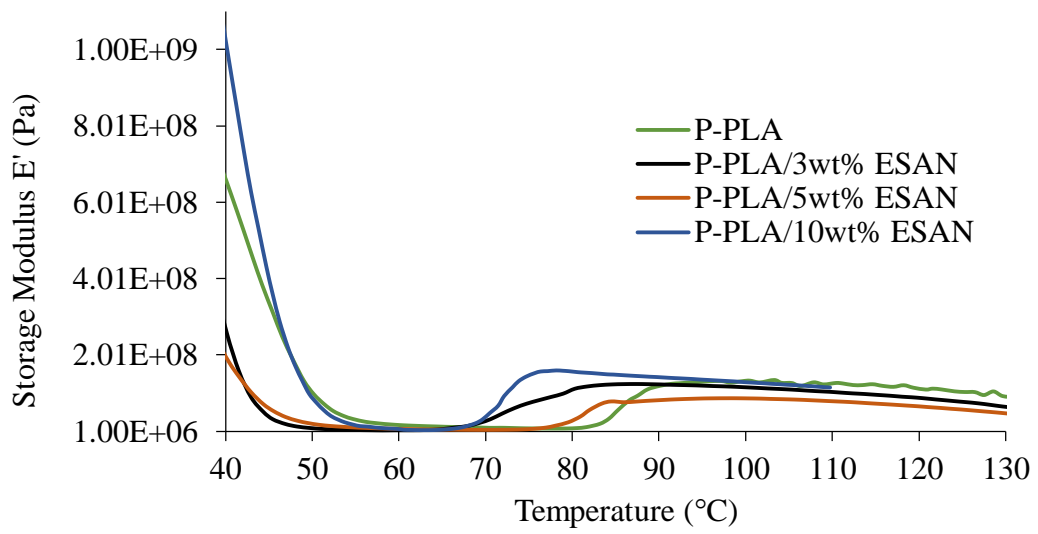


Figure 4.61. Storage Modulus (E') versus temperature data for P-PLA/ESAN HNT composites

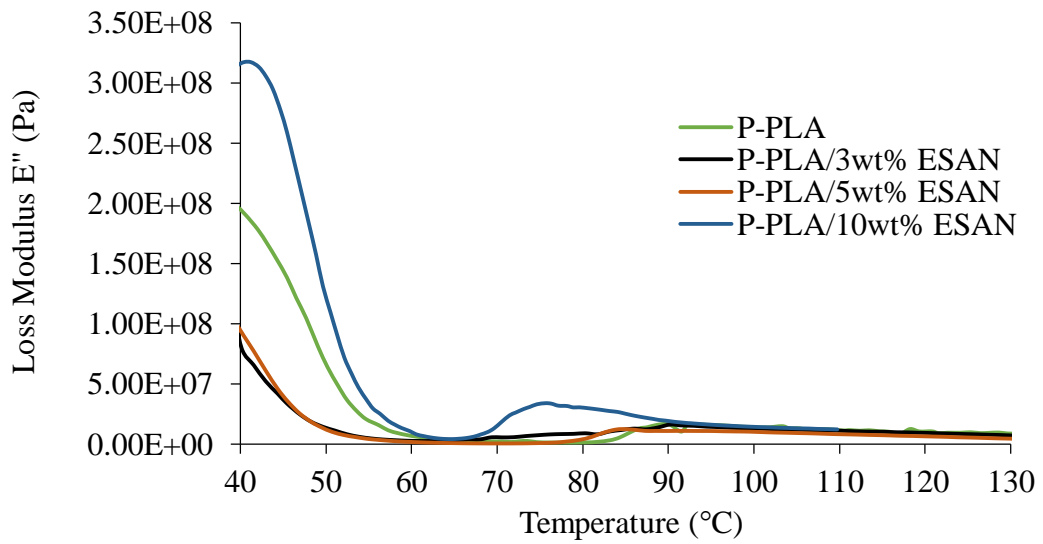


Figure 4.62. Loss Modulus (E'') versus temperature data for P-PLA/ESAN HNT composites

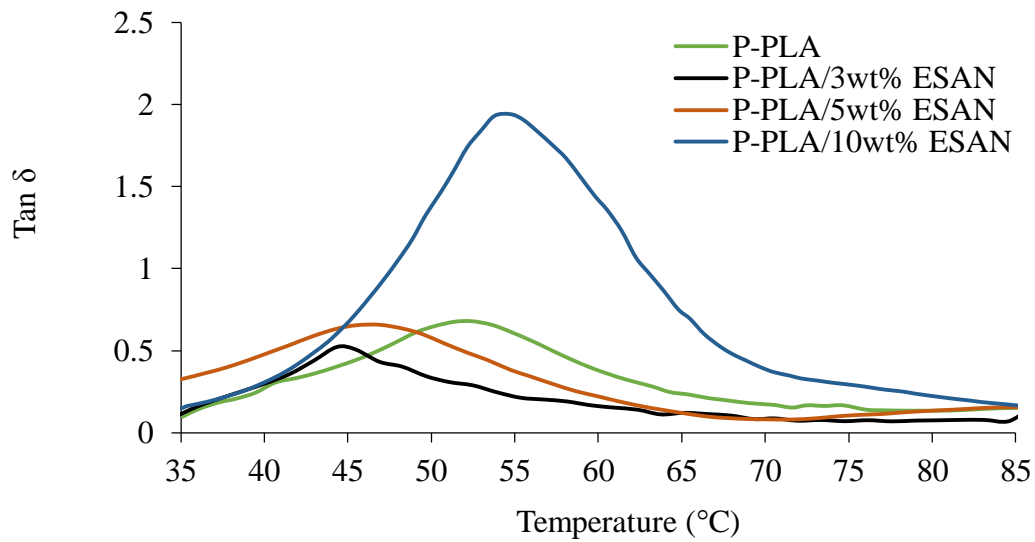


Figure 4.63. Tan δ versus temperature data for P-PLA/ESAN HNT composites

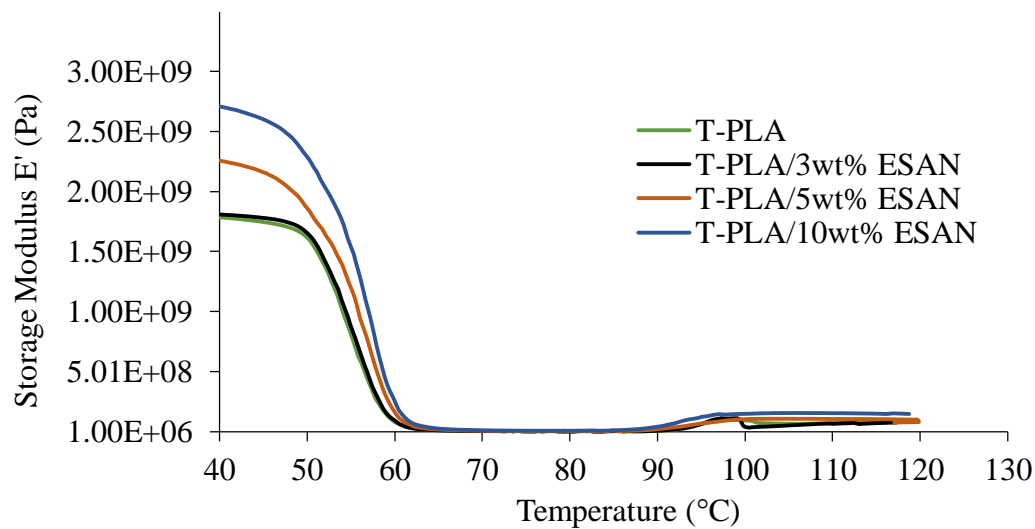


Figure 4.64. Storage Modulus (E') versus temperature data for T-PLA/ESAN HNT composites

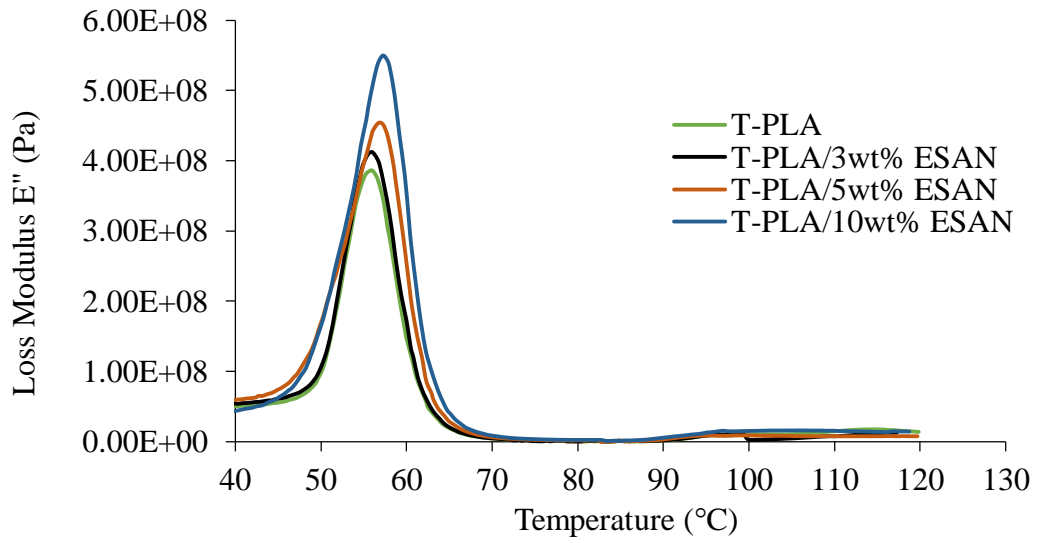


Figure 4.65. Loss Modulus (E'') versus temperature data for T-PLA/ESAN HNT composites

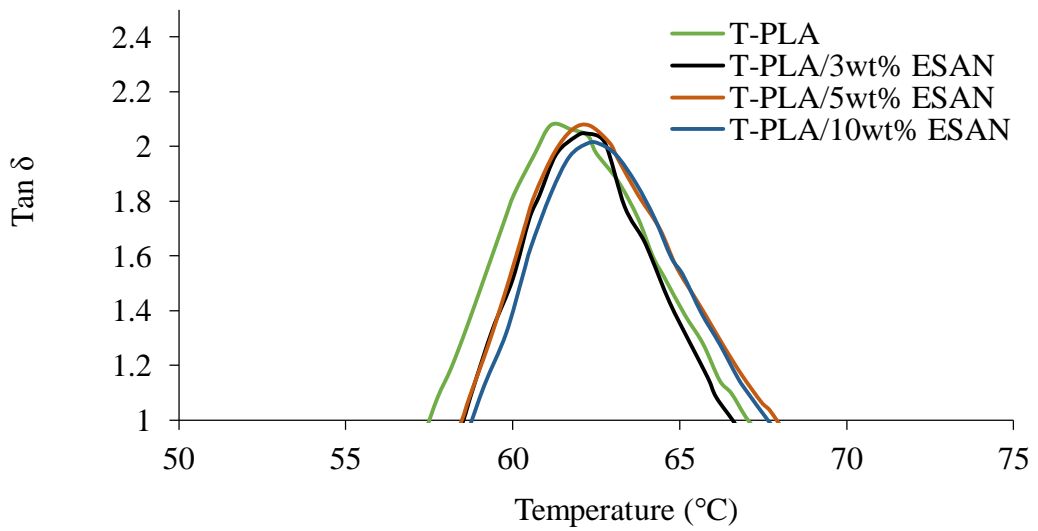


Figure 4.66. $\text{Tan } \delta$ versus temperature data for

4.4.7 Differential Scanning Calorimetry Analysis (DSC)

Plasticization of brittle polymers mainly affects the thermal properties in addition to mechanical properties. To investigate these effects, P-PLA polymer and its HNT based composites were subjected to DSC analysis. In order to eliminate the thermal history of the polymeric materials, two heating runs were performed and the second run was taken into account.

The thermograms for P-PLA/ESAN HNT composites can be seen from Figure 4.67 and the comparison of transition temperatures for PLA and P-PLA are given in Table 4.6. As expected, T_g and T_c of pure PLA shift approximately 25°C and 40°C to lower temperatures respectively due to higher macromolecular movement by the addition of small molecules. This is a result of physical interaction such as hydrogen bonding or dipolar interaction between the atoms of PLA and PEG which had entered between the PLA macromolecules during melt mixing. Hence, heterogeneous PLA-PEG interactions replace some rigid PLA-PLA interactions leading to decreased energy consumption during glass transition and more mobile molecules (Mohapatra et al. 2014).

The other observation obtained from the DSC results of plasticized PLA is decreased crystallization enthalpy (ΔH_c) and increased heat of melting (ΔH_m) compared to pure PLA. This is an indication of higher crystallinity as shown in Table 4.6. The cooling thermograms of P-PLA and P-PLA/ESAN HNT composites can be seen from Figure 4.68. PLA does not show an indication of crystallization on its cooling thermogram, whereas addition of PEG results in cold crystallization peak formation owing to increased crystallinity and different crystal forms which become more intense with HNT introduction as explained below.

Following the increased crystalline fraction with addition of PEG insertion, a shoulder formation is observed in the melting peak region. This is a result of the

melting of two crystalline types formed with the addition of PEG as explained above. In the literature, some grades of PLA show two melting peaks indicating formation of different crystal structures (Murariu et al. 2012, Fukushima et al. 2011). However, in this study, only a single melting peaks was observed in the DSC thermogram of pure PLA. The formation of these two melting peaks with the addition of PEG might be the indication of extreme tendency of PLA to nucleation in the presence of a nucleating agent, such as highly crystalline PEG molecule. The shoulder peaks observed around 140°C and 150°C can be classified as the melting of β -crystal and α -crystal forms respectively. The α -crystal form (pseudo-orthorhombic, pseudo-hexagonal or orthorhombic) is the most common form and melts at higher temperatures, whereas, the β -crystal form (orthorhombic or trigonal) is interpreted as an imperfect crystal structure melting at lower temperatures (Yasuniwa et al. 2008, Yasuniwa et al. 2006). However, the helical conformations of the chains in α - and β - forms have approximately the same energy.

With the addition of HNT to P-PLA, T_g of the composites shift to higher temperatures indicating the nucleating effect of the clay mineral. The broad and weak endotherm caused by enthalpy relaxation also becomes more visible with addition of HNT and it overlaps with T_g which makes it hard to observe the true value of glass transition temperature. However, it can be said that the reduction in T_g with plasticization is recovered by the help of clay which acts as nucleating agent for crystallization of P-PLA (Lewitus et al. 2006). The mentioned weak endotherm due to enthalpy relaxation also suppresses the formation of cold crystallization peak. Hence, the weak endotherm might be considered as an unstable crystalline form.

The mentioned unstable crystalline form explained as enthalpy relaxation might be the reason of unimproved mechanical properties as mentioned in the former parts of this section. In addition, the formation of this weak endotherm around T_g becomes more intense with increasing clay content.

The shoulder formation is clearer for P-PLA/HNT composites compared to P-PLA and it becomes more significant with increasing clay content. This can be attributed to increased fraction of β -crystal forms in the composites due to nucleating ability of HNT minerals. In addition, cooling thermograms of the composites proves this result with more intense cold crystallization peaks around 140°C indicating β -crystal formation. This result is consistent with the study performed by Liu. The study mentions the β -nucleating ability of nanotubes on the isotactic polypropylene (iPP) polymer which shows only α -crystal form in the absence of clay mineral.

For Nanoclay based P-PLA composites, the same observations obtained in P-PLA/ESAN HNT composites are observed as can be seen from Figure 4.69. With HNT addition T_g of the composites overlap with weak endotherm formed due to melting of imperfect crystals other than β - form and its intensity decreases with increasing clay content. Also, there is no cold crystallization peak in the presence of Nanoclay HNT, and shoulder formation around melting point of PLA becomes more significant with increasing clay content.

For T-PLA/ESAN HNT and T-PLA/Nanoclay HNT composites, the thermograms can be seen from Figure 4.70 and Figure 4.71 respectively. In contrast to plasticization with PEG, the transition temperature; T_g , of PLA remains almost the same with the addition of TPU. This might be evaluated as there are two separate glass transition slopes in the DSC thermograms confirming the immiscibility of TPU with PLA. The first one belongs to TPU and could not be observed in the experiments that had started from room temperature. The second one is the unchanged T_g mentioned above and belongs to PLA.

According to the thermograms crystallization peak of the PLA also remains the same indicating no nucleating effect of TPU on PLA. On this subject there are two different results in the literature. Mi's study mentions a shift of crystallization peak to lower temperatures which is attributed to nucleating activity of TPU (Mi et al. 2013). However, according to the study performed by Lai and his co-

workers, the crystallinity of PLA decreases with TPU addition (Lai and Lan 2013). The second case, i.e. crystallinity reduction, is also observed in this study and the crystalline fraction of PLA is decreased from 2.3 to 0.8

The melting temperature of PLA and its composites decreases with the addition of TPU phase according to the study performed by Jia and his friends (Jia et al. in press). This suggests that the mobility of the PLA chains is enhanced when TPU phase is added. This phenomenon indicates that TPU can effectively enhance the toughness. However, in this study, the melting temperature of the blend remained the same. Still, the toughness of the PLA/TPU blends is much better than that of pure PLA as can be seen from impact results part.

As can be seen from both Figure 4.70 and Figure 4.71, addition of HNT does not give rise to a change in transition temperatures and crystalline fractions. However, as mentioned formerly in the mechanical results part, HNT has a great effect on the toughness improvement, although there is no increase in the crystalline fraction. Hence, this enhancement can be attributed to the higher attraction between TPU and HNT as compared to the attraction between PLA and HNT.

Table 4.6. Thermal transition behavior and crystalline fraction (%) of P-PLA/HNT composites

Sample	T_g (°C)	T_c (°C)	ΔH_c (J/kg)	T_{m1} / T_{m2} (°C)	ΔH_m (J/kg)	X_c (%)
PLA	57.8	120.3	22.04	148.1	24.21	2.3
P-PLA	32.4	81.6	11.15	140.1 / 149.8	27.89	18
T-PLA	57.8	119.7	20.76	148.0	19.99	0.8

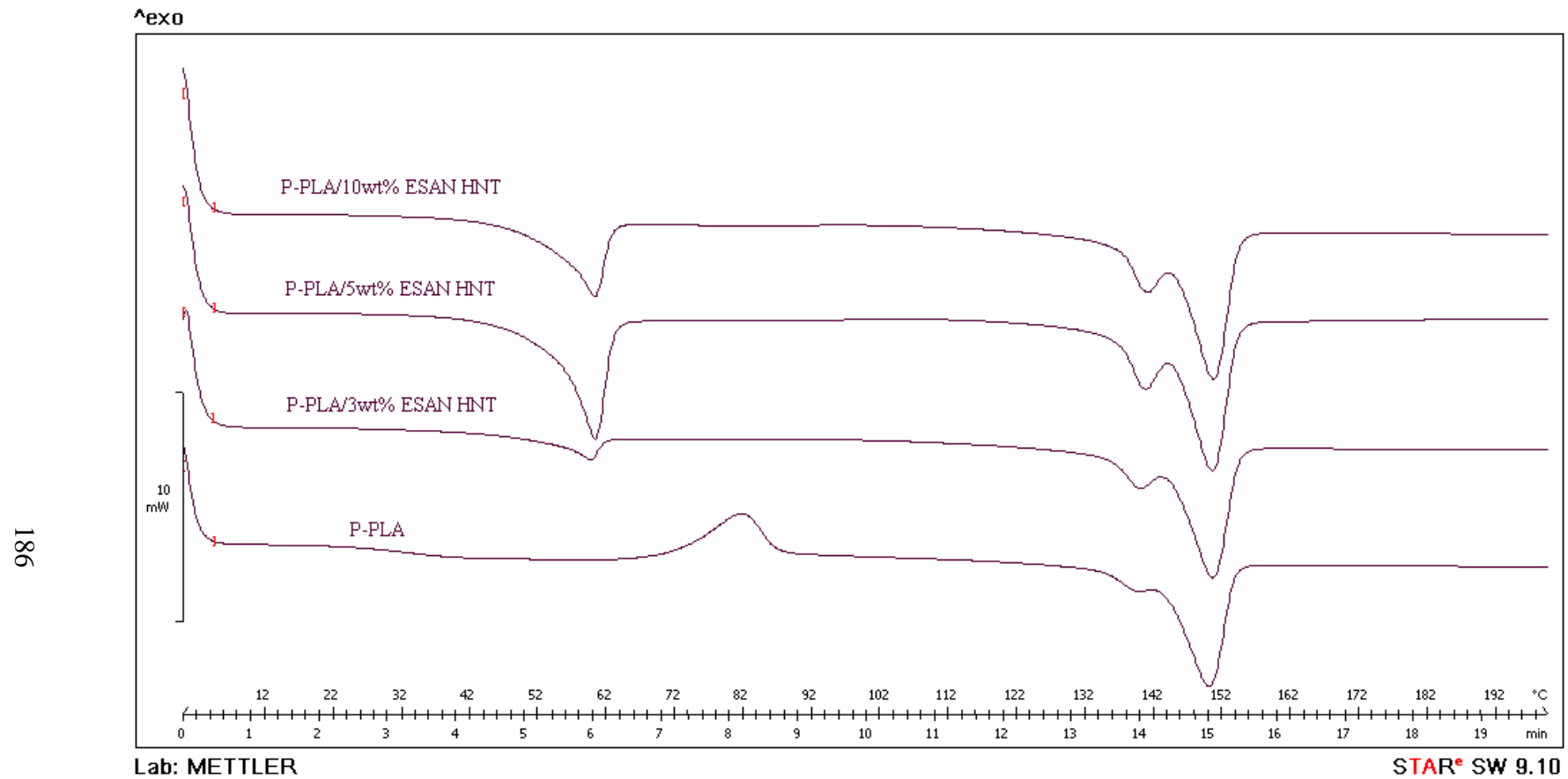


Figure 4.67. DSC thermograms of P-PLA/ESAN HNT composites

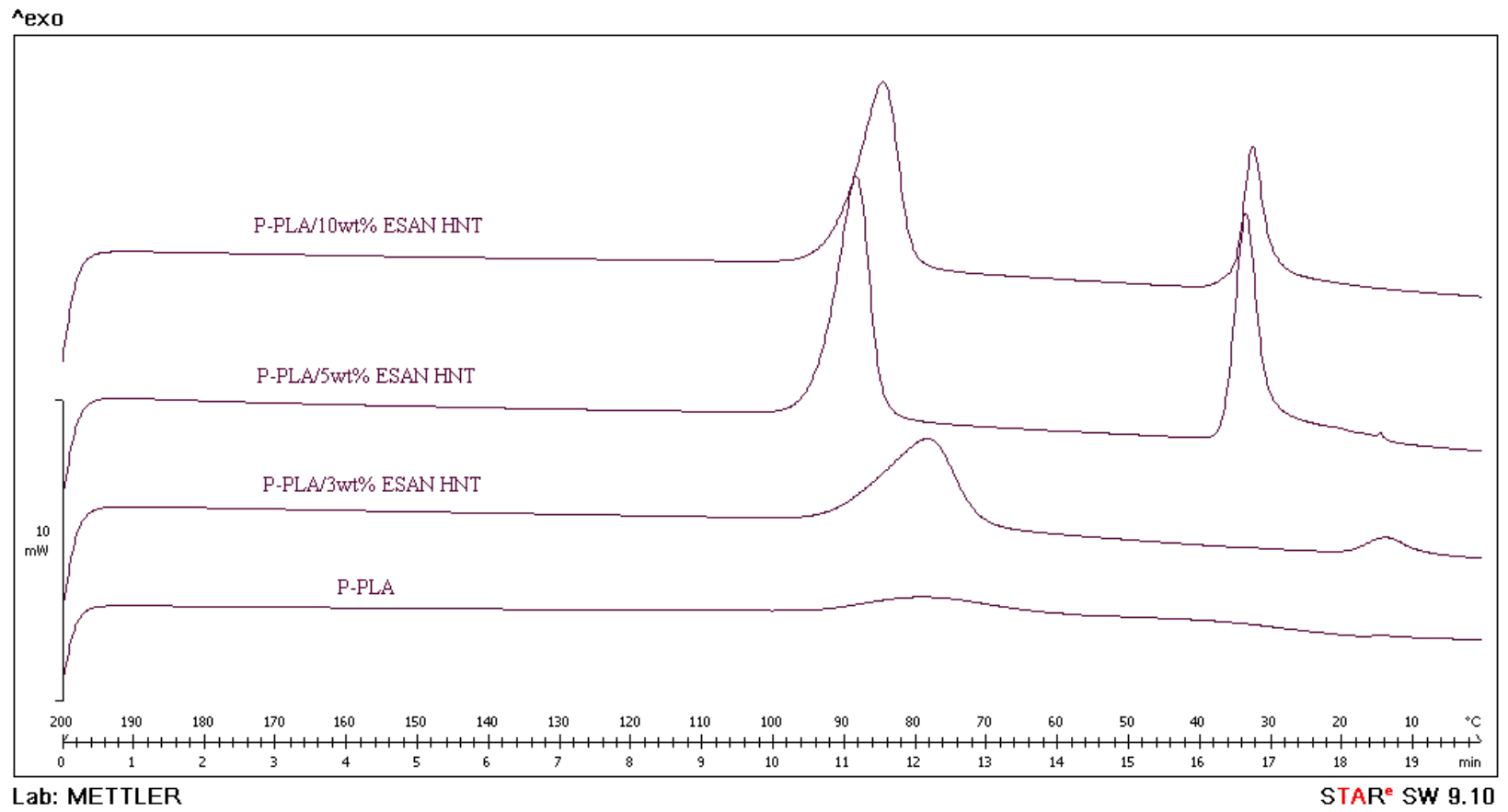


Figure 4.68. Cooling thermograms for P-PLA/ESAN HNT composites

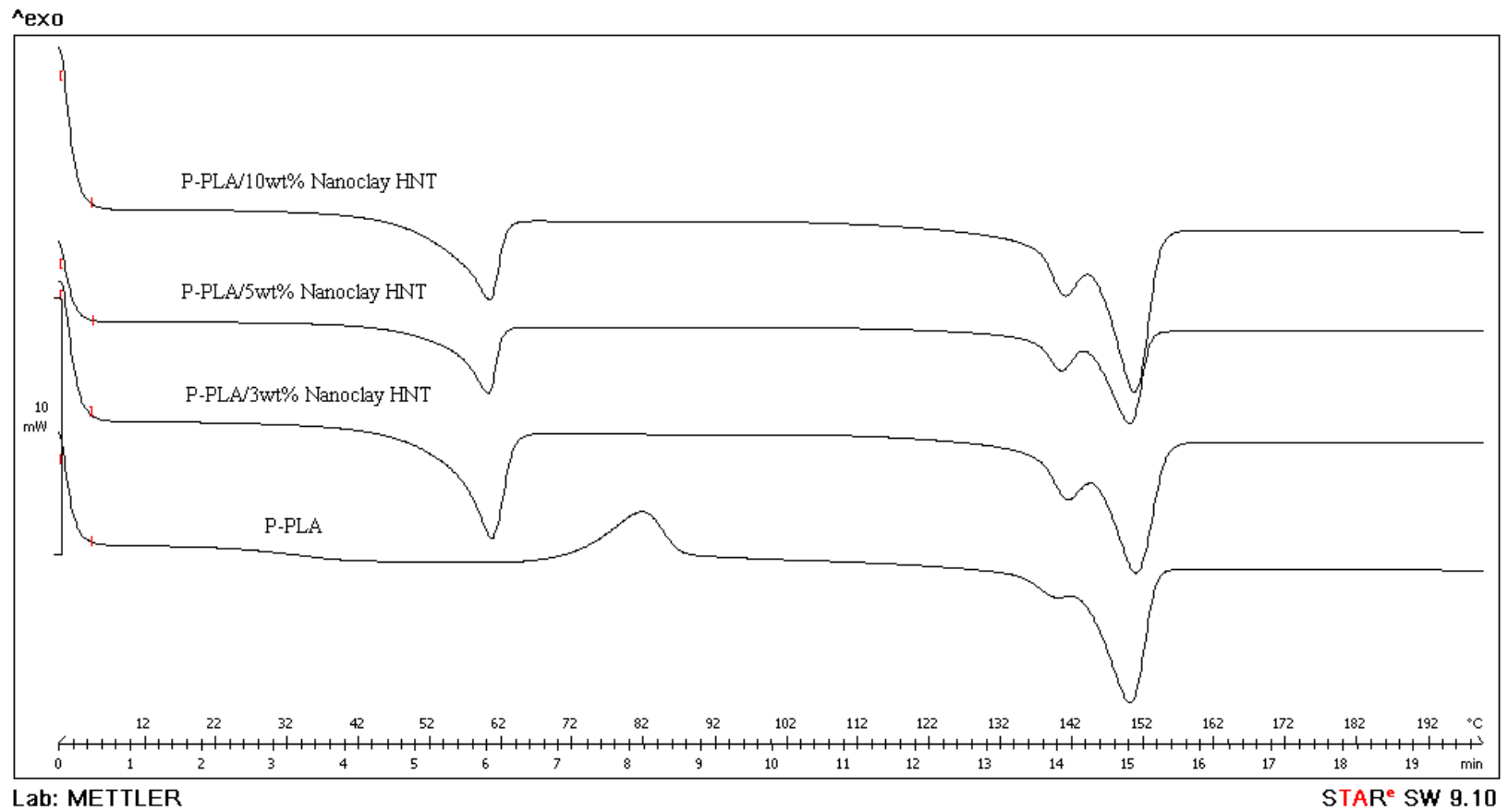


Figure 4.69. DSC thermograms of P-PLA/Nanoclay HNT composites

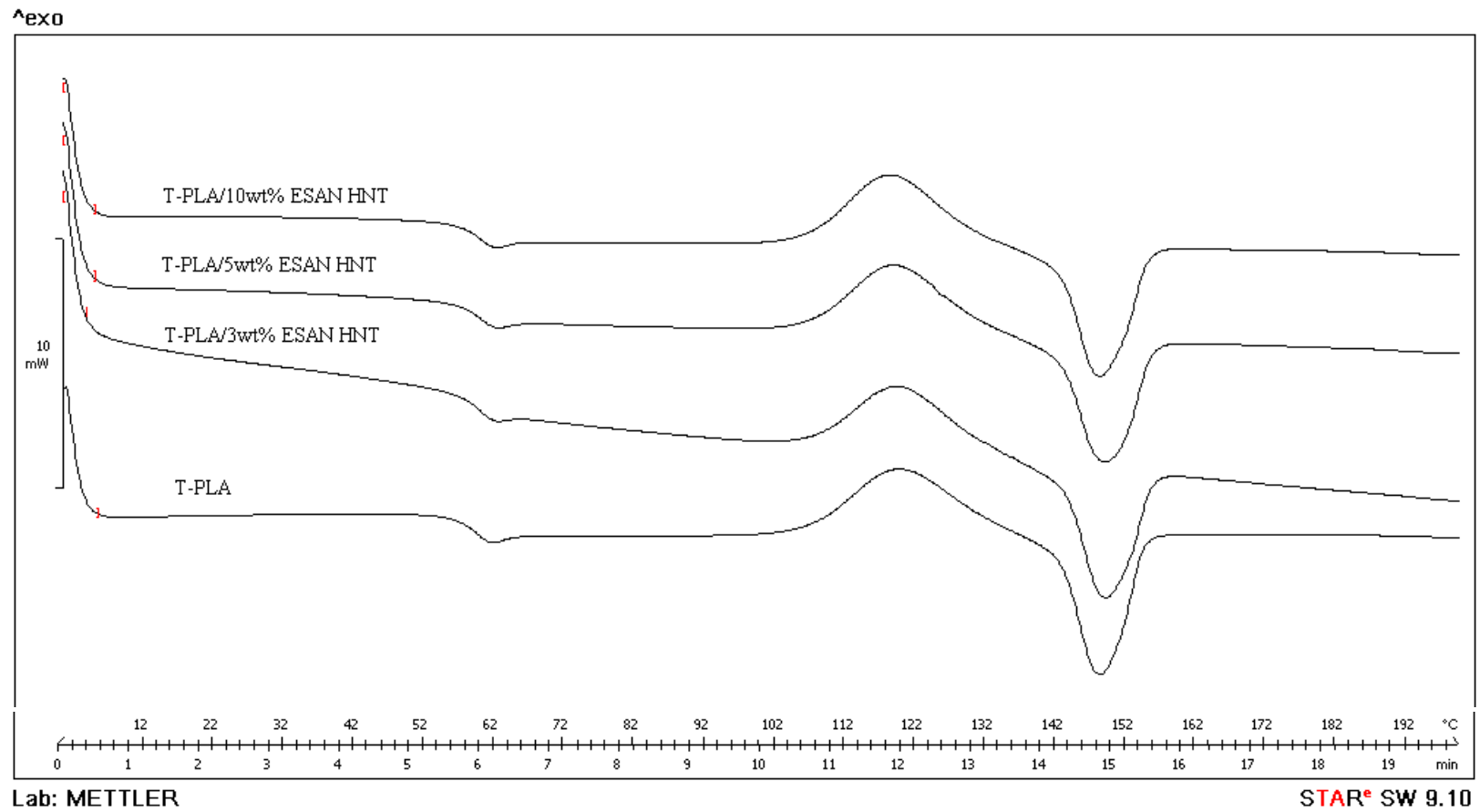


Figure 4.70. DSC thermograms of T-PLA/ESAN HNT composites

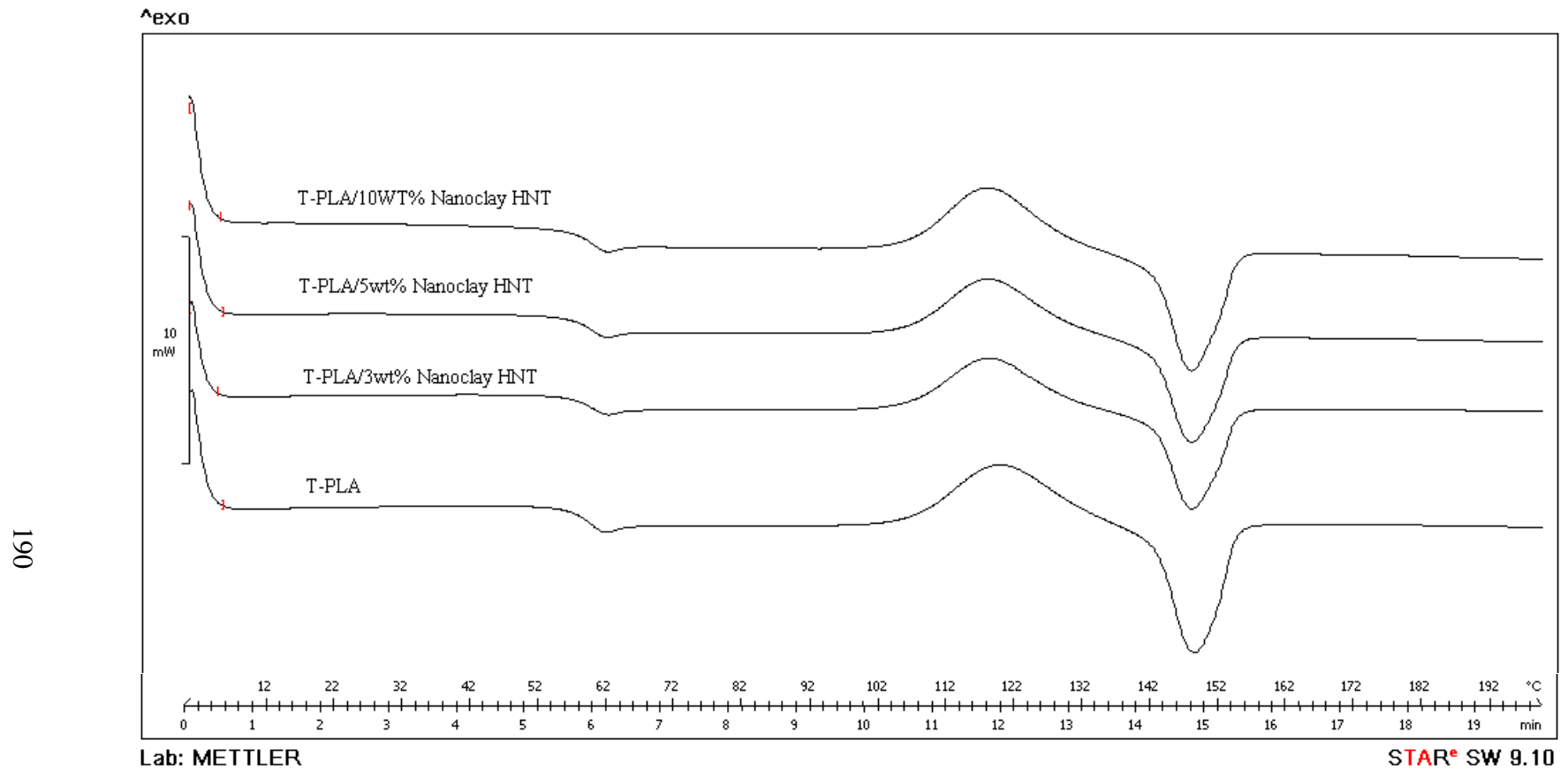


Figure 4.71. DSC thermograms of T-PLA/Nanoclay HNT composites

4.4.8 Hydrolytic Degradation

The impact of the plasticizers, PEG and TPU, on the hydrolytic degradation behavior of the semi-crystalline PLA was investigated in this part of the dissertation. Visual results for PLA, P-PLA and T-PLA polymers and the % of weight loss versus hydrolysis time plot can be seen from Figure 4.72 and Figure 4.73 respectively.

As mentioned previously, PLA does not display a weight loss until the 20th day. Then, a fast degradation starts and after the 40th day it becomes difficult to measure the weight of the samples due to extensive fragmentation. However, for P-PLA polymer the weight loss starts before the 20th day. Although it is not clear in Figure 4.73, 1% weight loss occurs for P-PLA on the 10th day. In the first stage of the degradation bulk erosion is balanced by increased crystallinity and no weight loss is observed for the sample. The difference between PLA and P-PLA in the first stage might be attributed to the initial higher crystalline fraction of P-PLA which balances between bulk erosion and crystallization. The visual observations also reveal that after 40 days of hydrolysis, PLA and P-PLA polymers show complete fragmentation of the samples. This higher weight loss of P-PLA during the secondary stage can be attributed to the migration of the low molecular weight PEG molecules.

However, for T-PLA, the case is a bit different than P-PLA. In the first stage of the degradation no change is observed for T-PLA as in the degradation of PLA. However, contrary to the impact of PEG, the degradation of PLA is impeded by TPU in the second stage of the degradation. As can be seen from Figure 4.72, there still remains some large pieces at the end of the 40th day. The bulkier molecules of TPU might be the reason of longer degradation period and lower weight loss (%).

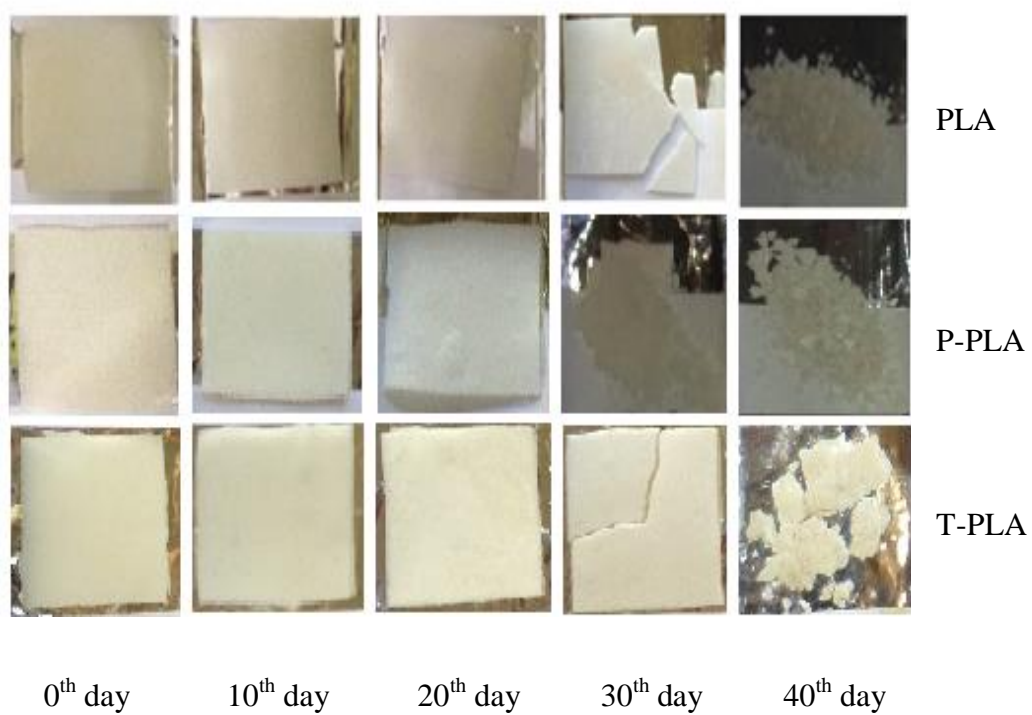


Figure 4.72. Hydrolysis samples of PLA, P-PLA and T-PLA polymers

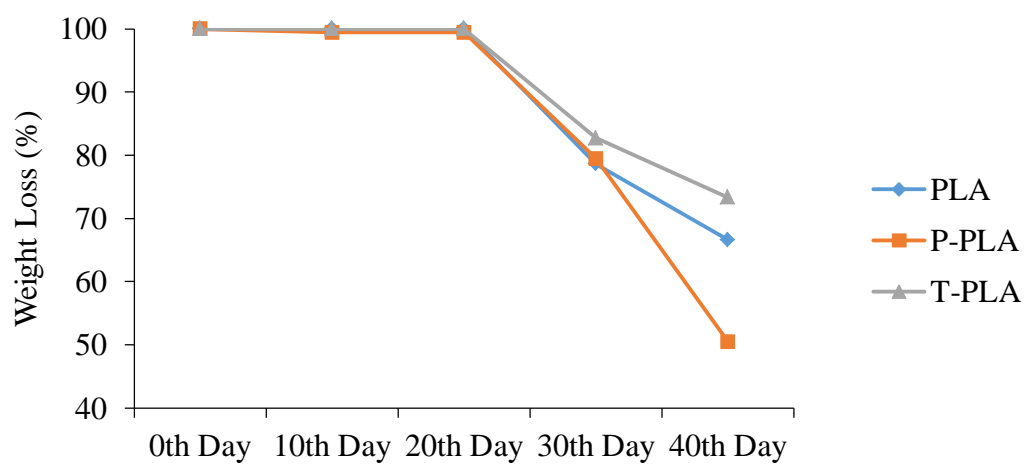


Figure 4.73. Hydrolytic degradation results of PLA, P-PLA and T-PLA polymers

Addition of HNT mineral into P-PLA and T-PLA causes a delay in the second degradation stage of the hydrolysis which gives the main idea about the degradation behavior of the composites. In PLA/HNT hydrolytic degradation results part, it was mentioned that hydrolytic degradation of polyester chains take place in the amorphous phase of the polymer matrix and the lowered crystalline fraction of the polymer matrix by addition of HNT or the poor nucleating ability of HNT itself might result in slower degradation rates. The same observation and explanation is also valid for P-PLA and T-PLA composites which show a decreasing degradation rate with increasing clay content (see Figure 4.74 and Figure 4.75).

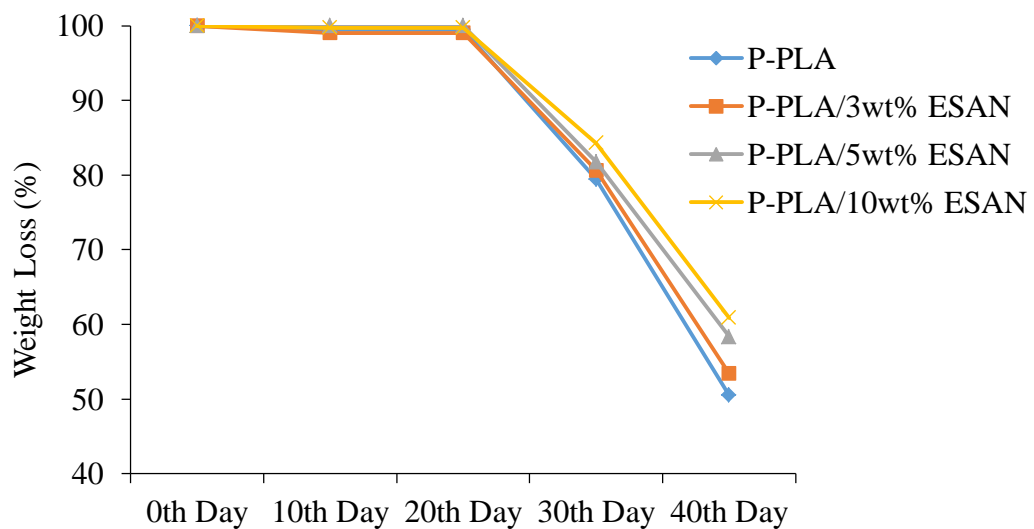


Figure 4.74. Hydrolytic degradation results of P-PLA/ESAN HNT composites

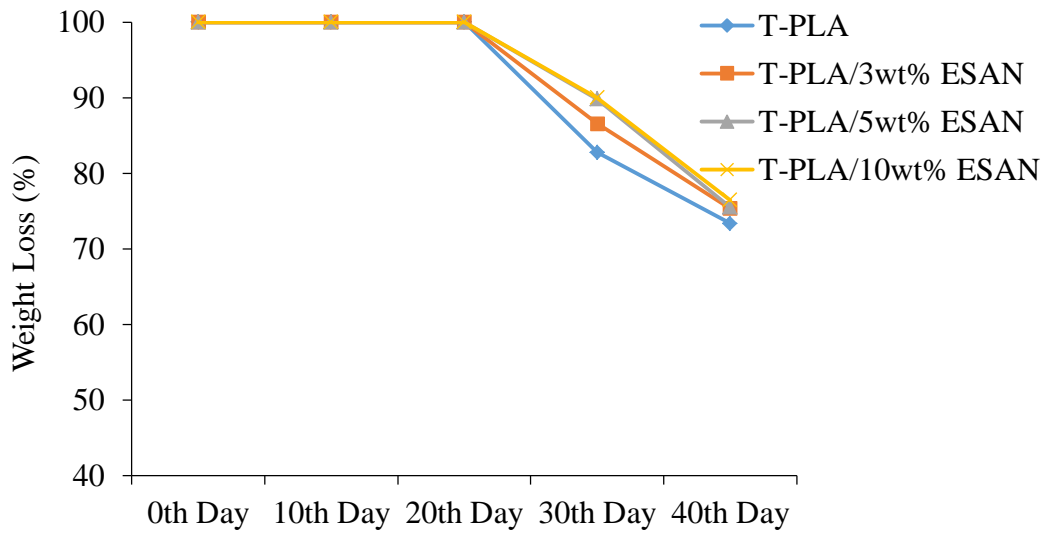


Figure 4.75. Hydrolytic degradation results of T-PLA/ESAN HNT composites

Plasticization of PLA with PEG and TPU was investigated in this section of the dissertation. One of the main reasons for PLA plasticization is to achieve more flexible materials. This could be achieved with both PEG and TPU. However, the desired compatibilization effect which is expected to provide a much better distribution of clay particles and nanocomposite formation could not be obtained with either of them. These results are again attributed to the degradation of PLA and plasticizer molecules in the presence water that had remained between the layers of HNT and blocked HNT layer spacing that makes the intercalation process impossible. On the contrary, TPU was observed to act as a better compatibilizer between HNT and PLA matrix. This can be understood from well enhanced elongation at break properties of T-PLA matrix with increasing clay content.

4.5 Use of Chain Extender in PLA/HNT P-PLA/HNT Composites and Their Properties

In the previous sections, degradation of biopolymer molecules due to high processing temperatures and water molecules that had remained between the layers of HNT mineral was mentioned. During the degradation of PLA, undesirable reactions take place. Some of them are hydrolysis, inter-chain transesterification, and intra-molecular trans-esterification. Hydrolysis is a water based degradation mechanism and results in splitting of PLA chains into smaller chains. The hidden water between HNT layers may accelerate the rate of this reaction and results in un-improved physical properties for the composites.

In order to increase the stability of PLA during the melt extrusion with HNT particles, 1,4-phenylene diisocyanate (PDI) was used as a chain extender at 3wt% concentration. The chain extension mechanism occurs through the reaction between the hydroxyl functional groups of both PLA and PEG and isocyanate functional groups of PDI. Also, a reaction might occur between the carboxyl functional group of PLA and isocyanate. As a result, the chain extender acts to connect the split chains that are formed during the melt mixing of composites.

PDI is expected to recover the reduction in the mechanical properties of PLA/HNT composites by providing higher molecular weight and formation of a long chain branched structure. The long chain branching increases the entanglement density of the polymer structure and thus further hinders the slippage and orientation of the chains upon elongation (Najafi et al. 2012b).

The effect of chain extender on the morphological, mechanical, and thermal properties of PLA and P-PLA composites containing 5wt% HNT are investigated in this section of the dissertation.

4.5.1 X-Ray Diffraction Results

The effect of addition of chain extender, PDI, into PLA and plasticized PLA composites were investigated and the basal spacing results are tabulated in Table 4.7. As mentioned before, PLA/HNT composites do not display an intercalated structure due to lack of interactions between PLA and HNT.

Chain extender is responsible for the increase of the molecular weight of PLA during melt mixing. For platelet structure filler containing nanocomposites the increased shear force provided by the higher molecular weight generally results in an easier delamination of the clay particles (Meng et al. 2012). However, for HNT minerals exfoliation is nearly impossible due to their crystal structure. Hence, it can be said that, increased molecular weight and higher shear stress do not contribute to the formation of an intercalated structure.

Table 4.7. Basal spacing (\AA) results of ESAN based PLA and P-PLA composites containing 3wt% PDI

	2theta	Basal Spacing (\AA)
ESAN HNT	12.17	7.27
Nanoclay HNT	12.15	7.28
PLA/5wt% ESAN	11.85	7.46
PLA/5wt% Nanoclay	12.01	7.36
PLA/5wt% ESAN/3wt%PDI	11.85	7.46
PLA/5wt% Nanoclay/3wt%PDI	11.57	7.64
P-PLA/5wt% ESAN/3wt% PDI	12.03	7.35
P-PLA/5wt% Nanoclay/3wt%PDI	11.91	7.42

4.5.2 Scanning Electron Microscopy

Figure 4.76 and Figure 4.77 display the effect of PDI on the morphology of PLA and P-PLA respectively. For both matrices, PDI increases the roughness of the surface and hence results in better mechanical properties as will be shown in the next part. However, its effect is much more significant in P-PLA matrix. When PDI is introduced to PLA, the smooth surface partly becomes rough. However, there are still some parts at which crack propagation lines are visible. For P-PLA matrix, PDI addition completely roughens the surface indicating a higher attraction between PEG molecules and PDI compared to the interaction between PLA and PDI molecules.

Addition of HNT to plasticized and un-plasticized PLA/PDI matrices roughens the surface of the matrix, and it is expected to improve the mechanical properties. However, the agglomerated particles dominating the structure are observed. When the sizes of the agglomerates in PLA/PDI matrix are compared with the ones observed in the neat PLA matrix, the former exhibit larger domains. Hence, PLA/PDI/HNT composites display worse mechanical properties than PLA/HNT composites do, as will be mentioned in the next part.

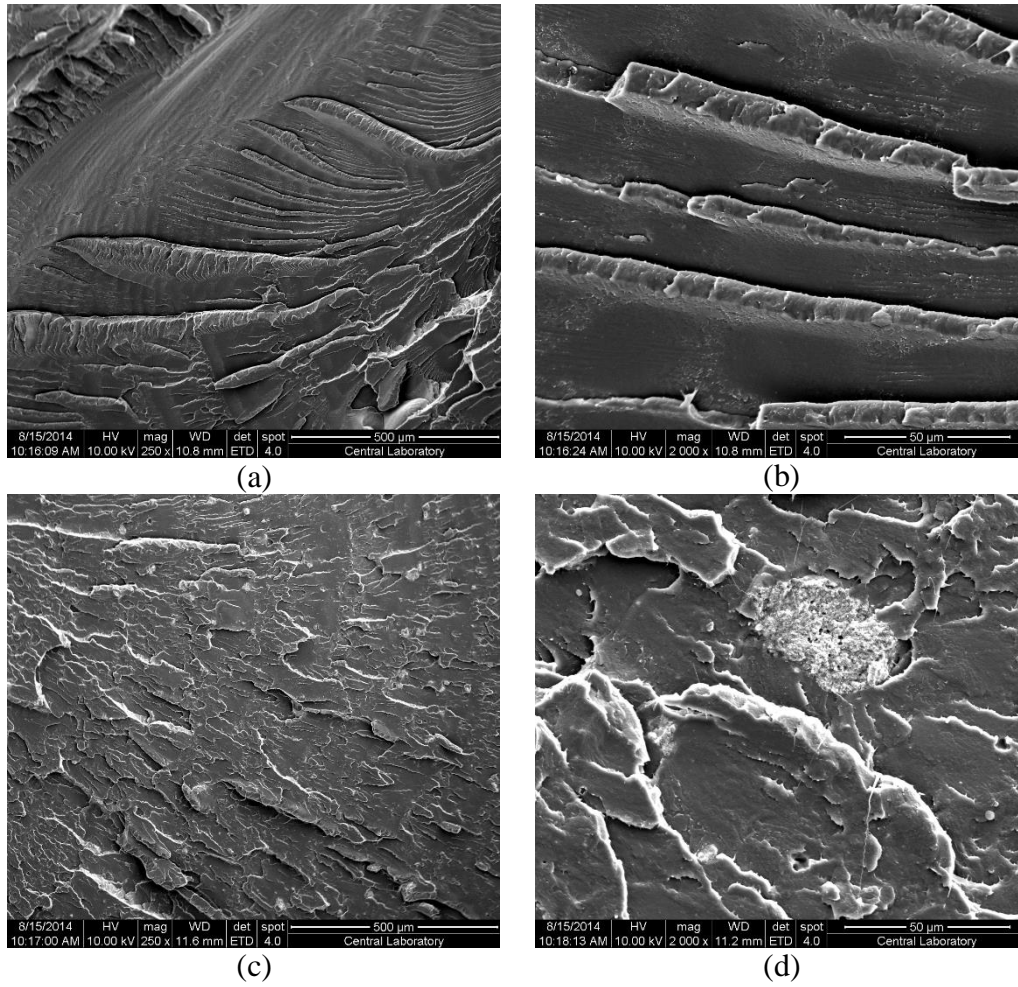


Figure 4.76. SEM Micrographs of PLA/PDI composite (a) 0wt% ESAN HNT250x, (b) 0wt% ESAN HNT 2000x, (c) 5wt% ESAN HNT 250x, (d) 5wt% ESAN HNT 2000x

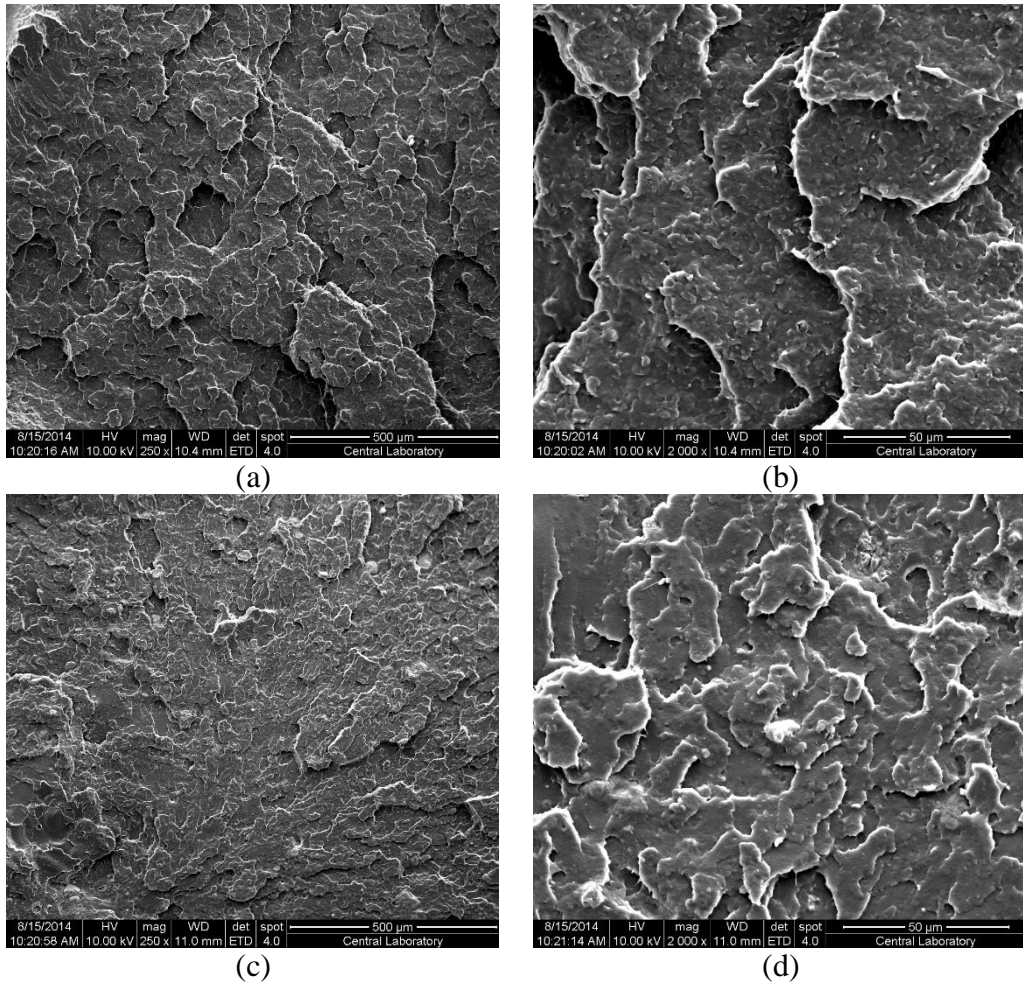


Figure 4.77. SEM Micrographs of P-PLA/PDI composite (a) 0wt% ESAN HNT 250x, (b) 0wt% ESAN HNT 2000x, (c) 5wt% ESAN HNT 250x, (d) 5wt% ESAN HNT 2000x

4.5.3 Tensile Properties

Tensile properties of PLA/HNT and P-PLA/HNT composites are given in Figure 4.78 – Figure 4.79 and Figure 4.80 – Figure 4.81 respectively. During melt mixing, addition of PDI into PLA enhances the tensile strength insignificantly. However, the tensile strength of P-PLA polymer increases from 32.7 to 45.7 MPa. This might be attributed to the higher interaction of PEG molecules with PDI compared to the interaction between PLA and PDI molecules. In the presence of PEG, the molecular weight increases much more rapidly and results in an increase in the vertical force during melt mixing. As can be seen from Figure 4.82, decrease in vertical force during melt mixing of PLA is recovered up to only a certain level in the presence of PDI. However, for P-PLA polymer there is a distinct increase in the vertical force indicating molecular weight buildup. In addition to improvement of tensile strength, elongation at break values also increase significantly in the presence of PDI for P-PLA polymers.

In the presence of HNT mineral, tensile properties of PLA/PDI mixtures show a reduction in contrast to the improvement in the properties of pure PLA. The clay particles may hinder the function of PDI molecules to act as chain extender during melt mixing. Although the increase in shear stress due to higher molecular weight is expected to cause a finer distribution and hence better physical properties, no improvement was observed.

For P-PLA composites the situation is a bit different. PLA/HNT composites do not show a reduction in their tensile strength with addition of PDI. However, the improvement in the strength of the composites is not as distinct as the one achieved with pure PLA. In addition, PDI addition results in lower strain at break values in PLA/HNT composites, whereas the improvement is obvious for pure PLA.

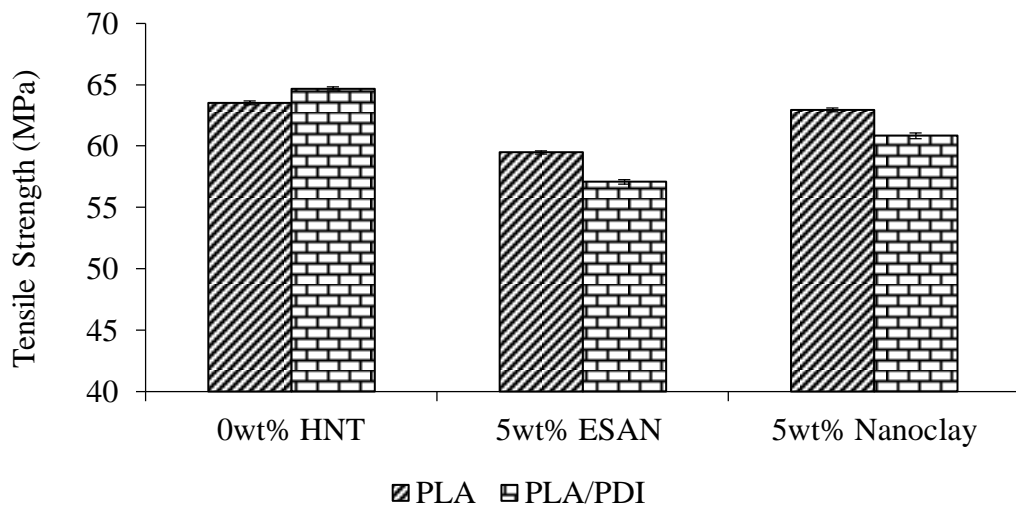


Figure 4.78. Effect of chain extender on tensile strength (MPa) of PLA/HNT composites

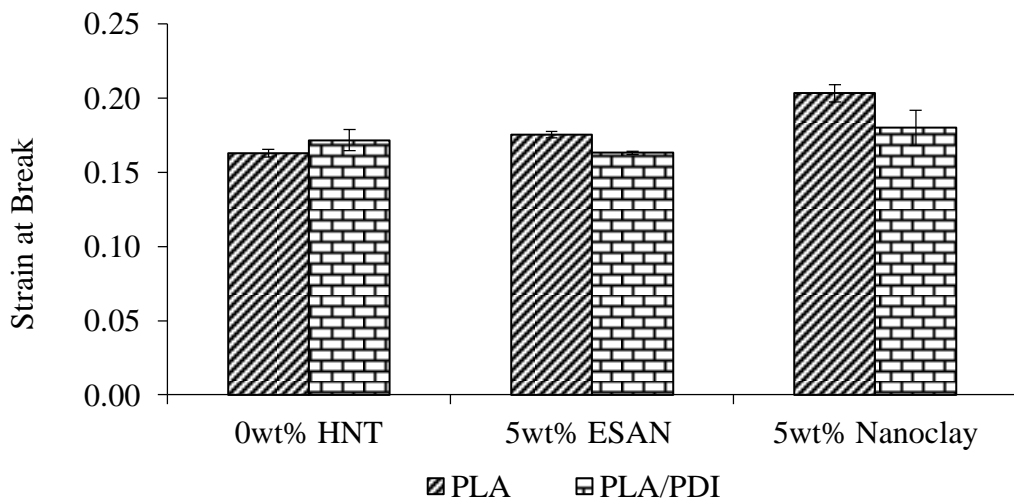


Figure 4.79. Effect of chain extender on strain at break of PLA/HNT composites

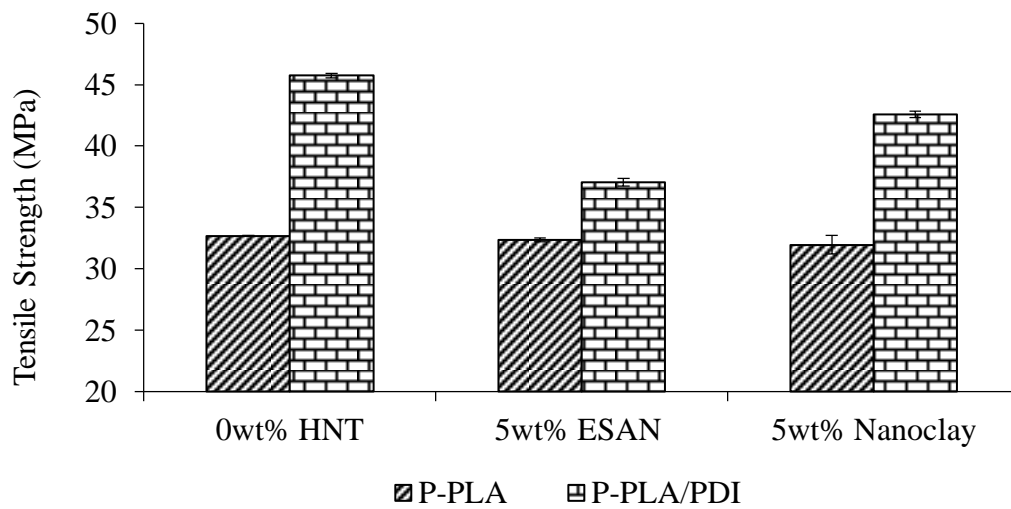


Figure 4.80. Effect of chain extender on tensile strength (MPa) of P-PLA/HNT composites

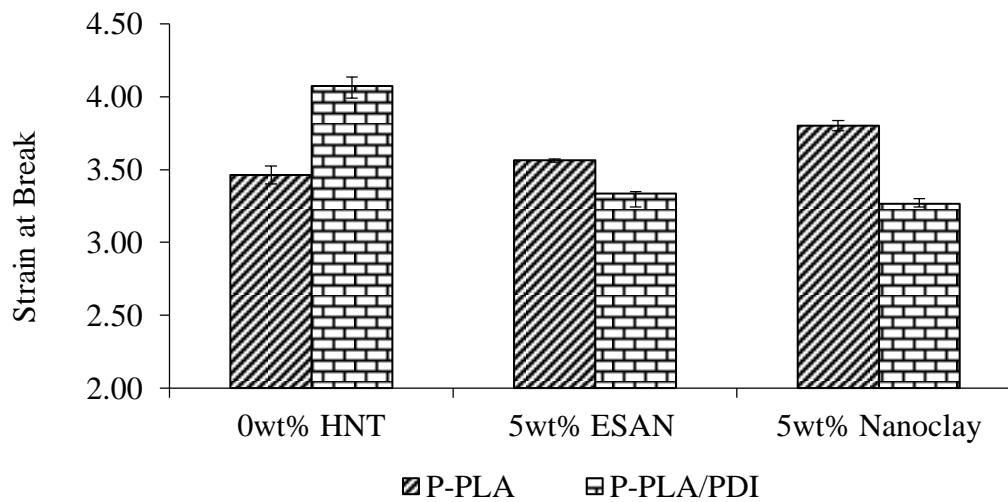
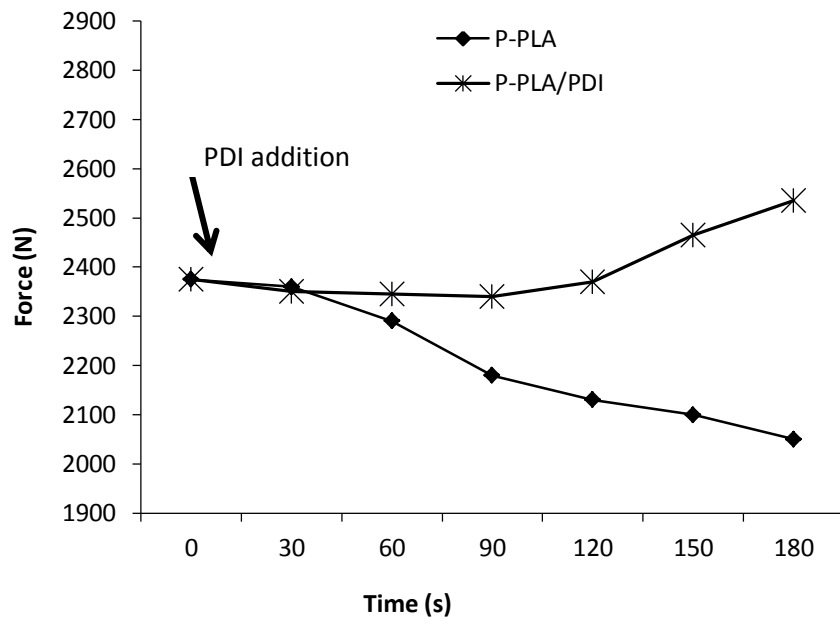
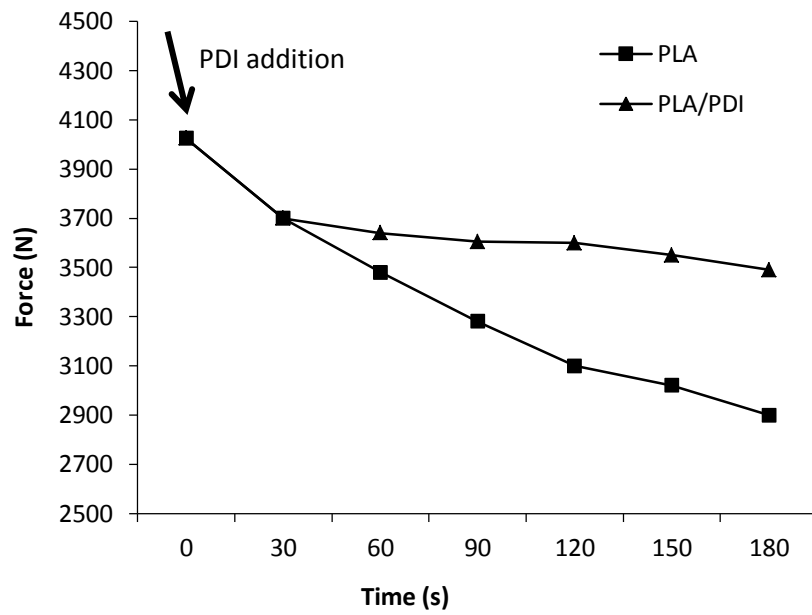


Figure 4.81. Effect of chain extender on strain at break of P-PLA/HNT composites



(a)



(b)

Figure 4.82. Vertical force measurements for PLA and P-PLA blends in the presence of PDI

It is a well-known fact that the mechanical properties of P-PLA blends are lost over time and crystallization and phase separation takes place (Mohapatra et al. 2014). The main factor which affects this mechanical loss is the degradation of the constituents of the blend with time. However, there is another factor which affects this phenomenon. It is the migration of PEG molecules to the surface of the samples. Migration of plasticizers can be described with a first order kinetic equation, which depends on the initial and final plasticizer concentration, temperature and time (Wool and Sun 2005).

Low molecular weight plasticizers should be miscible with PLA and create a homogeneous blend. Also, they should not be prone to migration which would cause contamination of food in PLA based beverages. Migration to surface would also cause the blended material to regain the brittleness of pure PLA (Ren 2010).

In this study, the PEG molecules tend to migrate to the surface of the sample, and cause increased brittleness. However, in PDI containing samples, PEG molecules show a lower tendency for migration as shown in Figure 4.83, and this result in less recession of the mechanical properties with time.

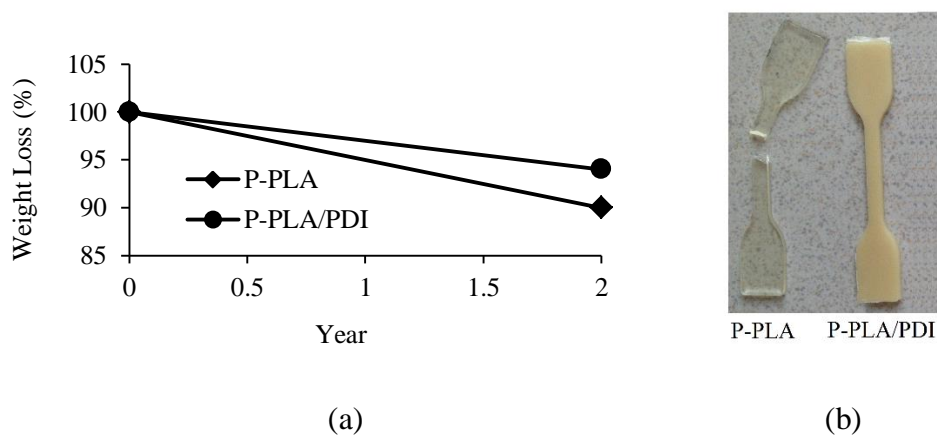


Figure 4.83. Effect of chain extender on the PEG migration; (a) Weight loss (%) versus time plot, (b) P-PLA and P-PLA/PDI samples at the end of 2 years

4.5.4 Dynamic Mechanical Analysis (DMA)

Stiffness of the polymeric materials is directly proportional to the molecular weight. Hence chain extended polymers are expected to yield higher dynamic mechanical properties compared to PLA. However, Figure 4.84 – Figure 4.86 show that the addition of chain extender, PDI, results in a reduction in both storage and loss modulus values at room temperature and also shifts the T_g of PLA to lower temperatures. With the addition of HNT to PLA/PDI mixtures, the reduced dynamic mechanical properties are partially recovered. Especially, for Nanoclay HNT containing composites the properties are recovered to a greater extent compared to the properties of ESAN HNT containing composites.

When compared with PLA/PDI mixtures, P-PLA/PDI mixtures show an opposite trend in their dynamic responses as can be seen through Figure 4.87 to Figure 4.89. P-PLA shows an increase in its modulus values in the presence of PDI molecules. As mentioned before this can be attributed to the higher interactions provided between PEG and PDI molecules compared to the interaction between PLA and PDI. Hence, it can be said that PDI does not function as a chain extender for PLA polymer as it does for P-PLA blends. In contrast to the contribution of clay particles to the dynamic mechanical properties of PLA polymer, these particles prevent a further improvement in P-PLA composites. This might be due to inhibited chain extension reactions owing to relatively immobilized P-PLA chains in the presence of HNT minerals.

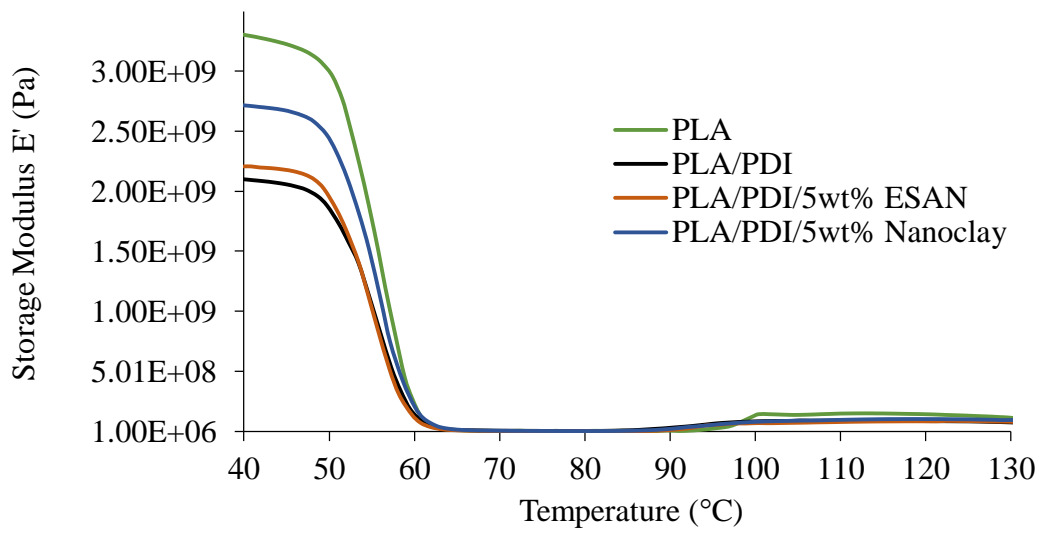


Figure 4.84. Storage Modulus (E') versus temperature data for PLA/PDI/5wt%HNT composites

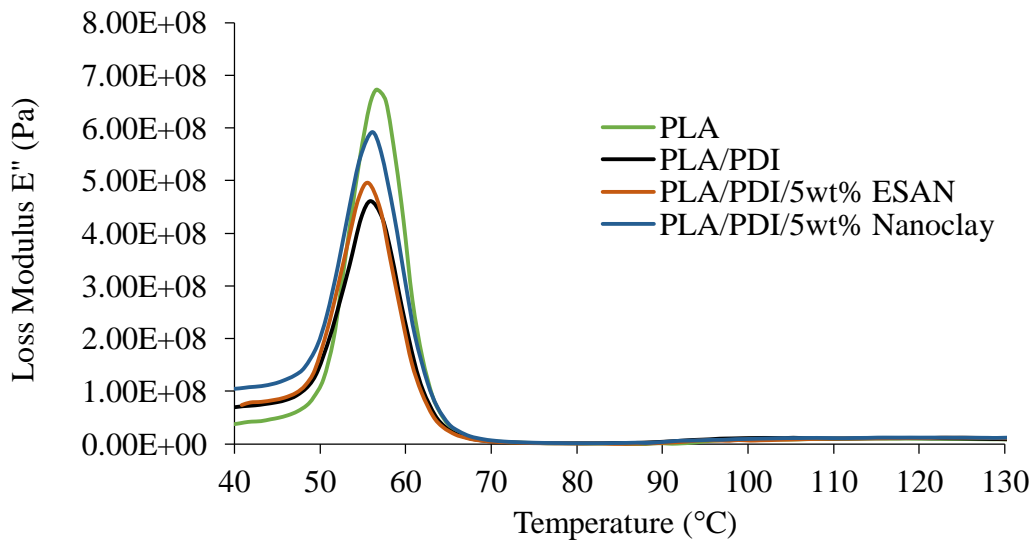


Figure 4.85. Loss Modulus (E'') versus temperature data for PLA/PDI/5wt%HNT composites

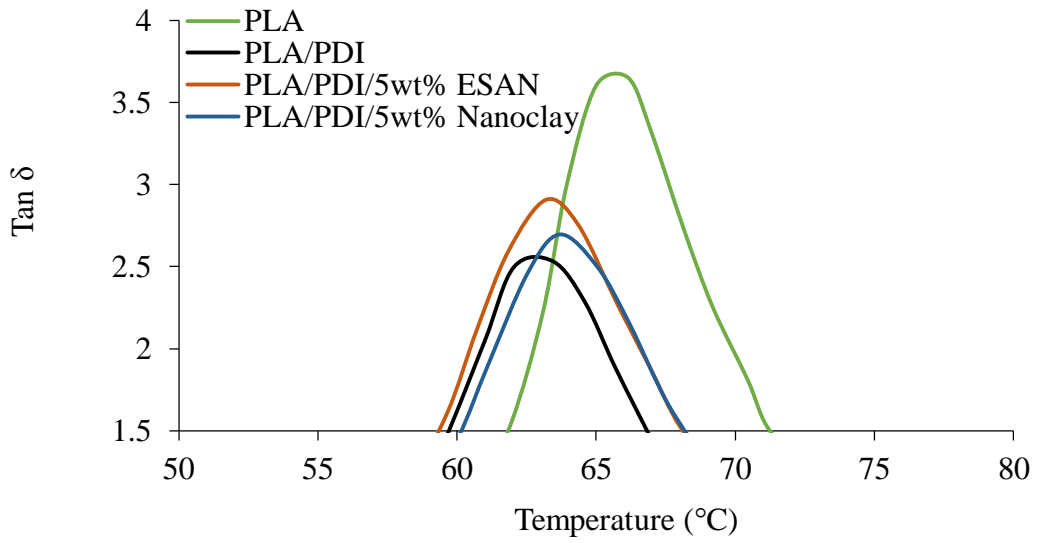


Figure 4.86. Tan δ versus temperature data for PLA/PDI/5wt% HNT composites

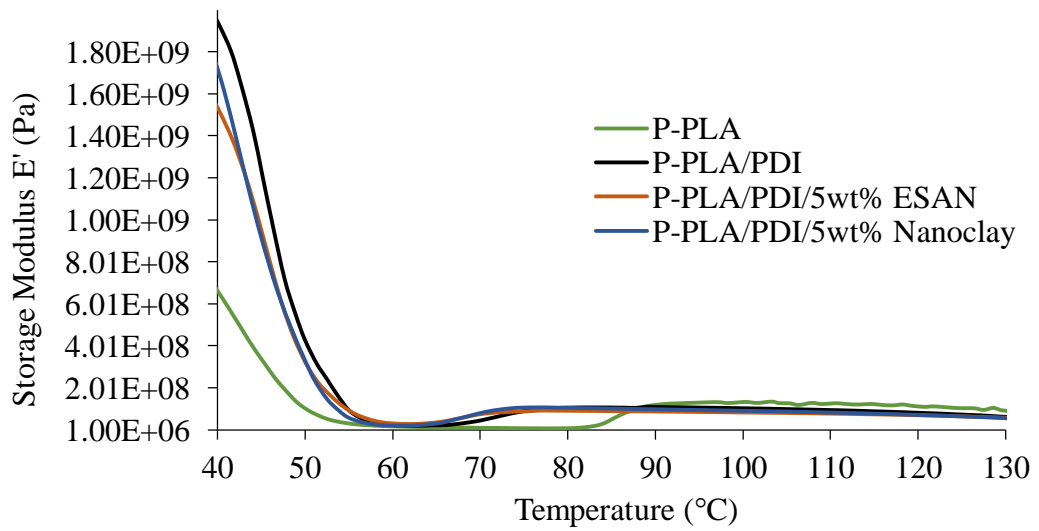


Figure 4.87. Storage Modulus (E') versus temperature data for P-PLA/PDI/5wt% HNT composites

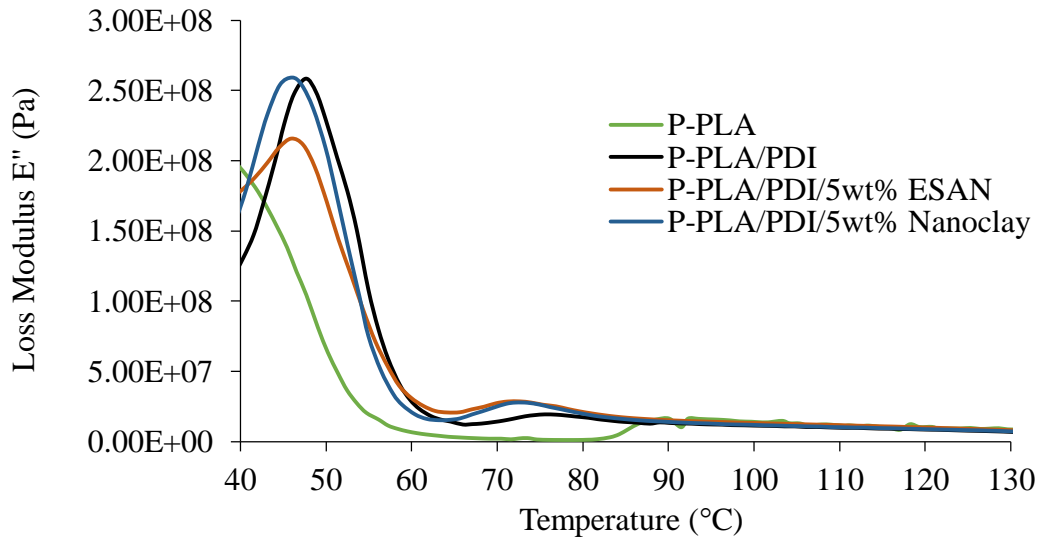


Figure 4.88. Loss Modulus (E'') versus temperature data for P-PLA/PDI/5wt%HNT composites

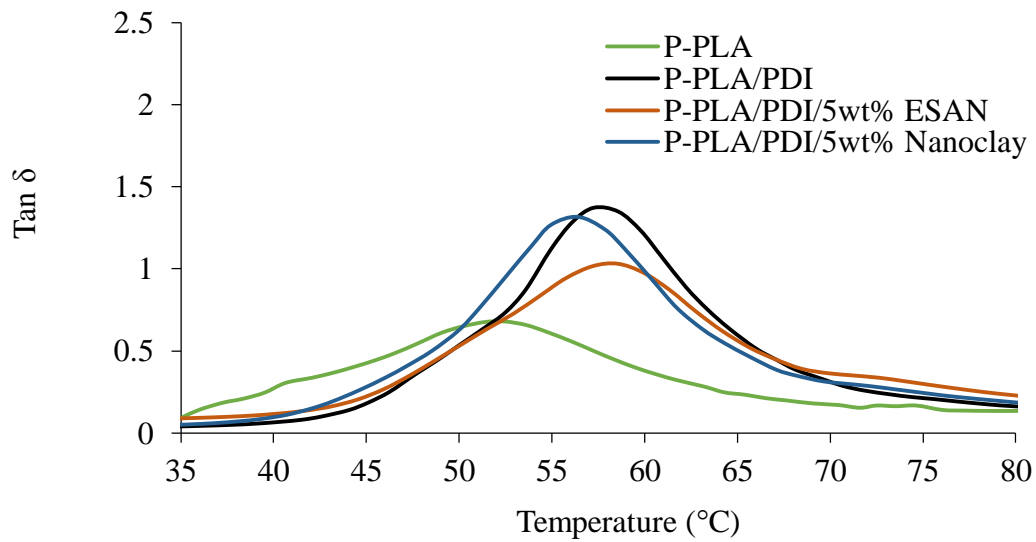


Figure 4.89. Tan δ versus temperature data for P-PLA/PDI/5wt%HNT composites

4.5.5 Differential Scanning Calorimetry Analysis (DSC)

Effects of chain extender on the thermal properties of PLA and P-PLA composites are tabulated in Table 4.8. For PLA, chain extender results in an increase in T_g , T_c and T_m values due to increased molecular weight of PLA. The increased molecular weight also decreases the crystal formation. In addition, heat required for crystallization or melting decreases approximately to half of their initial value with addition of PDI. Clay containing PLA/PDI composites show no significant change in their thermal transition behavior.

The same trend, i.e. increasing T_g , T_c and T_m values with addition of PDI, is also observed for the P-PLA blends, but, more explicitly. When the PLA based composites are plasticized with PEG, a shoulder formation is observed in the melting peak region due to melting of two crystalline types. The shoulder peaks observed around 140°C and 150°C can be classified as the melting of β -crystal and α -crystal forms respectively. This shoulder formation becomes more visible with the introduction of HNT minerals due to the β -nucleating ability of nanotubes on the P-PLA blends. However, with PDI addition this formation is suppressed as can be seen from Figure 4.90. However, the increased T_g in the presence of HNT indicates the nucleating effect of the clay minerals. As a result, although the β -nucleating ability of HNT minerals is suppressed in the presence PDI, their nucleating ability for α -crystal formation is still active.

In addition, the weak endotherm observed for P-PLA/HNT composites is also suppressed with addition of PDI as shown in Figure 4.90. Previously this endotherm was mentioned as enthalpy relaxation. As the endotherm becomes more visible with addition of HNT to P-PLA, it suppresses the formation of cold crystallization peak. Although the endotherm still exists in PDI containing composites, its reduced intensity results in the formation of a crystallization peak.

Table 4.8. Effects of PDI on thermal transition behavior and crystalline fraction (%) of PLA/5wt% HNT composites

Sample	T_g (°C)	T_c (°C)	ΔH_c (J/kg)	T_{m1} / T_{m2} (°C)	ΔH_m (J/kg)	X_c (%)
PLA	57.8	120.3	22.04	148.1	24.21	2.3
PLA/PDI	59.5	126.8	10.88	150.5	10.80	0
PLA/PDI/ESAN	59.8	125.6	15.54	150.7	15.05	0
PLA/PDI/Nanoclay	59.6	125.7	14.37	150.6	14.34	0
P-PLA	32.4	81.6	11.15	140.1/149.8	27.89	18
P-PLA/PDI	X*	108.1	20.76	150.4	21.20	0
P-PLA/PDI/ESAN	X	95.3	19.84	151.4	19.48	0
P-PLA/PDI/Nanoclay	X	93.3	18.87	153.0	18.55	0

*X: Not observed due to overlap with endothermic peak which is around 50°C

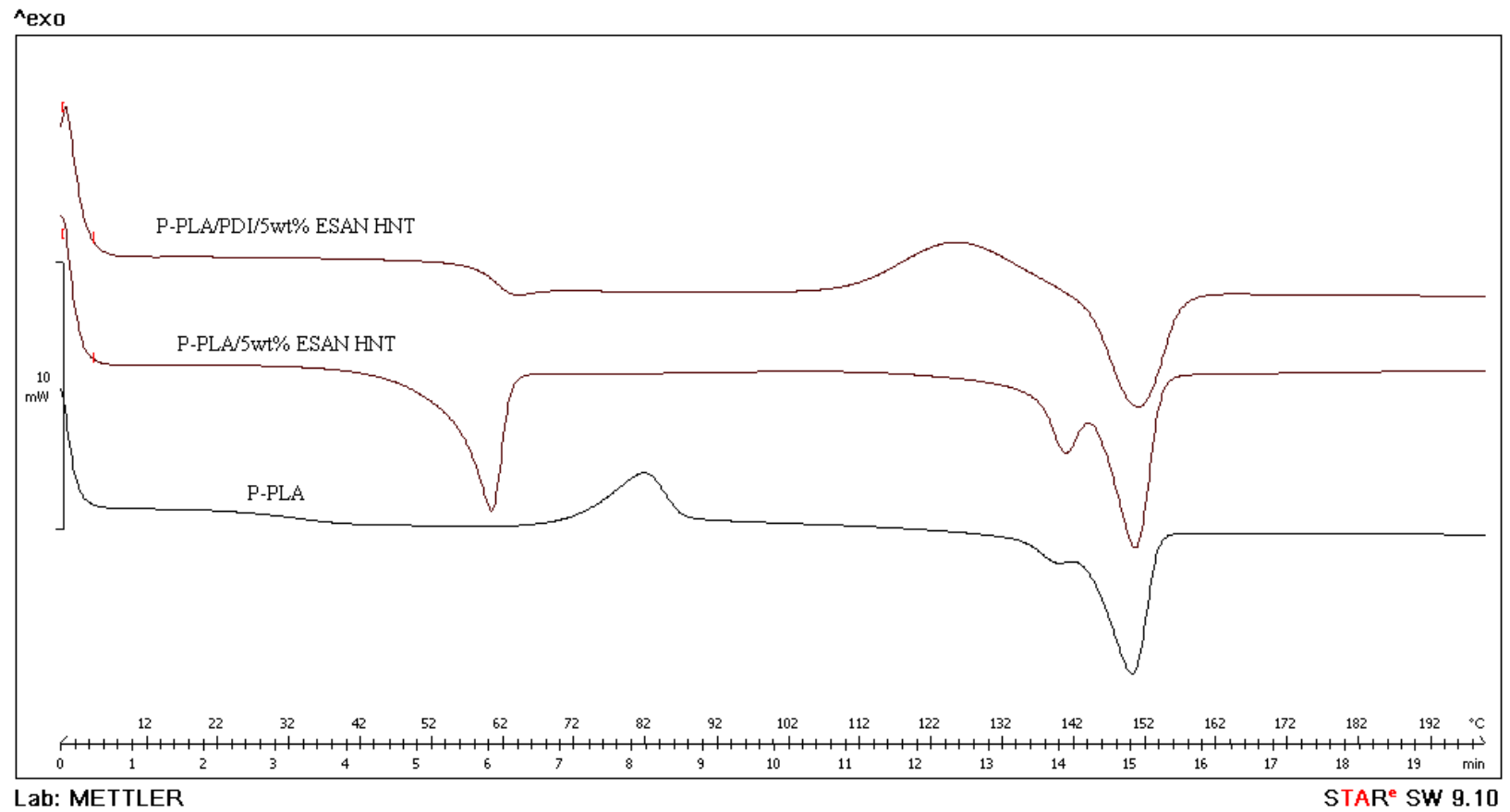


Figure 4.90. Effect of PDI on the crystallization behavior of P-PLA/HNT composite

4.5.6 Hydrolytic Degradation

Hydrolytic test observations on PLA and P-PLA polymers and composites containing PDI molecules are given in Figure 4.91 and Figure 4.92. As can be seen from the figures, addition of PDI to PLA matrix results in a lower degradation rate. This is mainly due to increased molecular weight as mentioned before. For P-PLA blends, the retardation in the second stage of the hydrolytic degradation is much more explicit. Higher molecular weight of the P-PLA due to chain extension with PDI molecules is the main cause of this result. When HNT is added into PLA/PDI mixtures no change is observed both in the first and second stages of the hydrolytic degradation, in contrast to the results obtained on PLA/HNT composites.

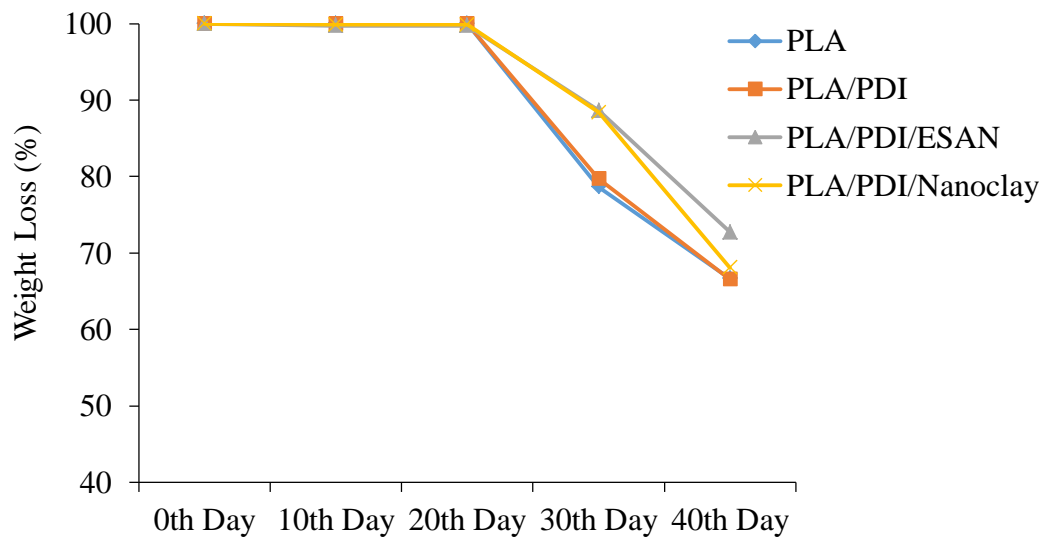


Figure 4.91. Hydrolytic degradation results on PLA/PDI mixture and PLA/PDI/HNT composites

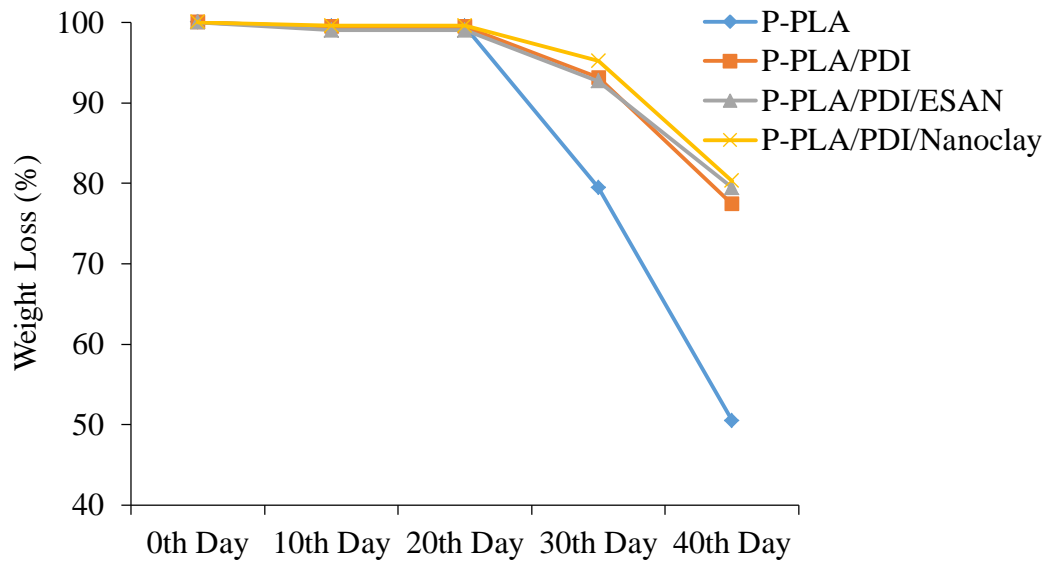


Figure 4.92. Hydrolytic degradation results of P-PLA/PDI mixture and P-PLA/PDI/HNT composites

4.6 Comparison between the Properties of PLA/CNT and PLA/HNT Unplasticized and Plasticized Composites

Up to this point of the study, PLA/HNT based composites are investigated. The results obtained by different methodologies showed that PLA and HNT are incompatible unless the hidden water that had remained between the layers of silicate is removed or the right compatibilizer is used as toughening agent.

Compared to HNT minerals, carbon nanotubes (CNT) are not easily available, abundant and biocompatible which allow HNT applications to be used in drug delivery and biomedical applications. In addition, CNT's extremely high cost and the difficulties faced during composite preparation reduced the interest on their biopolymer nanocomposites and directed the studies onto other natural fillers. Another important advantage of HNTs compared to CNTs is their effect on human health. According to European Union standards, HNT contains only trace amount of heavy metals which is much lower than the maximum limits of restriction of harmful substances (Du, Guo and Jia 2010).

However, their high elastic modulus and exceptional tensile strength led CNT to be used in nanocomposites which exhibit improved features, such as sensitivity to pressure, temperature and gas, and improved electrical, mechanical and thermal properties (Yesil 2013). In spite of its many disadvantages PLA bio-based composites containing CNT might be used in heavier industries such as manufacturing of automotive parts.

In this section of the study, CNT based PLA composites were prepared and plasticized with both PEG and TPU at concentration of 20wt%. As in the case of PLA/HNT composites, PLA/CNT composites were prepared by DM3 method and the CNT concentration was varied from 3 to 10wt%. Also, all of the results are compared with the results obtained on PLA/HNT, P-PLA/HNT and T-PLA/HNT composites prepared with local ESAN HNT.

4.6.1 Scanning Electron Microscopy

SEM micrographs given through Figure 4.93 to Figure 4.95 compare the morphology of PLA/HNT plasticized and un-plasticized composites with PLA/CNT plasticized and un-plasticized composites.

CNT particles are distributed better in PLA matrix compared to HNT mineral owing to better attraction between PLA and synthetic CNT. Also, further growing crack propagation lines are observed with the use of CNT. This might be expected to reduce the stiffness of PLA, whereas it improves the tensile strength as will be mentioned in the mechanical analysis part.

PEG plasticized CNT composite and its comparison with P-PLA/HNT can be examined from Figure 4.94. CNT based composite displays morphology with larger agglomerates dominating the structure compared to HNT based composites. Hence, it can be said that plasticization with low molecular weight materials has no positive effect on the dispersion of both HNT and CNT particles.

When TPU toughened materials are considered it can be said that the filler materials change the domain size of the dispersed phase. HNT particles reduce the size to an optimum level, whereas CNT particles almost completely destroy the droplet structure of the TPU phase. This destruction is a result of too small domains which might be formed owing to finely dispersed particles that hinder the coalescence of domains during melt mixing. The small domains might also be a result of increased viscosity of the continuous phase, PLA, with the addition of CNT particles. Owing to increased viscosity, the shear stress applied on the dispersed phase might be increased and this may reduce the domain size. It is a well-known fact that the size of the domain should not be too small or too big. When ultra-fine domains of elastomers are formed they cause low impact strength values because of the crack propagation lines that propagate without touching the elastomer domains.

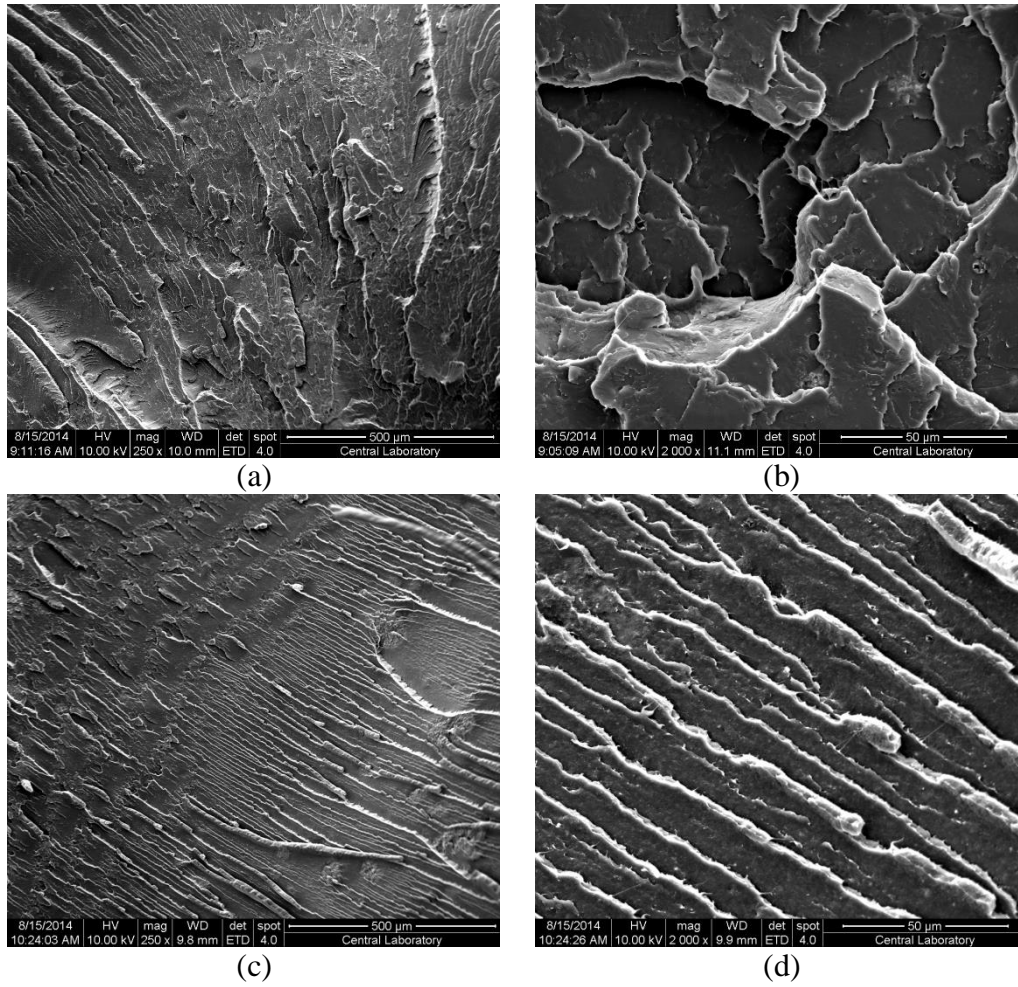


Figure 4.93. SEM Micrograph of PLA composites containing 5wt% (a) ESAN HNT 250x, (b) ESAN HNT 2000x, (c) CNT 250x, (d) CNT 2000x

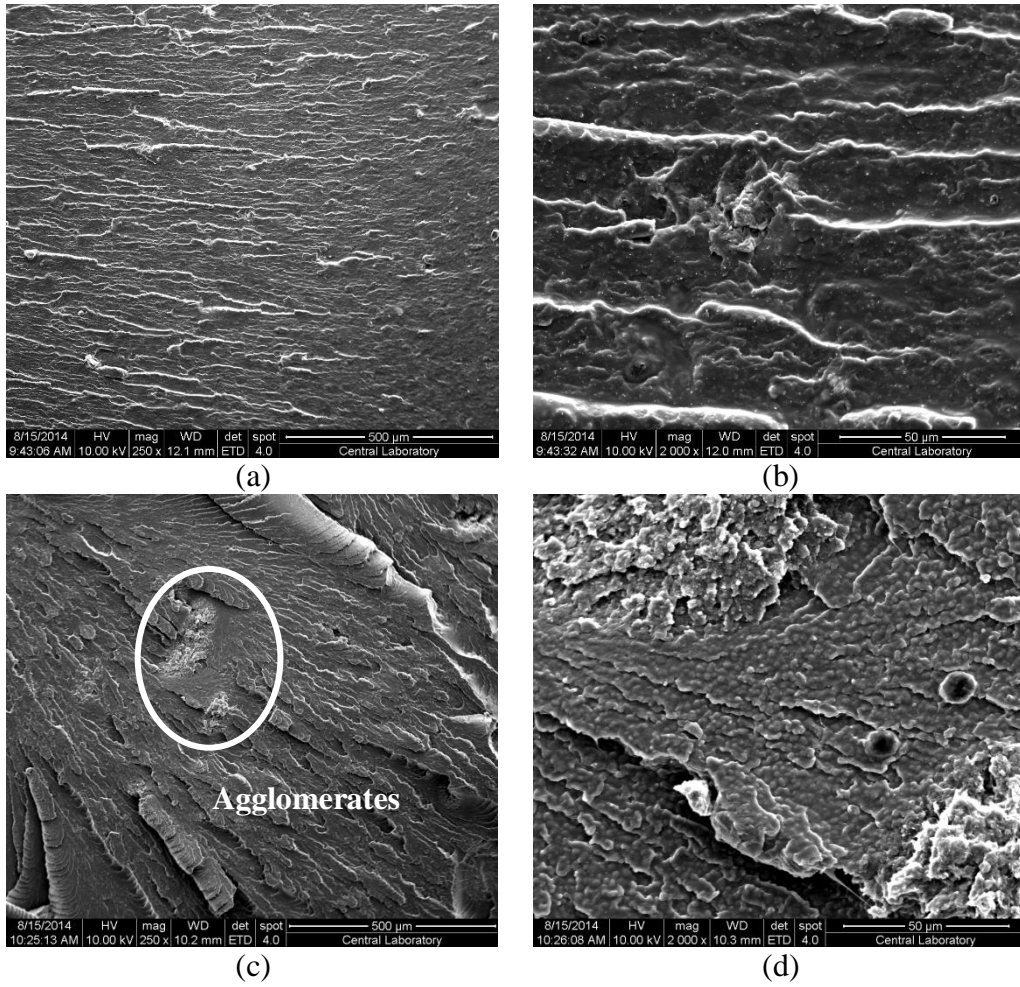


Figure 4.94. SEM Micrograph of P-PLA composites containing 5wt% (a) ESAN HNT 250x, (b) ESAN HNT 2000x, (c) CNT 250x, (d) CNT 2000x

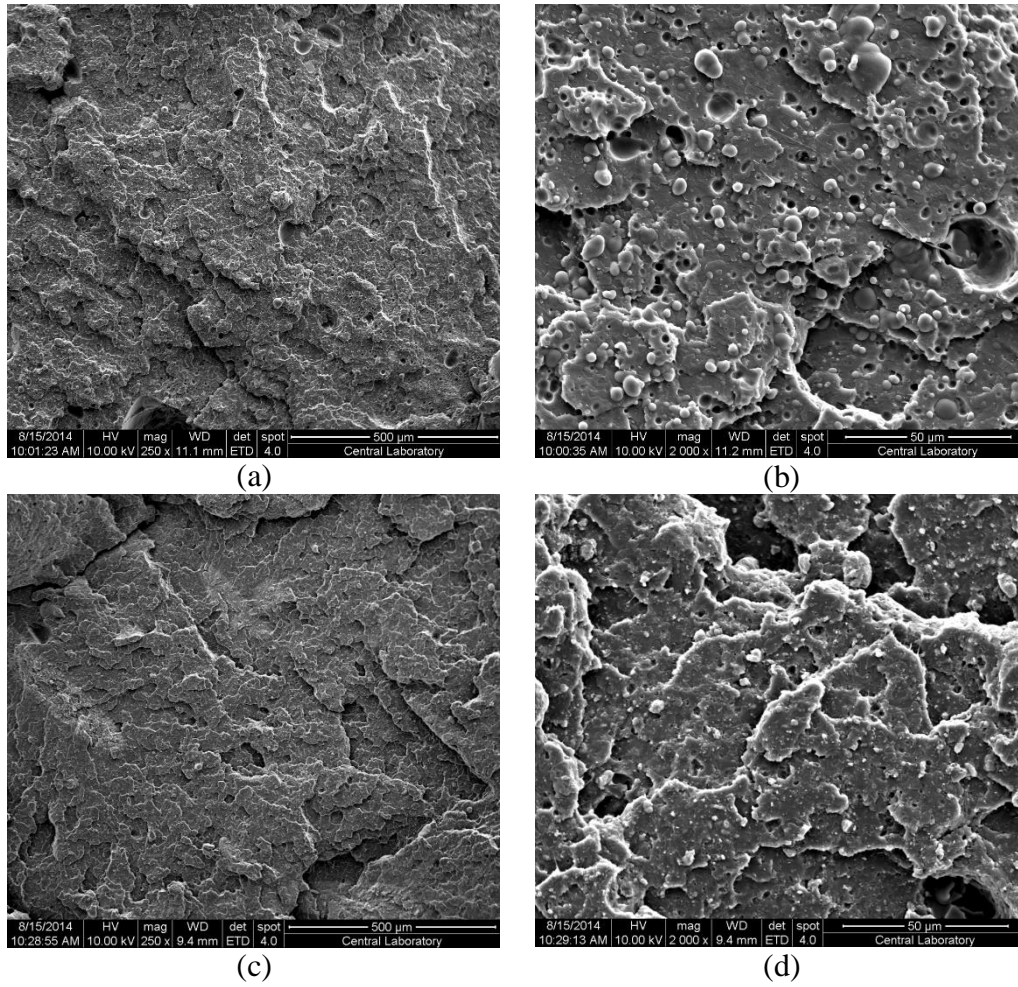


Figure 4.95. SEM Micrograph of T-PLA composites containing 5wt% (a) ESAN HNT 250x, (b) ESAN HNT 2000x, (c) CNT 250x, (d) CNT 2000x

4.6.2 Transmission Electron Microscopy

Well distribution of CNT particles in polymer matrix at a 5wt% loading was also proven by TEM analysis as shown in Figure 4.96. At this loading, uniform dispersion of CNT bundles results in more elongated CNT content which improves load transfer and mechanical properties. Figure 4.97 shows the TEM micrographs of P-PLA and T-PLA composites containing 5wt% CNT. As in the case of P-PLA/HNT composite, CNT particles do not show the desired distribution in the PLA/PEG blend, and they form agglomerated structures with entangled CNT bundles. T-PLA/CNT composite also displays an entangled structure. Contrary to T-PLA/HNT composites, the filler CNT locates itself in the TPU phase and destroys the droplet structure of the TPU phase. The location of CNT might be assumed to result in larger domain size. However, CNT particles located in the TPU phase results in ultra-fine domains

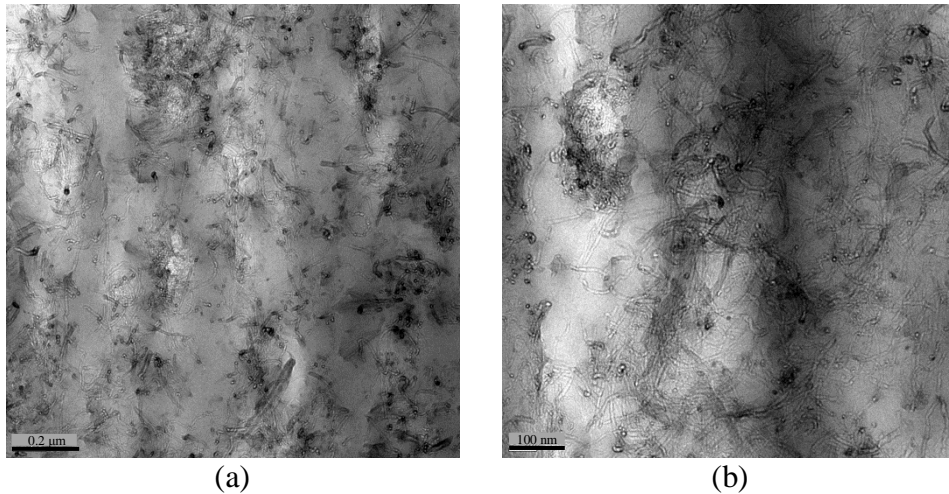


Figure 4.96. TEM Micrographs of PLA/5wt% CNT composite; (a) Scale bar is 0.2 μ m, (b) Scale bar is 100nm

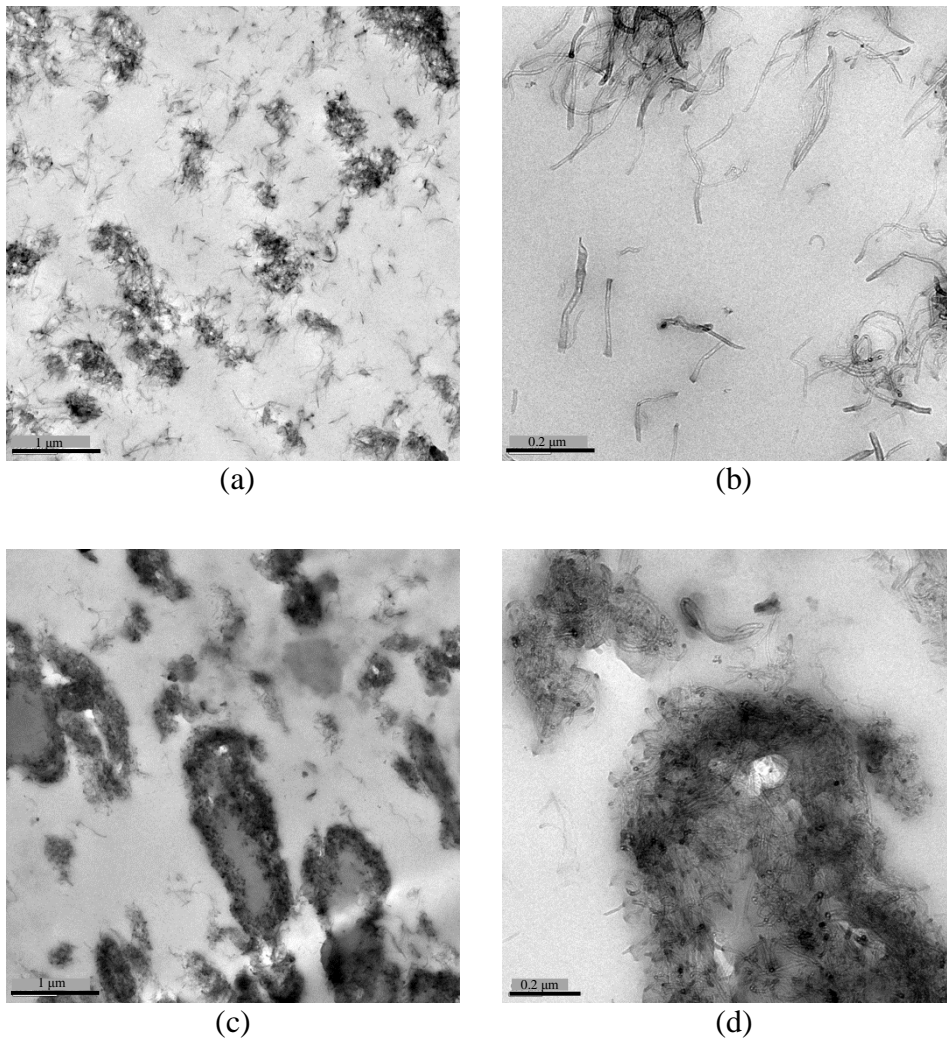


Figure 4.97. TEM Micrographs of composites containing 5wt% CNT; (a) P-PLA Scale bar is 1μm, (b) P-PLA Scale bar is 0.2μm, (c) T-PLA Scale bar is 1μm, (d) T-PLA Scale bar is 0.2μm

4.6.3 Tensile Properties

In Figure 4.98 and Figure 4.99, tensile properties of the CNT containing PLA nanocomposites are shown. Although the CNT surfaces are not subjected to purification and functionalization (Kuan et al. 2008, Chiu et al. 2008, Li et al. 2013), they display an improvement in the tensile properties of PLA. With increasing CNT content, the strength of the material increases up to 5wt% and then remains the same. This result is in contrast with the results obtained from the PLA/HNT composites. However, CNT causes a rapid reduction in the elongation at break independent of the content. According to these results, it can be said that CNT acts better compared to HNT.

However, for plasticized composites, the result is completely different. As can be seen from Figure 4.100 and Figure 4.101, increasing CNT content causes a distinct reduction in both tensile strength and strain at break values of P-PLA. This might be the cause of an activated phase separation in the presence of CNT molecules. As discussed previously and shown in the following figures, there is no improvement in tensile properties of the P-PLA/HNT composites, but after all, tensile properties of PLA do not show reduction with addition of HNT. Instead, as the clay content increases the strength reduction is recovered.

When the tensile properties of T-PLA/CNT composites are investigated from Figure 4.102 and Figure 4.103, it is seen that there is an improvement in tensile properties at the expense of elongation at break properties. Hence, compared to HNT fillers, which improves the strain at break values of T-PLA extremely, CNT acts as a better filler in terms of material strength. However, for the T-PLA applications which require higher flexibility, HNT filler type is much more desired.

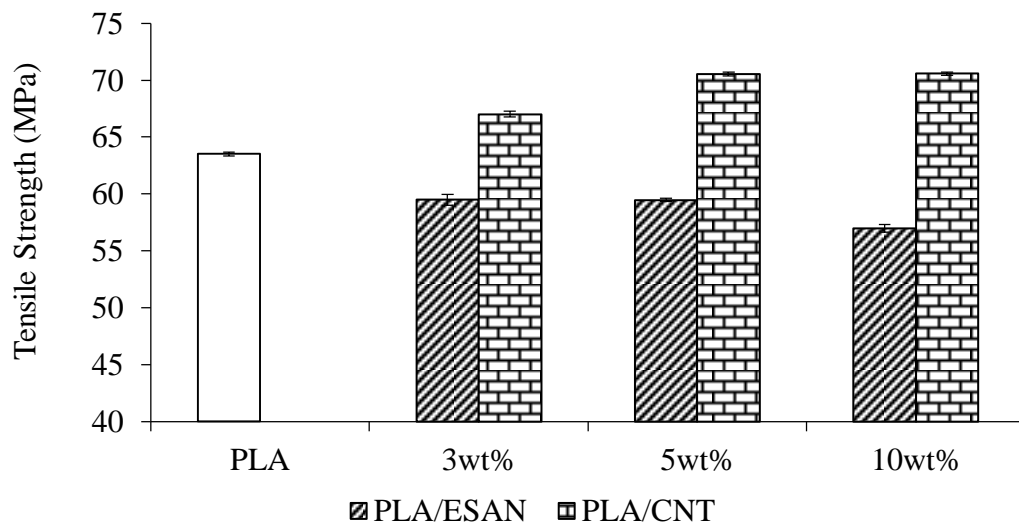


Figure 4.98. Tensile strength (MPa) of PLA/CNT nanocomposites and their comparison with PLA/ESAN HNT composites

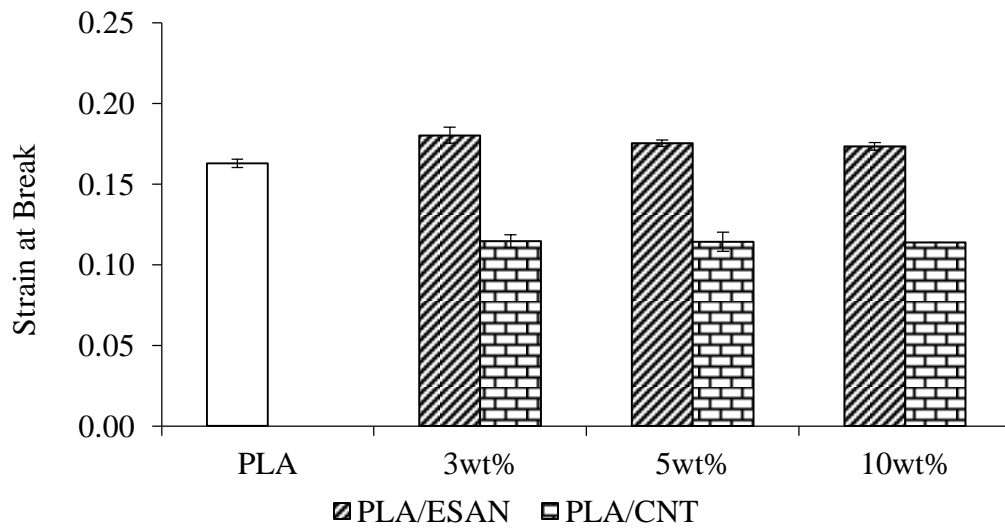


Figure 4.99. Strain at break values of PLA/CNT nanocomposites and their comparison with PLA/ESAN HNT composites

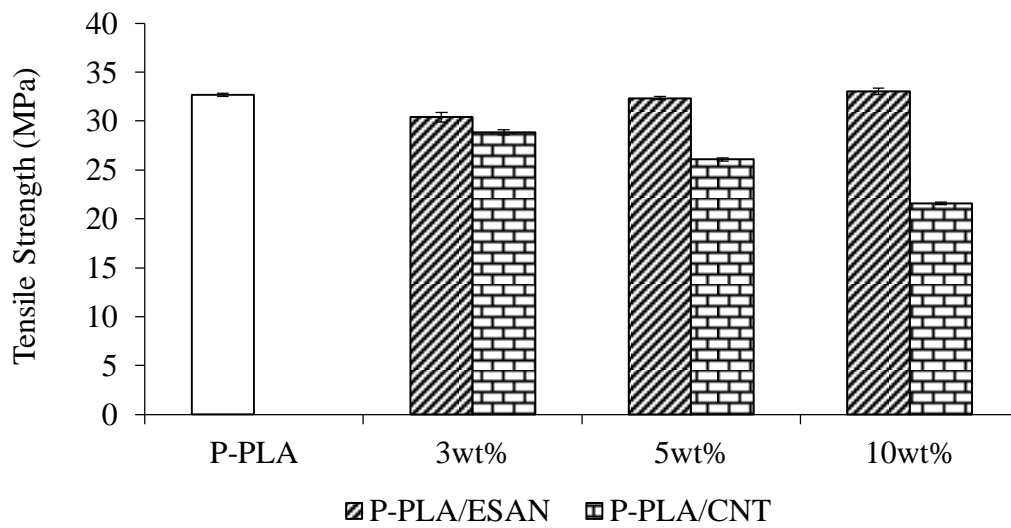


Figure 4.100. Tensile strength (MPa) of P-PLA/CNT nanocomposites and their comparison with P-PLA/ESAN HNT composites

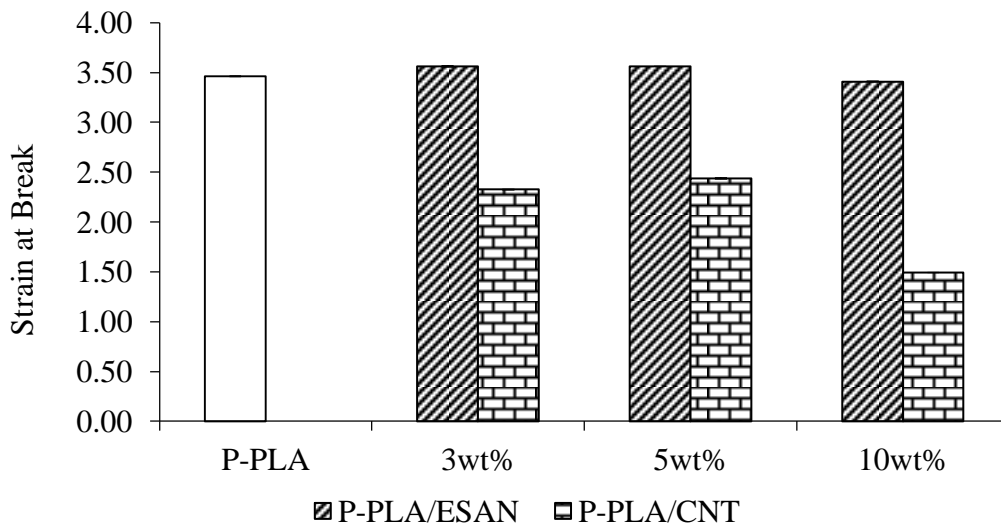


Figure 4.101. Strain at break values of P-PLA/CNT nanocomposites and their comparison with P-PLA/ESAN HNT composites

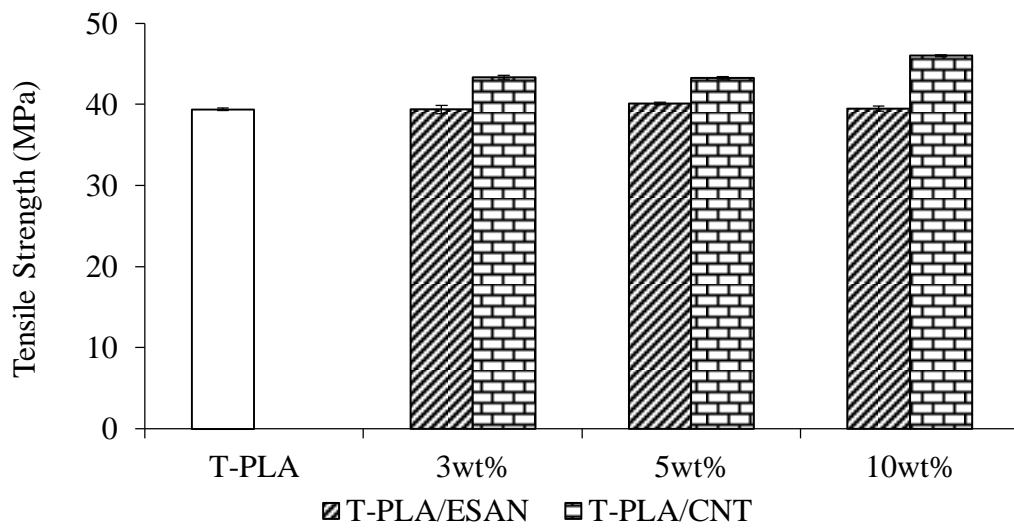


Figure 4.102. Tensile strength (MPa) of T-PLA/CNT nanocomposites and their comparison with T-PLA/ESAN HNT composites

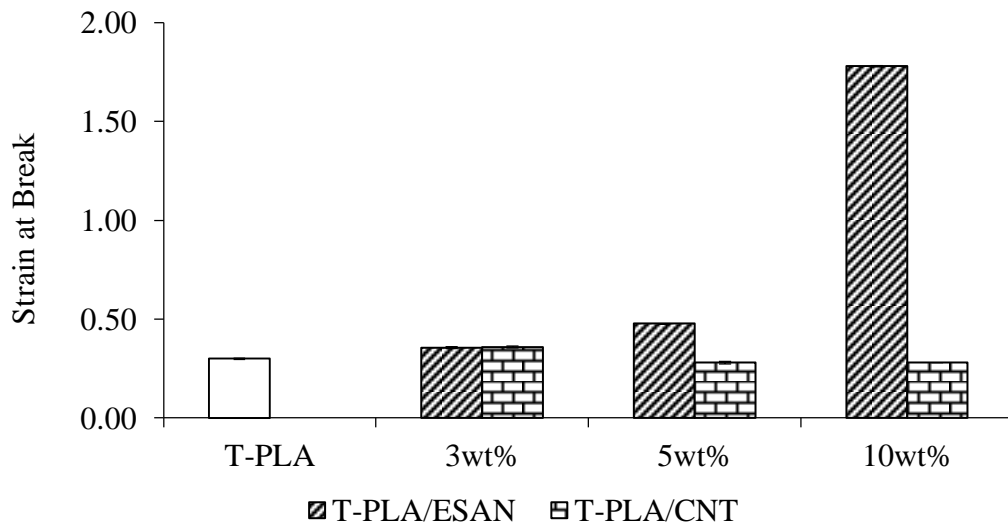


Figure 4.103. Strain at break values of T-PLA/CNT nanocomposites and their comparison with P-PLA/ESAN HNT composites

4.6.4 Impact Results

Impact results of the PLA composites prepared with CNT and their comparison with HNT based PLA composites can be seen from Figure 4.104. Addition of CNT to the system results in lower impact strength and this reduction rises as the CNT content increases. This might be related to the growing crack propagation lines with addition of CNT as can be seen from their SEM micrographs.

In contrast to the contribution of HNT mineral to the toughness of T-PLA blend, CNT yields in a reduction in the impact strength as can be seen from Figure 4.105. CNT particles destroy the droplet structure of dispersed phase, TPU, domains by forming ultra-fine domains and reduce the toughness of the material.

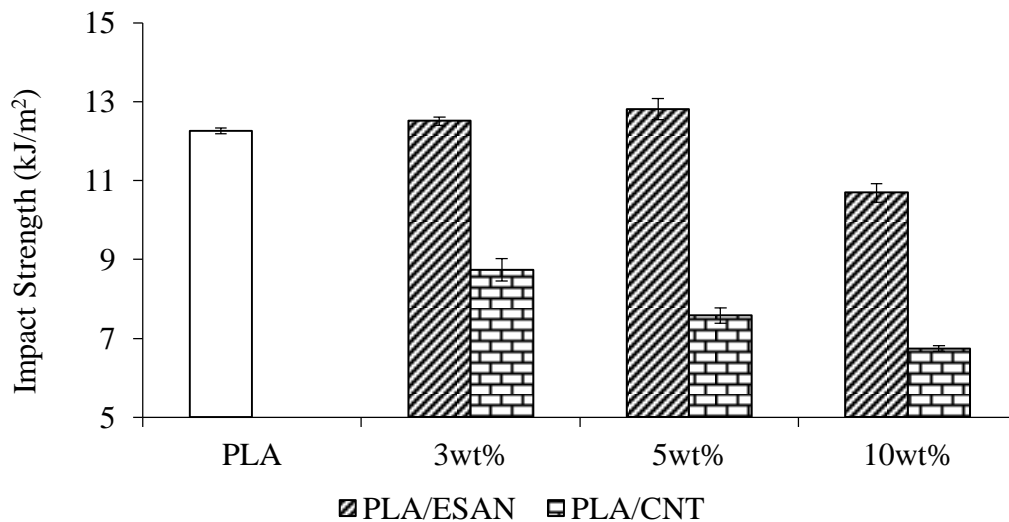


Figure 4.104. Impact strength (kJ/m²) of PLA/CNT nanocomposites and their comparison with PLA/ESAN HNT composites

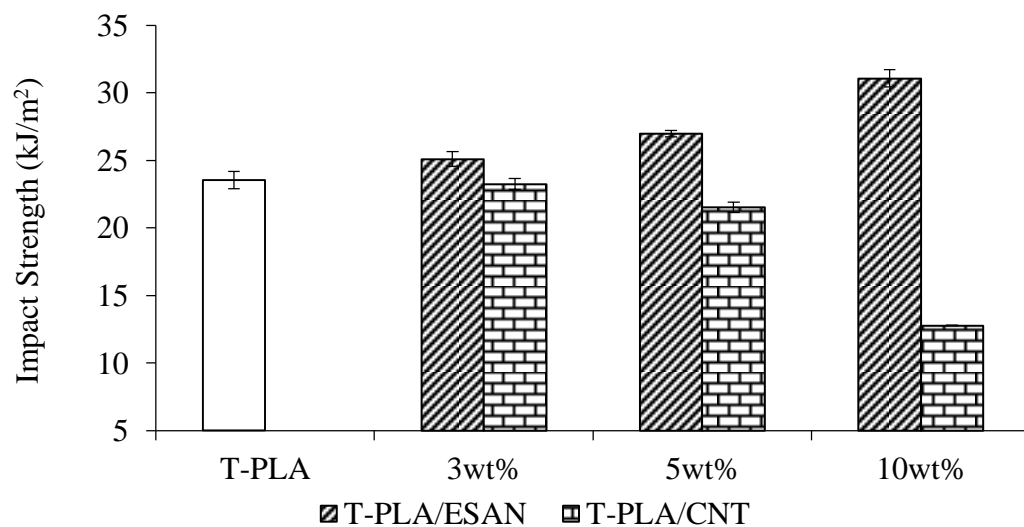


Figure 4.105. Impact strength (kJ/m²) of T-PLA/CNT nanocomposites and their comparison with T-PLA/ESAN HNT composites

4.6.5 Dynamic Mechanical Analysis (DMA)

Dynamic mechanical analysis of CNT based PLA, P-PLA and T-PLA composites are given in this part. The properties of PLA/CNT composites are given in Figure 4.106 and Figure 4.108.

Addition of CNT to PLA gives rise to slight enhancement in storage modulus, whereas it reduces the intensity of loss modulus maximum peak. This might be the sign of the nano reinforcing effect tendency of the high aspect ratio CNT suppressed by high nanotube-nanotube interactions causing agglomeration and interconnected structures of CNT in the polymer matrix.

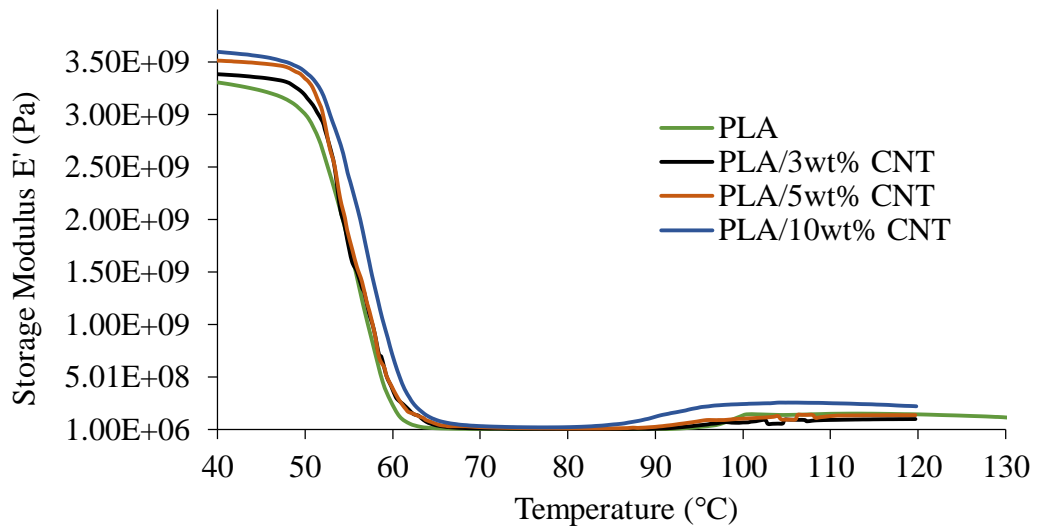


Figure 4.106. Storage Modulus (E') versus temperature data for PLA/CNT composites

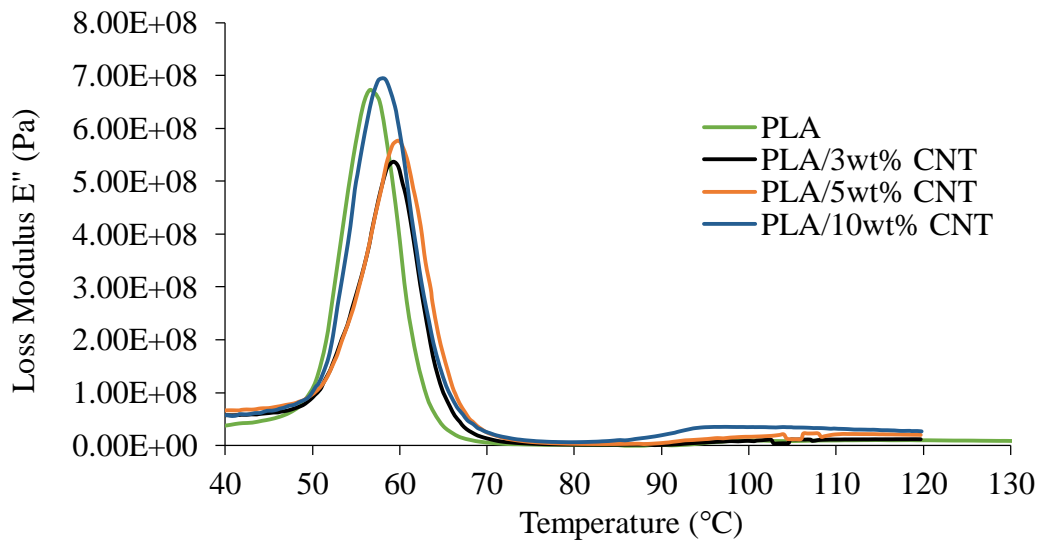


Figure 4.107. Loss Modulus (E'') versus temperature data for PLA/CNT composites

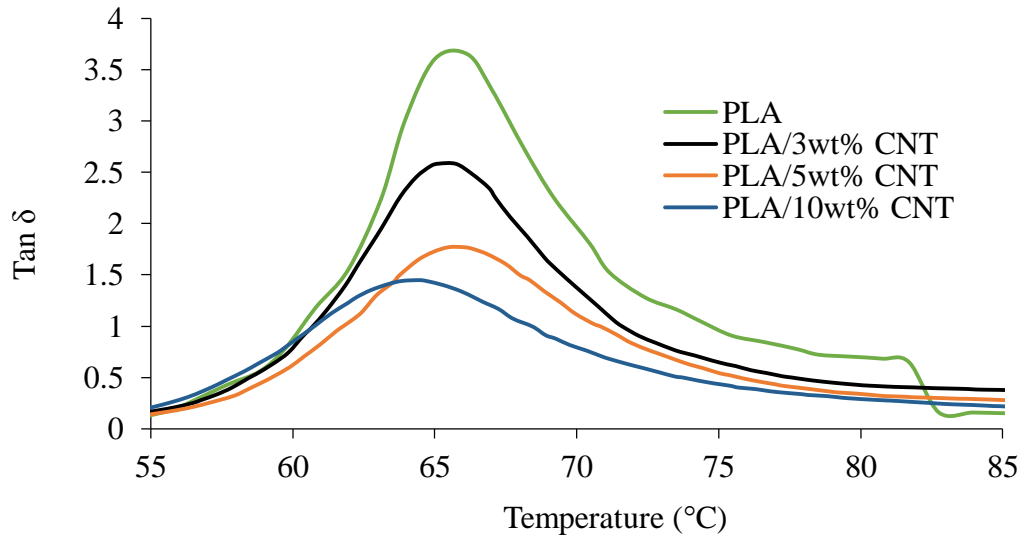


Figure 4.108. Tan δ versus temperature data for PLA/CNT composites

DMA results obtained for P-PLA/CNT and T-PLA/CNT composites are given through Figure 4.109 to Figure 4.111 and Figure 4.112 to Figure 4.114 respectively. CNT particles affect the dynamic mechanical properties of P-PLA blend in a similar way that HNT minerals did. When the filler is introduced to the system it reduces the stiffness of the material up to 5wt% clay loading and after that point it starts to increase. The same trend is also observed in the E'' and tan δ versus temperature plots indicating a recession in DMA properties with addition of CNT, whereas the properties are well recovered with increasing HNT loading up to 10wt%.

When T-PLA composites are analyzed with dynamic mechanical analysis, it is observed that CNT particles improve storage modulus values, whereas they do not affect the loss modulus values. Also, no significant change is observed in the loss tangent value with addition of CNT to T-PLA matrix.

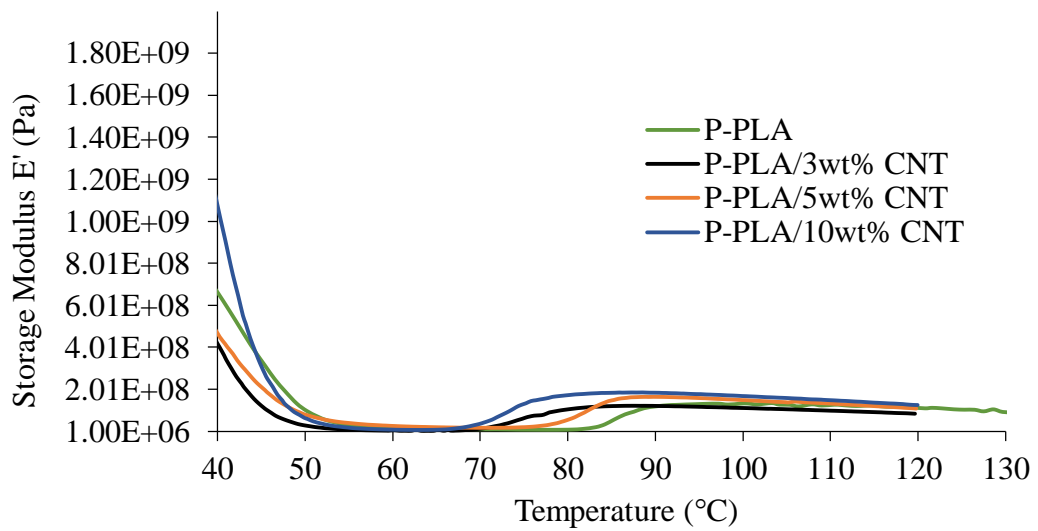


Figure 4.109. Storage Modulus (E') versus temperature data for P-PLA/CNT composites

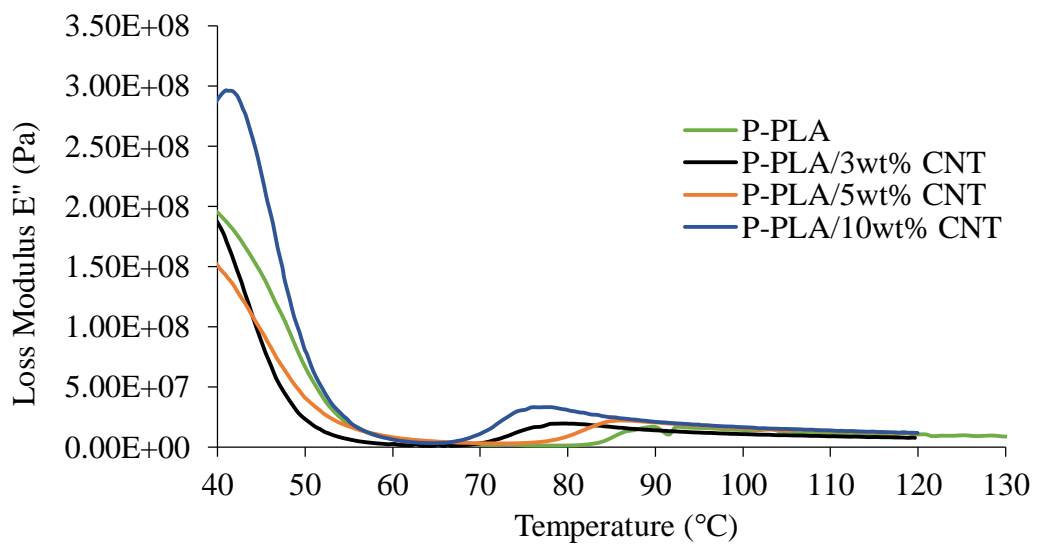


Figure 4.110. Loss Modulus (E'') versus temperature data for P-PLA/CNT composites

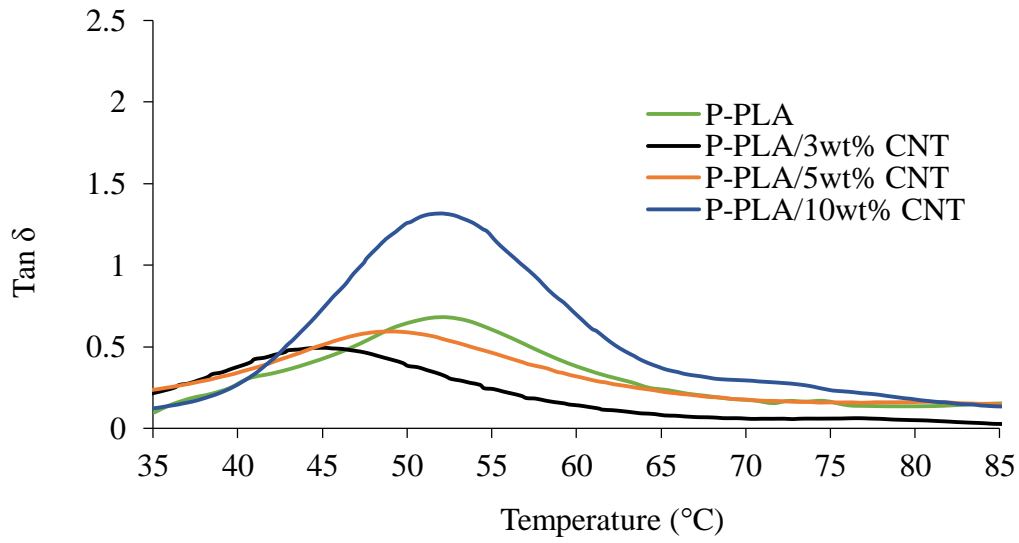


Figure 4.111. Tan δ versus temperature data for P-PLA/CNT composites

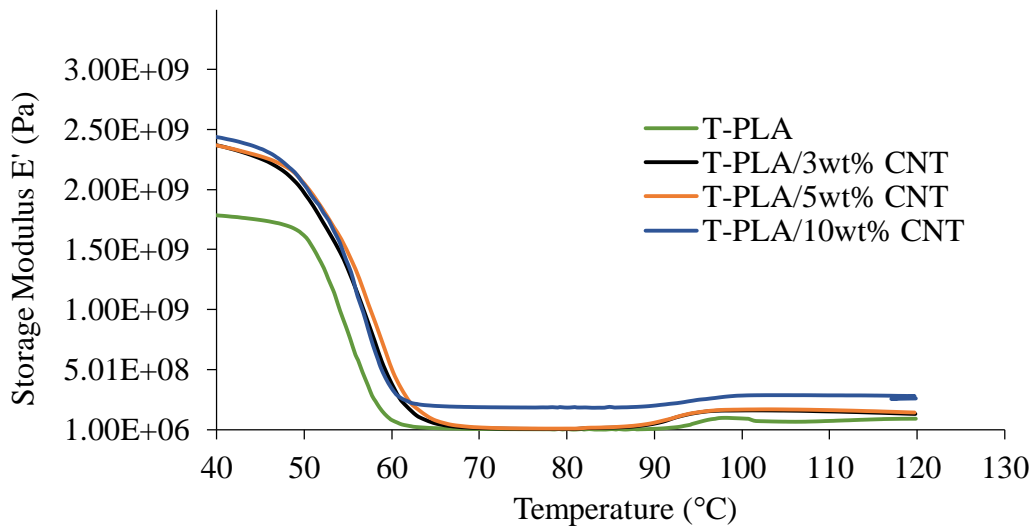


Figure 4.112. Storage Modulus (E') versus temperature data for T-PLA/CNT composites

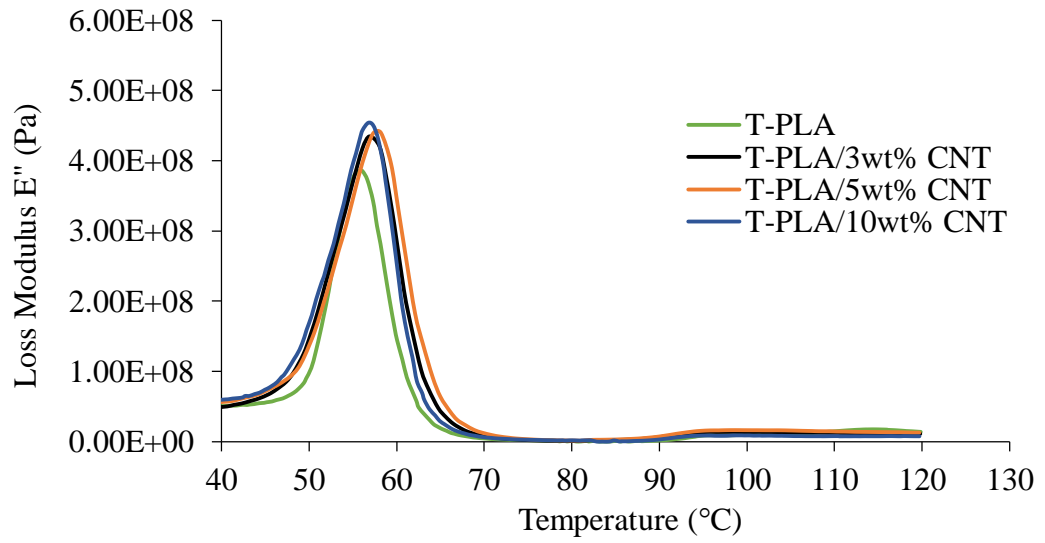


Figure 4.113. Loss Modulus (E'') versus temperature data for T-PLA/CNT composites

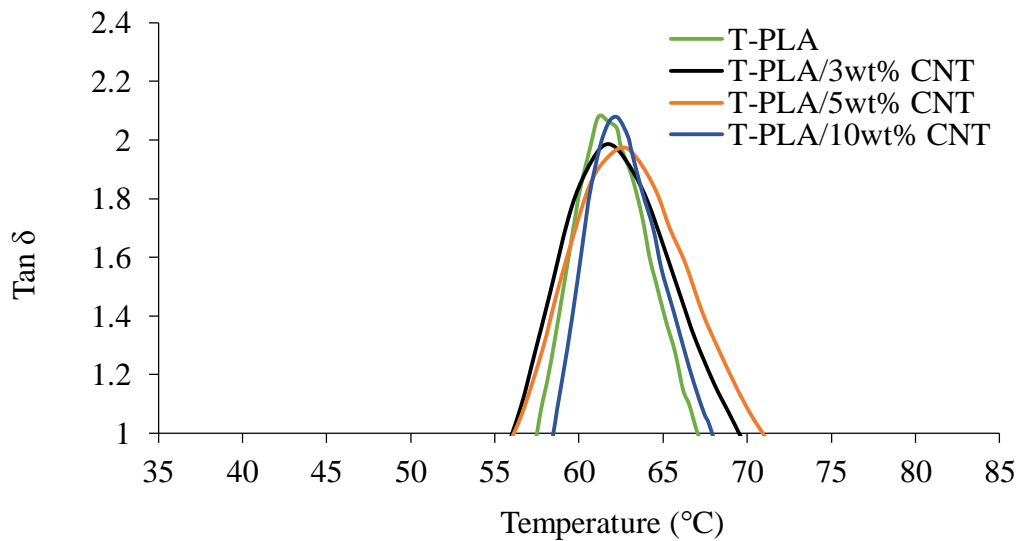


Figure 4.114. $\text{Tan } \delta$ versus temperature data for T-PLA/CNT composites

4.6.6 Differential Scanning Calorimetry Analysis (DSC)

Thermal transition behavior and crystalline fraction (%) of PLA/CNT composites are given in Table 4.9. There is slight effect of CNT on the T_g , T_c and T_m of the PLA composites. However, CNT induces heterogeneous nucleation and hence the crystalline fraction is increased.

For P-PLA/CNT composites, the same results observed on P-PLA/HNT composites are obtained. As can be seen from Figure 4.115, clear shoulder formation indicating β -nucleating ability is also observed for P-PLA/CNT composites. In addition, weak endotherm formation occurs due to the melting of imperfect crystals other than the β -crystal form, and also crystallization peak is suppressed with this formation in P-PLA/CNT composites.

Table 4.9. Thermal transition behavior and crystalline fraction (%) of PLA/CNT composites

Sample	T_g (°C)	T_c (°C)	ΔH_c (J/kg)	T_{m1} / T_{m2} (°C)	ΔH_m (J/kg)	X_c (%)
PLA	57.8	120.3	22.04	148.1	24.21	2.3
PLA/3wt% CNT	59.5	120.5	22.14	149.5	24.33	2.4
PLA/5wt% CNT	60.3	120.4	21.45	150.4	24.25	3.0
PLA/10wt% CNT	59.2	120.3	20.2	150.1	24.42	4.0

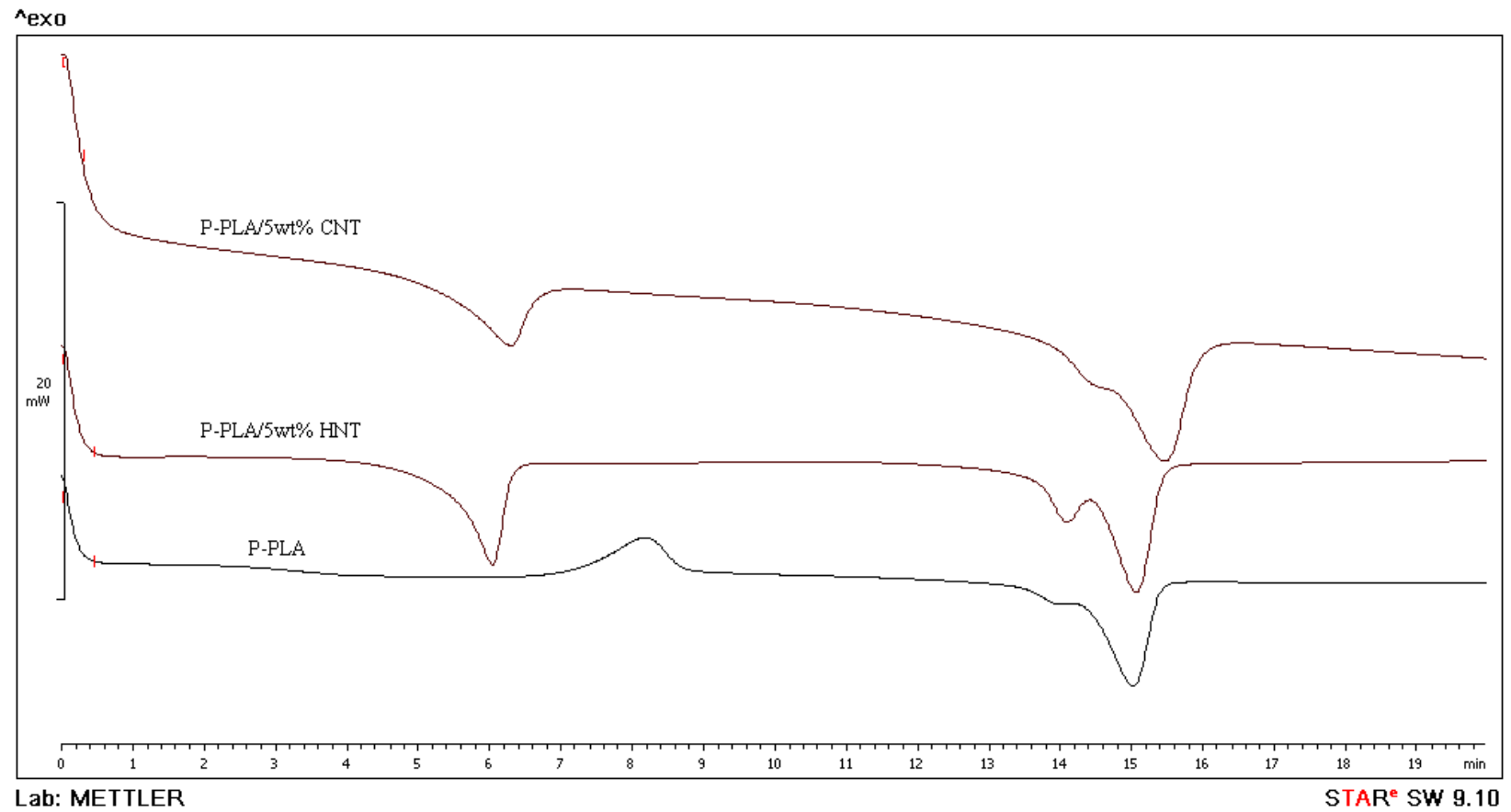


Figure 4.115. DSC thermograms of P-PLA, P-PLA/ESAN HNT and P-PLA/CNT composites

4.6.7 Hydrolytic Degradation

Weight loss plot and stages in the hydrolytic degradation of PLA/CNT composite samples and the can be seen from Figure 4.116 and Figure 4.117 respectively. As in the case of PLA/HNT composites, the samples go through two simultaneous stages: the first one is the stage in which bulk erosion is balanced with weight loss, in the second stage weight loss and fragmentation of the sample starts. With CNT addition while the first stage remains the same, the second stage slows down due to restricted chain movements. However, compared to ESAN HNT based composites, the inhibition in the degradation rate is lower for CNT composites.

The results obtained on the CNT based composites of PEG plasticized P-PLA and TPU toughened T-PLA are given in Figure 4.118 and Figure 4.119 respectively. The tendency of CNT molecules to slow down the degradation rate does not change for plasticized and toughened polymers.

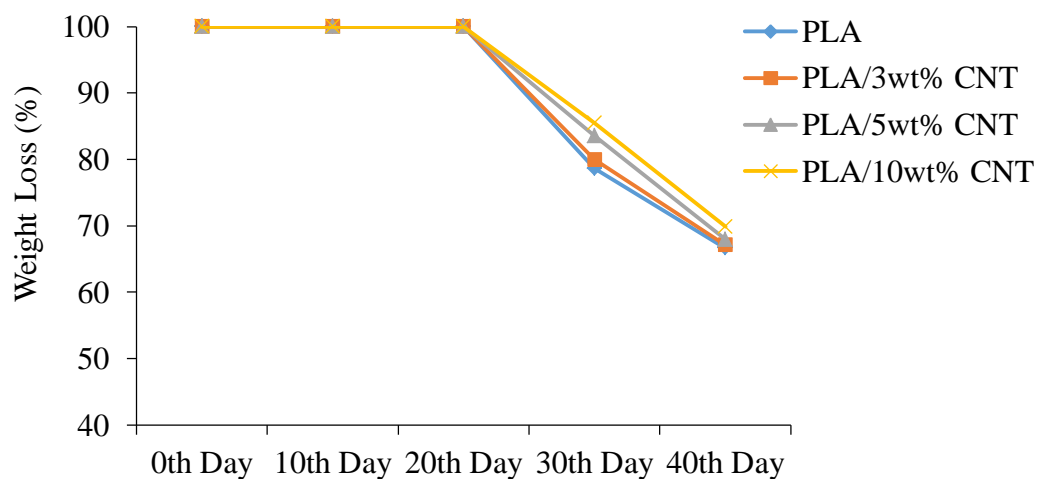


Figure 4.116. Hydrolytic degradation results of PLA/CNT composites

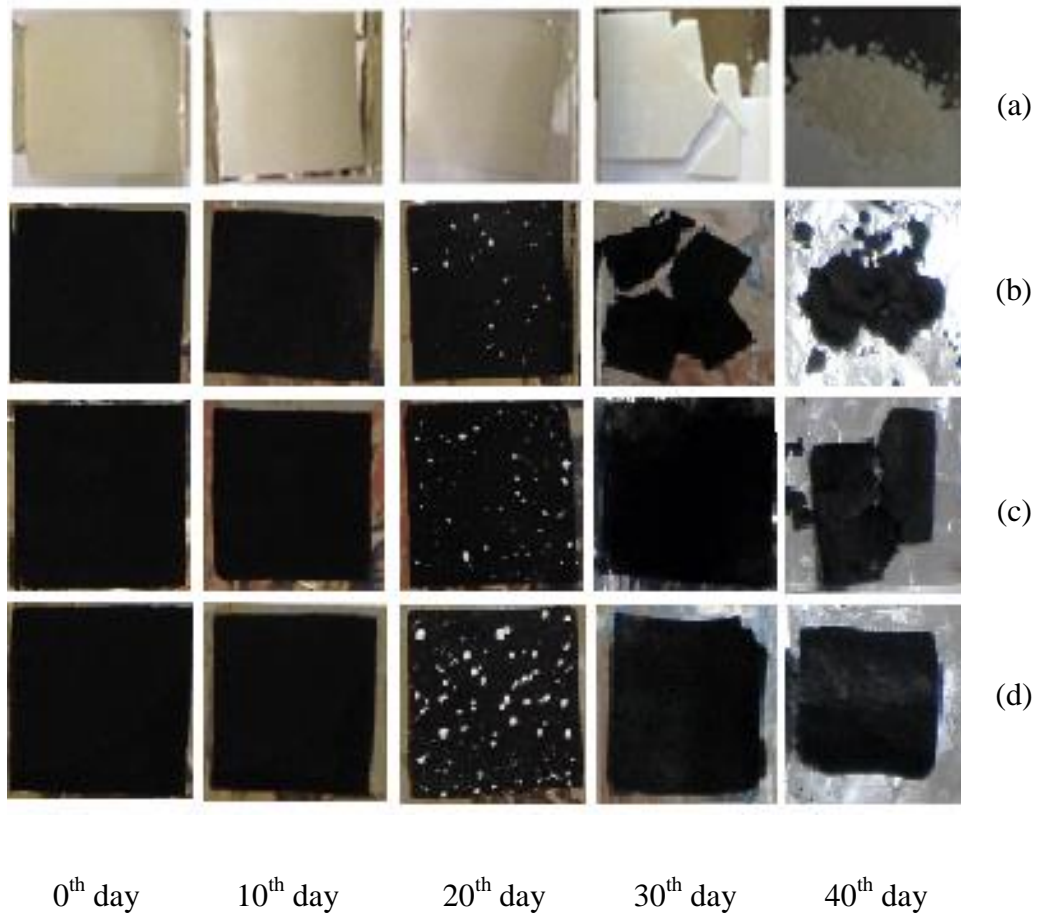


Figure 4.117. Hydrolysis samples of PLA/CNT composites; (a) 0wt% CNT, (b) 3wt% CNT, (c) 5wt% CNT, (d) 10wt% CNT

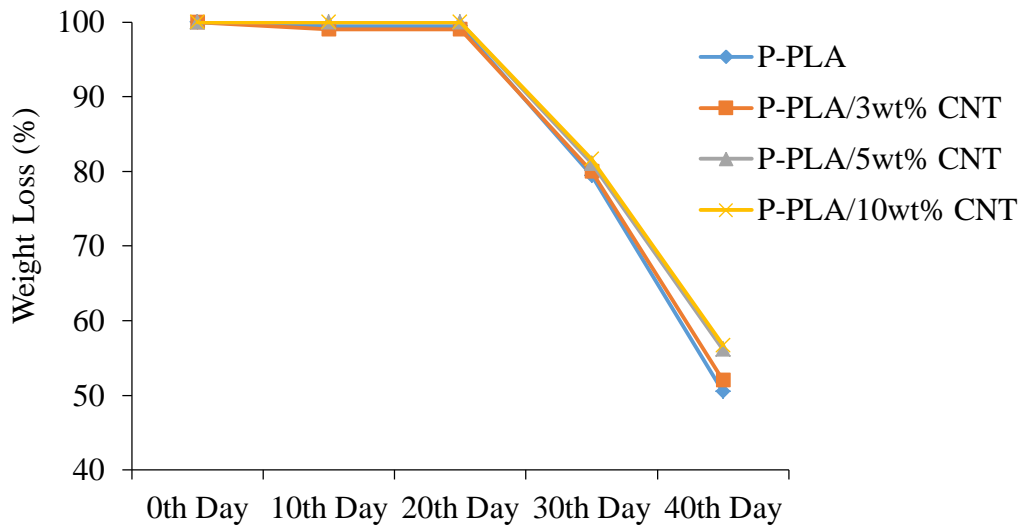


Figure 4.118. Hydrolytic degradation results of P-PLA/CNT composites

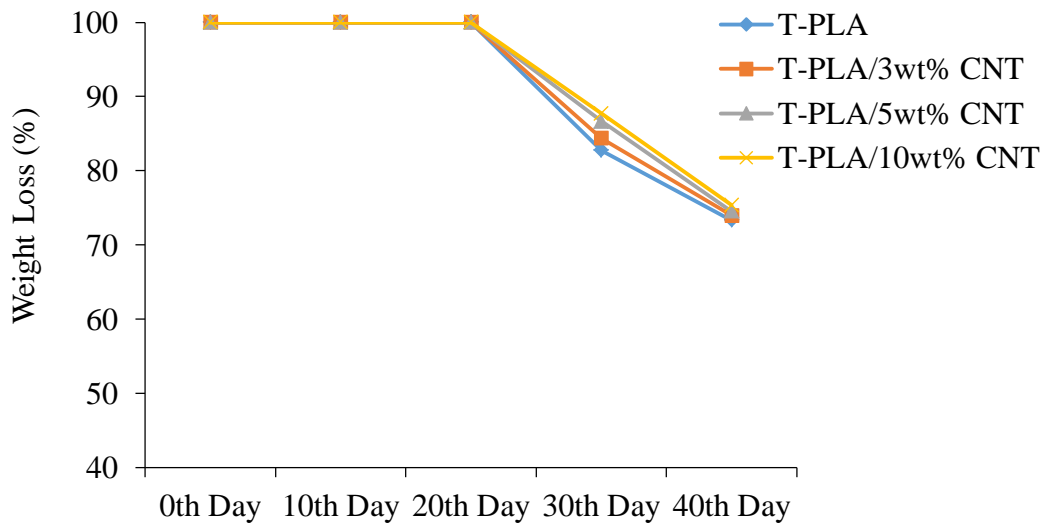


Figure 4.119. Hydrolytic degradation results of T-PLA/CNT composites

CHAPTER 5

CONCLUSIONS

Lower fracture toughness of PLA compared to many petro-chemical polymers restricts its usage area. To secure its foothold, it is desirable to optimize its physical properties. In this study, two types of Halloysite (HNT) were used as the reinforcing agent. The first one is a local mineral and called as ESAN HNT, and the second one is an imported mineral, Nanoclay HNT, used as the reference.

Owing to their unique tubular morphology, and the same chemical structure as that of layered silicates, HNT is an attractive research topic. In the first part of the study, ESAN HNT was characterized and then purified. For characterization, Ethylene Glycol (EG) treatment was performed, and it was concluded that the sample is composed of HNT and does not contain kaolin mineral. For purification, the sample was subjected to sedimentation procedure, XRD and chemical analyses showed that purification had been achieved successfully.

When melt mixing method was applied to PLA/HNT composites, it was seen that the constituents are not compatible and HNT particles form agglomerates in the matrix. Hence, the control factors considered to affect the dispersion state of the nano-fillers were changed and direct melt mixing method have been modified to achieve better mechanical and thermal results. The respective methods are;

- Direct Melt Mixing Method (DM)
 - o 3 minute mixing time (DM3)
 - o 10 minute mixing time (DM10)
- Masterbatch Melt Mixing Method (MMA)

- Solvent Casting Followed by Melt Mixing Method (SC)
- Suspension Addition to Melt Mixing (SA)

According to the results obtained in this part of the study: although there is insignificant interaction between PLA and HNT, they can be designated to be incompatible. In addition, no improvement could be obtained in the physical properties by different melt mixing methods. Owing to its simple, environmental friendly and relatively cheap characteristics DM3 method can be preferred for the composite preparation. There are two more options to provide enhancement in the physical properties. One of these ways is applying pre-treatment to HNT minerals to form a compatible surface with the polymer matrix. The second way is to use a third material which serves as a compatibilizer between PLA and HNT.

The pre-treatments applied to HNT minerals to create a surface interaction between filler and the polymer matrix were:

- Purification of HNT (p-HNT)
- Functionalization of HNT by Grafting with Organo-silane (o-HNT)
- Modification of HNT With Quaternary Salt (m-HNT)
- Evacuation pre-treatment (e-HNT)

Among the pretreatments, only evacuation led to better mechanical and thermal properties compared to those of neat PLA, and according to XRD results only e-HNT mineral showed a good dispersion in the polymer matrix. During this pre-treatment, HNT mineral was subjected to very high vacuum and all the water that had remained between the clay galleries were removed. Hence, it can be said that water layer is the main cause of reduced mechanical properties. In addition to poor distribution and mechanical properties, residual water causes a reduction in the thermal stability of PLA. However, in industrial applications evacuation is hard to achieve due to vacuum application. Hence, the use of third material was investigated.

These types of materials are called compatibilizer, impact modifier or plasticizer depending on intended use. The main aim of these types of materials is to toughen the matrix by preventing crazes from developing into cracks. In addition, they might enhance the compatibility between the matrix and filler to aid the penetration of polymer chains between the silicate layers. In this study two types of materials with different characteristics were used as the impact modifier for PLA; Poly(ethylene glycol) (PEG) and Thermoplastic polyurethane (TPU). The blends are called as:

- PEG plasticized PLA (P-PLA)
- TPU toughened PLA (T-PLA)

Although no significant improvement could be observed with P-PLA blend, addition of HNT was observed to greatly contribute to the elongation at break improvement of T-PLA blend without deteriorating the tensile strength. This was attributed to the relatively better compatibilization effect of TPU and the role of nanotubes to act as bridges between the cracks formed in the interphase between TPU and PLA.

Degradation of biopolymer molecules due to high processing temperatures and water molecules that had remained between the layers of HNT mineral might be the main reason of unimproved mechanical and thermal properties. In order to increase the stability of PLA during the melt extrusion with HNT particles, 1,4-phenylene diisocyanate (PDI) was used as a chain extender. PDI is expected to recover the reduction in the mechanical properties of PLA/HNT composites by providing higher molecular weight and formation of long chain branching. When the effect of chain extender on the properties of PLA and P-PLA composites were investigated, it was observed that PDI has no significant impact on PLA while it gives better properties for P-PLA.

In the last part of the study, the results obtained with HNT were compared with the results obtained by using CNT. The results, showed that HNT is not a compatible mineral with PLA if it does not well dried or compatibilized with a

third material. When all the properties are compared for the two types of fillers, it was observed that CNT can be a choice for PLA matrix instead of HNT mineral. However, for T-PLA, natural HNT is the best so far in terms of higher mechanical and thermal properties.

REFERENCES

- Akkapeddi, M. K., W. E. Baker, G. H. Hu & C. E. Scott. 2001. *Reactive polymer blending*. Munich: Hanser Gardner Publications.
- Alexandre, M. & P. Dubois (2000) Polymer-layered silicate nanocomposites: preparation, properties and uses of a new class of materials. *Materials Science & Engineering R-Reports*, 28, 1-63.
- Amass, W., A. Amass & B. Tighe (1998) A review of biodegradable polymers: Uses, current developments in the synthesis and characterization of biodegradable polyesters, blends of biodegradable polymers and recent advances in biodegradation studies. *Polymer International*, 47, 89-144.
- Aminabhavi, T. M., R. H. Balundgi & P. E. Cassidy (1990) A Review on Biodegradable Plastics. *Polymer-Plastics Technology and Engineering*, 29, 235-262.
- Baiardo, M., G. Frisoni, M. Scandola, M. Rimelen, D. Lips, K. Ruffieux & E. Wintermantel (2003) Thermal and mechanical properties of plasticized poly(L-lactic acid). *Journal of Applied Polymer Science*, 90, 1731-1738.
- Barrientos-Ramirez, S., G. M. de Oca-Ramirez, E. V. Ramos-Fernandez, A. Sepulveda-Escribano, M. M. Pastor-Blas & A. Gonzalez-Montiel (2011) Surface modification of natural halloysite clay nanotubes with aminosilanes. Application as catalyst supports in the atom transfer radical polymerization of methyl methacrylate. *Applied Catalysis a-General*, 406, 22-33.
- Billmeyer, F. W. 1984. *Textbook of polymer science*. New York: John Wiley & Sons.
- Bower, D. I. 2002. *An introduction to polymer physics*. USA: Cambridge University Press.

- Brigatti, M. F., E. Galan & B. K. G. Theng. 2006. Structures and mineralogy of clay minerals. In *Handbook of clay science: Developments in clay science*, eds. F. Bergaya, B. K. G. Theng & G. Lagaly. Amsterdam: Elsevier.
- Brindley, G. W. & J. Goodyear (1948) X-ray studies of halloysite and meta-halloysite, II. The transition of halloysite to meta-halloysite in relation to relative humidity. *Mineralogical Magazine*, 28, 407 - 422.
- Bucknall, C. B. 1977. *Toughened plastics*. London: Applied Science Publishers.
- Byun, Y., S. Whiteside, R. Thomas, M. Dharman, J. Hughes & Y. T. Kim (2012) The effect of solvent mixture on the properties of solvent cast polylactic acid (PLA) film. *Journal of Applied Polymer Science*, 124, 3577-3582.
- Cabedo, L., J. L. Feijoo, M. P. Villanueva, J. M. Lagaron & E. Gimenez (2006) Optimization of biodegradable nanocomposites based on aPLA/PCL blends for food packaging applications. *Macromolecular Symposia*, 233, 191-197.
- Callister, W. D. 1997. *Materials science and engineering: An introduction*. New York: John Wiley and Sons Inc.
- Carli, L. N., J. S. Crespo & R. S. Mauler (2011) PHBV nanocomposites based on organomodified montmorillonite and halloysite: The effect of clay type on the morphology and thermal and mechanical properties. *Composites Part a-Applied Science and Manufacturing*, 42, 1601-1608.
- Carroll, D. (1959) Ion Exchange in Clays and Other Minerals. *Geological Society of America Bulletin*, 70, 749-779.
- Chen B., E. J. R. G., Greenwell H. C., Boulet P., Coveney P. V., Bowdenf A. A., and Whiting A. (2008) A Critical Appraisal of Polymer - Clay Nanocomposites. *Chemical Society Reviews*, 37, 568–594.
- Chiu, W. M., Y. A. Chang, H. Y. Kuo, M. H. Lin & H. C. Wen (2008) A study of carbon nanotubes/biodegradable plastic polylactic acid composites. *Journal of Applied Polymer Science*, 108, 3024-3030.
- Cho, J. W. & D. R. Paul (2001) Nylon 6 nanocomposites by melt compounding. *Polymer*, 42, 1083-1094.

- Chow, W. S., W. L. Tham & P. C. Seow (2013) Effects of maleated-PLA compatibilizer on the properties of poly(lactic acid)/halloysite clay composites. *Journal of Thermoplastic Composite Materials*, 26, 1349-1363.
- Churchman, G. J. (1990) Relevance of Different Intercalation Tests for Distinguishing Halloysite from Kaolinite in Soils. *Clays and Clay Minerals*, 38, 591-599.
- Churchman, G. J. & R. M. Carr (1975) Definition and Nomenclature of Halloysites. *Clays and Clay Minerals*, 23, 382-388.
- Corre, Y. M., J. Duchet, J. Reignier & A. Maazouz (2011) Melt strengthening of poly (lactic acid) through reactive extrusion with epoxy-functionalized chains. *Rheologica Acta*, 50, 613-629.
- Deng, S. Q., J. N. Zhang, L. Ye & J. S. Wu (2008) Toughening epoxies with halloysite nanotubes. *Polymer*, 49, 5119-5127.
- Dennis, H. R., D. L. Hunter, D. Chang, S. Kim, J. L. White, J. W. Cho & D. R. Paul (2001) Effect of melt processing conditions on the extent of exfoliation in organoclay-based nanocomposites. *Polymer*, 42, 9513-9522.
- Dorgan, J. R., H. Lehermeier & M. Mang (2000) Thermal and rheological properties of commercial-grade poly(lactic acid)s. *Journal of Polymers and the Environment*, 8, 1-9.
- Du, M. L., B. C. Guo & D. M. Jia (2006a) Thermal stability and flame retardant effects of halloysite nanotubes on poly(propylene). *European Polymer Journal*, 42, 1362-1369.
- Du, M. L., B. C. Guo & D. M. Jia (2010) Newly emerging applications of halloysite nanotubes: a review. *Polymer International*, 59, 574-582.
- Du, M. L., B. C. Guo, M. X. Liu & D. M. Jia (2006b) Preparation and characterization of polypropylene grafted halloysite and their compatibility effect to polypropylene/halloysite composite. *Polymer Journal*, 38, 1198-1204.

- Ebbesen, T. W. 1997. *Production and Purification of Carbon Nanotubes*, in *Carbon Nanotubes Preparation and Properties*. Boca, Raton: CRC Press.
- Finnigan, B., D. Martin, P. Halley, R. Truss & K. Campbell (2004) Morphology and properties of thermoplastic polyurethane nanocomposites incorporating hydrophilic layered silicates. *Polymer*, 45, 2249-2260.
- Fisher, E. G. 1976. *Extrusion of Plastics*. New York: John Wiley & Sons.
- Fukushima, K., D. Tabuani, C. Abbate, M. Arena & P. Rizzarelli (2011) Preparation, characterization and biodegradation of biopolymer nanocomposites based on fumed silica. *European Polymer Journal*, 47, 139-152.
- Giannelis, E. P. (1999) Polymer-Layered Silicate Nanocomposites: Emerging Scientific and Commercial Opportunities. *Proceedings of 57th SPE Annual Technical Conference (ANTEC)*, 155, 3966-3968.
- Hakkarainen, M. (2002) Aliphatic polyesters: Abiotic and biotic degradation and degradation products. *Degradable Aliphatic Polyesters*, 157, 113-138.
- Halász, K. & L. Csóka (2013) Plasticized biodegradable poly(lactic acid) based composites containing cellulose in micro- and nanosize. *Journal of Engineering*, 2013, 1-9.
- Hapuarachchi, T. D. & T. Peijs (2010) Multiwalled carbon nanotubes and sepiolite nanoclays as flame retardants for polylactide and its natural fibre reinforced composites. *Composites Part A-Applied Science and Manufacturing*, 41, 954-963.
- Hashemifard, S. A., A. F. Ismail & T. Matsuura (2011) Mixed matrix membrane incorporated with large pore size halloysite nanotubes (HNT) as filler for gas separation: Experimental. *Journal of Colloid and Interface Science*, 359, 359-370.
- Hedicke-Hochstotter, K., G. T. Lim & V. Altstadt (2009a) Halloysite nanocomposites: Natural occurring silicate nanotubes as reinforcement in polyamide 6. *Journal of Plastics Technology*, 5, 71 - 86.

- Hedicke-Hochstotter, K., G. T. Lim & V. Altstadt (2009b) Novel polyamide nanocomposites based on silicate nanotubes of the mineral halloysite. *Composites Science and Technology*, 69, 330-334.
- Henton, D. E., P. Gruber, J. Lunt & J. Randall. 2005. Polylactic acid technology. In *Natural fibers, biopolymers, and biocomposites*, eds. A. K. Mohanty, M. Misra & L. T. Drzal. Boca Raton, Florida: CRC Press.
- Hillier, S. & P. C. Ryan (2002) Identification of halloysite (7 angstrom) by ethylene glycol solvation: the 'MacEwan effect'. *Clay Minerals*, 37, 487-496.
- Homminga, D., B. Goderis, S. Hoffman, H. Reynaers & G. Groeninckx (2005) Influence of shear flow on the preparation of polymer layered silicate nanocomposites. *Polymer*, 46, 9941-9954.
- Hong, H. L. & J. X. Mi (2006) Characteristics of halloysite associated with rectorite from Hubei, China. *Mineralogical Magazine*, 70, 257-264.
- Hu, Y., Y. S. Hu, V. Topolkaev, A. Hiltner & E. Baer (2003a) Aging of poly(lactide)/poly(ethylene glycol) blends. Part 2. Poly(lactide) with high stereoregularity. *Polymer*, 44, 5711-5720.
- Hu, Y., Y. S. Hu, V. Topolkaev, A. Hiltner & E. Baer (2003b) Crystallization and phase separation in blends of high stereoregular poly(lactide) with poly(ethylene glycol). *Polymer*, 44, 5681-5689.
- Hu, Y., M. Rogunova, V. Topolkaev, A. Hiltner & E. Baer (2003c) Aging of poly(lactide)/poly(ethylene glycol) blends. Part 1. Poly(lactide) with low stereoregularity. *Polymer*, 44, 5701-5710.
- Huang, L. M., X. D. Cui, B. White & S. P. O'Brien (2004) Long and oriented single-walled carbon nanotubes grown by ethanol chemical vapor deposition. *Journal of Physical Chemistry B*, 108, 16451-16456.
- Immergut, E. H. & H. F. Mark. 1965. Principles of plasticization. In *Plasticization and plasticizer processes*. Washington, D.C.: American Chemical Society.

- Ismail, H., P. Pasbakhsh, M. N. A. Fauzi & A. Abu Bakar (2008) Morphological, thermal and tensile properties of halloysite nanotubes filled ethylene propylene diene monomer (EPDM) nanocomposites. *Polymer Testing*, 27, 841-850.
- Jamshidian, M., E. A. Tehrani, M. Imran, M. Jacquot & S. Desobry (2010) Poly-Lactic Acid: Production, Applications, Nanocomposites, and Release Studies. *Comprehensive Reviews in Food Science and Food Safety*, 9, 552-571.
- Jang, W. Y., B. Y. Shin, T. X. Lee & R. Narayan (2007) Thermal properties and morphology of biodegradable PLA/starch compatibilized blends. *Journal of Industrial and Engineering Chemistry*, 13, 457-464.
- Jia, S., J. Qu, R. Chen, C. Wu, Z. Huang, S. Zhai, W. Liu & Y. Feng (in press) Effects of thermoplastic polyurethane on the properties of poly(lactic acid)/organo-montmorillonite nanocomposites based on novel vane extruder. *Polymer Engineering & Science*.
- Jordan, S. N. & G. J. Mullen (2007) Enzymatic hydrolysis of organic waste materials in a solid-liquid system. *Waste Management*, 27, 1820-1828.
- Joussein, E., S. Petit, J. Churchman, B. Theng, D. Righi & B. Delvaux (2005) Halloysite clay minerals - A review. *Clay Minerals*, 40, 383-426.
- Keller, W. D. & W. D. Johns (1976) Endellite Will Reduce Ambiguity and Confusion in Nomenclature of Halloysite. *Clays and Clay Minerals*, 24, 149-149.
- Kennedy, B. A. 1990. Mine operations. In *Surface mining*, ed. B. A. Kennedy. Society for Mining, Metallurgy, and Exploration.
- Keskkula, H. & D. R. Paul. 1996. Polymer blends. In *Kirk othmer encyclopedia of chemical technology*. John Willey & Sons.
- Kim, S. Y., K. S. Shin, S. H. Lee, K. W. Kim & J. R. Youn (2010) Unique Crystallization Behavior of Multi-Walled Carbon Nanotube Filled Poly(lactic acid). *Fibers and Polymers*, 11, 1018-1023.

- Kodal, M., H. Sirin & G. Ozkoc (2014) Effects of reactive and nonreactive POSS types on the mechanical, thermal, and morphological properties of plasticized poly(lactic acid). *Polymer Engineering and Science*, 54, 264-275.
- Kolybaba, M., L. G. Tabil, S. Panigrahi, W. J. Crerar, T. Powell & B. Wang (2003) Biodegradable polymers: past, present, and future. *CSAE/ASAE Annual Intersectional Meeting*, 3 - 7.
- Kornmann, X., H. Lindberg & L. A. Berglund (2001) Synthesis of epoxy-clay nanocomposites: influence of the nature of the clay on structure. *Polymer*, 42, 1303-1310.
- Kramer, E. J. & H. H. Krauch. 1983. *Crazing in polymers*. Berlin: Springer.
- Krishnamoorti, R., Vaia R.A, and Giannelis E.P. (1996) Structure and Dynamics of Polymer-Layered Silicate Nanocomposites. *Chemistry of Materials*, 8, 1728-1734.
- Kroschwitz, J. I. 1990. *Concise Encyclopedia of Polymer Science and Engineering*. New York: John Wiley and Sons.
- Krul, L. P., A. I. Volozhyn, D. A. Belov, N. A. Poloiko, A. S. Artushkevich, S. A. Zhdanok, A. P. Solntsev, A. V. Krauklis & I. A. Zhukova (2007) Nanocomposites based on poly-D,L-lactide and multiwall carbon nanotubes. *Biomolecular Engineering*, 24, 93-95.
- Kuan, C. F., H. C. Kuan, C. C. M. Ma & C. H. Chen (2008) Mechanical and electrical properties of multi-wall carbon nanotube/poly(lactic acid) composites. *Journal of Physics and Chemistry of Solids*, 69, 1395-1398.
- Kulinski, Z. & E. Piorkowska (2005) Crystallization, structure and properties of plasticized poly(L-lactide). *Polymer*, 46, 10290-10300.
- Lagaly, G. 2006. Colloid Clay Science. In *Handbook of Clay Science: Developments in Clay Science*, eds. F. Bergaya, B. K. G. Theng & G. Lagaly. Amsterdam: Elsevier.

- Lai, S. M. & Y. C. Lan (2013) Shape memory properties of melt-blended polylactic acid (PLA)/thermoplastic polyurethane (TPU) bio-based blends. *Journal of Polymer Research*, 20.
- Lecouvet, B., J. G. Gutierrez, M. Sclavons & C. Bailly (2011) Structure-property relationships in polyamide 12/halloysite nanotube nanocomposites. *Polymer Degradation and Stability*, 96, 226-235.
- Leng, J., S. Du & H. Lu. 2010. Multifunctional shape-memory polymers and actuation methods. In *Shape-memory polymers and multifunctional composites*, eds. J. Leng & S. Du. Boca Raton, Florida: CRC Press.
- Lewitus, D., S. McCarthy, A. Ophir & S. Kenig (2006) The effect of nanoclays on the properties of PLLA-modified polymers part 1: Mechanical and thermal properties. *Journal of Polymers and the Environment*, 14, 171-177.
- Li, Q. H., Q. H. Zhou, D. Deng, Q. Z. Yu, L. Gu, K. D. Gong & K. H. Xu (2013) Enhanced thermal and electrical properties of poly (D,L-lactide)/multi-walled carbon nanotubes composites by in-situ polymerization. *Transactions of Nonferrous Metals Society of China*, 23, 1421-1427.
- Liu, C., Y. F. Luo, Z. X. Jia, B. C. Zhong, S. Q. Li, B. C. Guo & D. M. Jia (2011) Enhancement of mechanical properties of poly(vinyl chloride) with polymethyl methacrylate-grafted halloysite nanotube. *Express Polymer Letters*, 5, 591-603.
- Liu, M. X., B. C. Guo, M. L. Du, Y. D. Lei & D. M. Jia (2008) Natural inorganic nanotubes reinforced epoxy resin nanocomposites. *Journal of Polymer Research*, 15, 205-212.
- Liu, M. X., Y. Zhang & C. R. Zhou (2013) Nanocomposites of halloysite and polylactide. *Applied Clay Science*, 75-76, 52-59.
- Macewan, D. M. C. (1946) Halloysite-Organic Complexes. *Nature*, 157, 159-160.
- Macewan, D. M. C. (1948) Complexes of Clays with Organic Compounds .1. Complex Formation between Montmorillonite and Halloysite and Certain Organic Liquids. *Transactions of the Faraday Society*, 44, 349-367.

- Maldanis, R. (2009) Eco-friendly requirements in the automotive industry create growth opportunity for recycling technology innovators / end-of-life vehicles (ELV) directive 2000/53/EC. *Industry & Innovation Marketplace Review*.
- Mark, H. F. & J. I. Kroschwitz. 2003. *Encyclopedia of Polymer Science and Technology*. Hoboken, NJ: Wiley-Interscience.
- Marney, D. C. O., L. J. Russell, D. Y. Wu, T. Nguyen, D. Cramm, N. Rigopoulos, N. Wright & M. Greaves (2008) The suitability of halloysite nanotubes as a fire retardant for nylon 6. *Polymer Degradation and Stability*, 93, 1971-1978.
- Martin, O. & L. Averous (2001) Poly(lactic acid): plasticization and properties of biodegradable multiphase systems. *Polymer*, 42, 6209-6219.
- Matusik, J., E. Stodolak & K. Bahranowski (2011) Synthesis of polylactide/clay composites using structurally different kaolinites and kaolinite nanotubes. *Applied Clay Science*, 51, 102-109.
- Meng, Q. K., M. C. Heuzey & P. J. Carreau (2012) Control of thermal degradation of polylactide/clay nanocomposites during melt processing by chain extension reaction. *Polymer Degradation and Stability*, 97, 2010-2020.
- Mi, H. Y., M. R. Salick, X. Jing, B. R. Jacques, W. C. Crone, X. F. Peng & L. S. Turng (2013) Characterization of thermoplastic polyurethane/polylactic acid (TPU/PLA) tissue engineering scaffolds fabricated by microcellular injection molding. *Materials Science & Engineering C-Materials for Biological Applications*, 33, 4767-4776.
- Middleman, S. 1977. *Fundamentals of Polymer Processing*. New York: McGraw-Hill.
- Mohanty, A. K., L. T. Drzal & M. Misra (2003) Nano reinforcements of bio-based polymers - The hope and the reality. *Abstracts of Papers of the American Chemical Society*, 225, U665-U665.

- Mohapatra, A. K., S. Mohanty & S. K. Nayak (2014) Effect of PEG on PLA/PEG Blend and Its Nanocomposites: A Study of Thermo-Mechanical and Morphological Characterization. *Polymer Composites*, 35, 283-293.
- Murariu, M., A. L. Dechief, Y. Paint, S. Peeterbroeck, L. Bonnaud & P. Dubois (2012) Polylactide (PLA)-Halloysite Nanocomposites: Production, Morphology and Key-Properties. *Journal of Polymers and the Environment*, 20, 932-943.
- Najafi, N., M. C. Heuzey & P. J. Carreau (2012a) Polylactide (PLA)-clay nanocomposites prepared by melt compounding in the presence of a chain extender. *Composites Science and Technology*, 72, 608-615.
- Najafi, N., M. C. Heuzey, P. J. Carreau & P. M. Wood-Adams (2012b) Control of thermal degradation of polylactide (PLA)-clay nanocomposites using chain extenders. *Polymer Degradation and Stability*, 97, 554-565.
- Ndazi, B. S. & S. Karlsson (2011) Characterization of hydrolytic degradation of polylactic acid/rice hulls composites in water at different temperatures. *Express Polymer Letters*, 5, 119-131.
- Nielsen, L. & R. Landel. 1993. *Mechanical properties of polymers and composites*. USA: Marcel Dekker.
- Nielsen, L. E. 1962. *Mechanical Properties of Polymers*. New York: Reinhold.
- Ning, N. Y., Q. J. Yin, F. Luo, Q. Zhang, R. Du & Q. Fu (2007) Crystallization behavior and mechanical properties of polypropylene/halloy site composites. *Polymer*, 48, 7374-7384.
- Ogawa, M., and Kuroda K. (1997) Preparation of inorganic-organic nanocomposites through intercalation of organoammonium ions into layered silicates. *Bulletin of the Chemical Society of Japan* 70, 2593-2618.
- Ozkoc, G., G. Bayram & M. Quaedflieg (2008) Effects of microcompounding process parameters on the properties of ABS/polyamide-6 blends based nanocomposites. *Journal of Applied Polymer Science*, 107, 3058-3070.

- Ozkoc, G. & S. Kemaloglu (2009) Morphology, biodegradability, mechanical, and thermal properties of nanocomposite films based on PLA and plasticized PLA. *Journal of Applied Polymer Science*, 114, 2481-2487.
- Pasbakhsh, P., H. Ismail, M. N. A. Fauzi & A. Abu Bakar (2009) Influence of maleic anhydride grafted ethylene propylene diene monomer (MAH-g-EPDM) on the properties of EPDM nanocomposites reinforced by halloysite nanotubes. *Polymer Testing*, 28, 548-559.
- Pasbakhsh, P., H. Ismail, M. N. A. Fauzi & A. Abu Bakar (2010) EPDM/modified halloysite nanocomposites. *Applied Clay Science*, 48, 405-413.
- Paul, M. A., M. Alexandre, P. Degee, C. Henrist, A. Rulmont & P. Dubois (2003) New nanocomposite materials based on plasticized poly(L-lactide) and organo-modified montmorillonites: thermal and morphological study. *Polymer*, 44, 443-450.
- Paul, M. A., C. Delcourt, M. Alexandre, P. Degee, F. Monteverde & P. Dubois (2005) Polylactide/montmorillonite nanocomposites: study of the hydrolytic degradation. *Polymer Degradation and Stability*, 87, 535-542.
- Pavlidou, S. & C. D. Papaspyrides (2008) A review on polymer-layered silicate nanocomposites. *Progress in Polymer Science*, 33, 1119-1198.
- Pethrick, R. A. 2000. Polymer-Clay Nanocomposites. eds. T. J. Pinnavaia & G. W. Beall. UK: John Wiley&Sons.
- Pilla, S., A. Kramschuster, L. Q. Yang, J. Lee, S. Q. Gong & L. S. Turng (2009) Microcellular injection-molding of polylactide with chain-extender. *Materials Science & Engineering C-Biomimetic and Supramolecular Systems*, 29, 1258-1265.
- Pillin, I., N. Montrelay & Y. Grohens (2006) Thermo-mechanical characterization of plasticized PLA: Is the miscibility the only significant factor? *Polymer*, 47, 4676-4682.
- Ping, P., W. S. Wang, P. B. Zhang, X. S. Chen & X. B. Jing (2007) Shape-memory and biocompatibility properties of segmented polyurethanes

- based on poly(L-lactide). *Chemical Journal of Chinese Universities-Chinese*, 28, 371-375.
- Pinnavaia, T. J. & G. W. Beall. 2000. *Polymer-clay nanocomposites*. England: John Wiley & Sons.
- Pluta, M. & A. Galeski (2002) Crystalline and supermolecular structure of polylactide in relation to the crystallization method. *Journal of Applied Polymer Science*, 86, 1386-1395.
- Pluta, M., A. Galeski, M. Alexandre, M. A. Paul & P. Dubois (2002) Polylactide/montmorillonite nanocomposites and microcomposites prepared by melt blending: Structure and some physical properties. *Journal of Applied Polymer Science*, 86, 1497-1506.
- Pluta, M., M. A. Paul, M. Alexandre & P. Dubois (2006a) Plasticized polylactide/clay nanocomposites. I. The role of filler content and its surface organo-modification on the physico-chemical properties. *Journal of Polymer Science Part B-Polymer Physics*, 44, 299-311.
- Pluta, M., M. A. Paul, M. Alexandre & P. Dubois (2006b) Plasticized polylactide/clay nanocomposites. II. The effect of aging on structure and properties in relation to the filler content and the nature of its organo-modification. *Journal of Polymer Science Part B-Polymer Physics*, 44, 312-325.
- Prashantha, K., B. Lecouvet, M. Sclavons, M. F. Lacrampe & P. Krawczak (2013) Poly(lactic acid)/halloysite nanotubes nanocomposites: Structure, thermal, and mechanical properties as a function of halloysite treatment. *Journal of Applied Polymer Science*, 128, 1895-1903.
- Prashantha, K., J. Soulestin, M. F. Lacrampe, P. Krawczak, G. Dupin & M. Claes (2009) Masterbatch-based multi-walled carbon nanotube filled polypropylene nanocomposites: Assessment of rheological and mechanical properties. *Composites Science and Technology*, 69, 1756-1763.

- Qi, R. L., R. Guo, M. W. Shen, X. Y. Cao, L. Q. Zhang, J. J. Xu, J. Y. Yu & X. Y. Shi (2010) Electrospun poly(lactic-co-glycolic acid)/halloysite nanotube composite nanofibers for drug encapsulation and sustained release. *Journal of Materials Chemistry*, 20, 10622-10629.
- Rauwendaal, C. 1990. *Polymer Extrusion*. New York: Hanser Gardner Publications.
- Ray, S. S. & M. Bousmina (2005) Biodegradable polymers and their layered silicate nano composites: In greening the 21st century materials world. *Progress in Materials Science*, 50, 962-1079.
- Ray, S. S., P. Maiti, M. Okamoto, K. Yamada & K. Ueda (2002a) New polylactide/layered silicate nanocomposites. 1. Preparation, characterization, and properties. *Macromolecules*, 35, 3104-3110.
- Ray, S. S. & M. Okamoto (2003) New polylactide/layered silicate nanocomposites, 6 - Melt rheology and foam processing. *Macromolecular Materials and Engineering*, 288, 936-944.
- Ray, S. S., K. Yamada, M. Okamoto, Y. Fujimoto, A. Ogami & K. Ueda (2003a) New polylactide/layered silicate nanocomposites. 5. Designing of materials with desired properties. *Polymer*, 44, 6633-6646.
- Ray, S. S., K. Yamada, M. Okamoto & K. Ueda (2002b) Polylactide-layered silicate nanocomposite: A novel biodegradable material. *Nano Letters*, 2, 1093-1096.
- Ray, S. S., K. Yamada, M. Okamoto & K. Ueda (2003b) New polylactide-layered silicate nanocomposites. 2. Concurrent improvements of material properties, biodegradability and melt rheology. *Polymer*, 44, 857-866.
- Ren, J. 2010. *Biodegradable poly(lactic acid); Synthesis, modification, processing and application*. Beijing: Tsinghua University Press.
- Roy, P. K., M. Hakkarainen & A. C. Albertsson (2012) Nanoclay effects on the degradation process and product patterns of polylactide. *Polymer Degradation and Stability*, 97, 1254-1260.

- Schey, J. A. 1987. *Introduction to Manufacturing Processes*. New York: McGraw Hill.
- Seyidoglu, T. & U. Yilmazer (2012) Use of purified and modified bentonites in linear low-density polyethylene/organoclay/compatibilizer nanocomposites. *Journal of Applied Polymer Science*, 124, 2430-2440.
- Seyidoglu, T. & U. Yilmazer (2013) Production of modified clays and their use in polypropylene-based nanocomposites. *Journal of Applied Polymer Science*, 127, 1257-1267.
- Seymour, R. B. 1996. *Polymer Chemistry: An Introduction*. New York: Marrel Dekker.
- Song, S. X., Y. M. Zhang, T. Liu & M. Zhang (2005) Beneficiation of montmorillonite from ores by dispersion processing. *Journal of Dispersion Science and Technology*, 26, 375-379.
- Sperling, L. 2006. *Introduction to physical polymer science*. Hoboken, New Jersey: John Wiley & Sons Inc.
- Strong, A. B. 2000. *Plastics, Materials & Processing*. New York: Prentice Hall.
- Tanoue, S., A. Hasook, Y. Iemoto & T. Unryu (2006) Preparation of poly(lactic acid)/poly(ethylene glycol)/organoclay nanocomposites by melt compounding. *Polymer Composites*, 27, 256-263.
- Theng, B. K. G. 1974. *The Chemistry of Clay-Organic Reactions*. New York: John Wiley & Sons.
- Ting, S. P., E. M. Pearce & T. K. Kwei (1980) Compatibility Studies of Poly(Styrene-Co-Vinylphenyl Hexafluorodimethyl Carbinol) with Bisphenol a Polycarbonate, Poly(Butyl Methacrylate), and Poly(2,6-Dimethyl-1,4-Phenylene Oxide). *Journal of Polymer Science Part C-Polymer Letters*, 18, 201-209.
- Tjong, S. C. (2006) Structural and mechanical properties of polymer nanocomposites. *Materials Science & Engineering R-Reports*, 53, 73-197.

- Touny, A. H., J. G. Lawrence, A. D. Jones & S. B. Bhaduri (2010) Effect of electrospinning parameters on the characterization of PLA/HNT nanocomposite fibers. *Journal of Materials Research*, 25, 857-865.
- Usuki, A., A. Koiwai, Y. Kojima, M. Kawasumi, A. Okada, T. Kurauchi & O. Kamigaito (1995) Interaction of Nylon-6 Clay Surface and Mechanical-Properties of Nylon-6 Clay Hybrid. *Journal of Applied Polymer Science*, 55, 119-123.
- Utracki, L. A. 2002. Introduction to polymer blends. In *Polymer blends handbook*, ed. L. A. Utracki. The Netherlands: Kluwer Academic Publishers
- Vable, M. 2009. Mechanical properties of materials. In *Mechanics of materials*, ed. M. Vable. Online Book
- Vaia, R. A., H. Ishii & E. P. Giannelis (1993) Synthesis and Properties of 2-Dimensional Nanostructures by Direct Intercalation of Polymer Melts in Layered Silicates. *Chemistry of Materials*, 5, 1694-1696.
- Vaia, R. A., K. D. Jandt, E. J. Kramer & E. P. Giannelis (1995) Kinetics of Polymer Melt Intercalation. *Macromolecules*, 28, 8080-8085.
- Vansant, E. F., P. Van Der Voort & K. C. Vrancken. 1995. *Characterization and chemical modification of the silica surface*. New York: Elsevier.
- Verhoogt, H., C. R. J. Willems, J. Vandam & A. P. Deboer (1994) Blends of a Thermotropic LCP and a Thermoplastic Elastomer .2. Formation and Stability of Lcp Fibers. *Polymer Engineering and Science*, 34, 453-460.
- Vroman, I. & L. Tighzert (2009) Biodegradable Polymers. *Materials*, 2, 307-344.
- Wan, C. Y., M. Li, X. Bai & Y. Zhang (2009) Synthesis and Characterization of Photoluminescent Eu(III) Coordination Halloysite Nanotube-Based Nanohybrids. *Journal of Physical Chemistry C*, 113, 16238-16246.
- Wang, L. P., Y. P. Wang, X. W. Pei & B. Peng (2008) Synthesis of poly(methyl methacrylate)-b-poly(N-isopropylacrylamide) (PMMA-b-PNIPAM) amphiphilic, diblock copolymer brushes on halloysite substrate via reverse ATRP. *Reactive & Functional Polymers*, 68, 649-655.

- Wilkinson, A. N., Z. Man, J. L. Stanford, P. Matikainen, M. L. Clemens, G. C. Lees & C. M. Liauw (2006) Structure and dynamic mechanical properties of melt intercalated polyamide 6 - Montmorillonite nanocomposites. *Macromolecular Materials and Engineering*, 291, 917-928.
- Wool, R. & S. Sun. 2005. *Bio-based polymers and composites*. USA: Elsevier Academic Press
- Wu, D. F., L. Wu, M. Zhang & Y. L. Zhao (2008) Viscoelasticity and thermal stability of polylactide composites with various functionalized carbon nanotubes. *Polymer Degradation and Stability*, 93, 1577-1584.
- Wu, S. H. (1985) Phase-Structure and Adhesion in Polymer Blends - a Criterion for Rubber Toughening. *Polymer*, 26, 1855-1863.
- Xanthos, M. 2005. *Functional fillers for plastics*. Germany: Wiley-VCH.
- Yao, Z., C. L. Kane & C. Dekker (2000) High-field electrical transport in single-wall carbon nanotubes. *Physical Review Letters*, 84, 2941-2944.
- Yasuniwa, M., K. Sakamo, Y. Ono & W. Kawahara (2008) Melting behavior of poly(L-lactic acid): X-ray and DSC analyses of the melting process. *Polymer*, 49, 1943-1951.
- Yasuniwa, M., S. Tsubakihara, K. Iura, Y. Ono, Y. Dan & K. Takahashi (2006) Crystallization behavior of poly(L-lactic acid). *Polymer*, 47, 7554-7563.
- Ye, Y. P., H. B. Chen, J. S. Wu & L. Ye (2007) High impact strength epoxy nanocomposites with natural nanotubes. *Polymer*, 48, 6426-6433.
- Yeniova, C. E. & U. Yilmazer (2013) Effect of different types of organoclays and compatibilizers on the properties of polystyrene-based nanocomposites. *Journal of Applied Polymer Science*, 127, 3673-3680.
- Yesil, S. (2013) Effect of carbon nanotube reinforcement on the properties of the recycled poly(ethylene terephthalate)/poly(ethylene naphthalate) (r-PET/PEN) blends containing functional elastomers. *Materials & Design*, 52, 693-705.
- Yuan, P., P. D. Southon, Z. W. Liu, M. E. R. Green, J. M. Hook, S. J. Antill & C. J. Kepert (2008) Functionalization of halloysite clay nanotubes by grafting

- with gamma-aminopropyltriethoxysilane. *Journal of Physical Chemistry C*, 112, 15742-15751.
- Zanetti, M., S. Lomakin & G. Camino (2000) Polymer layered silicate nanocomposites. *Macromolecular Materials and Engineering*, 279, 1-9.
- Zanetti, M., Lomakin S., and Camino G. (2000) Polymer-Layered Silicate Nanocomposites. *Macromolecular Materials and Engineering*, 279, 1-9.
- Zhang, X. Q., M. Espiritu, A. Bilyk & L. Kurniawan (2008) Morphological behaviour of poly(lactic acid) during hydrolytic degradation. *Polymer Degradation and Stability*, 93, 1964-1970.
- Zhang, Y. W., J. Q. Jiang, Q. H. Liang & B. Zhang (2010) Modification of Halloysite Nanotubes with Poly(styrene-butyl acrylate-acrylic acid) via In Situ Soap-Free Graft Polymerization. *Journal of Applied Polymer Science*, 117, 3054-3059.
- Zhao, M. & P. Liu (2008) Halloysite Nanotubes/Polystyrene (Hnts/Ps) Nanocomposites Via in Situ Bulk Polymerization. *Journal of Thermal Analysis and Calorimetry*, 94, 103-107.
- Zhou, Q. & M. Xanthos (2008) Nanoclay and crystallinity effects on the hydrolytic degradation of polylactides. *Polymer Degradation and Stability*, 93, 1450-1459.

APPENDIX A

TGA RESULTS OF PLA/HNT COMPOSITES

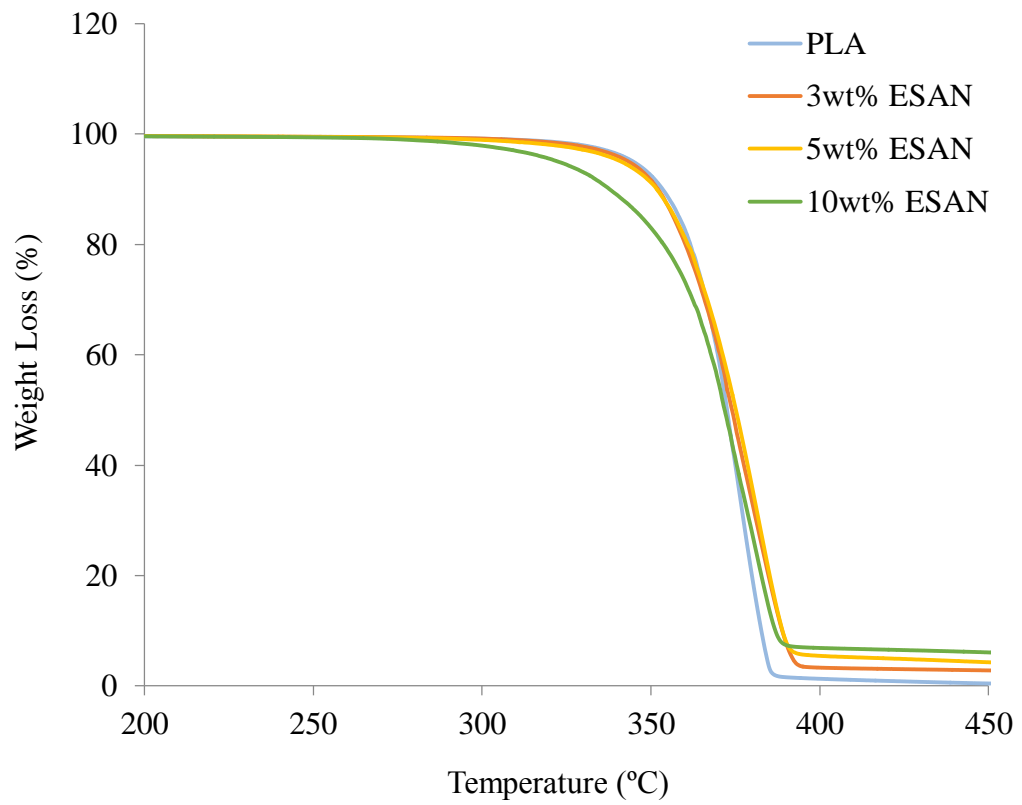


Figure A. 1 TGA spectrums of PLA/ESAN HNT composites prepared by DM3 method

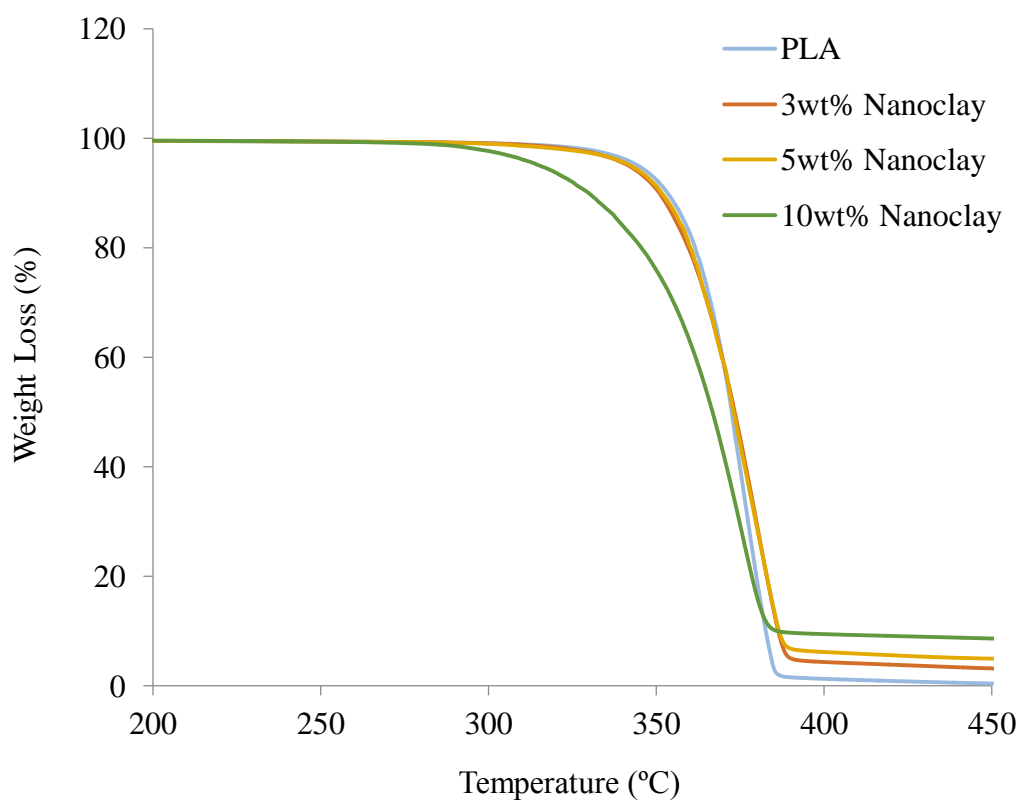


Figure A. 2 TGA spectrums of PLA/Nanoclay HNT composites prepared by DM3 method

Table A.1. TGA data of PLA/HNT composites prepared by DM3 method

	5wt% Loss Temperature (°C)	5wt% Loss Temperature (°C)	Temperature at max. rate of weight loss (from d-TG)
PLA (processed)	345	353	376
PLA/3wt%ESAN	343	352	379
PLA/5wt%ESAN	341	352	378
PLA/10wt%ESAN	322	337	378
PLA/3wt% Nanoclay	342	351	379
PLA/5wt% Nanoclay	342	351	378
PLA/10wt% Nanoclay	315	330	376

APPENDIX B

MECHANICAL TEST RESULTS

Table B.1. Tensile strength results (MPa)

Sample	Filler (wt%)	Tensile Strength (MPa)	Standard Deviation
PLA	---	63.5	0.16
PLA/ESAN HNT (DM3)	3	59.5	0.48
PLA/ESAN HNT (DM3)	5	59.5	0.14
PLA/ESAN HNT (DM3)	10	57.0	0.34
PLA/Nanoclay HNT (DM3)	3	61.8	0.25
PLA/Nanoclay HNT (DM3)	5	63.0	0.17
PLA/Nanoclay HNT (DM3)	10	59.4	0.14
PLA/ESAN HNT (DM10)	3	61.1	0.01
PLA/ESAN HNT (DM10)	5	63.3	0.65
PLA/ESAN HNT (DM10)	10	57.6	0.24
PLA/Nanoclay HNT (DM10)	3	62.3	0.12
PLA/Nanoclay HNT (DM10)	5	63.0	0.27
PLA/Nanoclay HNT (DM10)	10	61.8	0.18
PLA/ESAN HNT (MMA)	3	62.6	0.08
PLA/ESAN HNT (MMA)	5	59.7	0.01
PLA/ESAN HNT (MMA)	10	59.5	0.16
PLA/Nanoclay HNT (MMA)	3	61.6	0.30
PLA/Nanoclay HNT (MMA)	5	62.1	0.30
PLA/Nanoclay HNT (MMA)	10	61.7	0.05

Table B.1. (continued) Tensile strength results (MPa)

Sample	Filler (wt%)	Tensile Strength (MPa)	Standard Deviation
PLA/ESAN HNT (SC)	3	61.3	0.03
PLA/ESAN HNT (SC)	5	62.1	0.50
PLA/ESAN HNT (SC)	10	60.0	0.40
PLA/Nanoclay HNT (SC)	3	62.5	0.40
PLA/Nanoclay HNT (SC)	5	61.9	0.60
PLA/Nanoclay HNT (SC)	10	60.8	0.05
PLA/ESAN HNT (SA)	3	57.2	0.05
PLA/ESAN HNT (SA)	5	58.1	0.50
PLA/ESAN HNT (SA)	10	56.3	0.10
PLA/Nanoclay HNT (SA)	3	58.0	0.20
PLA/Nanoclay HNT (SA)	5	58.7	0.30
PLA/Nanoclay HNT (SA)	10	57.5	0.40
PLA/p-HNT	5	59.0	0.34
PLA/o-HNT	5	64.4	0.41
PLA/m-HNT	5	64.4	0.26
PLA/e-HNT	5	66.7	0.02
PLA/PEG	---	32.7	0.03
PLA/PEG/ESAN HNT	3	30.4	0.08
PLA/PEG/ESAN HNT	5	32.4	0.16
PLA/PEG/ESAN HNT	10	33.1	0.42
PLA/PEG/Nanoclay HNT	3	32.7	0.03
PLA/PEG/Nanoclay HNT	5	30.8	0.06
PLA/PEG/Nanoclay HNT	10	31.9	0.76
PLA/TPU	---	39.4	0.43

Table B.1. (continued). Tensile strength results (MPa)

Sample	Filler (wt%)	Tensile Strength (MPa)	Standard Deviation
PLA/TPU/ESAN HNT	3	39.4	0.37
PLA/TPU/ESAN HNT	5	40.1	0.39
PLA/TPU/ESAN HNT	10	39.5	0.01
PLA/TPU/Nanoclay HNT	3	39.4	0.43
PLA/TPU/Nanoclay HNT	5	40.2	0.79
PLA/TPU/Nanoclay HNT	10	40.7	0.82
PLA/PDI	---	64.7	0.13
PLA/PDI/ESAN HNT	5	57.1	0.18
PLA/PDI/Nanoclay HNT	5	60.8	0.23
PLA/PDI/PEG	---	45.7	0.19
PLA/PDI/PEG/ESAN HNT	5	37.0	0.31
PLA/PDI/PEG/Nanoclay HNT	5	42.6	0.27
PLA/CNT	3	67.0	0.31
PLA/CNT	5	70.5	0.14
PLA/CNT	10	70.6	0.22
PLA/PEG/CNT	3	28.8	2.07
PLA/PEG/CNT	5	26.1	0.62
PLA/PEG/CNT	10	21.6	0.02
PLA/TPU/CNT	3	43.4	0.61
PLA/TPU/CNT	5	43.3	0.45
PLA/TPU/CNT	10	46.0	0.00

Table B.2. Elongation at break results

Sample	Filler (wt%)	Strain at Break	Standard Deviation
PLA	---	0.16	0.0026
PLA/ESAN HNT (DM3)	3	0.18	0.0050
PLA/ESAN HNT (DM3)	5	0.18	0.0020
PLA/ESAN HNT (DM3)	10	0.17	0.0024
PLA/Nanoclay HNT (DM3)	3	0.19	0.0039
PLA/Nanoclay HNT (DM3)	5	0.20	0.0060
PLA/Nanoclay HNT (DM3)	10	0.16	0.0000
PLA/ESAN HNT (DM10)	3	0.16	0.0037
PLA/ESAN HNT (DM10)	5	0.16	0.0026
PLA/ESAN HNT (DM10)	10	0.14	0.0027
PLA/Nanoclay HNT (DM10)	3	0.16	0.0023
PLA/Nanoclay HNT (DM10)	5	0.15	0.0016
PLA/Nanoclay HNT (DM10)	10	0.20	0.0103
PLA/ESAN HNT (MMA)	3	0.18	0.0102
PLA/ESAN HNT (MMA)	5	0.20	0.0041
PLA/ESAN HNT (MMA)	10	0.20	0.0057
PLA/Nanoclay HNT (MMA)	3	0.22	0.0037
PLA/Nanoclay HNT (MMA)	5	0.23	0.0077
PLA/Nanoclay HNT (MMA)	10	0.20	0.0084
PLA/ESAN HNT (SC)	3	0.22	0.0037
PLA/ESAN HNT (SC)	5	0.23	0.0026
PLA/ESAN HNT (SC)	10	0.22	0.0024
PLA/Nanoclay HNT (SC)	3	0.24	0.0023
PLA/Nanoclay HNT (SC)	5	0.25	0.0060
PLA/Nanoclay HNT (SC)	10	0.23	0.0103

Table B.2. (cont'd) Elongation at break results

Sample	Filler (wt%)	Strain at Break	Standard Deviation
PLA/ESAN HNT (SA)	3	0.25	0.0102
PLA/ESAN HNT (SA)	5	0.27	0.0041
PLA/ESAN HNT (SA)	10	0.24	0.0027
PLA/Nanoclay HNT (SA)	3	0.26	0.0037
PLA/Nanoclay HNT (SA)	5	0.28	0.0016
PLA/Nanoclay HNT (SA)	10	0.26	0.0084
PLA/p-HNT	5	0.14	0.0012
PLA/o-HNT	5	0.15	0.0074
PLA/m-HNT	5	0.16	0.0015
PLA/e-HNT	5	0.14	0.0011
PLA/PEG	---	3.46	0.0610
PLA/PEG/ESAN HNT	3	3.56	0.0429
PLA/PEG/ESAN HNT	5	3.56	0.0105
PLA/PEG/ESAN HNT	10	3.41	0.0341
PLA/PEG/Nanoclay HNT	3	3.58	0.0273
PLA/PEG/Nanoclay HNT	5	3.80	0.0091
PLA/PEG/Nanoclay HNT	10	3.70	0.0097
PLA/TPU	---	0.30	0.0300
PLA/TPU/ESAN HNT	3	0.36	0.0005
PLA/TPU/ESAN HNT	5	0.48	0.0180
PLA/TPU/ESAN HNT	10	1.78	0.0324
PLA/TPU/Nanoclay HNT	3	0.35	0.0025
PLA/TPU/Nanoclay HNT	5	0.55	0.0205
PLA/TPU/Nanoclay HNT	10	2.08	0.0025

Table B.2. (cont'd) Elongation at break results

Sample	Filler (wt%)	Strain at Break	Standard Deviation
PLA/PDI	---	0.17	0.0071
PLA/PDI/ESAN HNT	5	0.16	0.0011
PLA/PDI/Nanoclay HNT	5	0.18	0.0119
PLA/PDI/PEG	---	4.07	0.0849
PLA/PDI/PEG/ESAN HNT	5	3.34	0.0942
PLA/PDI/PEG/Nanoclay HNT	5	3.27	0.0226
PLA/CNT	3	0.11	0.0022
PLA/CNT	5	0.11	0.0019
PLA/CNT	10	0.11	0.0020
PLA/PEG/CNT	3	2.33	0.0525
PLA/PEG/CNT	5	2.44	0.0758
PLA/PEG/CNT	10	1.49	0.0250
PLA/TPU/CNT	3	0.36	0.0191
PLA/TPU/CNT	5	0.28	0.0130
PLA/TPU/CNT	10	0.28	0.0130

Table B.3. Impact strength (kJ/m²) results

Sample	Filler (wt%)	Strain at Break	Standard Deviation
PLA	---	12.26	0.071
PLA/ESAN HNT	3	12.51	0.106
PLA/Nanoclay HNT	3	12.90	0.360
PLA/ESAN HNT	5	12.81	0.267
PLA/Nanoclay HNT	5	12.81	0.306
PLA/ESAN HNT	10	10.69	0.234
PLA/Nanoclay HNT	10	11.02	0.292
PLA/p-HNT	5	12.7	0.2
PLA/o-HNT	5	12.3	0.15
PLA/m-HNT	5	12.5	0.3
PLA/e-HNT	5	12.1	0.2
PLA/TPU	---	23.56	0.628
PLA/TPU/ESAN HNT	3	25.10	0.534
PLA/TPU/ESAN HNT	5	26.97	0.244
PLA/TPU/ESAN HNT	10	31.07	0.623
PLA/TPU/Nanoclay HNT	3	24.79	0.263
PLA/TPU/Nanoclay HNT	5	27.20	0.180
PLA/TPU/Nanoclay HNT	10	32.35	0.499
PLA/CNT	3	8.74	0.288
PLA/CNT	5	7.58	0.195
PLA/CNT	10	6.74	0.078
PLA/TPU/CNT	3	23.26	0.396
PLA/TPU/CNT	5	21.52	0.366
PLA/TPU/CNT	10	12.78	0.018

CURRICULUM VITAE

PERSONAL INFORMATION

Surname, Name: Yeniova Erpek, Canan Esma

Nationality: Turkish (TC)

Date and Place of Birth: 03.08.1983 / Edmonton – CANADA

e-mail: cananyeniova@gmail.com

cananerpek@erpekmuhendislik.com

EDUCATION

2006 September – 2009 January

Middle East Technical University / Ankara / TURKEY

M.Sc in Chemical Engineering, CGPA: 3.86 / 4.00

2001 September – 2006 June

Middle East Technical University / Ankara / TURKEY

B.Sc in Chemical Engineering, CGPA: 3.51 / 4.00

1999 September – 2001 June

Çağrıbey Anatolian High School / Ankara / TURKEY

Mathematics – Science Branch, CGPA: 4.62 / 5.00

WORK EXPERIENCE

2013 April – Continue

ERPEK Engineering & Consulting / İstanbul / TURKEY

Technical Manager

2011 July – 2013 April

TÜBİTAK Marmara Research Center- Chemistry Institute/ Gebze / TURKEY

Researcher

Projects:

- Waste Oil Recycling Pilot Plant Design and Optimization
- Aluminum Salt Cake Recycling Process Performance Improvement

2010 June – 2011 June

KORDSA GLOBAL Endüstriyel İplik A.Ş. / İzmit / TURKEY
Technical Engineer (Industrial Yarn Line 2)

2006 September – 2010 May

Middle East Technical University / Ankara / TURKEY
Teaching Assistant

- Process Control
- Fluid Mechanics
- Rheology
- Chemical Engineering Laboratory I and II

RESEARCH TOPICS

- Process Design and Detailed Engineering
- Hydrocarbon Processes
- Waste Oil Recycling Technologies
- Polymeric Nanocomposites
- Polymer Processing
- Layered Silicates

COMPUTER SKILLS

- ChemCad
- Aspen HYSYS
- MATLAB Simulink
- AutoCAD
- Ansys Fluent

PUBLICATIONS**Journal Publications**

- Yeniova C., Ozkoc G., Yilmazer U., Use of Halloysite Nanotubes for the Production of Poly (lactic acid) Nanocomposites, Materials Research Society, 1504 (2013).
- Yeniova C., Yilmazer U., Effect of Different Types of Organoclays And Compatibilizers on the Properties of Polystyrene Based Nanocomposites, Journal of Applied Polymer Science, 127(5), s. 3673 – 3680 (2012).
- Yeniova C., Yilmazer U., Characteristics of Impact Modified Polystyrene/ (SEBS-g-MA) / Organoclay Nanocomposites, Polymer Composites, 31, s. 1853 – 1861 (2010).

National and International Congresses

- Yeniova C., Özkoç G., Yilmazer Ü., Joint Turkey-Germany Workshop on Polymeric Nanocomposites, 29-31 August 2014, Istanbul, TURKEY.
- Yeniova C., Özkoç G., Yilmazer Ü., Material Research Society (MRS) Fall Meeting, Use of Halloysite Nanotubes For the Production of Poly(lactic acid) Nanocomposites, 25-30 November 2012, Boston, USA.
- Yeniova C., Özkoç G., Yilmazer Ü., III. Uluslararası Polimerik Kompozitler Sempozyumu, PLA/Halloysit Nanokompozitlerinin Üretimi Ve Karakterizasyonu, 9-11 November 2012, Izmir, TURKEY.
- Yeniova C., Özkoç G., Yilmazer Ü., 7th Chemical Engineering Conference for Collaborative Research in East Mediterranean Countries (EMCC-7), Production of Poly(lactic acid) Nanocomposites by Using Halloysite Nanotubes Originated from a Local Source, s. 15, 27 April – 3 May 2012, Corfu, GREECE.
- Yeniova C., Baykan A., Vehbioğlu Ö. Erpek E., 7th Chemical Engineering Conference for Collaborative Research in East Mediterranean Countries (EMCC-7), Recycling of Used Oil by Thin Film Evaporation plus Hydrotreating Process, s. 72, 27 April – 3 May 2012, Corfu, GREECE.
- Yeniova C., Yilmazer Ü., 6th Chemical Engineering Conference for Collaborative Research in Eastern Mediterranean Countries (EMCC-6), *Effect of Organoclay on Phase Inversion Point Polystyrene / Organoclay Nanocomposites*, s. 139, 7 – 12 March 2010, Antalya, TURKEY.
- Yeniova C., Yilmazer Ü., 17th Annual International Conference on Composites/Nano Engineering (ICCE - 17), *Use of Organically Modified Montmorillonite In the Preparation of Impact Modified Polystyrene*, 26 – 31 July 2009, Hawaii, USA.
- Yeniova C., Yilmazer Ü., Bayramlı E., International Polymeric Composites Symposium – Workshop and Exhibition, *Impact Modification of Polystyrene Based Nanocomposites*, 28 – 30 November 2008 Izmir, TURKEY.
- Yeniova C., Yilmazer Ü., Bayramlı E., 8th National Chemical Engineering Congress (UKMK-8), *Preparation of High Impact Polystyrene Nanocomposites by Melt Intercalation Method*, pg. 611-612, 26 – 29 August 2008, İnönü University, Malatya, TURKEY.
- Yeniova C., Yilmazer Ü., Bayramlı E., Polymer Processing Society 24th Annual Meeting, *Impact Modified Polystyrene Based Nanocomposites: Production By Melt Intercalation and Characterization*, 15 – 19 June 2008 Salerno, ITALY.
- Yeniova C., Yilmazer Ü., Bayramlı E., II. National Polymer Science and Technology Congress, *Preparation and Characterization of Organoclay/Polystyrene Nanocomposites at Different Microstructures*, pg. 88, 30 April – 2 May 2008 Harran University, Şanlıurfa, TURKEY.

TRAINING PROGRAMS

- “Ansys Fluent Training” Anova Proje ve Danışmanlık Tic. Ltd. Şti., Ankara, TURKEY, February 2013
- “Uygulamalı Arge’de Temel yaklaşımlar” TÜBİTAK Marmara Research Center, TURKİYE, May 2012
- “6 Sigma Green Belt Training Module 1-2”, Matris Danışmanlık, Kocaeli, TURKEY, April 2011.
- “Advanced Excell Training”, Bilginç IT Academy, Kocaeli, March 2011,
- “Internal Auditor Training”, Bereau Veritas, Kocaeli, TÜRKİYE, February 2011.
- “Basic Principles of Extrusion and Rheology and Their Applications on Polymer Technology” Anamed-Thermo Companies, Hacettepe University, Ankara, TÜRKİYE, November 2007.

HONORS

- METU, Department of Chemical Engineering, 2003 - 2nd Semester, 3rd Degree Certificate.
- METU, Department of Chemical Engineering, 2004 – 2nd Semester, 3rd Degree Certificate.
- METU, 2008 – 2009 Graduate Courses Performance Award.